Volume

1

Conseil national de recherches
Canada

Institut de génie des
matériaux

Boucherville (Québec)

National Research Council
Canada

Industrial Materials
Research Institute

Boucherville, Quebec

COMPOSITES 86

28434 - Part 1

POLYMER COMPOSITES

VOLUME 8/NO. 5/OCTOBER 1987

Composites '86—Part 1

National Research Council of Canada
Industrial Materials Research Institute

CONTENTS

289 T. VU-KHANH and L.A. UTRACKI/Preamble

291 M.R. PIGGOTT/The Effect of the Interface/Interphase of Fiber Composite Properties

298 P.X. NGUYEN and A. MOET/The Effect of Fiber-Matrix Adhesion on the Fatigue Fracture of Glass-Fiber-Reinforced Poly(Vinyl Chloride)

308 P.S. CHUA/Dynamic Mechanical Analysis Studies of the Interphase

314 A.C. ROULIN-MOLONEY, W.J. CANTWELL, and H.H. KAUSCH/Parameters Determining the Strength and Toughness of Particulate-Filled Epoxy Resins

324 A.C. ROULIN-MOLONEY, N. CUDRÉ-MAUROUX, and H.H. KAUSCH/In Situ Fracture Tests in the Scanning Electron Microscope

331 T. VU-KHANH/Crack-Arrest Study in Mode II Delamination in Composites

342 A.J. RUSSELL/Micromechanisms of Interlaminar Fracture and Fatigue

352 M. TASNON and C. ROY/Damage Tolerance in Graphite Epoxy Composite: Comprehensive Monitoring Method

PUBLISHED BY THE SOCIETY OF PLASTICS ENGINEERS, INC.

POLYMER COMPOSITES

Published by the Society of Plastics Engineers

EDITOR—Roger S. Porter
℅ Polymer Science and Engineering
University of Massachusetts
Amherst, Mass 01003

ASSOCIATE EDITORS—Richard E. Ball and Robert A. Weiss
℅ Western New England College
Springfield, Mass 01119
℅ University of Connecticut
Storrs, Conn 06268

ADVISORY BOARD

Lawrence J. Broutman
Illinois Institute of Technology
Anthony T. DiBenedetto
University of Connecticut
Nikolay Enikolopyan
USSR Academy of Sciences
David H. Kaelble
Arroyo Computer Center
John L. Kardos
Washington University
Lon Mathias
University of Southern Mississippi
Frederick J. McGarry
Massachusetts Institute of Technology
L. Nicolais
University of Naples
R. Byron Pipes
University of Delaware
N. S. Schneider
Army Materials and Mechanics Research Center
James C. Seferis
University of Washington
J. G. Williams
Imperial College of Science & Technology

PUBLICATIONS COMMITTEE

E. W. Rowan, Jr., Chairman
Parkway Plastics, Inc

R. P. Braddicks, Jr.
Plastics Consultant
A. T. DiBenedetto
University of Connecticut
H. Finkel
Industrial Designer
R. D. Forger
Society of Plastics Engineers
J. L. Hull
Hull Corporation
M. A. Mendelsohn
Westinghouse Electric Corp
R. S. Porter
University of Massachusetts
D. W. Riley
Extrusion Engineers
A. A. Schoengood
Society of Plastics Engineers
A. E. Whitney, Jr.
Plastics Consultant

Copyright by Society of Plastics Engineers, 1987. POSTMASTER: Send address changes to Polymer Composites, 14 Fairfield Dr., Brookfield Center, CT 06805. Telephone (203) 775-0471, TELEX 643-712. Reproduction in whole or in part without written permission is strictly prohibited.

Polymer Composites (ISSN 0272-8397) is published at Waverly Press, Easton, MD 21601. Address changes, undeliverable copies, and orders for subscriptions should be sent to Circulation Manager, Society of Plastics Engineers, 14 Fairfield Dr., Brookfield Center, CT 06805.

Published bimonthly (February, April, June, August, October, December). Second class postage paid at Brookfield Center, Conn., and additional entry offices. Accepted at special postal rate provided in P.M. Sec. 132.122.

Neither the Society of Plastics Engineers nor Polymer Composites is responsible for the views expressed by individual contributors either in articles published in Polymer Composites or in technical papers presented at meetings of the Society.

Subscription rates for 1987: SPE members, 1 year—$40. Nonmembers, 1 year—$100. Delivery outside North America, add $12 per year.

SOCIETY OF PLASTICS ENGINEERS
Business and Executive Offices, 14 Fairfield Dr., Brookfield Center, CT 06805

Daniel J. Domoff
Managing Editor
Marie J. Bruckenthal
Production Manager
Becky Borgatti
Copy Editor
Michael R. Cappelletti
Circulation Manager

OFFICERS OF THE SOCIETY

John R. Kretzschmar
President
Bruce A. Petersen
President-elect
Vivian E. Malpass
First Vice President
Leonard H. Drexler
Second Vice President
Jacques de Craene
Vice President for International Affairs
Kishor S. Mehta
Secretary
George W. Thorne
Treasurer
Robert D. Forger
Executive Director and Publisher

POLYMER COMPOSITES is indexed by:—Chemical Abstracts—Engineering Index, Inc.

PREAMBLE

After a period of sustained growth in plastics consumption, their volume now exceeds that of raw steel. However, since the beginning of the 70s, forecasts made by extrapolating from past data have proven too optimistic. The gap between capacity and sales of plastics in the Western world is widening. Pressure of competition forces companies to focus on materials offering higher performance.

The production of reinforced plastics has constantly increased since the Second World War. With a forecast annual growth rate of 8% to 12% over the next decade, composites are the fastest growing sector of the plastics industry. Advanced composites show the largest expansion, mainly because of a strong increase in demands in aerospace and military applications. Penetration of advanced composites into big-volume markets has not occurred, but it is believed that advances in fiber and matrix performance as well as in the method of fabrication will accelerate the mass production of these materials.

High-volume composites will see a less rapid growth, but demand will continue to increase at a higher rate than that of matrix resin. Land transportation is and will remain the largest and fastest growing market for high-volume composites.

The next potential market for high-performance plastics will be found in the area of substitution for metals in structural parts. To fulfil this function, the mechanical properties of plastics must be improved. The most attractive method seems to be through addition of stiffer and stronger reinforcements.

However, the bright future of reinforced plastics is impossible without sustained efforts in research and development as well as in education of the user about the possibilities of these new materials. The composites offer unique properties that require imagination and ingenuity from scientists and engineers. Besides the technical problems, the particularity of composites necessitates an extensive training program on new approaches to design. These hurdles are many, but they will have to be overcome before composites can be used to their full potential.

The symposium "Composites-'86" of November 25 and 26 was the sixth in a series on "Polymer Composites" and the 16th organized and sponsored by the Industrial Materials Research Institute of the National Research Council of Canada. The remaining symposia are part of the two other series on "Mathematical Modeling of Plastics Processing and Properties" and on "Polymer Blends."

Proceedings of these symposia have been published in the technical journals of the Society of Plastics Engineers: "Composites" in *Polymer Composites*, "Modeling" and "Polyblends" in *Polymer Engineering and Science*. In addition, the entire symposia are recorded, and the tapes stored in the Institute library for two years, available to anyone interested in the subject. The meetings provide a source of the most recent information and an open forum for discussion and consultation; in addition, they facilitate contacts between academic and commercial competence and improve understanding, mutual respect, and cooperation between the participants.

In organizing this symposium, we tried to create a forum for discussions between people from different areas of both theory and practice. We hope that it was a fruitful meeting for those involved in the development of composites. Because of the diversity of composite materials, sharing opinions and experiences constitutes a necessary and fertile element for the advancement.

The main topic of the meeting was the solid state behavior of advanced, fiber-reinforced composites. Accordingly, the papers are grouped into two parts. The first starts with an invited review by M. R. Piggott on the influence of interface on composite properties followed by seven papers on interface characterization and mechanism of fracture and delamination in advanced composites.

The second part, starting with a review by T. Vu-Khanh on current status and future trends in reinforced plastics and ending with a transcript of discussion on the subject of thermoplastics vs. thermosets in advanced composites, deals primarily with analysis and performance of composites and compositelike materials.

It is our pleasant duty to express once again our gratitude and thanks to the authors and participants of the symposium. As evidenced by the discussion transcripts, the meeting was a lively one with a frank exchange of concepts and opinions. It made a small but important contribution toward better understanding of these materials.

T. Vu-Khanh and L. A. Utracki
Symposium Organizers

The Effect of the Interface/Interphase on Fiber Composite Properties

M. R. PIGGOTT

*Department of Chemical Engineering
and Applied Chemistry
University of Toronto
Toronto, Ontario M5S 1A4*

The interfacial region between fibers and matrix in fiber composites governs the transfer of forces between the relatively weak and compliant matrix and the reinforcing fibers. An effective interphase can ensure that the mechanical properties of the composite reflect the high strength and modulus of the fibers. Although composites can be made with the expected strengths and moduli, it is not entirely clear why this is achieved: Tests with critical composites, i.e., those containing very short aligned fibers, do not show the expected stress-strain behavior. This paper examines the effect of an interphase having a shear modulus that is less than that of the matrix. It is found that to explain the Young's moduli of the short fiber composites, the interphase must have a very low modulus indeed; i.e., a few kPa at most. In addition, the strength results can be accounted for only if we assume that the short lengths of fiber used in the experiments had higher strengths than anticipated. Although agreement between experiments and theory is thus not very good, the small amount of experimental evidence available indicates a need for further systematic experiments on critical (i.e. short aligned fiber) composites before firm conclusions are drawn.

INTRODUCTION

In the earliest treatment of fiber composites (1), the interface between the fibers and the matrix was assumed to transmit stresses perfectly. This permitted the estimation of the Young's modulus of composites containing fibers having lengths from very short to infinitely long, and any orientation relative to each other and to the direction of an applied stress. This treatment was developed to explain the remarkably good properties of wood fiber products such as paper and cardboard and since has been widely used, refined, and developed by researchers into fiber composites. It is now commonly referred to as shear lag analysis.

It was eventually realized (2) that the shear lag theory involved very high shears at the fiber-matrix interface, near the fiber ends. At quite low composite stresses, these reached the shear strength of the matrix. Thus, some sort of failure in this region is to be expected. It has been suggested that debonding and frictional sliding can take place with reinforced polymers (3), while shear yielding has been suggested for metal matrix composites (4).

This approach has led to the concept of the fiber critical length L_c or aspect ratio s_c:

$$s_c = L_c/d = \sigma_{fu}/2\tau_i \tag{1}$$

where d is the fiber diameter, σ_{fu} its strength, and τ_i is the shear stress due to friction or matrix yielding at the interface. τ_i is usually assumed to be constant.

s_c can be measured by embedding a single fiber in a plastic and stressing the plastic until the fiber has been broken into small pieces. Further stressing leads to still more breakage, but eventually no further fiber breakage is observed. At this stage, the lengths of the pieces of fiber are measured. These lengths range from $L_c/2$ to L_c (5).

The implications of this slip and/or shear yielding process have been thoroughly examined, and two conclusions were drawn that have serious implications for use of fiber composites in critical load-bearing situations (6):

1. There exists a slip point. This is the point on the stress-strain curve at which the stresses near the fiber ends become so great that they exceed the matrix shear strength, τ_{mu}. In an aligned fiber composite this occurs at a composite strain ϵ_{1s} where we can write, approximately
$$\epsilon_{1s} \cong 2\tau_{mu}/\sqrt{E_f E_m}. \tag{2}$$
Here E_f and E_m are the Young's moduli of fibers and matrix. A typical aligned carbon-fiber-reinforced polymer could have a strength of 2 GPa and a breaking strain of 1.5%, while the matrix shear strength is typically only 40 MPa. ϵ_{1s} might be regarded as a danger point for the composite. Debonding is expected to start at this strain, with slip taking over as the predominant stress transfer mechanism at higher stresses.
2. Stress-strain curves are straight lines up to the slip point; beyond this they deviate more and more from the straight line. *Figure 1* shows typical theoretical plots for glass-epoxies. Note the effect of fiber aspect (length/diameter) ratio.

Although this analysis has wide support, it lacks experimental evidence. Some support was indicated from experiments with glass-nylon extrusions in which the molding process aligned the fibers (7). Unfortunately, these workers seem subsequently to have changed their minds (8), and a recent, careful investigation of short carbon fiber reinforced epoxies lends no support to the theory at all, except when interface sliding was artificially promoted.

In this work (9, 10), straight stress-strain curves were obtained for sized fibers with lengths of 1, 2, 3, and 5 mm (aspect ratios 125, 250, 375, and 625); see *Fig. 2*. Reducing the fiber-matrix adhesion reduced the Young's modulus of the composites, but still gave straight lines for stress vs. strain (*Fig. 3*). Only by coating the fibers with silicone oil could curved stress vs. strain plots be obtained (*Fig. 4*), and these only for the shortest of fibers. These results are summarized in *Fig. 5*, which shows the breaking strains of the composites, together with the form taken by the stress-strain plot, for the different fiber lengths.

The failure to observe the curves predicted suggests that slip is only playing a minor role in the reinforcement process. Note that there is an assumption concerning interface failure that is a key element in the analysis. This is that the failure is governed by a stress criterion.

Recent results of experiments in which single fibers were embedded in blocks of polymer and pulled out under carefully controlled conditions suggest that this assumption may not always be tenable (11). *Figure 6* shows the force, F_A,

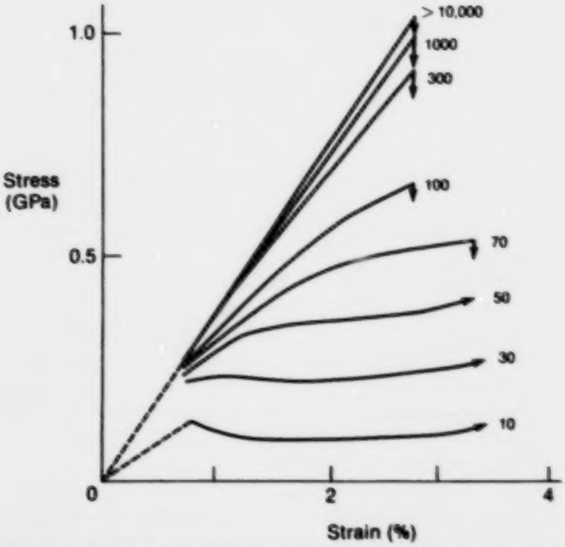

Fig. 1. Theoretical stress-strain curves for glass-epoxies. The fibers were aligned in the stress direction and had aspect ratios indicated on the curves.

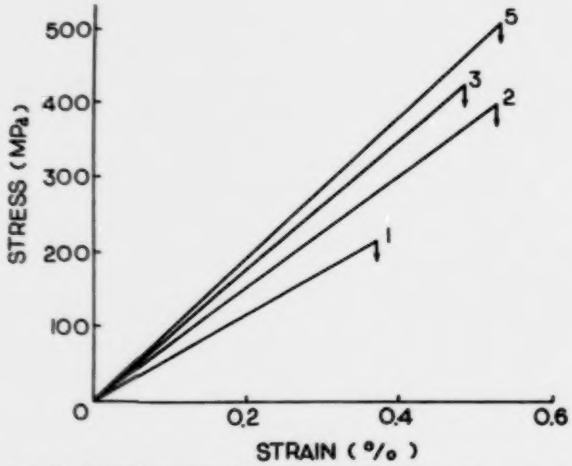

Fig. 2. Experimental stress-strain plots for carbon-epoxies [sized fibers; fiber lengths 1, 2, 3, and 5 mm, as indicated on the plots; V_f = 0.35; fibers aligned along stress direction (9)]. V_f is the fiber volume fraction.

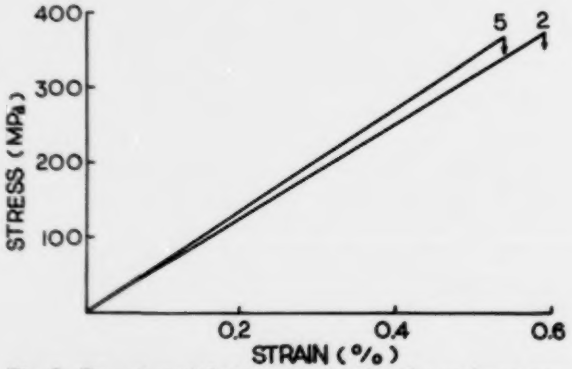

Fig. 3. Experimental stress-strain plots for carbon-epoxies [fibers desized to reduce adhesion with matrix; fiber lengths 2 and 5 mm; V_f = 0.35; fibers aligned along the stress direction (9)].

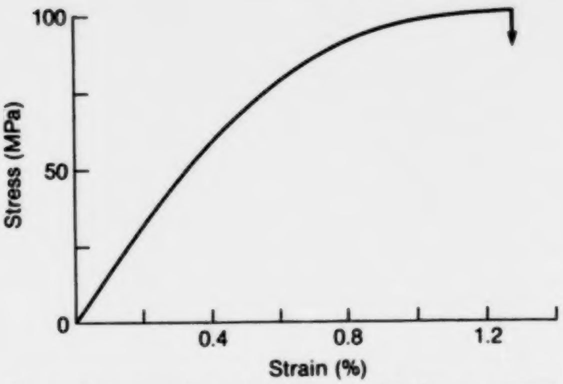

Fig. 4. Experimental stress-strain plot for a carbon-epoxy in which the fibers had been coated with silicone oil [fiber length 1 mm; $V_f = 0.20$; fibers aligned along the stress direction (9)].

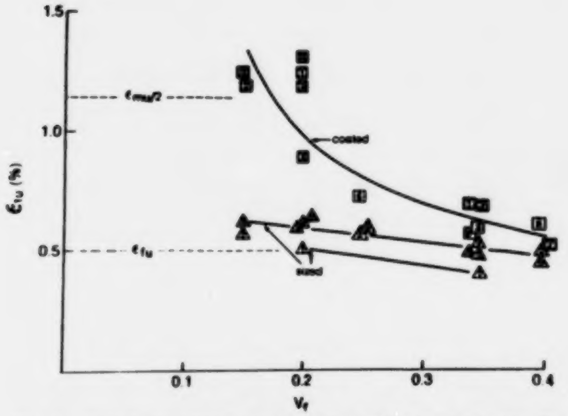

Fig. 5. Breaking strains of aligned fiber composites. Fiber length is indicated by figures on curves. Square and triangular shapes indicate silicone-coated and sized fibers, respectively. Circles indicate curved stress-strain plot.

that had to be exerted on the fiber to cause debonding vs. embedded fiber length, *L*. The results fit the relation

$$F_A = \pi d\ \sqrt{G_i L E_{fm}} \qquad (3)$$

where $E_{fm} \cong 0.33\ \sqrt{E_f E_m}$ (the constant, 0.33, depends on the exact geometry of the test setup). G_i is the work of fracture of the interphase or interface. G_i is small and very much less than the work of fracture of the matrix. It is typically 10 to 40 $\mathrm{Jm^{-2}}$ for carbon in epoxies and 50 to 200 $\mathrm{Jm^{-2}}$ for glass in epoxies and polyester, compared with 1000 to 5000 $\mathrm{Jm^{-2}}$ for the polymer matrices themselves (12).

The $L^{1/2}$ relation, *Eq 3*, suggests very strongly that a fracture process is involved in interphase failure: The Griffith equation is analogous to *Eq 3*. The forces required to pull the fibers out, shown in *Fig. 6*, greatly exceeded the maximum stress criterion for failure. (These were calculated on the basis of the interphase having the same shear strength as the matrix; i.e., about 40 MPa.) For the longer embedded lengths, the interphase region did not have enough energy to fracture until the shear stress, if the material were still elastic, reached 100 MPa.

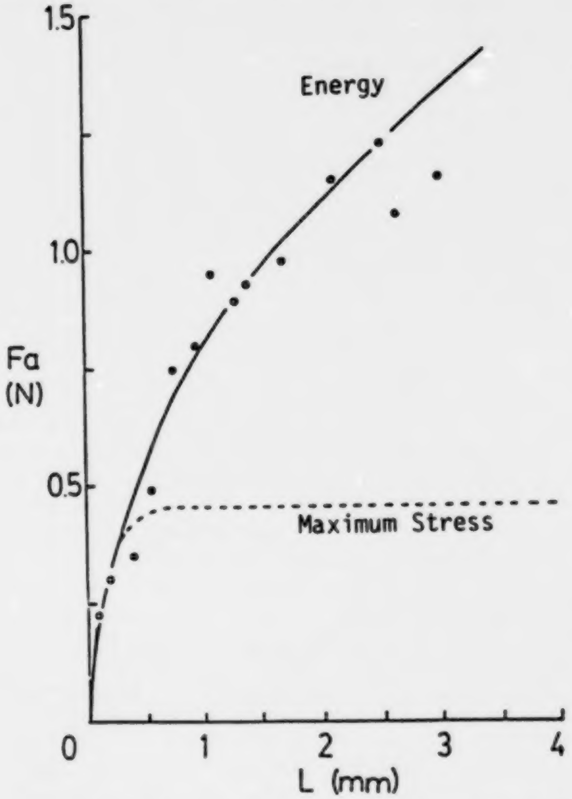

Fig. 6. Force required to debond the fiber vs. fiber embedded length in a single-fiber pullout test. Lines indicate theoretical plots.

We can estimate the composite strain, ϵ_{1i}, needed to generate the energy required for interface failure near the fiber ends in the composite. This gives (11)

$$\epsilon_{1i} = \sqrt{8G_i/dE_f}. \qquad (4)$$

For glass fibers, with $E_f = 72$, $d = 10\ \mu\mathrm{m}$, and $G_i = 190\ \mathrm{Jm^{-2}}$, ϵ_{1i} comes to 4.6%. For carbon, with $E_f = 250$ GPa, $d = 8\ \mu\mathrm{m}$, and $G_i = 20\ \mathrm{Jm^{-2}}$, ϵ_{1i} comes to 0.89%; i.e., about three times greater than ϵ_{1s}. Thus, in both glass and carbon fiber composites, the progressive slip process could be suppressed until the fibers are close to their breaking points. When progressive slip is initiated at such a high stress, it is likely to be catastrophic when the fibers are short. Thus, we might expect composite failure to occur, for short fiber composites at least, at strains that are somewhat less than the fiber breaking strain. This is indeed the case with the aligned short carbon fiber reinforced epoxies at the higher fiber volume fractions (9).

Since the Young's modulus of the composite made with aligned short fibers is affected by the adhesion between the fibers and the matrix (9), we are perforce obliged to look elsewhere than progressive slip theory, or simple shear lag theory, for an explanation of the behavior of short fiber composites.

An attempt has been made to explain the straight line stress-strain plots, based on some initial debonding of the fibers (13). The slope of the plot (i.e., the effective composite Young's modulus) was given approximately by

$$E_1 = V_f E_f (1 - m_d - \sqrt{E_f/E_m}/s) + V_m E_m \quad (5)$$

where m_d is the fraction of the fiber surface area that has debonded and s is the fiber aspect (length/diameter) ratio. Debonding was assumed to take place at the end regions of the fibers. However, inconsistent values of m_d were obtained when values of m_d calculated from the composite strengths were compared with those calculated from the composite modulus.

Another possible approach is to assume that the system is truly elastic and that the decrease in modulus, caused by the fiber surface treatments, is due to the interphase having a modulus that is different from that of the matrix (and the fibers).

Composite With a Distinctive Interphase

The idea of a composite having an interphase with different mechanical properties from either fiber or matrix is not a new one; see, for example, Kaeble (14). In the appendix is set out a treatment of this that follows the terminology of the author's test (15). Here, we will discuss the interpretation of what little experimental data are available on the basis of the distinctive interphase.

The only difference between the results with the interphase and those without is the value of n (*Eq A13*). With no interphase, A (see *Eq A7*) is just $\ln(P_f/V_f)$ which comes to $\ln(3.63/V_f)$ for hexagonal packing of the fibers ($P_f = 2\pi/\sqrt{3}$ for hexagonal packing).

First, we note that for $G_i < G_m$, n is decreased by the interphase. Here, G_i is the shear modulus of the interphase and G_m that for the matrix; these G's should not be confused with G's for the works of fracture. Thus, the composite modulus is decreased (*Eq A16*). The distinctive interphase concept is therefore in qualitative agreement with the experiment (10), so long as the surface treatment reduces the value of G_i.

Figure 7 shows a plot of E_1 estimated from *Eq A16*, with n given by *Eq A13*, A by *Eq A8*, and $P_f = 2\pi/\sqrt{3}$. For these curves, $E_f = 380$ GPa, $E_m = 2.4$ GPa, $s = 125$, $\upsilon_m = 0.35$, and $V_f = 0.5$. This was the same carbon fiber-epoxy system used by Sanadi and Piggott (9). The volume fraction of the interphase material was varied, taking values 0.1, 0.03, and 0.01, as indicated on the graph. Unless the interphase is relatively thick ($V_i = 0.1$), G_i has to be several hundred times less than G_m before a substantial reduction in modulus of the composites could be obtained, even though the fibers were only 1 mm long ($s = 125$).

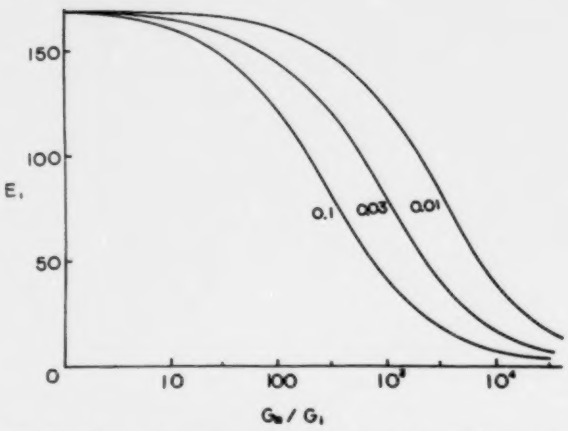

Fig. 7. Effect of interphase shear modulus (G_i) on the Young's modulus of an aligned short fiber composite (E_1). Volume fraction of interphase material is 0.01, 0.03, and 0.1, as indicated on the curves.

It is notable, though, that a very low modulus material like a rubber, with $G_i < G_m/10{,}000$, has a profound effect on the modulus. It should be noted also that V_i and G_i work in concert. The curves for the different V_i's can be approximately superposed. This is because for $V_i \ll V_f$, $\ln((V_f + V_i)/V_f) \cong V_i/V_f$. Thus *Eq A8* simplifies to

$$A \cong \ln(P_f/V_f) + (G_m/V_f)(V_i/G_i). \quad (6)$$

For quantitative agreement we compare the pseudo rule of mixtures formulae. For Young's modulus in the fiber direction of an aligned short fiber composite, we write

$$E_1 = \chi_1 \chi_2 V_f E_f + V_m E_m \quad (7)$$

where χ_1 represents the effect on modulus of imperfect fiber alignment and has the values 0.67 and 0.68 for the 2-mm and 5-mm fibers respectively, χ_2 represents the effect of finite fiber aspect ratio, and comparison with *Eq A16* gives

$$\chi_2 = 1 - \tanh(ns)/ns. \quad (8)$$

Using the experimental values for the modulus reduction, A_E, which should be equal to $\chi_1\chi_2$, we can estimate n and hence G_m/G_i. The results for 2-mm and 5-mm long fibers are given in *Table 1*.

We can treat the results for strength similarly, writing

$$\sigma_{1u} = \chi_3 \chi_4 V_f \sigma_{fu} + V_m E_m \sigma_{fu}/E_f \quad (9)$$

where χ_3 represents the effect of imperfect alignment, equal to 0.74 and 0.76 for 2-mm and 5-mm fibers respectively. χ_4 represents the effect of fiber length.

To estimate χ_4 we use *Eq A17* with $\sigma_{fmax} = \sigma_{fu}$ to determine ϵ_{1u}, and substitute this for ϵ_1 in *Eq A15*. This gives the average fiber stress at the breaking point of the composite, σ_{fbp}.

Table 1.

Fiber Length (mm)	Surface Treatment	Estimated χ_2	G_m/G_i	Estimated χ_4	G_m/G_i	χ_4/χ_2
2	sized	0.87	300	1.00		1.15
	desized	0.66	2,700	0.82	700	1.24
	etched	0.66	2,700	0.82	700	1.24
	coated	0.37	12,000	0.62	4,000	1.68
5	sized	0.99	—*	1.21	—	1.22
	desized	0.76	8,500	1.04	—	1.37
	etched	0.87	2,500	1.04	—	1.20
	coated	0.41	62,000	0.72	15,000	1.76

* With a perfect interphase ($G_i = G_m$), χ_2 comes to 0.98.

$$\sigma_{fbp} = \sigma_{fu}(1 - \tanh(ns)/ns)(1 - \mathrm{sech}(ns)). \quad (10)$$

Now $\chi_4 = \sigma_{fbp}/\sigma_{fu}$; hence

$$\chi_4 = \frac{1 - \tanh(ns)/ns}{1 - \mathrm{sech}(ns)}. \quad (11)$$

Using the experimental data for the strength reduction factor, A_s, which should be equal to $\chi_3\ \chi_4$, we can estimate G_m/G_i. The values so obtained do not correlate with G_m/G_i estimated from the modulus (see *Table 1*).

DISCUSSION AND CONCLUSIONS

That strength and modulus results do not give the same values of G_m/G_i is not surprising since the strength of carbon fibers is length dependent (16). Thus, the fibers in short fiber composites could well behave as though they were stronger than expected, based on measurements of fiber strengths. The usual length used for measuring fiber strength is more than ten times the 2-mm fiber length giving the results shown in *Table 1*. [What is a more serious problem is that the strength results fit the slip theory quite well except in the case of the silicone-coated fibers (9)].

If we look at the ratio χ_4/χ_2 (*Table 1*) we see that for the silicone-coated fibers it is 1.68 to 1.76, while for the uncoated fibers it varies from 1.15 to 1.37. It seems possible that the disagreement between the strength and modulus results could be accounted for by deviations in the fiber strength caused by (1) using short lengths of fiber; (2) treating the fiber surface by the various techniques used. That the results are not entirely consistent could be due to the notorious variability in fiber strength and to imperfections introduced during the composite manufacturing process.

However, we only have one set of results to go on. What is needed, above all, is more systematic study of aligned short fiber composites, with interfaces (or interphases) modified in a controlled fashion. To draw many conclusions at this time would be premature.

APPENDIX: SHEAR LAG THEORY WITH DISTINCT INTERPHASE

We follow the treatment given by Piggott (15) derived from that of Cox (1). Consider the element of a fiber composite shown in *Fig. 8*. The fiber, diameter $2r_f$, is surrounded by an interphase having a thickness $r_i - r_f$. The fibers are hexagonally packed, with nearest neighbor fibers having their axes a distance r_m away from the fiber axis.

For equilibrium, the shear stresses at the three boundaries obey the equation

$$r_f\tau_f = r_i\tau_i = r_m\tau_m. \quad (A1)$$

Hookes Law for the interphase gives

$$\frac{dw_i}{dz} = \frac{\tau}{G_i} \quad (A2)$$

where w_i is the displacement of the interphase at a distance z from the fiber axis, and G_i the shear modulus of the interphase. We can determine the displacement of the interphase at its outer face by integration:

$$\int_{u_f}^{u_i} dw_i = \frac{\tau_f r_f}{G_i}\int_{r_f}^{r_i}\frac{dz}{z} \quad (A3)$$

where we have substituted $\tau_f r_f$ for τz, in accordance with the same equilibrium condition as used for *Eq 1*. Doing the integration gives

$$u_i - u_f = \frac{\tau_f r_f}{G_i}\ln(r_i/r_f). \quad (A4)$$

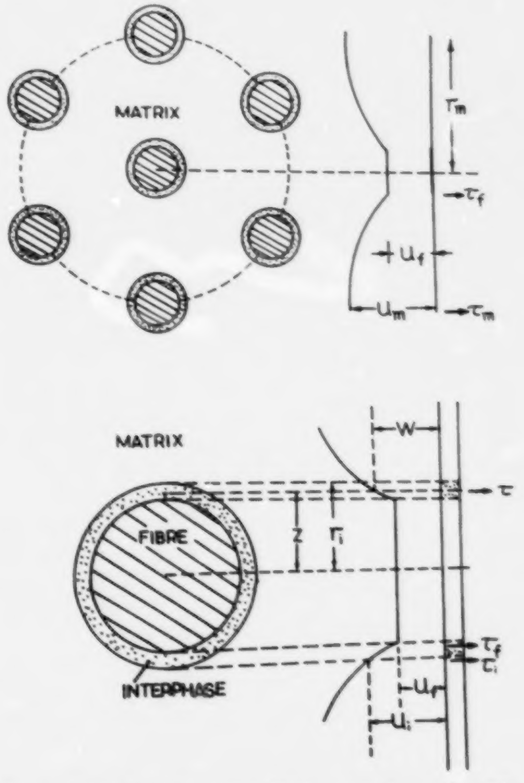

Fig. 8. Top: On left is one fiber, near its end, with six nearest neighbor fibers and interphases; on right are relative displacements along fiber direction. Bottom: magnified view of region around the central fiber.

The same treatment for the matrix gives

$$u_m - u_i = \frac{\tau_i r_i}{G_m}\ln(r_m/r_i) \qquad \text{(A5)}$$

where G_m is the shear modulus of the matrix. We neglect the shear deformation of the fiber. Eliminating u_i between *Eqs A4* and *A5*, we obtain the relative displacement at the boundaries of the element:

$$u_m - u_f = \tau_f r_f \frac{\ln(r_m/r_i)}{G_m} + \frac{\ln(r_i/r_f)}{G_i}. \qquad \text{(A6)}$$

Let

$$A = 2\ln(r_m/r_i) + (2G_m/G_i)\ln(r_i/r_f). \qquad \text{(A7)}$$

For hexagonal packing with fiber, interphase, and matrix volume fractions V_f, V_i, and V_m, we have

$$\begin{aligned} A = {} & \ln[P_f/(V_i + V_f)] \\ & + (G_m/G_i)\ln((V_i + V_f)/V_f) \end{aligned} \qquad \text{(A8)}$$

where $P_f = 2\pi/\sqrt{3}$.

τ_f transfers stress to the fibers, and equilibrium of a fiber element, length dx with stresses σ_f at distance x from the fiber center section and $\sigma_f + d\sigma_f$ at $x + dx$, requires that

$$\frac{d\sigma_f}{dx} = \frac{2\tau_f}{r_f}. \qquad \text{(A9)}$$

Using *Eqs A6* and *A7* we have

$$\frac{d\sigma_f}{dx} = \frac{2G_m(u_m - u_f)}{Ar}. \qquad \text{(A10)}$$

Since u_f is related to σ_f by Hookes Law,

$$\frac{d^2\sigma_f}{dx^2} = \frac{n^2}{r^2}(\sigma_f - E_f\epsilon_1) \qquad \text{(A12)}$$

and the matrix tensile strain $\epsilon_m(=du_m/dx)$ is assumed equal to the composite strain, ϵ_1, we have

$$\frac{d^2_{\sigma f}}{dx^2} = \frac{n^2}{r^2}(\sigma_f - E_f\epsilon_1) \qquad \text{(A12)}$$

where

$$n^2 = 2E_m/(AE_f(1 + \nu_m)). \qquad \text{(A13)}$$

For a fiber with zero stress at the ends, *Eq A12* may be solved to give the well-known solution (1):

$$\sigma_f = E_f\epsilon_1(1 - \cosh(nx/r)/\cosh(ns)) \qquad \text{(A14)}$$

where s is the fiber aspect ratio.

The average fiber stress, obtained by integration, is

$$\bar{\sigma}_{fb} = E_f\epsilon_1(1 - \tanh(ns)/ns) \qquad \text{(A15)}$$

and the composite stress, σ_1, thus comes to

$$\begin{aligned} \sigma_1 = {} & V_f E_f\epsilon_1(1 - \tanh(ns)/ns) \\ & + V_m E_m \epsilon_1. \end{aligned} \qquad \text{(A16)}$$

Finally, the maximum fiber stress, at the center, is

$$\sigma_{fmax} = E_f\epsilon_1(1 - \operatorname{sech}(ns)). \qquad \text{(A17)}$$

REFERENCES

1. H. L. Cox, *Br. J. Appl. Phys.*, **16**, 199 (1952).
2. A. Kelly, *Strong Solids*, 2nd Ed., p. 179, Clarendon Press, Oxford (1973).
3. J. Outwater, *Modern Plastics*, **33**, 37 (1956).
4. A. Kelly and G. Davies, *Metall. Rev.*, **10**, 1 (1965).
5. J. D. Hughes, AERE (UK) Report R8683 (1977).
6. M. R. Piggott, *J. Mater. Sci.*, **13**, 1709 (1978).
7. W. H. Bowyer and M. G. Bader, *J. Mater. Sci.*, **7**, 1315 (1972).
8. P. T. Curtis, M. G. Bader, and J. E. Bailey, *J. Mater. Sci.*, **13**, 377 (1978).
9. A. R. Sanadi and M. R. Piggott, *J. Mater. Sci.*, **20**, 421 (1985).
10. A. R. Sanadi and M. R. Piggott, *J. Mater. Sci.*, **20**, 431 (1985).
11. M. R. Piggott and P. S. Chua, *Ind. Eng. Chem.—Product R/D* (accepted for publication, 1986).
12. M. R. Piggott, A. Sanadi, P. S. Chua, and D. Andison, in *Proc. ICCI*, H. Ishida and J. L. Koenig, eds., p. 109, Elsevier Sci. Publ. Co. (1986).
13. M. R. Piggott (accepted by *Materials Forum*, 1987).
14. D. H. Kaeble, *Proc. 16th National SAMPE Tech. Conf.*, 340 (1984).
15. M. R. Piggott, "Load Bearing Fibre Composites," Ch. 5, Pergamon, Oxford (1980).
16. J. W. Hitchon and D. C. Phillips, *Fib. Sci. Technol.*, **12**, 217 (1979).

DISCUSSION

S. V. Hoa: When you are calculating the theoretical distribution for the stresses, do you use finite element or other techniques to get the variations?

M. R. Piggott: I haven't used the finite element method (FEM) much for two reasons: (1) it uses a lot of computer time, funding for which has been a problem; and (2) my aim always has been to develop simple relationships that tell me directly what happens when I change this or that parameter (e.g., yield stress of the interphase, work of fracture of interphase, modulus of fiber, etc.). The aim is to design better interphases. If I used FEM, I would have to do the computations many times over to determine the effect of all the different variables. Since the number of possible variables is very large, the computer time would be prohibitive. I realize that my assumptions are somewhat sweeping, and I haven't rejected FEM altogether. I have used it to determine interfacial and matrix stresses in composites with fibers in square and hexagonal arrays (1).

S. Newman: Is there any indication that chemistry of the system, as, for example, state of cure, is different at the interface than in the bulk?

M. R. Piggott: Yes. My impression is that the curing agent tends to be in a higher concentration near the interface, and indeed the chemistry is different there. This leads to nonuniform properties in the matrix. The interphase should be regarded as a phase with a gradient of properties instead of a mathematical surface.

S. Newman: A number of years ago people tried to put a rather thick layer on the fiber; as much as 10% to 20% of the original fiber diameter. They tried materials that were considerably softer than the fiber itself so it would have a ductile boundary layer. I wonder if this could be used as a model of gradual boundary layer?

M. R. Piggott: Yes. Ductile layers, especially rubbery ones, have been considered by many workers; e.g., Plueddeman in the United States (2) and Hancox and Wells (3) in the United Kingdom (see also U.S. Patent 4,035,550). The idea has great merit, but is difficult to apply in practice. The problem is that if the interphase is too soft, the off-axis properties are degraded. This effect is particularly noticeable with the shear strength.

References for Discussion

1. J. Ostrowski, G. Will, and M. R. Piggott, *J. Strain Analysis*, 19(1), 43 (1984).
2. E. P. Plueddeman, 29th Ann. Tech. Conf. SPI, Section 2 A (1974).
3. N. L. Hancox and H. Wells, *Fib. Sci. Tech.*, 10, 9 (1977).

The Effect of Fiber-Matrix Adhesion on the Fatigue Fracture of Glass-Fiber-Reinforced Poly(Vinyl Chloride)

P. X. NGUYEN *and* A. MOET

Department of Macromolecular Science
Case Western Reserve University
Cleveland, Ohio 44106

Fatigue crack propagation (FCP) of injection-molded glass-fiber-reinforced poly(vinyl chloride) was examined as a function of fiber-matrix adhesion (coupling) and fiber content at different load levels. Considering the entire FCP history, from crack initiation to critical propagation, it is shown that fatigue lifetime and fracture toughness of coupled composites increase with fiber weight fraction. Uncoupled material exhibits the highest fracture toughness at 10 wt% fiber, yet its fatigue life is considerably shorter. Damage analysis indicates that fiber debonding, pullout, and particularly fiber fracture seem to contribute to the higher fatigue lifetime noted in coupled composites. The Crack Layer Theory is employed to describe the observed FCP behavior. The effective enthalpy of damage parameterizes the resistance of the composite to FCP in terms of the observed mechanisms.

INTRODUCTION

Structural variables such as fiber-matrix adhesion, fiber content, and fiber orientation are known to play important roles in the fracture behavior of fiber-reinforced composites. Studies of their effects on fatigue crack propagation (FCP) resistance are mostly devoted to continuous fiber composite laminates; only a few are concerned with short-fiber-reinforced thermoplastics. Friedrich (1, 2) recently examined the fatigue behavior of poly(ethylene terephthalate) composites as a function of the above variables. The fracture toughness K_{Ic} and FCP resistance of the studied composite increased with strong fiber-matrix adhesion, with fiber weight fraction, and with cracks propagating in the direction transverse to the fiber length axis. Hertzberg, Manson, and co-workers (3, 4) investigated FCP in nylon 66 composites and obtained similar results; however, no, or only slight, effect of orientation was observed. These investigators, in a separate study (5), also found that FCP resistance of notched styrene-acrylonitrile composite significantly increased with increasing amount of fibers forming small angles with the loading direction. They attributed this increase to the increase in the fiber load-carrying capacity. Lomax and O'Rourke (6) reported that the endurance limit of polycarbonate at two million cycles was increased by a factor of seven when the plastic was filled with 40 wt% glass fibers. On the other hand, Shaver and Abrams (7) found that a randomly reinforced glass/nylon composite had only half the endurance of the unfilled polymer. These studies indicate that the effects of the structural variables discussed are characteristically different for different composites.

In an earlier publication (8), we found the resistance of poly(vinyl chloride) (PVC)/glass composites to crack propagation to be enhanced with increasing fiber content despite the lack of fiber-matrix adhesion. This paper examines FCP response and micromechanisms of failure as a function of enhanced fiber-matrix adhesion, fiber weight fraction, and applied stress level. The effect of fiber-matrix adhesion is particularly emphasized.

EXPERIMENTAL

Materials and Sample Preparation

The injection-molded fiber-reinforced PVC composites used in this study were supplied by the B. F. Goodrich Company. Detailed formulation for the composites is given elsewhere (8). To improve fiber-matrix adhesion, a proprietary silane coupling agent was used. The glass loadings are 10%, 20%, and 30% by weight for composites without coupling agent (uncoupled) and 6%, 20%, 30%, and 38% by weight for composites with coupling agent (coupled).

The stress-strain properties were determined using standard ASTM dog-bone shaped specimens molded under the same conditions. The elastic modulus, the ultimate stress, and strain for various composites are tabulated in *Table 1*.

Fatigue Testing

Single-edge notches (SEN) of 1 mm were introduced into injection-molded plaques (152 by 25.4 by 3.2 mm). The specimens' mold was end gated, and the initial notch was normal to the mold fill direction. FCP tests were conducted in a laboratory atmosphere using a 25-kip MTS servohydraulics test system. This provided a sine waveform loading with a constant load amplitude, a load ratio $R = 0.1$, and a frequency of 0.5 Hz. The maximum stress was 70% of the fracture stress of the notched 10 wt% uncoupled composite. These parameters allow the measurement of a reasonable crack range for every composite tested. Crack growth in the composite was monitored through a travelling optical microscope equipped with a video recorder. This system yielded 50 times magnification on the TV screen, which allowed direct observation of the crack tip position during cyclic loading. Crack propagation profile was recorded on a video tape at selected loading cycles for later measurement and detailed analysis.

The energy release rate was calculated from the following expression:

$$J_1 = \frac{\sigma^2 \pi l f^2(l/B)}{E} \tag{1}$$

where $f(l/B) = 1.12 - 0.231(l/B) + 10.55(l/B)^2 - 21.72(l/B)^3 + 30.39(l/B)^4$ (9), l is the measured crack length, B is the width of the specimen, and E is Young's modulus. Since the load ratio was kept constant ($R = 0.1$), the energy release rate averaged over the cyclic load excursion is proportional to the maximum energy release rate, J_{1max}. Accordingly, the crack propagation data are presented in terms of the latter quantity. The critical energy release rate, J_{1c} was computed from actual measurement of the critical crack length using scanning electron microscopy (SEM) together with the value of the actual fatigue fracture stress. The J_{1c} values evaluated as such are considered as a measure of fracture toughness.

Table 1. Elastic Properties of Glass-Fiber-Reinforced PVC of Varying Fiber Content, With and Without Coupling Agent, Indicated by U and C, Respectively.

Material (wt % glass)	E (GPa)	σ_{ult} (MPa)	ϵ_{ult} (%)
PVC Resin	1.2 ± .1	54.5 ± .5	20.5 ± 7.5
6%, C	2.5 ± .1	62.0 ± .6	3.2 ± .1
10%, U	2.0 ± .1	67.7 ± .5	4.2 ± .1
20% U	2.5 ± .1	78.6 ± .3	3.3 ± .1
C	3.2 ± .1	97.8 ± .9	3.2 ± .1
30% U	3.0 ± .1	86.6 ± 1.1	3.0 ± .1
C	4.1 ± .1	106.6 ± 1.3	3.0 ± .1
38%, C	4.4 ± .1	121.5 ± 1.5	3.0 ± .1

Microscopic Analysis

Micromechanisms of fatigue damage were investigated from micrographs of the fracture surface obtained from a Jeol 35CF scanning electron microscope. For this purpose, the specimens were sputter-coated with a thin film of gold-palladium. The fracture profiles were also studied by optical microscopy using a Zeiss microscope.

Sections at the critical crack length and perpendicular to the fracture surface were cut from the fatigued specimens using a slow speed Isomet diamond saw equipped with a diamond wafer blade. These sections were then processed through a series of conventional metallographic grinding and micropolishing operations (10). The final polished sections were sputter-coated with a thin film of gold-palladium and observed under the scanning electron microscope.

RESULTS

Mechanism of Crack Growth

Before crack initiation, damage was observed to accumulate ahead of the notch tip. At a certain level of damage, the notch extended into the damaged zone signaling crack initiation. Subsequently, fatigue fracture occurred as the propagation of a main crack preceded and surrounded by a zone of diffuse damage; i.e., crack layer. A typical crack layer profile recorded during stable FCP is shown in *Fig. 1*. The horizontal arrow indicates the crack growth direction.

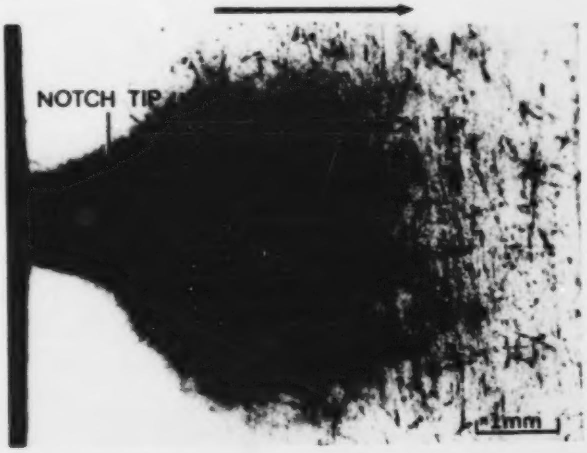

Fig. 1. Optical micrograph showing the shape of the crack and the accompanied damage of 20 wt% coupled PVC composite during slow crack propagation. The horizontal arrow indicates crack growth direction.

The crack tip is estimated as the end point of the darkened path at which a change in darkness level is observed. SEM examination of the crack tip region (*Fig. 2*) confirms its location as estimated from optical micrographs. The crack path is brightened because of electrostatic charging. The crack on the surface appears to avoid the fibers by local shifts in direction, but propagates along the center of the damage zone. Local directional shifts in the crack trajectory were observed more frequently in coupled composites than in uncoupled ones. The damage zone (seen under transmitted light source in *Fig. 1*) does not appear at low magnification in the SEM micrograph (*Fig. 2*). In this experiment, the width of the damage zone measured at the crack tip (*Fig. 1*) is taken as a first-order approximation for the extent of damage growth assuming self-consistent damage during crack propagation.

Kinetics of Crack Growth

Stable crack propagation in this composite involves a series of alternating crack jumps and crack arrests. A crack arrest period can be significantly long (up to 100 cycles) during which damage preceding the main crack is intensified. Because of this discontinuous nature of the crack propagation, the crack speed presented here is averaged over a selected number of loading cycles sufficiently large to provide more or less a smooth behavior. At least three identical runs were done for each crack propagation test reported.

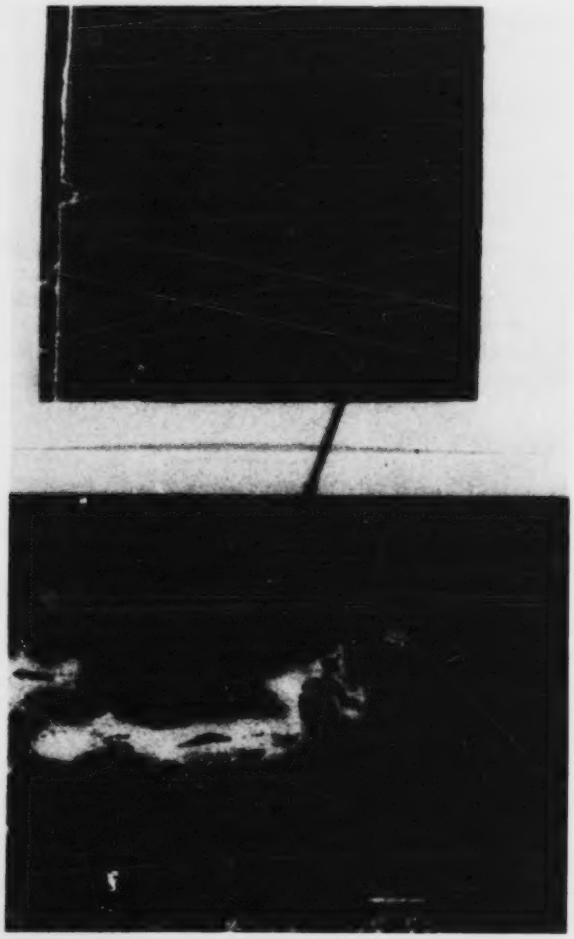

Fig. 2. SEM micrograph indicating the position and morphology of the crack tip in Fig. 1.

Effect of Interfacial Adhesion

Figure 3 shows the logarithm of the crack speed (dl/dN) as a function of the energy release rate (J_{max}) for composites containing 20% glass with and without coupling agent. The vertical dashed lines in *Fig. 3* represent the asymptotic behavior of FCP where the speed becomes unlimited. The initial crack speed is higher in the uncoupled relative to the coupled, suggesting a shorter life for the former. In the latter part of FCP, this trend is reversed. The crack accelerates more slowly in the uncoupled material, giving rise to a higher critical energy release rate, J_c.

The effect of coupling on the crack propagation resistance of composites with high fiber content is displayed in stable crack propagation

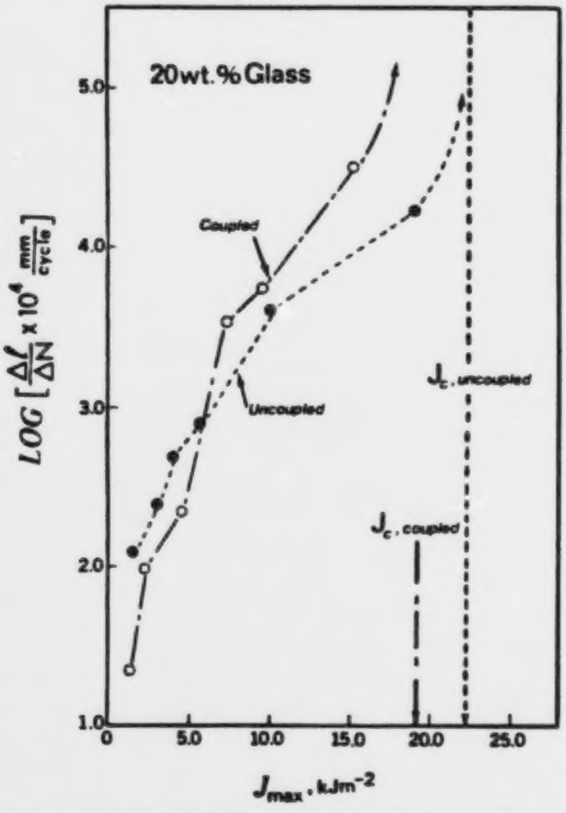

Fig. 3. FCP rates (dl/dN) as a function of energy release rate, J_{max}, for 20 wt% glass composite with and without coupling agent. The vertical dashed lines indicate the critical energy release rates at the respective points of fracture.

and fracture toughness (*Fig. 4*). A composite with 30 wt% glass fibers coupled to the matrix exhibits a lower FCP rate over its entire history than the uncoupled material. In addition, an increase in the critical energy release rate of 50% is observed because of fiber-matrix coupling.

Effect of Fiber Weight Fraction

Comparison of the FCP behavior of coupled composites containing 6%, 20%, and 38% by weight of glass fibers is displayed in *Fig. 5*. At any fixed value of energy release rate, the crack growth rate is slower for composites with higher fiber content. Both the FCP life and the fracture toughness (J_c) increase with fiber content. The former is reflected in terms of the range of the crack speed and the latter in the range of energy release rate within which reduced acceleration (lower rates of acceleration) occurs. Only a modest increase in FCP resistance is observed from 6 wt% to 20 wt% glass composites, whereas a marked improvement is seen from 20 wt% to 38 wt%. The energy required for the first observable crack jump (threshold energy) is approximately the same for the various composites.

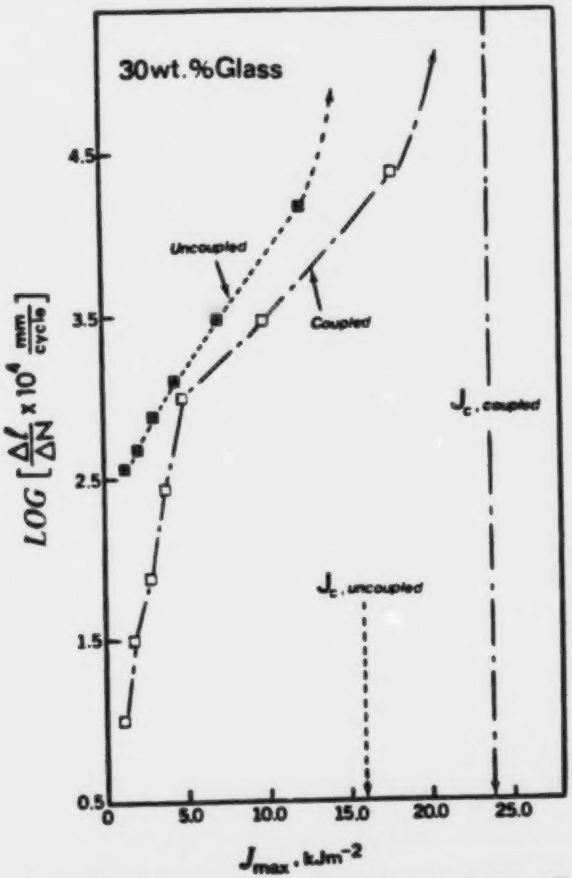

Fig. 4. Comparison between the FCP rates in 30 wt% glass composites with and without coupling agent.

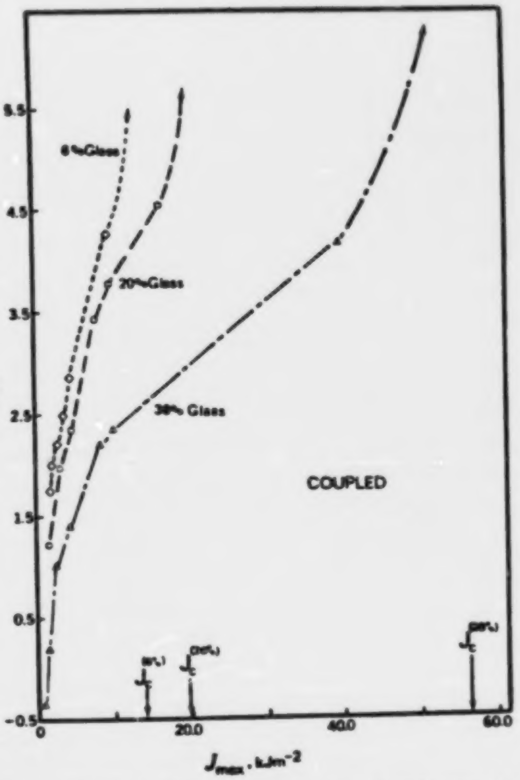

Fig. 5. Variation of FCP rate and fracture toughness (J_c) with fiber weight percent for coupled composites.

Effect of Stress Level

Crack growth data were obtained for the 38% glass coupled composite under three different applied cyclic stress levels as shown in *Fig. 6*. Clearly, at any fixed energy release rate, the crack speed is slower at lower stress level. The fracture toughness is not constant but increases with decreasing stress level.

Fracture Toughness and Life Time

The effect of interfacial adhesion and fiber glass content on the fracture toughness (J_c in *Figs. 3, 4*, and *5*) and FCP time of the composites considered is illustrated in *Fig. 7*. The fracture toughness as a function of glass content is shown here for composites with and without coupling agent. The number of cycles to failure, N_f, is total FCP life for each composite composition. These data were obtained from tests conducted under identical conditions. The total FCP life is markedly higher for composites with higher glass content and strong interfacial adhesion. For uncoupled composites, J_c is highest for 10 wt% glass fiber, then it gradually decreases with increasing glass content. For coupled composites, however, the inverse trend is observed.

Micromechanisms of Fatigue Damage

The fracture surfaces of the fatigue specimens were examined microscopically to identify

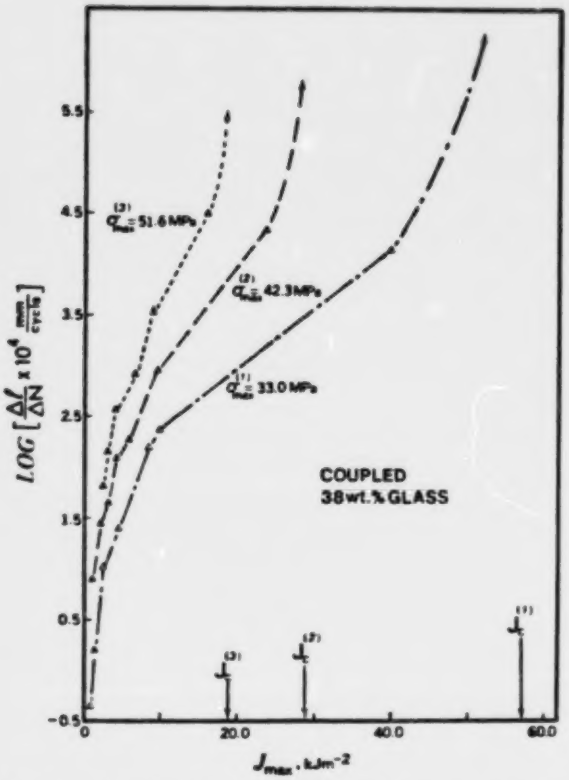

Fig. 6. Variation of FCP rate and fracture toughness with different applied stress levels for 38 wt% glass coupled composites.

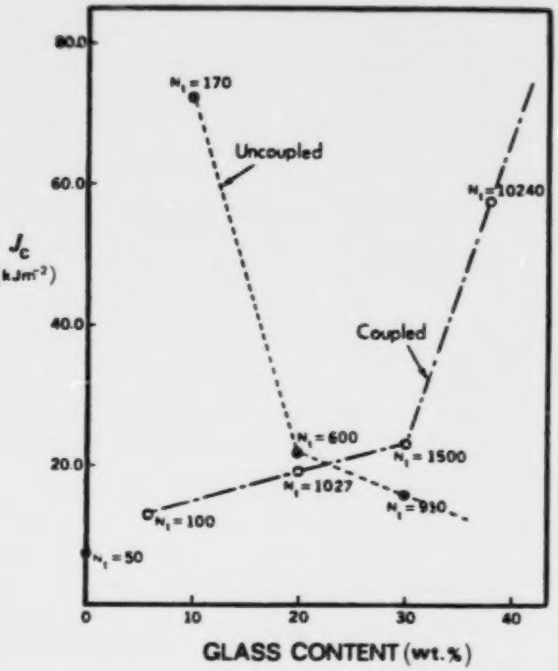

Fig. 7. Fracture toughness (J_c) and total fatigue (N_t) as a function of fiber content for coupled and uncoupled composites.

fatigue fracture mechanisms. Shown in *Fig. 8* is a scanning electron micrograph of a typical fracture surface of a 6 wt% coupled glass composite in the slow crack growth region. The white arrow indicates the crack growth direction. Matrix adhering to the exposed fiber "A" indicates significant coupling between the fiber and the matrix. The mirror zone followed by the hackle pattern on the fiber fracture surface as indicated by the arrow in *Fig. 8A* suggests that this fiber was broken as a result of an applied tensile stress (11). The area "B" in *Fig. 8* exhibits matrix shear yielding and is shown at higher magnification in *Fig. 8B*. Matrix crazing appears in the smooth area "C" in *Fig. 8*, a higher magnification of which (*Fig. 8C*) indicates the craze fibrillar structure. Deformation due to fiber-matrix interlocking as shown in *Fig. 8D* is also shown by "D" in *Fig. 8*. The magnitude of this fiber-induced matrix deformation is minimal in contrast with that in the uncoupled material where it is extremely severe (8).

SEM examination of polished sections taken at the critical crack length, normal to the direction of crack propagation, reveals five damage species: matrix cracks induced by fiber (*Fig. 9A*), fiber debonding and breakage (D and B, respectively, in *Fig. 9B*), fiber pullout (*Fig. 9C*), and matrix crazing (*Fig. 9D*). To estimate the

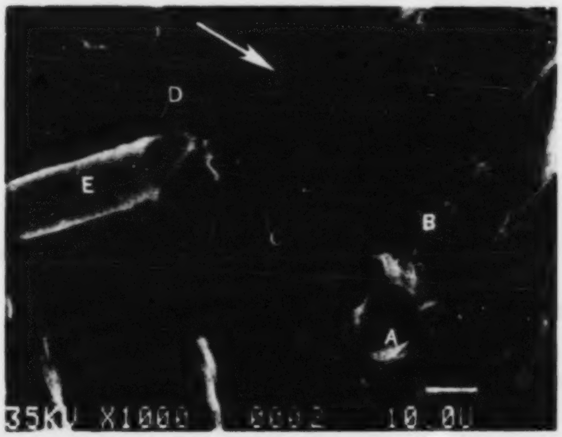

Fig. 8. SEM micrograph of a selected area on the fracture surface of 6 wt% glass coupled composite during slow crack growth showing fiber breakage (A), matrix shear yielding (B), crazing (C), and mechanical fiber-matrix interlocking (D).

relative contribution of these various damage species in resistance to FCP, the number of occurrences of each species was counted at a magnification of 500× across the entire damage zone. The results are tabulated in *Table 2* for coupled composites with 20 wt% and 38 wt% glass fibers. This analysis does not account for the size of each species, which is significant. It merely aims to identify the relative contribution of each damage mechanism in crack propagation resistance. Fiber-induced matrix cracks

X7200 0002
1.0U

Fig. 8A. High magnification of fiber breakage shown in Fig. 8.

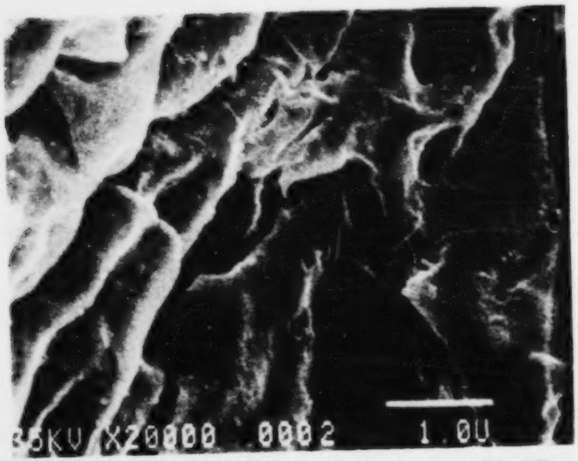

Fig. 8B. Matrix shear yielding shown in area "B" of Fig. 8.

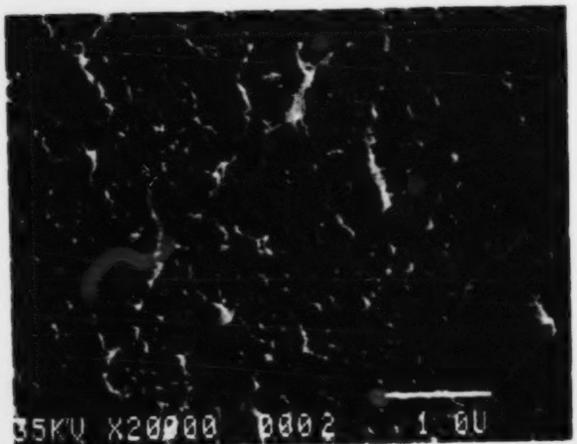

Fig. 8C. High magnification of area "C" in Fig. 8 shows craze fibrillar microstructure.

and fiber debonding seem to dominate the fracture process.

This type of analysis was not possible in an

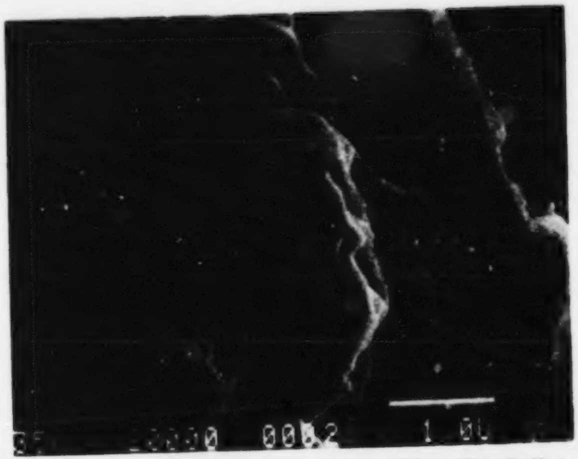

Fig. 8D. High magnification of area "D" in Fig. 8 illustrates matrix deformation induced by fiber-matrix interlocking.

uncoupled composite because of the lack of fiber-matrix adhesion. On polishing of the sections, the fibers were simply removed from the matrix. Fractographic analysis of uncoupled composites, however, reveals that matrix crazing, fiber-induced matrix deformation, and fiber interlocking are the main mechanisms involved in FCP resistance in the uncoupled compound of this composite (8).

DISCUSSION

Kinetics and mechanisms of FCP in fiber-reinforced PVC are strongly influenced by the improved fiber-matrix adhesion resulting from the use of the coupling agent (*Figs. 4, 5, 8*, and *9*). Stronger interfacial adhesion can prolong the FCP life significantly, although it reduces the fracture toughness of the composite, particularly at low fiber content. This appears to be due to additional damage mechanisms. Fiber debonding and fiber-induced matrix cracking (*Table 2*) seem to dominate energy-absorbing processes causing reduced crack speed, thus prolonging the FCP time of coupled composites (*Fig. 7*). In addition, fiber fracture acts as a high energy-absorbing mechanism, providing strong resistance to crack propagation especially at high fiber concentration. In the absence of significant interfacial adhesion, only matrix deformation and mechanical fiber-matrix interlocking seem to provide the major resistance to crack propagation (8).

The array of various damage species discussed above constitutes the crack tip damage zone (*Fig. 1*). Its influence on FCP and fracture toughness in PVC composites has been elucidated using the Crack Layer Theory (8), which treats the crack and the surrounding damage as a single thermodynamic entity; i.e., a crack layer (CL). The rate of CL translation (dl/dn) has been derived as (12)

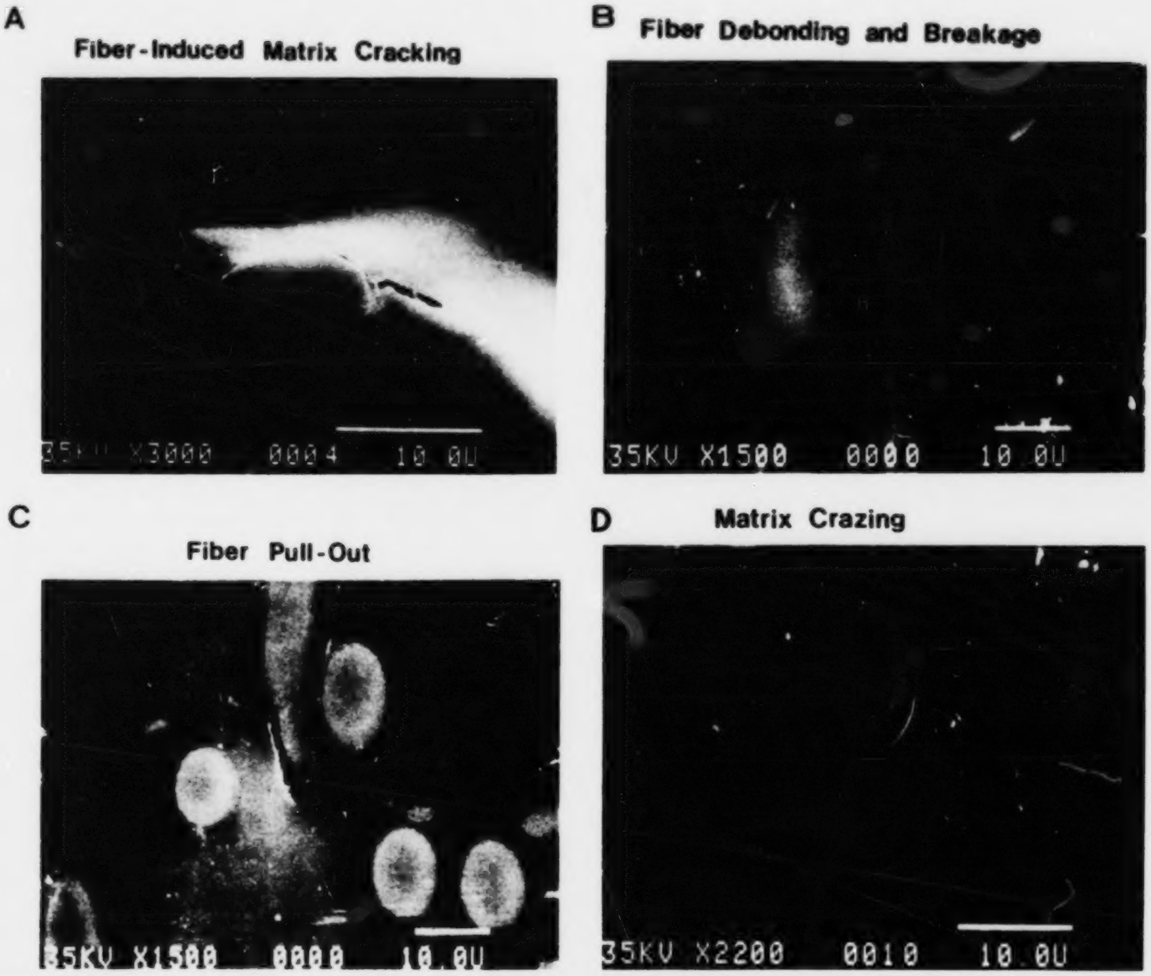

Fig. 9. SEM micrograph of a polished section normal to the crack propagation direction within the active zone in 20 wt% coupled glass fiber PVC composite showing (A) fiber-induced matrix cracking, (B) fiber debonding and fracture, (C) fiber pullout, and (D) matrix crazing.

Table 2. Number of Damage Species on Polished Sections at the Critical Crack Length in Coupled Composites.

	No. of Events/mm²	
Mechanisms	**20 wt. %**	**38 wt. %**
Fiber-induced matrix cracks	18	13
Fiber debonding	10	19
Fiber fracture	3	6
Fiber pullout	3	3
Matrix crazing	7	4

$$\frac{dl}{dN} = \frac{dD/dN}{\gamma^* R_1 - J_1} \tag{2}$$

where D is the energy dissipated on damage growth in the active zone (the zone ahead of the crack tip), γ^* is the specific enthalpy of damage, R_1 is the amount of damage associated with crack advance, and J_1 is the energy release rate. At critical crack propagation, dl/dN approaches infinity; i.e.,

$$J_{1c} = \gamma^* R_{1c} \tag{3}$$

where the subscript c denotes the critical condition. The amount of damage, R_{1c}, is expressed as

$$R_{1c} = \langle \rho\gamma^* \rangle w_c \tag{4}$$

where ρ is the damage density and w is the width of the damage measured at the crack tip. In view of the fact that crack tip damage involves a mixture of damage mechanisms, each mechanism has its own γ^*, $\langle \rho\gamma^* \rangle$ is an average quantity that may be considered as a characteristic of a particular composite. Therefore, the extent of damage at any crack length may be estimated from the measurement of the width of the damage zone (*Fig. 1*). From *Eqs 3* and *4*, $\gamma^* R_{1c}$ of *Eq 2* may be expressed as

$$\gamma^* R_{1c} = J_{1c}(w/w_c). \tag{5}$$

On the other hand, the energy dissipated on damage growth within the active zone per cycle dD/dN is part β of the irreversible work W_i; i.e., $dD/dN = \beta W_i$. The remainder could evolve as heat.

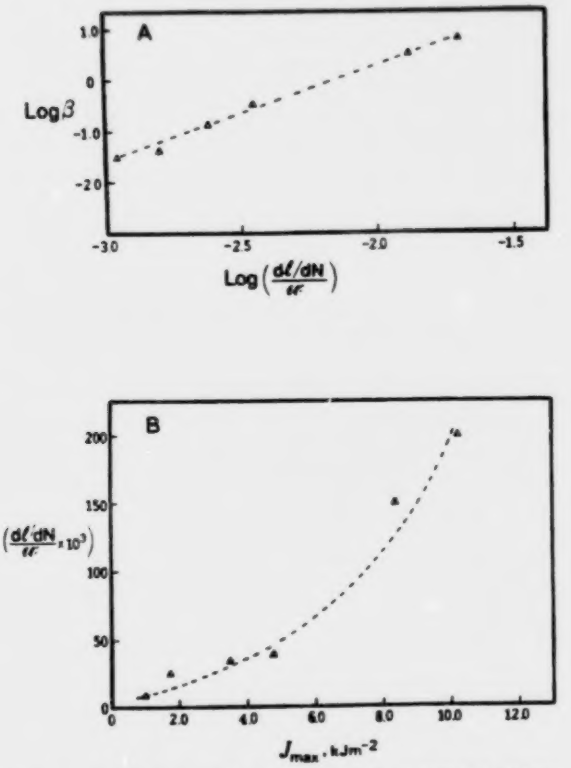

Fig. 10. Plots of (A) log β vs. log dl/ωdN and (B) dl/ωdN vs. J_{max} (see text).

The above argument suggests that *Eq 2* now can be expressed in the form

$$\frac{dl}{dN} = \frac{\beta W_i}{J_{1c}\left(\frac{\omega}{\omega_c}\right) - J_1}. \qquad (6)$$

All the parameters but β in the FCP law expressed by *Eq 6* are experimentally accessible. The phenomenological coefficient β has a dimension of 1/cycle. Examination of *Eq 5* reveals that the only parameter associated with active zone translation which is coincident with crack extension is $[(dl/dN)/\omega]$. Analysis of the experimental results indicates that β is a linear function of $[(dl/dN)/\omega]$. This quantity, in the meantime, appears to be an exponential function (power 2) of J_{max}. A demonstration of these relationships is exhibited in *Figs. 10A* and *B*, respectively. It is therefore suggested that the coefficient β in *Eq 5* be expressed as

$$\beta = \beta_o J_{max}^2. \qquad (7)$$

The coefficient β_o is the only fitting parameter used to describe the rate of CL extension. A similar relationship is found to describe FCP behavior in epoxy resin (13) and high-density polyethylene (14). The experimental FCP data (dotted lines) and the predictions of *Eq 5* (solid lines) of 38 wt% and 6 wt% coupled glass composites are shown in *Figs. 11* and *12*, respec-

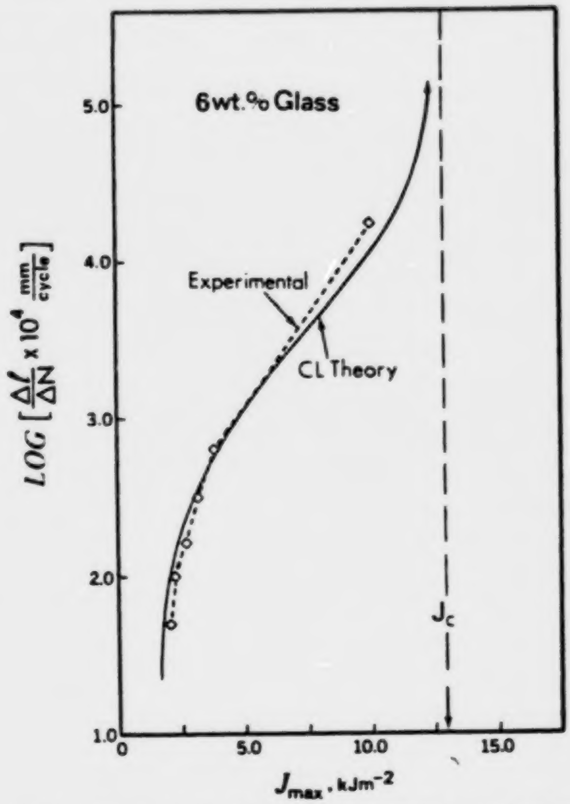

Fig. 11. Comparison of experimental FCP curve to that calculated from Eq 6 for 6 wt% coupled glass composites.

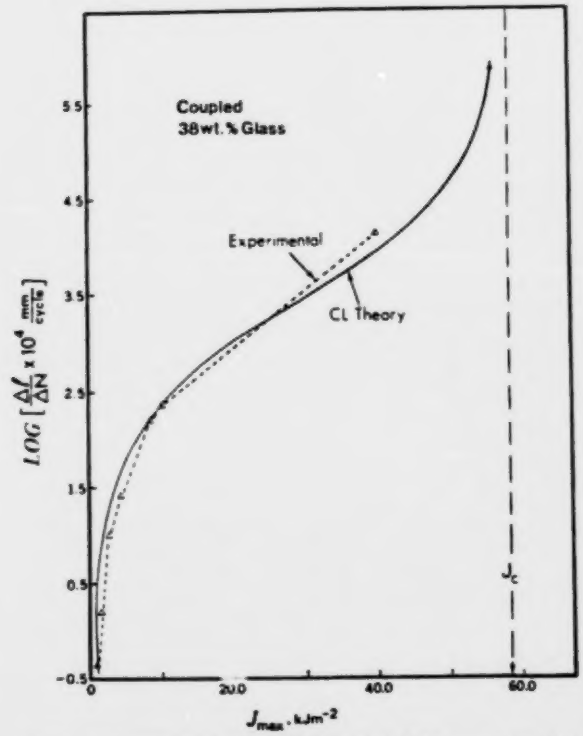

Fig. 12. Comparison of experimental FCP curve to that calculated from Eq 6 for 38 wt% coupled glass composite.

tively. Evidently, the proposed model provides very good agreement with the experimental results.

The observed difference in the rates of FCP and fracture toughness (J_c) at different stress levels (*Fig. 6*) is considered in light of the proposed formalism. Since fracture occurs via the same deformation mechanisms in the same composite, γ^* is expected to be the same regardless of the applied stress levels. As a consequence, the increase in fracture resistance at a lower stress level is due to an increase in the extent of damage $R_1 = \mathcal{W} \langle \rho \rangle$. The increase in the active zone width at the critical crack length ($\mathcal{W}_c$) at lower stress levels (*Table 3*) provides some supporting evidence. The increased amount of damage appears responsible for enhanced FCP resistance.

Because of the unavailability of quantitative values of the damage density $\langle \rho \rangle$, an effective enthalpy of damage, $\langle \gamma \rho \rangle$, rather than γ^* is used as a parameter characterizing the composite's resistance to crack growth. It is readily determined from *Eq 6* and shown in *Table 4* for various compositions. Glass reinforcement of PVC increases its effective enthalpy of damage about five times over that of the neat resin. It is also noted that improved coupling between the glass and the matrix displays its toughening effect through the dissemination of damage evaluated from measurement of the width of the active zone.

CONCLUSIONS

Fatigue cracks in glass-fiber-reinforced poly(vinyl chloride) propagate preceded and surrounded by a layer of damage whose magnitude and intensity depend on the loading conditions, fiber weight fraction, and fiber-matrix adhesion. Considering the entire FCP history, from crack initiation to critical (avalanchelike) propagation, it is shown that fatigue lifetime and fracture toughness of coupled composites increase with fiber weight fraction. Uncoupled material exhibits the highest fracture toughness at 10 wt% fiber, yet its fatigue life is much shorter than the other composites. The resistance to crack propagation is controlled by the type of damage mechanisms and the magnitude of damage dissemination. Damage analysis indicates that fiber debonding, fiber-induced matrix cracking, and particularly fiber fracture, which is more effective in energy absorption, contribute to the higher fatigue lifetime noted in coupled composites. A crack layer approach is used to characterize toughness and lifetime in terms of the damage mechanisms and magnitude of damage dissemination associated with crack propagation.

Table 3. Fracture Toughness and Width of Damage Layer at the Critical Crack Length for the Different Stress Levels in the 38 wt % Glass Composites.

σ_{max} (MPa)	J_c (kJm^{-2})	$\mathcal{W}_c$ (mm)
51.6	18.4	0.5
42.3	28.2	0.8
33.0	57.0	1.2

Table 4. Effective Enthalpy of Damage for Composites of Varying Fiber Weight Fraction, With and Without Coupling Agent ($\langle \gamma \rho \rangle_{eff.}$, Jmm^{-3} × 10^{-2}).

Wt. % Glass	Coupled	Uncoupled
0	0.8	
6	2.3	—
10	—	3.5
20	4.0	3.1
30	3.9	4.1
38	4.8	—

REFERENCES

1. K. Friedrich, *Colloid Polym. Sci.*, **259**, 801 (1981).
2. K. Friedrich, *Plast. Rubber. Process. Appl.*, **3**, 255 (1983).
3. R. W. Lang, J. A. Manson, and R. W. Hertzberg, *ACS Org. Coat. Plast. Chem.*, **45**, 778 (1981).
4. R. W. Lang, J. A. Manson, and R. W. Hertzberg, *Polym. Eng. Sci.*, **22**, 982 (1981).
5. R. W. Lang, J. A. Manson, and R. W. Hertzberg, "Proceedings Org. Coat. Appl. Polym.," **48**, 816 (1983).
6. J. W. Lomax and J. T. O'Rourke, "Proceedings of the 24th Annual Tech. Conf., Reinforced Plastics/Composites Institute of SPE," Paper X-5 (1966).
7. R. G. Shaver and E. F. Abrams, *SPE ANTEC Tech. Papers*, **17**, 378 (1971).
8. P. X. Nguyen and A. Moet, *J. Vinyl Technol.*, **1**, 140 (1985).
9. H. Tada, P. C. Paris, and G. P. Irwin, "The Stress Analysis of Cracks Handbook," Del Research Corporation, Hellertown, Pa. (1983).
10. A. S. Holik, R. P. Kambour, D. G. Fink, and S. Y. Hobbs, *Microstructural Science*, **7**, 357 (1979).
11. A. C. Jara, B. J. Norman, and S. C. Simmens, *J. Mater. Sci.*, **18**, 2459 (1983).
12. A. Chudnovsky and A. Moet, *J. Mater. Sci.*, **20**, 630 (1985).
13. X. Wang, K. Sehanobish, and A. Moet, *Polym. Eng. Sci.* (in press).
14. K. Sehanobish, A. Chudnovsky, and A. Moet, *Polymer* (in press).

DISCUSSION

M. Takemori: Did you look at different geometries and different crack loading to see if you get the same γ^* for the same material?

A. Moet: Recently we have done this for polycarbonate. If you can introduce the same mechanism, γ^* is independent of these parameters. Unfortunately we did not do it on composites. I imagine that if fiber breaking dominates over pullout we may have a problem. The γ^* describes a sum of all those mechanisms.

S. V. Hoa: The concept of diffusion coefficient* is very interesting. What is the unit of your *t*?

A. Moet: It is meter, because we said that the time "*t*" is measured by crack length. For crack propagation you cannot measure *t* in seconds since you cannot do it under high and low load, or high and low frequency; you cannot crack any time you wish. So the crack length we take as a measure of the process time.

---

* This and subsequent questions refer to another part of the lecture which is published in *Phil. Mag.*, in press, on Crack Diffusion Coefficient.

L. A. Utracki: What is the meaning of your diffusion parameter? Does it have any significance on the molecular level? By definition, it is related to the ratio of moduli divided by square of stress, but physically what does it mean? Is it related to any diffusion process?

A. Moet: You mean the crack diffusion coefficient, *D*? The best way to explain it is to say that you have to design a system to confuse the crack, passing the crack through a long low energy path, to make the material tougher. So the process is not molecular, but rather related to microstructure discussed in terms of radius of correlation on the scale of the supermolecular structure.

S. Newman: Are you implying that *D* gives you length as it would be a domain structure?

A. Moet: You are dealing with domain structure: polyester, glass beads, short fibers, and the last two are coated. So indeed you have domains of filler particles in brittle matrix.

S. Newman: But I can argue from another point. How would you interpret *D* for unreinforced material?

A. Moet: In unreinforced matrix, the crack will go all the way, with a small diffusion coefficient. The higher *D*, the more tortuous is the crack path and the tougher the material is.

S. Newman: So the diffusion coefficient is rather related to multiplicity of modes of propagation. In the past, people expressed the opinion that cross-linked systems actually have domain structure because of fluctuation in cross-link density. I wonder if you would see more of this wandering around for a cross-linked vs. a noncross-linked, amorphous system.

A. Moet: This comment should be coupled with Utracki's. I believe that domains as I see them are seven to eight orders of magnitude larger than the molecular level which is influenced by cross-links.

Dynamic Mechanical Analysis Studies of the Interphase

PING SENG CHUA

Fiberglas Canada Inc.
Guelph Technical Center
Guelph, Ontario N1E 3G1

The dynamic mechanical properties of unidirectional glass-fiber-reinforced polyester measured along the fiber direction were recently investigated. In the same polyester, the type of organosilane coated on the glass fiber, the amount of organosilane, the fiber volume fraction, and the fiber diameter affect the value of the loss tangent, tan δ, at the glass-transition temperature of the glass-fiber-reinforced polyester. The interfacial shear strength and the tan δ at the glass-transition temperature of the glass-fiber-reinforced polyester show good correlation suggesting that the latter can be used to characterize the quality of the interphase. Factors affecting the glass-transition temperature and the application of Zorowski and Murayama's equation in the characterization of the interfacial adhesion are also discussed.

INTRODUCTION

The past 2½ decades have witnessed the emergence of fiber-reinforced polymers as strong candidates for load-bearing structures. Fiber-reinforced polymers are usually made up of polymer matrix and high strength and high modulus reinforcing fibers. The region where the fiber meets the matrix is called the interphase. High strength, stiffness, and off-axis properties of fiber-reinforced polymers require a good interfacial bond and an efficient load transfer between the fiber and the matrix.

The problem of understanding and predicting the complex nature of the interphase has attracted considerable attention from both academic and industrial researchers. Pluedemann has written an excellent account of the many techniques developed for measuring the interfacial properties of fiber-reinforced polymers (1).

Recently, several dynamic mechanical methods of characterizing reinforced polymers have been reported. These studies show that dynamic mechanical analysis is a powerful technique for studying not only molecular structure and motion, but also phase morphology of polymers and polymer blends (2, 3), effects of filler addition (4–6), and fiber orientation effects in reinforced polymers (3, 7). Using nylon and poly(ethylene terephthalate) cords reinforced rubber, Zorowski and Murayama developed a method for determining the quality of the interfacial adhesion through energy loss measurements, using the following relationships (8):

$$\tan \delta_{adh} = \tan \delta_c - \tan \delta_{exp} \qquad (1)$$

$$\tan \delta_c = \left(\frac{\tan \delta_f E_f V_f + \tan \delta_m E_m V_m}{E_f V_f + E_m V_m} \right) \qquad (2)$$

where tan δ_{adh} is a relative measure of energy dissipated because of poor adhesion, tan δ_{exp} is the measured energy loss for a composite, and tan δ_c is the calculated energy loss for a composite. E is the modulus of elasticity and V represents volume fraction. Subscripts f and m refer to the fiber and matrix, respectively. Zorowski and Murayama's study showed an inverse correlation between the adhesion factor, tan δ_{adh}, and the adhesive strength (8).

Since the interphase of glass-fiber-reinforced polymer is viscoelastic in nature, Zorowski and Murayama's work clearly demonstrated the virtually untapped potential of the dynamic mechanical analysis toward the understanding of the interphase. This paper, the first in a series of dynamic mechanical studies of the interphase, is concerned with tests conducted along the fiber direction of unidirectional glass-fiber-reinforced polyester.

EXPERIMENTAL

One half percent aqueous solutions of the organosilanes shown in *Table 1* were acidified with acetic acid (Fisher Chemicals) to a pH of about 4 and then coated on glass fiber. Unless specified, the glass fiber (Fiberglas Canada Inc.) was 1100 Tex and the fiber diameter was 16 μm. Unidirectional glass-fiber-reinforced polyester was made by filament winding. The bis-

Table 1. Different Organosilanes Used in Coating Glass Fiber.

Organosilane	Abbreviation	Product Code	Supplier
γ-Methacryloxypropyltrimethoxysilane	MPS	A-174	Union Carbide Corp.
Vinyltriethoxysilane	VES	A-151	Union Carbide Corp.
m,p-Styrylethyltrimethoxysilane	SMS	S-1588	Dynamit Nobel Chemicals
3-Chloropropyltrimethoxysilane	CPS	Z-6076	Dow Corning
Methyltrimethoxysilane	MMS	A-163	Union Carbide Corp.
n-Hexyltrimethoxysilane	HMS	H-7334	Dynamit Nobel Chemicals

phenol type polyester used was DION 7000A (Fiberglas Canada Inc.). All samples were cured with 1% methyl ethyl ketone peroxide (Mia Chemical) at room temperature for 12 h followed by postcuring at 130°C for 4 h. The fiber volume fraction was maintained at 0.50 ± 0.01 for most of the tests.

The dynamic mechanical properties of a 70-mm long, 6-mm diameter polyester rod and unidirectional glass-fiber-reinforced polyester 70-mm long, 14-mm wide, and 3.2-mm thick were tested in a Du Pont 982 Dynamic Mechanical Analyzer (DMA). The samples were heated at a rate of 5°C/min. The glass-fiber-reinforced polyester was subjected to deformation along the fiber direction. The loss tangent, tan δ, determined in this instrument as the ratio between the flexural loss modulus and the flexural storage modulus, was measured as a function of temperature. The apparent interfacial shear strength was measured by the short beam test in accordance with ASTM D 2344.

RESULTS AND DISCUSSION

It is well known that the coating of glass fiber with organosilane coupling agents has improved the interfacial strength of glass-fiber-reinforced polymers especially under wet conditions (1, 9). Furthermore, chemical bonding is the most plausible theory of bonding in the interphase. Thus, this work is mainly concerned with organosilane-coated glass-fiber-reinforced polyester.

A plot of tan δ vs. temperature for MPS-coated (see *Table 1* for abbreviation) glass fiber, polyester, and MPS-coated glass-fiber-reinforced polyester is shown in *Fig. 1*. Tan δ is defined for viscoelastic materials as the ratio of the dissipated energy (i.e., due to molecular motion and phase transition) to the applied energy (2). As shown in *Fig. 1*, the tan δ peak at the highest temperature corresponds to a second-order transition, and this temperature is usually identified with the glass-transition temperature or T_g (2).

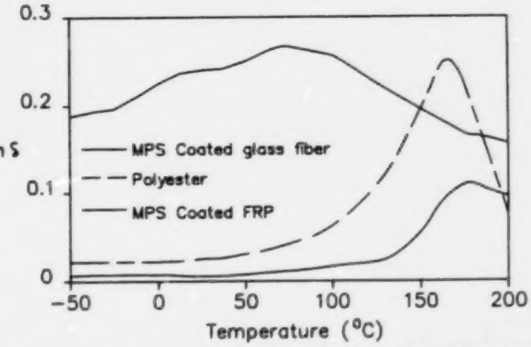

Fig. 1. Plot of tan δ against temperature for MPS-coated glass fiber, polyester, and MPS-coated glass-fiber-reinforced polyester.

Organofunctionality of the Organosilane

The amount of organosilane coated on the glass fiber, as measured by the % LOI (loss on ignition), is about 0.025% to 0.045% of the weight of the glass fiber (*Table 2*). A comparison between the tan δ and the interfacial shear strength in *Table 2* shows that when the organosilane contains an organic group capable of polymerization with the polyester matrix, i.e., MPS, VES, and SMS, the interfacial shear strength, τ_{12}, is high while the tan δ at the T_g of the glass-fiber-reinforced polyester, tan δ_{T_g}, is low.

In this study where the only variable is the organosilane in the interphase, the tan δ_{T_g} and the interfacial shear strength are obviously related to the reactivity of the organosilane in free radical polymerization either with itself or with the polyester matrix. The presence of unreactive organic groups from the organosilane suggests the presence of unrestrained or free end groups and, consequently, low cross-link density networks in the interphase. During the dynamic mechanical test, the strain and thermal energies introduced could be easily converted into the "mobilization" of the "plasticized" interphase. The amount of energy dissipated during the test will be large. Thus, a high tan δ value is observed, and this corresponds to a weak interfacial shear strength. The inverse relationship between the tan δ_{T_g} of the glass-fiber-reinforced polyester and the interfacial shear strength is shown in *Fig. 2*.

% LOI of Organosilanes

The effect of increasing the amount of organosilane on the tan δ_{T_g} of the glass-fiber-reinforced polyester appears to be related to the organofunctionality of the organosilanes (*Table 3*). Whereas increasing the amount of MPS and VES beyond the optimum LOI range of 0.040% to 0.045% only effected a small increase in the tan δ_{T_g} of the glass-fiber-reinforced polyester,

Table 2. Dynamic and Static Mechanical Properties of Glass Fiber, Glass-Fiber-Reinforced Polyester, and Polyester.

	Glass Fiber		0.5 V_f GFRP			
Organosilane	% LOI	Tan $\delta_{25°C}$	Tan $\delta_{25°C}$	Tan δ_{T_g}	T_g (°C)	τ_{12} (MPa)
MPS	0.045	0.190	0.0066	0.107	174	56 ± 1
VES	0.040	0.114	0.0066	0.122	175	42 ± 1
SMS	0.035	0.171	0.0083	0.123	172	54 ± 1
CPS	0.040	0.172	0.0097	0.136	168	26 ± 2
MMS	0.025	0.155	0.0071	0.146	175	24 ± 1
HMS	0.045	0.266	0.0125	0.152	174	19 ± 1
nil	—	—	0.0083	0.134	176	29 ± 2
Polyester	**Tan δ_m**	**E_m (GPa)**				
25°C	0.0228	3.13				
175°C	0.2320	0.21				

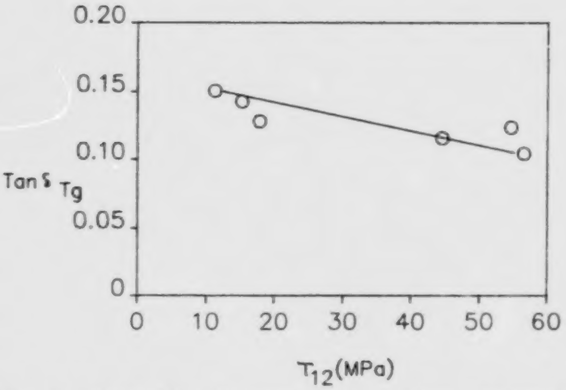

Fig. 2. Relationship between tan δ_{T_g} of glass-reinforced polyester and interfacial shear strength for organosilane-coated glass-fiber-reinforced polyester (data from Table 2).

Table 3. Effect of the Amount of Organosilane on the Tan δ at the T_g of the Glass-Fiber-Reinforced Polyester and Interfacial Shear Strength.

		0.5 V_f GFRP		
Organosilane	% LOI	Tan δ_{T_g}	τ_{12} (MPa)	T_g (°C)
MPS	0.045	0.107	56 ± 1	174
	0.113	0.110	56 ± 1	173
VES	0.040	0.122	42 ± 1	175
	0.070	0.125	41 ± 1	174
CPS	0.040	0.136	26 ± 2	168
	0.130	0.155	21 ± 2	166
MMS	0.025	0.146	24 ± 1	175
	0.050	0.155	18 ± 1	173

increasing the amount of CPS and MMS resulted in a large increase in the tan δ_{T_g} (*Table 3*). This observation suggests that some of the extra amount of organosilane in the interphase may be "used up" to some extent by its ability to polymerize with the polyester matrix or with itself. Thus, the increased presence of (short chain) organosilane molecules (e.g., MPS and VES) in the interphase did not drastically reduce the cross-link density of the interfacial network. On the other hand, adding extra CPS and MMS only serves to increase the population of short-chain molecules, thus plasticizing the interphase. Consequently, the cross-link density of the interfacial network becomes lower and tan δ increases dramatically as the interfacial shear strength becomes weaker.

Fiber Volume Fraction

As shown in *Fig. 1*, the tan δ of the polyester is considerably reduced by the addition of the glass-fiber reinforcement. The variation in the tan δ with fiber volume fraction appears to be related to the reactivity of the organosilane coated on the glass fiber (*Table 4*). With reactive organosilanes like MPS, the decrease in the tan δ_{T_g} of the glass-fiber-reinforced polyester with increasing fiber volume fraction is due to the increasing amount of MPS available for coupling glass fiber to the polyester matrix. On the contrary, increasing the amount of unreactive CPS results in a plasticizing effect. Thus, an increase in the tan δ_{T_g} with increasing fiber volume fraction is observed. The variation in the tan δ_{T_g} of the glass-fiber-reinforced polyester with increasing fiber volume fraction is inversely related to the interfacial shear strength (*Table 4*).

The relationship between tan δ_{T_g} of the glass-fiber-reinforced polyester and the fiber volume fraction cannot be satisfactorily predicted by the simple rule of mixtures (*Eqs 3, 4* and *Table 4*).

$$\tan \delta = V_{cf} \tan \delta_{cf} + V_m \tan \delta_m \qquad (3)$$

$$\tan \delta = V_f \tan \delta_f + V_m \tan \delta_m + V_i \tan \delta_i \qquad (4)$$

where subscripts cf and i represent coated fiber and interphase material, respectively. This is because no account is made of the effect of organosilane in the interfacial adhesion.

Fiber Diameter

With constant fiber volume fraction and depending on the reactivity of the organosilane, the change in the tan δ_{T_g} of the glass-fiber-reinforced polyester with decreasing fiber diameter (*Table 5*) is either insignificant (i.e., MPS) or great (i.e., CPS). The rationale behind this observation is due to the increase in bonding surface area with decreasing fiber diameter.

Table 4. Effect of Fiber Volume Fraction on the Tan δ at the T_g of the Glass-Fiber-Reinforced Polyester, Interfacial Shear Strength, and Tan δ Derived From the Rule of Mixtures.

	0.5 V_f GFRP					
Organosilane	V_f	Tan δ_{T_g}	τ_{12} (MPa)	T_g (°C)	Tan δ_{T_g} (*Eq. 3*)	Tan δ_{T_g} (*Eq. 4*)[a]
MPS	0.3	0.115	42 ± 2	169	0.213	0.162
	0.4	0.111	47 ± 1	171	0.207	0.139
	0.5	0.107	56 ± 1	174	0.201	0.116
CPS	0.3	0.130	26 ± 1	172	0.207	0.162
	0.4	0.133	28 ± 2	171	0.199	0.139
	0.5	0.136	26 ± 2	168	0.191	0.116

[a] Tan δ_f and V_f were considered negligible in *Eq. 4*.

Table 5. Effect of Fiber Diameter on the Tan δ at the T_g of Glass-Fiber-Reinforced Polyester and Interfacial Shear Strength.

		0.5 V_f GFRP		
Organosilane	Fiber Diameter (μm)	Tan δ_{T_g}	τ_{12} (MPa)	T_g (°C)
MPS	13	0.112	55 ± 2	174
	16	0.107	56 ± 1	174
	22	0.117	55 ± 2	174
CPS	13	0.130	31 ± 1	168
	16	0.136	26 ± 2	169
	22	0.149	25 ± 1	171

As in previous cases, the inverse relationship between tan δ_{T_g} of the glass-fiber-reinforced polyester and interfacial shear strength is observed.

Tan Delta and Interfacial Shear Strength

The results from the characterization of the interfacial adhesion using Zorowski and Murayama's equation (*Eqs 1* and *2*) are presented in *Table 6*. However, contrary to their work on rubber composites (8), no correlation between the adhesion factor, tan δ_{adh}, and the interfacial shear strength was found. As shown in *Table 6*, the tan δ_{T_g} derived from the rule of mixtures did not correlate with the interfacial shear strength either.

The inverse relationship between the tan δ_{T_g} of the glass-fiber-reinforced polyester and the interfacial shear strength has been observed throughout this study. *Figures 2* and *3* illustrate this relationship with respect to type of organosilane, variation in the amount of organosilane on the glass fiber, fiber volume fraction, and fiber diameter. This suggests that the value of the tan δ_{T_g} of the glass-fiber-reinforced polyester may be good enough for the characterization of the interfacial adhesion.

Glass-transition Temperature

Glass fiber does not show any T_g peak up to 200°C. Therefore, any T_g peak observed in glass-fiber-reinforced polyester can only be attributed to the organosilane coated on the glass fiber and to the polyester. The increase in the T_g of the polyester from 164°C to 176°C due to the presence of 0.5 V_f uncoated glass fiber (*Table 2*) may be related to the tightening up of the polyester through increased cross-linking and increased rigidity. This type of morphological change in polyester caused by the presence of the reinforcing fiber has been the basis for the Restrained Layer Theory (10, 11).

It is not clear from *Table 2* whether the organosilane, minute in quantity compared with the polyester matrix, affects the T_g of the glass-fiber-reinforced polyester. However, results from *Tables 3* through *5* suggest that the organic groups of the organosilanes play a minor role. Unreactive organosilane (i.e., CPS) shows a decrease in the T_g of the glass-fiber-reinforced polyester with increasing % LOI (*Table 3*), increasing fiber volume fraction (*Table 4*), and decreasing fiber diameter (*Table 5*). This is due to the plasticizing effect of the unreactive organosilane in the interphase. The magnitude of the change in T_g caused by this effect can be appreciated when one compares the T_g of uncoated glass-fiber-reinforced polyester (176°C) with that of CPS-coated glass-fiber-reinforced polyester (168°C). Organosilanes like MMS and HMS are also unreactive toward polyester. However, it is likely that the size of the MMS is small enough to fit into the network structure in the interphase; thus, the T_g of the glass-fiber-reinforced polyester remained high (*Table 3*). With respect to the HMS, entanglement of the hexyl group with the network structure could account for the value of T_g (*Table 2*). Reactive organosilanes such as MPS and VES are capable of polymerizing with the polyester matrix leaving the network cross-link density in the interphase relatively unaffected. Hence, there is no appreciable change in the T_g of the glass-fiber-reinforced polyester (*Tables 3* through *5*). There is no correlation, however, between the interfacial shear strength and the T_g of the glass-fiber-reinforced polyester, at least when tested in the fiber direction.

CONCLUSION

The results from the dynamic mechanical analysis of longitudinal glass-fiber-reinforced polyester showed that the quality of the interphase can be characterized by the tan δ_{T_g} of the glass-fiber-reinforced polyester. The tan δ_{T_g} is affected by the reactivity of the organosilane with the polyester matrix, the amount of the

Table 6. Tan δ Calculated According to Zorowski and Murayama's Equation.

Organosilane	25°C				T_g of GFRP			
	Tan δ_{exp}	Tan δ_f	Tan δ_c	Tan δ_{adh}	Tan δ_{exp}	Tan δ_f	Tan δ_c	Tan δ_{adh}
MPS	0.0066	0.190	0.2256	0.2190	0.107	0.170	0.1702	0.0632
VES	0.0066	0.114	0.1529	0.1463	0.122	0.101	0.1014	−0.0206
SMS	0.0083	0.171	0.2075	0.1992	0.123	0.171	0.1712	0.0482
CPS	0.0074	0.172	0.2084	0.2010	0.136	0.150	0.1502	0.0142
MMS	0.0070	0.155	0.1921	0.1850	0.152	0.110	0.1104	−0.0416
HMS	0.0125	0.266	0.2984	0.2859	0.152	0.248	0.2480	0.0960

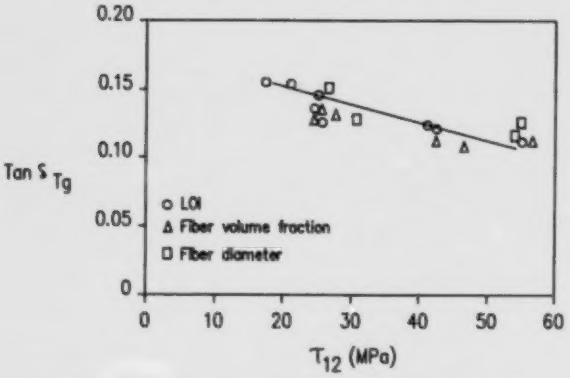

Fig. 3. Effect of the amount of organosilane, fiber volume fraction, and fiber diameter on the relationship between tan δ_{T_g} of glass-fiber-reinforced polyester and interfacial shear strength.

organosilane, the fiber volume fraction, and the fiber diameter. A good interfacial adhesion, associated with low energy dissipation, consistently exhibits low tan δ_{T_g} of the glass-fiber-reinforced polyester. No correlation was found between the interfacial adhesion and Zorowski and Murayama's equation as well as the T_g of the glass-fiber-reinforced polyester, at least when tested in the fiber direction.

REFERENCES

1. E. P. Pluedemann, "Interfaces in Polymer Matrix Composites," Vol. 6 of the series "Composite Materials," L. J. Broutman and R. H. Krock, eds., Academic Press, New York (1974).
2. L. E. Nielsen, "Mechanical Properties of Polymers and Composites," Marcel Dekker Inc., New York (1974).
3. J. W. Gearing and M. R. Stone, *Polym. Compos.*, **4**, 104 (1983).
4. T. B. Lewis and L. E. Nielsen, *J. Appl. Polym. Sci.*, **14**, 1449 (1970).
5. W. J. Mikols and J. D. Serifis, "Anisotropic Measurements on Single-Ply Lamina," in "Resins for Aerospace," C. A. May, ed., ACS Symp. Series 132, Washington, D.C. (1980).
6. J. R. Jennes and D. E. Kline, *J. Appl. Polym. Sci.*, **17**, 3991 (1973).
7. A. B. Schultz and S. W. Tsai, *J. Compos. Mater.*, **2**, 434 (1969).
8. C. F. Zorowski and T. Murayama, Proc. 1st Int. Conf. on Mechanical Behaviour of Materials, Soc. Mat. Sci., Kyoto, Japan, **5**, 28 (1972).
9. E. P. Pluedemann, "Silane Coupling Agents," Plenum Press, New York (1982).
10. C. A. Kumins and J. Roteman, *J. Polym. Sci.*, **1A**, 527 (1963).
11. T. K. Kwei, *J. Polym. Sci.*, **3A**, 3229 (1965).

DISCUSSION

L. A. Utracki: When using the viscoelastic measurements one should respect their terminology. The peak position of loss tangent, tan δ = E''/E', at an arbitrary frequency is not the glass-transition temperature. This point was settled more than 30 years ago by Tobolsky, Ferry, and other investigators of that time. The second point is the use of tan δ. For some applications where relative distribution of energy is important it is correct. For instance, Hoa used tan δ for optimization of sound-absorbing panels as a measure of energy lost-to-stored. You are following previous work by Zorowski and Murayama, but this does not make it right. In your application there are three phases, each with its own frequency dependent E' and E''. Instead of analyzing the behavior using these well-defined quantities, the proposed treatment mixes tan δ with, as I understand, low frequency E' called "modulus of elasticity." It seems that in the process a lot of information is lost, leading to a conclusion that there is little if any correlation between interfacial adhesion and Zorowski-Murayama parameter. Since you have done the experiments and you have E' and E'' values for the system, could you repeat the evaluation of data using these instead of tan δ? In principle, this should provide more direct means of interpretation, and we hope, a better correlation as far as the interphase character is concerned. Finally, could you tell us how you measured the interfacial shear stress, τ_{12}, against which you have been plotting tan δ in your figures?

P. S. Chua: The interfacial shear stress was measured using ASTM D 2344. This gives the apparent interfacial shear strength as long as the proper failure mode is observed. On the variation of storage modulus with the organosilane coating on the fiber, for continuous unidirectional glass-fiber-reinforced polyester no difference in E' at T_g was observed, at least in the case where testing was conducted in the fiber direction. I admit that for short fiber composites or for off-axis tests, this could be different. We are fully aware that dynamic mechanical analysis (DMA) is not used for fiber-reinforced polyester in this way, but part of our project is to look at new and different methods of testing fiber-reinforced polyester; DMA is just one of many we recently studied. DMA seems to show us something, but as I said earlier, the analytical window is small. As far as terminology is concerned, with respect to the thermoplastics, this has been well established. However, in the case of thermosets or reinforced thermosets, there seem to be many terms in the literature that refer to the same thing.

L. A. Utracki: Your observation that E' is constant at the temperature at which tan δ goes through a maximum is very intriguing. It may indicate that E' is determined by glass fiber modulus, whereas E'', by that of the matrix. It should be remembered that E' and E'' of the composite are averages of the three phases' response to the stress and strain fields. The "mixing rules" that result in the observed values should be investigated in much greater detail. Regarding your last comment, please note that principles of viscoelasticity are equally well applied to metals, plastics, or human body tissue. There is one science and one terminology.

S. V. Hoa: Following Utracki's question regarding the measurements of τ_{12}, the interfacial shear strength, I think that you are measuring it using filament wound sample. How did you flatten it?

P. S. Chua: We made flat unidirectional fiber-reinforced polyester samples by filament winding on a flat plate, with some compression.

S. Newman: I do not want to go into argument whether E'/E'' peak position is a good measure. However, the point is that with different surface treatments, this peak shifts by a fair amount. In fact, the highest transition temperature you obtained was for a system without coating. This may suggest that coating reduces the degree of cross-linking of the polyester; i.e., the shift in tan δ does not have anything to do with the interphase. Is there any ancillary evidence that would bear this out?

P. S. Chua: Yes. You can measure the degree of cross-linking by differential scanning calorimetry and the results can be duplicated.

L. Lamare: The relation between E' and interfacial strength is complex. If you increase the interfacial modulus, E' will follow the same trend. So if you plot tan δ vs. τ_{12} you may expect tan δ to go down if E' increases with τ_{12} faster than E'' does. Your graphs seem to indicate that both E' and E'' change with τ_{12}.

P. S. Chua: E'' changes, hence tan δ changes. The change in E' is insignificant in the case of unidirectional fiber-reinforced polyester tested in the fiber direction.

L. A. Utracki: Did you check the strain dependence of the dynamic data? Are you operating within the linear viscoelastic region?

P. S. Chua: Yes.

B. Favis: How did you characterize the silanes? Do you have a direct measure of the amount of silane with which you are dealing? It is known that different silanes have different affinity for glass fiber. How do you know that the amount you deposit is the same?

P. S. Chua: We measured silane content by the ignition losses. We also sent samples to our analytical laboratory in Sarnia where contents of the active groups were determined.

B. Favis: So you do it mainly by carbon analysis.

P. S. Chua: Yes.

S. V. Hoa: I still cannot understand how you can use solid sample to measure the interfacial strength between fiber and matrix.

P. S. Chua: I used ASTM D 2344 to get the apparent interfacial shear strength, τ_{12}.

S. V. Hoa: I think that what in fact you are measuring is the interlaminar shear strength, not the interfacial between fiber and matrix.

P. S. Chua: Yes. This is commonly done to obtain information about the interfacial strength, provided that the proper failure mode is observed. We also obtained the transverse flexural strength for comparative purposes. Generally, we use test methods that are simple and not time-consuming.

Parameters Determining the Strength and Toughness of Particulate-Filled Epoxy Resins

A. C. ROULIN-MOLONEY, W. J. CANTWELL, *and* H. H. KAUSCH

Laboratoire de Polymères
Ecole Polytechnique Fédérale de Lausanne
1007-Lausanne, Switzerland

The effects of such parameters as the filler volume fraction, particle size, aspect ratio, modulus and strength of filler, resin-filler adhesion, and toughness of the matrix on the stiffness, strength, and toughness of particulate-filled epoxy resins were evaluated. The mechanisms of crack initiation and subsequent crack propagation in these multiphase materials are discussed and illustrated by scanning electron microscopy of fracture surfaces.

INTRODUCTION

Particulate-filled polymers are extensively used in medium and high voltage insulators such as bushings, cable terminals, instrument transformers, and circuit breakers. The principal materials employed are epoxy resins with inorganic fillers such as silica, alumina, glass, and dolomite. These composites are brittle because of the high cross-link density of the organic matrix and the brittleness of the inorganic filler. The mechanical behavior of these materials results from a complex interplay of the constituent phases: resin, filler, and interfacial region. In formulating such systems the principal parameters, which may be varied, are the volume fraction of filler, the particle size, the filler aspect ratio, the modulus and strength of the filler, the resin-filler adhesion, and the toughness of the matrix.

Apart from the mechanical properties of the composite (toughness, stiffness, and strength), two other properties are of considerable importance in the processing and application of these materials. First, the viscosity of the uncured mixture must be sufficiently low to permit the evacuation of air bubbles. Second, for many uses the glass-transition temperature is critical, and often a minimum of 120°C is desired. Thus, these requirements restrict the unlimited variation of the above parameters.

The effects of formulation on these important properties having been established, the failure mechanisms in these materials will be discussed; that is, the source of the crack initiation and subsequent crack propagation. This work is illustrated by scanning electron microscopy of the fracture surfaces.

PARAMETERS DETERMINING STRENGTH AND TOUGHNESS

Volume Fraction

Epoxy resins in the uncured state have relatively high viscosities, as compared with polyesters for example. Thus, for most practical systems, the maximum volume fraction that may be incorporated is approximately 50% to avoid the presence of voids. The effect of increasing the volume fraction of the filler on the modulus of the composite is now well documented in the literature for a wide range of epoxy resins and filler materials (1–4). *Figure 1* shows the general parabolic relationship between these two quantities. For epoxy resins possessing high glass-transition temperatures, crack propagation is, in general, stable when particulate fillers are incorporated. For this type of system, a linear relationship exists between the stress intensity factor and the filler volume fraction, as shown in *Fig. 2*. This same type of relationship has been observed for a number of brittle unmodified epoxy resins. Increasing the volume fraction of the filler gives a composite with tensile strength at best equal to that of the unfilled matrix. This is shown in *Table 1* for a brittle epoxy resin filled with silica particles. At 20% volume fraction the tensile strength is lower than that of the matrix, and then it steadily increases until at 50% the matrix value of 75 MPa is achieved. A similar result was obtained by Spanoudakis and Young (5) for another epoxy resin filled with silane-treated glass beads. Thus, we may conclude that increasing filler volume fraction increases the modulus and toughness and can give castings with strength comparable to the matrix.

Changing the filler particle size at constant

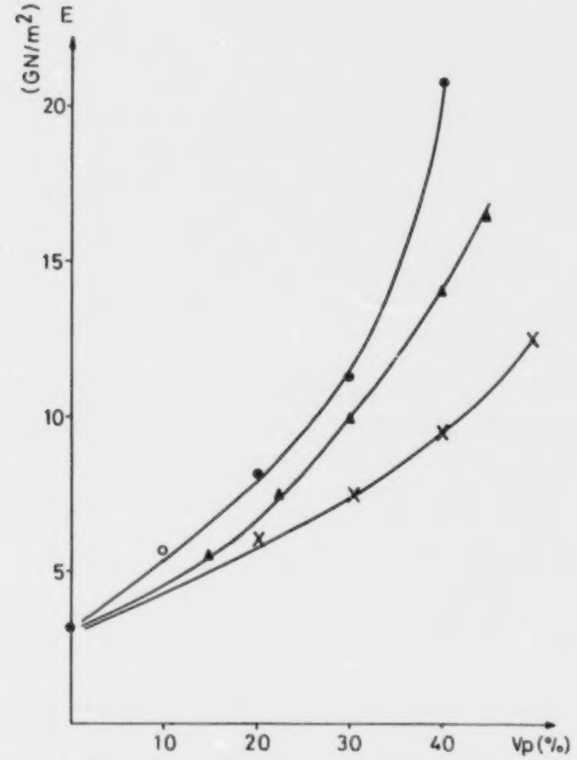

Fig. 1. Flexural modulus, E, as a function of volume fraction of filler: ×, silica; ▲, alumina; ●, silicon carbide.

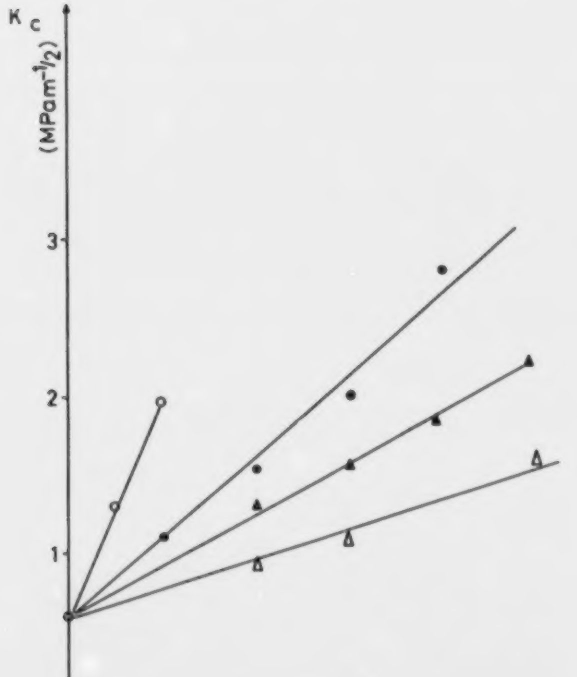

Fig. 2. Stress intensity factor as a function of volume fraction of filler: ▲, alumina and silica particles; △, A187-treated glass beads; ●, silicon carbide; ○, short glass fibers.

volume fraction does not have significant influence on the modulus of the composite. Spanoudakis and Young (5, 6) have used glass beads of 4.5 and 62 μm in diameter. The modulus of the composite with 4.5-μm particles was slightly higher, but in fact just outside the scatter band of the data. Similarly our own experiments on silica-filled resin showed that varying the particle size between 60 and 300 μm did not appreciably alter either the modulus or the stress intensity factor at constant volume fraction (*Table 2*). For the range of particle sizes investigated by Spanoudakis and Young, there was no difference in the strength of the castings at constant volume fraction for well-bonded beads. However, it is clear that there is an upper boundary in particle size where the strength is adversely affected because of the higher probability of a flaw being present within the particle. *Table 2* shows that the strength does indeed decrease with increasing size of silica particles. The inclusion of particles inferior in size to 4.5 μm may well improve the strength of the composite; however, a practical limit is imposed by the viscosity of the mixture. Smaller particles have a greater surface area and thus considerably increase the viscosity.

Modulus and Strength of Particles

Increasing the filler modulus increases the modulus of the resulting composite. This is clearly shown in *Fig. 1* for an epoxy resin filled with silica, alumina, and silicon carbide particles. The moduli of these filler materials are 94, 320, and 469 GPa respectively. Similarly, increasing the modulus of the filler increases the stress intensity factor (K_c) as shown in *Fig. 2*. The K_c values of the silicon carbide composites were significantly higher than those for the silica and alumina systems. In the case of dolomite-filled resin (4), above 25 vol% a plateau is reached in the stress intensity factor. This

Table 1. Mechanical Properties of a Silica-filled Resin as a Function of Volume Fraction.

Volume Fraction (%)	Tensile Strength (MPa)	Tensile Modulus (GPa)	Flexural Strength (MPa)	Flexural Modulus (GPa)	Compressive Yield Stress (MPa)
0	78.5	3.4	—	—	98.4
20	47.1	6.6	90.2	6.9	129.0
40	63.9	12.2	98.3	12.2	154.0
50	78.0	18.5	108.1	17.6	—

Table 2. The Effect of Filler Particle Size on Mechanical Properties of Silica-filled Resin (40 vol%).

Mean Particle Size (μm)	K_c ($MPam^{½}$)	Flexural Modulus (GPa)	Flexural Strength (MPa)
300	1.76	10.2	60.9
160	1.74	12.1	74.5
100	1.87	10.3	79.1
60	1.85	10.0	122.7

corresponds to the onset of transparticle fracture, dolomite particles being weak compared with silica and alumina. If extremely weak particles are used (such as hollow silica microspheres of mean diameter 50 μm and a wall thickness of 1.5 μm), no toughening at all is obtained. The stress intensity factor of the composite prepared from 30% by volume of the hollow spheres was exactly the same as that of the epoxy matrix (0.6 MPam$^{1/2}$). The micrograph in *Fig. 3* shows clearly that cracks have propagated directly through the particles.

The second phase material must have sufficient inherent toughness to be effective. It is evident that these "weak" particles such as dolomite and hollow spheres also diminish the strength of the casting, since the particles themselves act as sources of flaws.

Aspect Ratio

The aspect ratio of the filler is defined as the ratio of the length to the diameter of the particles. For the type of particles discussed here, it is difficult systematically to alter the aspect ratio; thus, this part of the discussion will consider fiber-reinforced materials since their fiber length may be varied relatively easily. The effect of aspect ratio on composite strength and toughness has been investigated by Kelly (7). The work of fracture increased with fiber length up to a critical size l_c; thereafter, the energy dropped. In the work of Hancock and Cuthbertson (8) the strength, however, attained a maximum asymptotic value above l_c. These results may be explained as follows: Below l_c, the principal mechanism is fiber pullout, whereas above l_c fiber failure occurs. The maximum composite strength is obtained only when the full fiber strength may be utilized; i.e., above l_c. Ideally, to give optimal strength and toughness in every direction, fibers slightly longer than the critical length should be used in a three-dimensional random array with a high volume fraction of fibers. This is extremely difficult to obtain in practice since most fabrication methods preferentially align fibers in a certain direction.

For particulate fillers, phenomena similar to those seen in fibers are observed. The data presented in *Fig. 2* are for fillers of differing aspect ratio, the glass beads having an aspect ratio of 1, alumina and silica particles one of 2 to 3, and silicon carbide ~4, whereas that for the short glass fibers is ~15. It can be seen from these data that increasing filler aspect ratio increases the resistance to crack propagation, short glass fibers being the most effective. How-

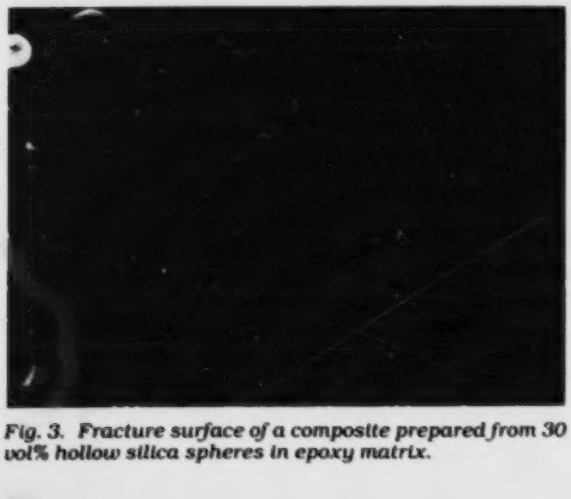

Fig. 3. Fracture surface of a composite prepared from 30 vol% hollow silica spheres in epoxy matrix.

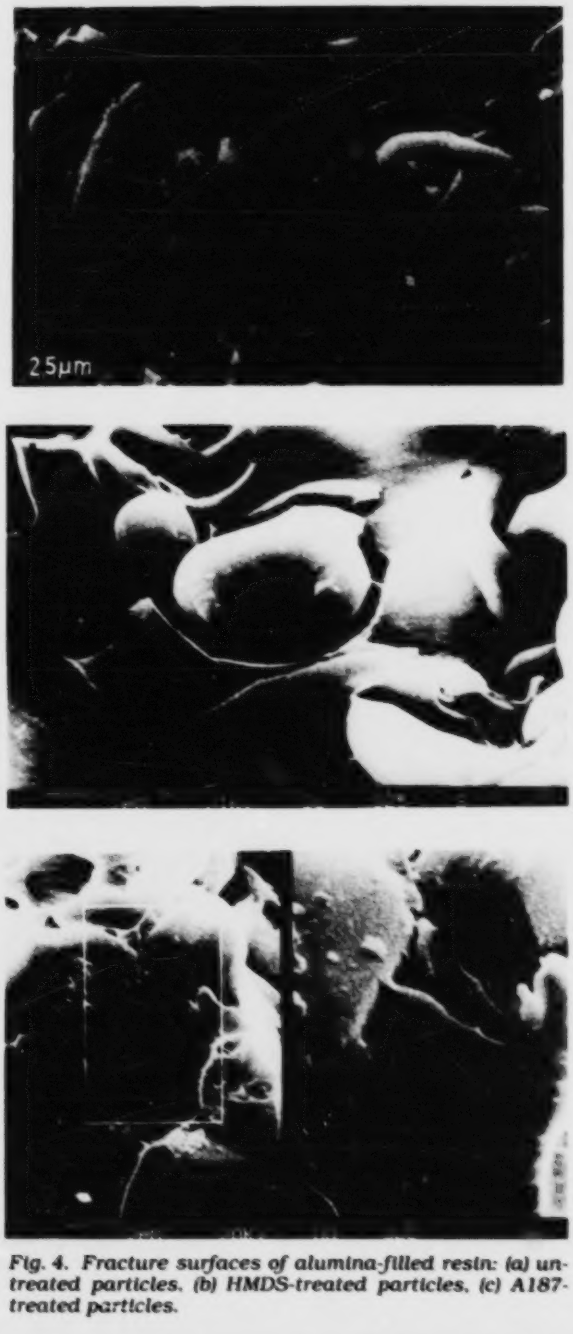

Fig. 4. Fracture surfaces of alumina-filled resin: (a) untreated particles, (b) HMDS-treated particles, (c) A187-treated particles.

ever, simple processing methods do not permit the incorporation of high volume fractions of short fibers because of the high viscosity of the uncured mixture.

Resin-Filler Adhesion

To investigate the effect of altering the resin-filler adhesion on composite mechanical properties, both alumina and glass beads were used. The particles were treated with either hexamethyldisilazane (HMDS) or chlorotrimethylsilane (CTMS), which would be expected to reduce the filler-resin adhesion, and two commercial silane coupling agents, y-glycidoxipropyl trimethoxy silane A187* and y-aminopropyl triethoxysilane A1100.* The micrographs of the fracture surfaces in *Fig. 4* indicate that the adhesion was modified in the manner desired.

* Trademarks of Union Carbide

Spanoudakis and Young (5, 6), who used glass beads treated with a mold release agent DC1107 and the silane coupling agent A187, found that surface treatment had little effect on the composite modulus. Similarly, we also observed that in the case of alumina particles, the filler-resin adhesion does not change the toughness (*Table 3*). For two epoxy resins, the K_c values for different filler surface treatments varied within the normal ~10% scatter. For glass-bead-filled systems, poorly bonded beads promoted crack tip blunting and unstable crack propagation (*Table 4*), whereas stable propagation was found for well-bonded beads. Clearly different mechanisms intervene here, and the K_c values do differ between surface treatments. These mechanisms were discussed in detail in *Ref. 9*.

Table 3. Effect of Surface Treatment on Strength and Toughness.

Resin	Filler	Treatment	Flexural Strength (MPa)	Tensile Strength (MPa)	K_c (MPam$^{1/2}$)
A	Alumina 30%	None	—	—	1.86
		HMDS	107	—	1.81
		A1100	145	—	1.99
		A187	155	—	2.04
B	Alumina 30%	None	96	45	1.53
		HMDS	82	—	1.46
		A1100	136	—	1.67
		A187	132	88	1.64

Table 4. The Effect of Surface Treatment on the Stress Intensity Factor of Glass Bead Composites (40% By Volume Beads).

		Mean Value K_{Ic} (MNm$^{-3/2}$)	
Resin	Treatment	Initiation	Arrest
A	none	1.88	1.52
	CTMS	2.26	1.37
	A187	1.89	1.74
	A1100	1.96	1.73
B	none	1.57	1.35
	CTMS	1.75	1.21
	A187	1.45	
	A1100	1.48	

Filler surface treatment does, however, have significant influence on the strength of the castings. Well-bonded fillers give composites with notably higher flexural and tensile strength (*Tables 3* and *4*). This may be explained by weakly bonded particles acting as sources of "inherent" flaws provoking crack initiation. Effective inherent flaw sizes may be calculated from the following equation:

$$K_{Ic} = \sigma Y a_i^{1/2} \tag{1}$$

where K_{Ic} is the critical stress intensity factor measured by, for example, the single-edge notch test, σ is the tensile strength, Y is a geometric factor ($\pi^{1/2}$ for infinitely wide specimens, ~1.99 for single-edge notched specimens), and a_i is the effective "inherent" flaw size.

In unfilled epoxy resins, calculations of this kind give values of 15 to 50 μm and for filled

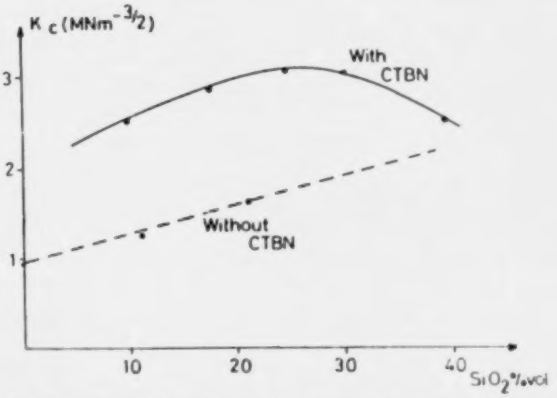

Fig. 5. Stress intensity factor as a function of volume fraction of silica particles.

Table 5. Mechanical Properties of an Unmodified Filled and Rubber-modified Filled Epoxy Resin.

Formulation	Modulus (GPa)	Flexural Strength (MPa)	Tensile Strength (MPa)	K_c (MPam$^{1/2}$)	G_c (Jm^{-2})	T_g (°C)
Epoxide 100p CTBN 15p Piperidine 5p Silica 90p	6.0	80	55	3.40	1540	96
Epoxide 100p Piperidine 5p Silica 90p	6.5	120	90	1.5	346	96

resins, values of 100 to 500 μm depending on the type of filler and the adhesion. The possible sources of these flaws will be discussed later.

It may be concluded that whereas poorly bonded glass beads give apparently higher toughness because of crack tip blunting, this is accompanied by a decrease in the strength of the composite and is therefore not beneficial for the overall performance.

Matrix Toughness

The most successful means of improving the toughness of epoxy resins to date is by incorporation of a secondary dispersed phase of carboxyl terminated acrylonitrile butadiene rubber (CTBN). Much information on these systems is available in the literature (10). Addition of CTBN at levels of 15 wt% gives fourfold increases in stress intensity factor (from 0.6 MPam$^{1/2}$ to ~2.5 MPam$^{1/2}$) with only a small sacrifice in the modulus (decrease from 3 GPa to ~2.7 GPa). Recently, Maxwell and co-workers (11, 12) reported results on hybrid systems containing epoxy resin, CTBN, and glass beads. Instead of a linear relationship between K_c and volume fraction, a maximum in K_c was observed at 10% glass. We have obtained similar results for a composite containing epoxy, CTBN, and silica particles, as shown in *Fig. 5*. The mechanical properties of the formulation with a maximum in K_c is given in *Table 5* and compared with the unmodified filled epoxy. It can be seen that the fracture energy is considerably increased without too great a loss in modulus or glass-transition temperature; however, the flexural and tensile strengths are somewhat impaired.

Pearson and Yee (13) investigated the effect of changing the resin cross-link density on the toughness of CTBN-modified epoxies. Varying the epoxy equivalent weight between 172 and 2000 increased fracture energies (G_{Ic}) from 0.162 to 11.5 kJm^{-2}. They concluded that intrinsic matrix ductility was the main source of toughness. Whether these high toughness systems could be used with particulate fillers to give hybrids with optimal toughness, moduli, and strength remains to be seen.

Unfortunately, once again, the high viscosity of these resins may well create problems, and their lower glass-transition temperature could limit applications. All these data are summa-

Table 6. Parameters Determining the Modulus, Toughness, and Strength of Particulate-filled Epoxy Resins.

Property	Effect on: Modulus	K_c	Strength
Increase volume filler	Increase	Increase	~Const. at matrix value
Particle size	Constant	Constant	Decrease
Increase aspect ratio	—	Increase	Increase
Increase modulus filler	Increase	Increase	Increase
Improved adhesion	Constant	Constant	Increase
Tougher matrix	Small decrease	Increase	Decrease

Table 7. Calculated "Inherent" Flaw Sizes For a Range of Filled Epoxy Resins.

Filler	Mean Particle Size (μm)	Volume Fraction (%)	Tensile Strength (MPa)	K_c MPam$^{1/2}$	Flaw Size (μm)
—	—	—	78	0.47	13
Silica	50	20	47	0.99	132
Silica	50	40	64	1.49	96
Silica	50	50	78	1.65	115
Alumina (untreated)	6	30	45	1.53	290
Alumina (silane-treated)	6	30	88	1.64	87
—	—	—	76	0.91	36
Alumina trihydrate*	5	29.5	33	1.33	412
"	8	10	30	1.22	413
"	8	21.5	34	1.51	493
"	8	29.5	45	1.51	282
"	8	43	38	1.44	359
"	12	29.5	35	1.60	522

* Data from *Ref. 14*.

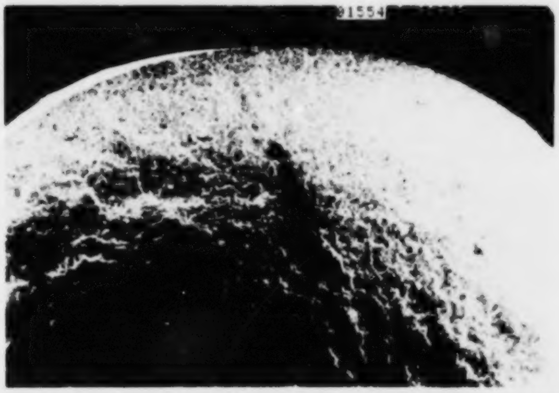

Fig. 6. Fractured tensile specimen of silica-filled epoxy resin showing rupture initiated within a resin-rich area.

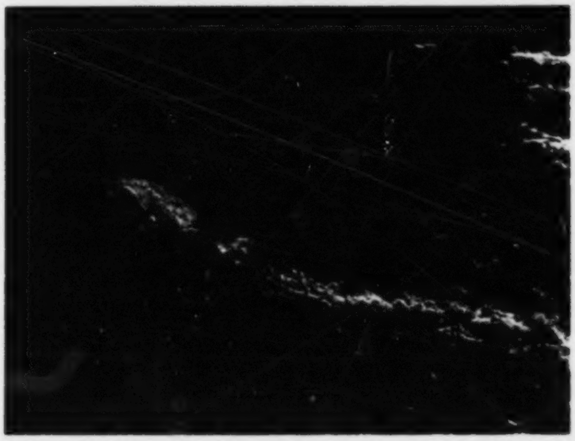

Fig. 7. Fractured tensile specimen of silica-filled epoxy resin showing rupture initiated at a foreign body incorporated into the casting during specimen preparation.

rized for clarity in *Table 6*, which gives the general trends in the composite strength, toughness, and stiffness by varying properties of the two phases.

CRACK INITIATION AND PROPAGATION IN FILLED EPOXY RESINS

Sources of Flaws

As mentioned earlier, calculations of effective "inherent" flaw sizes give values in the range of 15 to 500 μm depending on filler content, size, type, etc. The data for a number of systems have been collected in *Table 7*. To optimize the strength of filled resins, it is necessary to understand the origin of these flaws. Various possibilities are listed below:

1. *Specimen preparation:* Defects initiating fracture may arise during specimen preparation such as air bubbles (15), resin-rich areas (*Fig. 6*), or foreign matter (*Fig. 7*) such as dust particles (16). It is clear that precautions during sample manufacture can eliminate this type of flaw.

2. *Particle size:* The flaw sizes found for silica-filled composites are of the order of 100 μm; this may be explained by the presence of particles significantly larger than the mean size which, in this case, is 50 μm. Particles of size

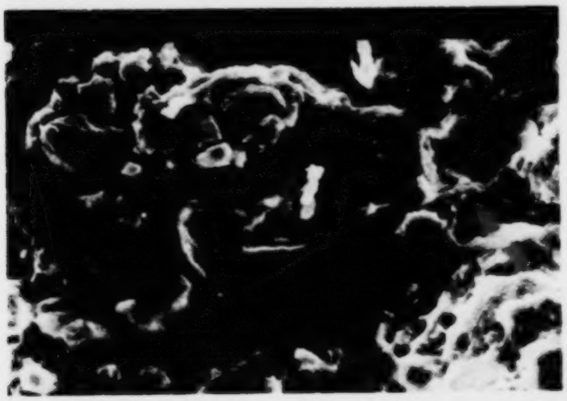

Fig. 8. Fracture surface of a silica-filled epoxy resin showing particles of size approaching the calculated "inherent flaw" size.

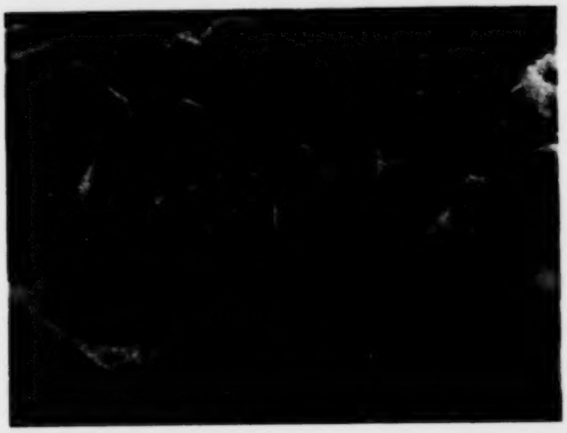

Fig. 9. The fracture surface of an alumina-filled resin showing how poorly bonded particles may link up to create large flaws.

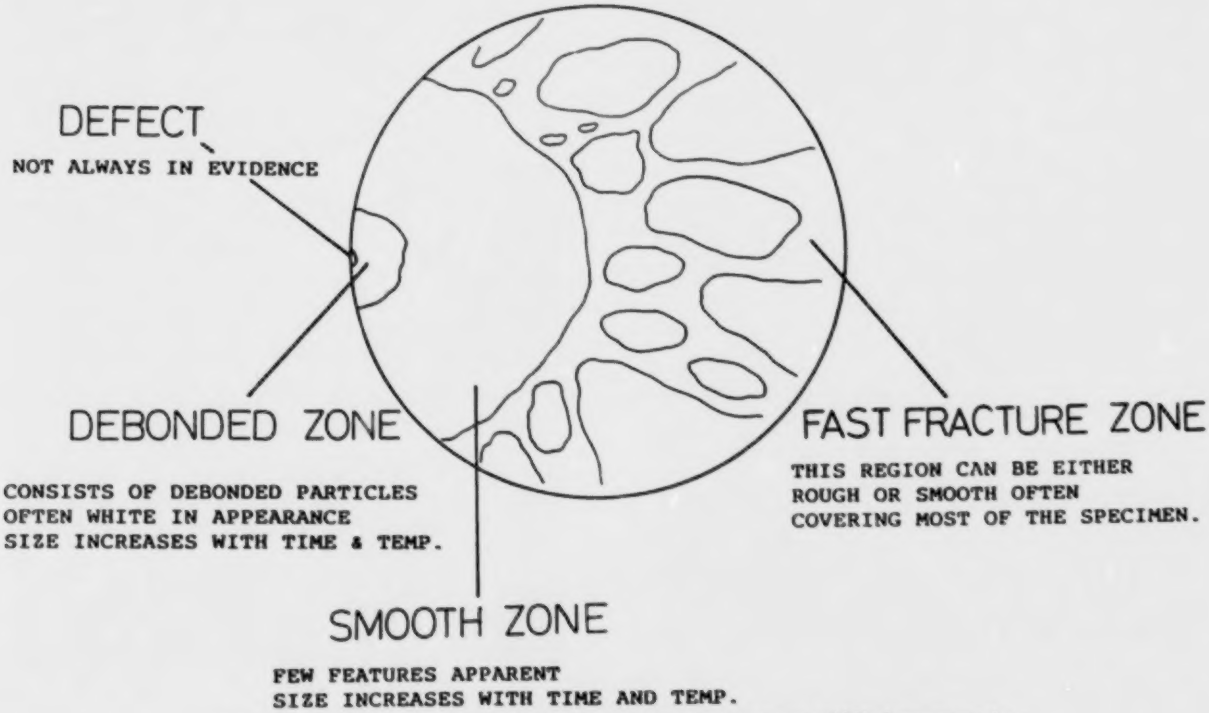
DEFECT
NOT ALWAYS IN EVIDENCE
DEBONDED ZONE
CONSISTS OF DEBONDED PARTICLES
OFTEN WHITE IN APPEARANCE
SIZE INCREASES WITH TIME & TEMP.
SMOOTH ZONE
FEW FEATURES APPARENT
SIZE INCREASES WITH TIME AND TEMP.
FAST FRACTURE ZONE
THIS REGION CAN BE EITHER
ROUGH OR SMOOTH OFTEN
COVERING MOST OF THE SPECIMEN.

Fig. 10. Zones on the fracture surface of a tensile specimen of filled epoxy resin.

50 to 100 μm indeed may be found on the fracture surface (*Fig. 8*).

3. *Poorly bonded or weak particles:* The large flaw sizes for untreated alumina-filled composites (290 μm) probably derive from the linking up of weakly bonded particles at low levels of stress. An example of this type may be seen in *Fig. 9*.

The flaw sizes of composites prepared from alumina trihydrate were in the range of 300 to 500 μm. These particles are relatively weak, and fractured particles are frequently found on the ruptured surface. Thus, in this case, flaws probably derive from a series of particles broken during the test.

Flaws Generated During Testing and Their Relation To Static Fatigue

It is clear that effective formulation (small "strong" particles, well-bonded to the matrix) and careful specimen preparation can avoid the above-mentioned flaws without great difficulty. In this case, it appears that the apparent flaw is generated during the test. A series of short-term tensile and creep tests have been conducted on a resin filled with 40% silica particles in the form of dumbbell specimens with circular cross-section. This work will be described in detail in a subsequent publication (17), but the principal results are outlined here. It has been found that there are three zones on the fracture surface as shown in *Fig. 10*. First is the zone of crack initiation where the particles are debonded from the matrix (*Fig. 11*); the second zone is a smooth region, and finally there is a rough area. In the latter two zones the fracture is matrix dominated, and the particles are well bonded to the resin matrix (*Fig. 12*). The size of each of these zones increases with temperature and time of loading so that at long times and elevated temperatures only the first two are observed and the rough region is forced off the specimen.

In a short-term tensile test at 23°C, the debonded zone is extremely small and corresponds to the previously mentioned calculated flaw sizes; that is, some hundred microns. In a creep test at 85°C, however, where the fracture time is perhaps 1000 to 2000 h, the debonded zone will be some 1 to 2 mm in diameter. The

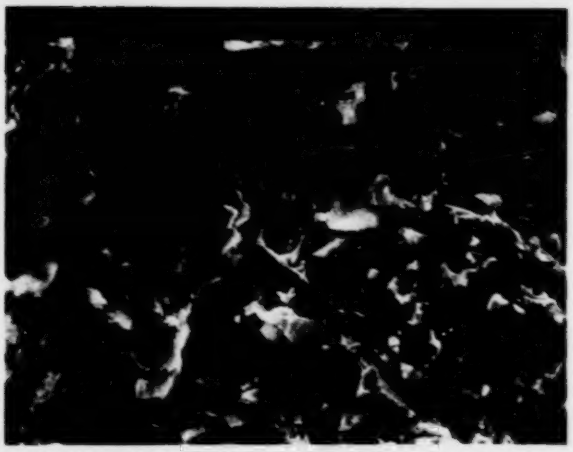

Fig. 11. Initiation zone of resin-particle debonding in a silica-filled resin tested in static tension at 85°C.

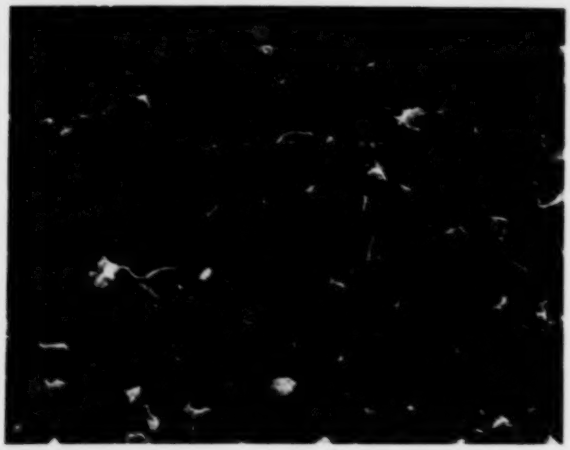

Fig. 12. Tensile fracture surface of a silica-filled resin typical of within the macroscopically smooth or rough zones where fracture is matrix dominated.

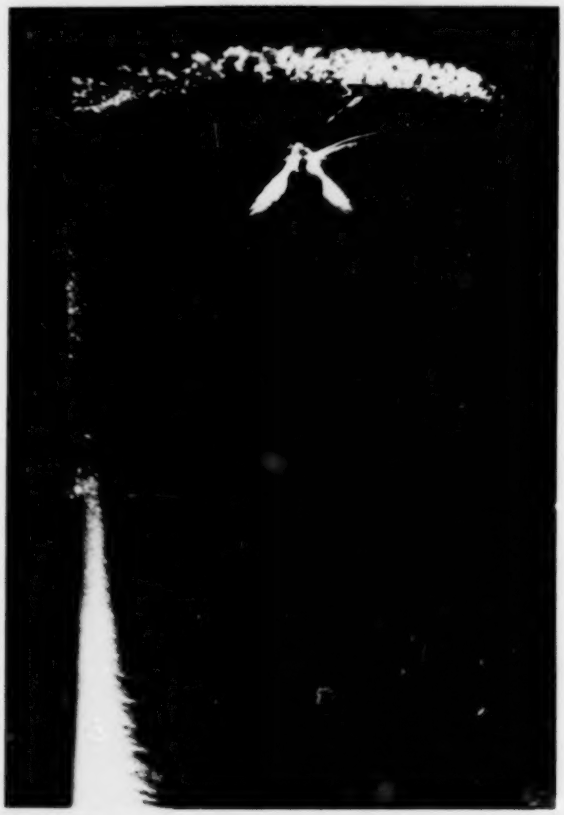

Fig. 13. Fracture initiated at the intersection of shear bands in an unfilled epoxy resin.

results indicate that for these systems the fracture is initiated originally at a much smaller defect than the calculated flaw size, which is on the submicroscopic or perhaps molecular level. An inhomogeneity provoking shear yielding in a certain region of the specimen is the most probable initial cause. An example is given in *Fig. 13* where the fracture of a tensile test specimen of an unfilled epoxy resin is clearly initiated at the intersection of shear bands.

After this initiation, slow subcritical crack growth occurs that results, in the case of filled resins, in debonding of the silica particles from the matrix. The crack gradually accelerates and this corresponds to the smooth region of the fracture surface. Finally, terminal velocities of some hundreds of meters per second may be reached in the rough zone. This roughness derives from energy consumed in crack branching because of the excess elastic energy stored in the sample at this point in the fracture process.

These results confirm previous work on these materials relating measured static fatigue lifetimes to predictions of time-to-failure on the basis of linear elastic fracture mechanics (18). Measurements of the variation of the stress intensity factor (K_c) with crack velocity (v) were carried out using the double torsion test technique. The results are shown in *Fig. 14*. These data may be used together with the short-term tensile strength to calculate the time-to-failure (t_L) from

$$t_L = [\tfrac{1}{2} Y^2 A K_{Ic}^{n-2}(n-2)]^{-1}(S_i^{n-2}\sigma^{-n}) \tag{2}$$

where Y is the geometric factor given in *Eq 1*, K_{Ic} is the critical stress intensity factor at which crack propagation becomes uncontrolled, S_i is the instantaneous fracture strength that is no subcritical crack growth before failure, and A and n are defined from the empirical power law relating K_c to v; that is,

$$v = AK_c^n. \tag{3}$$

The derivation of *Eq 2* is given in *Ref. 19*. The results are shown in *Fig. 15* for three temperatures. The points are the experimental fracture stresses and times for individual specimens, and the solid lines represent the predic-

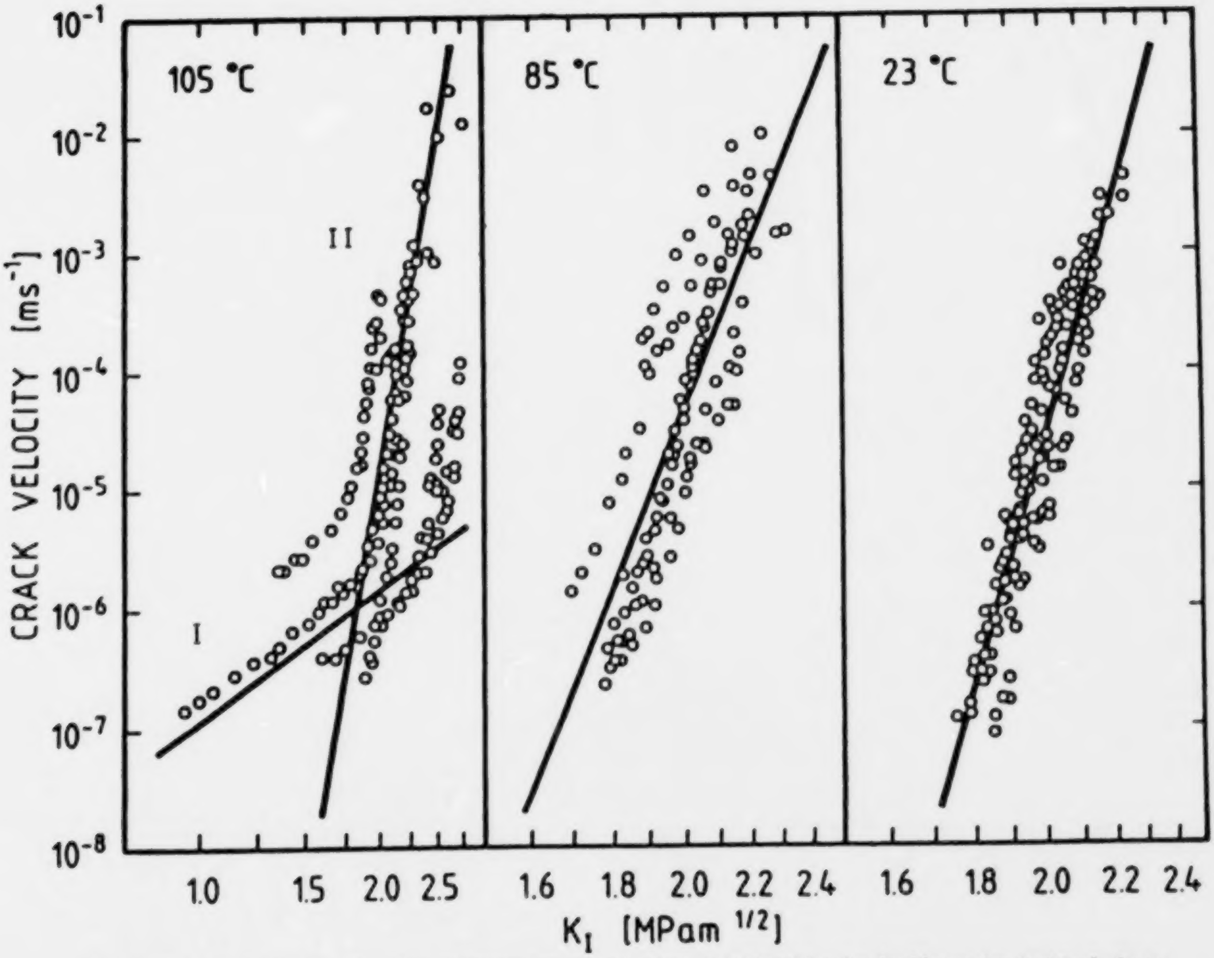

Fig. 14. Crack velocity as a function of stress intensity factor as obtained by the double torsion test technique.

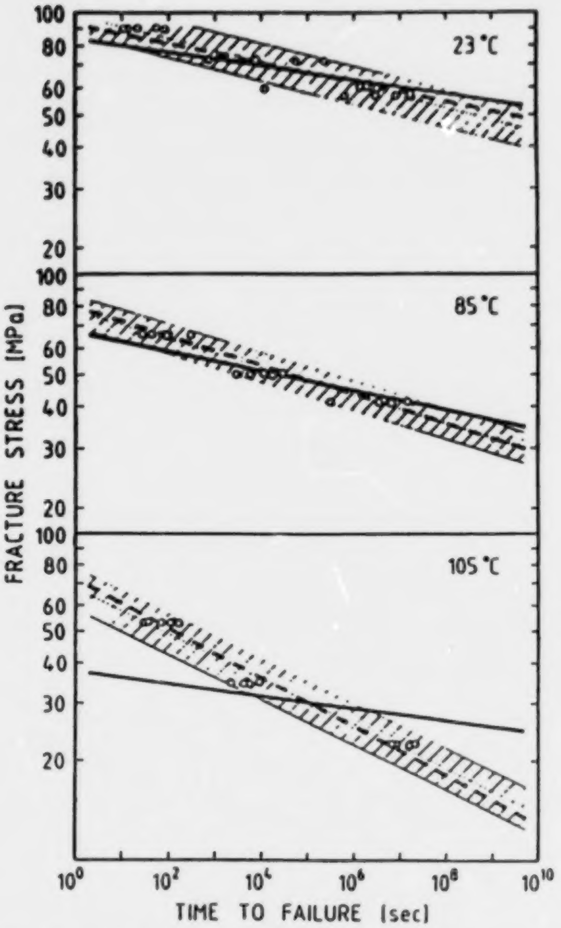

Fig. 15. Static fatigue and lifetime predictions at various temperatures: (○) fracture time/fracture stress of individual specimens: ——Prediction using parameters derived from double torsion experiments.

tions based on *Eq 2.* It can be seen that at 23°C and 85°C quite good agreement is obtained. At 105°C some deviation is noted, but this temperature is only 15°C below the glass transition and the material is no longer linearly elastic. Thus, at this temperature, predictions based on linear elastic fracture mechanics cannot be expected to give accurate results.

CONCLUSIONS

Using hybrid resin systems (resin, filler, and CTBN), it is possible to increase stress intensity factors by a factor of 5 and fracture energies by a factor of 15 above those of the unfilled resin. However, these increases are to the detriment of the tensile and flexural strength of the system, which is some 30% lower. Particulate-filled systems without second phase rubber can have stress intensity factors and fracture energies four times higher than the base resin without this loss in strength. It is clear that the choice of formulation will depend on the service loads of the structure, whether impact loads or high levels of stresses will be encountered. It has been shown that the mechanism of long-term failure in these particulate-filled resins is subcritical crack growth that is characterized by resin-particle debonding. Crack growth continues until a critical size is reached after which sudden failure occurs. Calculations of static fatigue life based on this mechanism predict the long-term strength with sufficient accuracy for engineering design.

REFERENCES

1. M. Narkis, *J. Appl. Polym. Sci.*, **22**, 2391 (1978).
2. J. A. Manson and L. J. Sperling, "Polymer Blends and Composites," Ch. 12, Plenum Press, New York (1976).
3. O. Ishai and L. J. Cohen, *Int. J. Mech. Sci.*, **9**, 539 (1967).
4. A. C. Moloney, H. H. Kausch, and H. R. Stieger, *J. Mater. Sci.*, **18**, 208 (1983).
5. J. Spanoudakis and R. J. Young, *J. Mater. Sci.*, **19**, 487 (1984).
6. J. Spanoudakis and R. J. Young, *J. Mater. Sci.*, **19**, 473 (1984).
7. A. Kelly, *Proc. R Soc. (London)*, **A 319**, 95 (1970).
8. P. Hancock and R. C. Cuthbertson, *J. Mater. Sci.*, **5**, 762 (1970).
9. A. C. Moloney, H. H. Kausch, T. Kaiser, and H. R. Beer, *J. Mater. Sci.* (in press).
10. A. J. Kinloch and R. J. Young, "Fracture Behaviour of Polymers," Applied Science, London (1983).
11. D. L. Maxwell, R. J. Young, and A. J. Kinloch, *J. Mater. Sci. Lett.*, **3**, 9 (1984).
12. A. J. Kinloch, D. L. Maxwell, and R. J. Young, *J. Mater. Sci.*, **20**, 4169 (1985).
13. A. F. Yee and R. A. Pearson, NASA Report 3718 "Toughening mechanisms in elastomer modified epoxy resins," Part I (August 1983).
14. F. F. Lange and K. C. Radford, *J. Mater. Sci.*, **6**, 1197 (1971).
15. K. C. Radford, *J. Mater. Sci.*, **6**, 1286 (1971).
16. R. P. Kambour and E. A. Farraye "Proc. Int. Conf. Def. Yield & Fracture of Polymers," Plastics & Rubber Inst. London (1985).
17. W. J. Cantwell, A. C. Roulin-Moloney (manuscript in preparation).
18. H. R. Beer, T. Kaiser, A. C. Moloney, and H. H. Kausch, *J. Mater. Sci.*, **21**, 3661 (1986).
19. B. J. Pletka and S. M. Wiederhorn, *J. Mater. Sci.*, **17**, 1247 (1982).

DISCUSSION

R. T. Woodhams: I noted from your manuscript that the particles you have been dealing with were more than 1 μm. In some publications this is a critical size; for submicron particles, the surface area sometimes dominates the fracture mechanics, strength, and toughness. It would be interesting to extend your measurement to the submicron particles.

A. C. Roulin-Moloney: Yes, certainly.

J. A. Radosta: What is the reason for the minimum in the tensile yield stress as a function of volume percent loading for the particulates? Does anyone know it?

S. Newman: The phenomenon of the minimum is a common one and has been discussed by B. D. Agarwal and L. J. Broutman in their 1980 book, "Analysis and Performance of Fiber Composites." The explanation is that if you add filler, you substantially reduce the strain to failure before you get the reinforcing effect. So you get these two conflicting effects; at the minimum you are not getting the reinforcing effect of the filler yet, but you already reduced the strain to failure of the matrix. Agarwal and Broutman gave the theory and calculations to support this argument.

I would like also to ask a question. In carboxyl-terminated polybutadiene modified samples, did you get shear band initiation on the surface? Did you see any evidence for crack termination by reason of the presence of rubber particles?

A. C. Roulin-Moloney: The shear bands started in the matrix by cavitation of the rubber particles. We have not observed crack termination by rubber particles.

In Situ Fracture Tests in the Scanning Electron Microscope

A. C. ROULIN-MOLONEY, N. CUDRÉ-MAUROUX, *and*
H. H. KAUSCH

Laboratoire de Polymères
Ecole Polytechnique Fédérale de Lausanne
1007-Lausanne, Switzerland

The experimental arrangement for conducting fracture tests in the scanning electron microscope (SEM) are described together with the particular problems in applying this technique to polymers and composite materials. Several examples are given of mechanisms of fracture in epoxy resins both unfilled and reinforced with particulate and fibrous fillers. The paper is illustrated by still photos taken from the video recording of the fracture experiments and by photos taken from the SEM raster.

INTRODUCTION

The fracture properties of highly cross-linked polymers, particularly epoxy resins, have been extensively studied in recent years (1). In view of their behavior in tensile tests, these materials have been generally considered brittle. However, it is now known that the stress concentrations at the crack tip are sufficient to produce local plastic yielding and flow (2). The objective of this work is to study in detail the deformation and fracture of epoxy resins, both unfilled and in the presence of particulate inclusions. The technique chosen for the investigation was conducting in situ fracture tests in the scanning electron microscope.

MATERIALS AND EXPERIMENTAL

Various epoxy resins were used in this investigation. Resin A is an unmodified epoxy cured with an anhydride hardener. Composites were prepared using this resin containing:

a. 30% volume of glass beads either untreated or treated with a silane coupling agent; b. 40% volume of silicon carbide particles; c. 8% volume of milled glass fibers.

Resin B is an epoxy based on the diglycidyl ether of bisphenol A and cured with piperidine modified with 15% weight of carboxy-terminated butadiene acrylonitrile (CTBN) from B. F. Goodrich.

Samples were cast in steel molds, rotating if necessary to prevent sedimentation. The specimen geometry used was the compact tension of dimensions 13 by 14 by 2.5 mm. The loading jig was developed in the Materials Department here in Lausanne by Dr. G. Zambelli. It fitted on the stage of Cambridge Instruments S250 scanning electron microscope as shown in *Fig. 1*. Strain gauges and a clip gauge enabled the simultaneous measurement of the load and the deformation of the specimen. The output was fed into a chart recorder. The loading stage had all the normal operations of a regular microscope stage; that is, movement in the x, y, and z directions. The sample was loaded manually to control crack propagation to speeds that could be followed under the electron beam. All the events during the fracture process were registered using a video recorder, but in some cases still photos were taken from the normal SEM raster giving better quality. Some events were too fast to be captured by a still photo, and then photos were taken subsequently from the video recording. The experimental arrangement is shown schematically in *Fig. 2*.

Certain problems are encountered when applying this technique to polymers: First, since these resins are cast from the liquid state, the surface is resin-rich and, to study fracture behavior of particulate-filled resins, this layer must be removed to reveal the particles below. Many polishing techniques were attempted, following for example the recommendations of Holik, *et al.* (3), but the resin-particle interface was inevitably damaged and particles were often torn out or damaged. To avoid these problems, the technique of argon ion etching was adopted. With careful control of the current, voltage, time and angle of attack, satisfactory results were obtained. An example is given in *Fig. 3*. Nevertheless, the rubber-modified systems were rather sensitive to the ion beam, and etching was kept to a minimum. Second, these polymeric materials are nonconducting and, to work at beam voltages above 1 kV, it is necessary to coat the sample with a metallic layer such as gold or platinum to render the surface conductive. For the majority of the tests, a 30-nm layer of gold was applied. Unfortunately,

Fig. 1. The experimental equipment showing the microscope stage and the test jig.

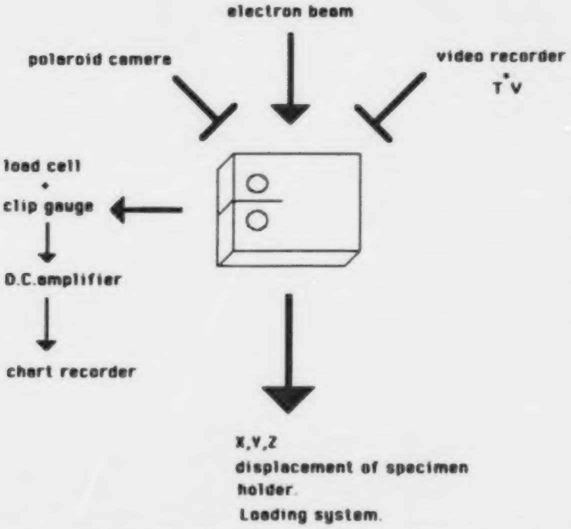

Fig. 2. Schematic diagram of the experimental equipment.

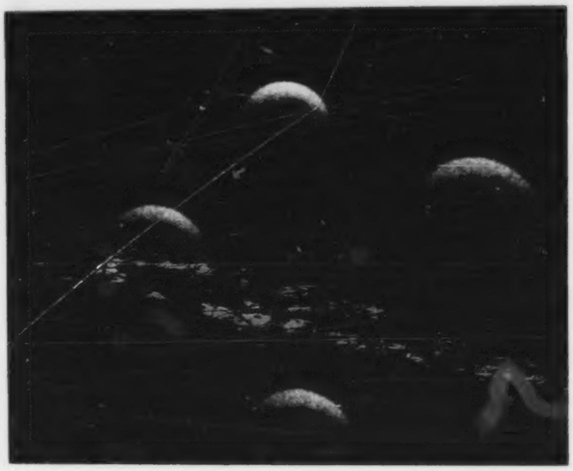

Fig. 3. Surface of a glass-bead-filled resin after argon ion etching.

the gold is incapable of following all the deformations of the polymer and it cracks during the test. This misled us in the early part of our experiments (4), and indeed other workers using this technique on epoxides (5) and polyamides (6) have reported the same observation. It is now clear that these "microcracks" are only within the gold layer.

It is possible to work without gold coating at low beam voltages (1 to 2 kV) using a LaB_6 filament. Obviously, this is with some loss of resolution and, in fact, the signal was not intense enough to work with the video recorder. In the work at low voltages, an image store system was used in conjunction with Polaroid photographs. To enable differentiation between any artifacts caused by either the argon ion etching or the gold coating, four approaches were used:

a. tests on gold-coated samples at 10 kV beam voltage to give the best resolution;
b. tests on uncoated samples at low beam voltage;
c. tests outside microscope with and without gold coating—both the deformed specimen and the fracture surface were observed in the scanning electron and optical microscopes;
d. tests on samples without treatment by argon ion etching and also on polished samples.

RESULTS AND DISCUSSION

Unfilled Resin A

In many unfilled epoxy resins, two types of crack propagation are observed—either stable, continuous or unstable stick-slip propagation. The load-displacement curves for each type are shown in *Fig. 4*, which is relevant for test geometries where the compliance is linear with the crack length (e.g., double torsion, tapered double cantilever beam). For resins exhibiting unstable crack propagation, the load-displacement diagrams have a sawtooth appearance, and values of the stress intensity factor (K_c) appropriate to crack initiation (K_{ci}) and crack arrest (K_{ca}) may be determined. Values of K_{ci} are, in general, strongly dependent on testing rate, whereas K_{ca} values are approximately constant and similar to values for stable propagation. At higher testing speeds propagation often becomes continuous. Yamini and Young (7) have tested a wide range of epoxy resins at various rates and determined K_{ci} and K_{ca} for different systems. They explained the transition from stable to stick-slip propagation in terms of blunting at the crack tip. For resins with a low yield stress, material in the vicinity of the crack tip may flow while the crack is

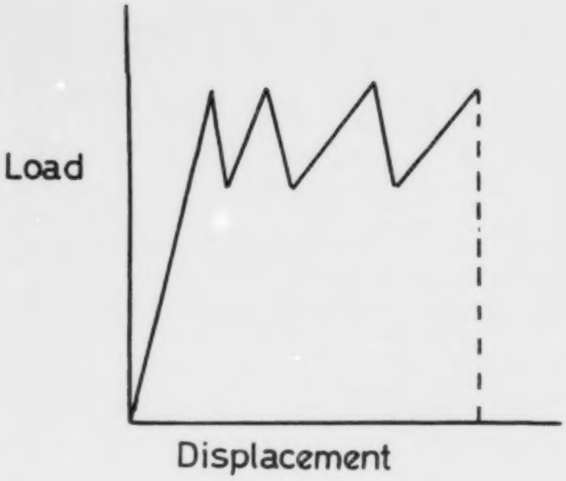

Stable propagation

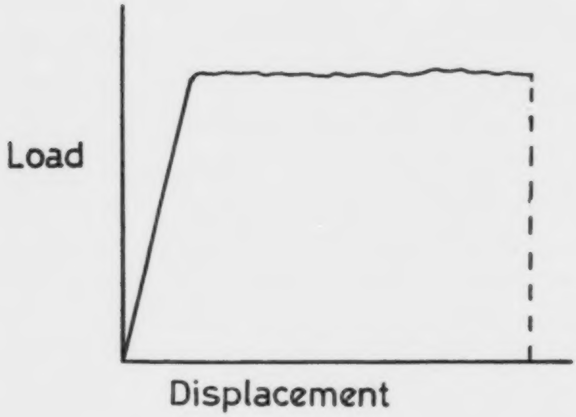

Fig. 4. Typical load-displacement diagrams for unstable and stable crack propagation.

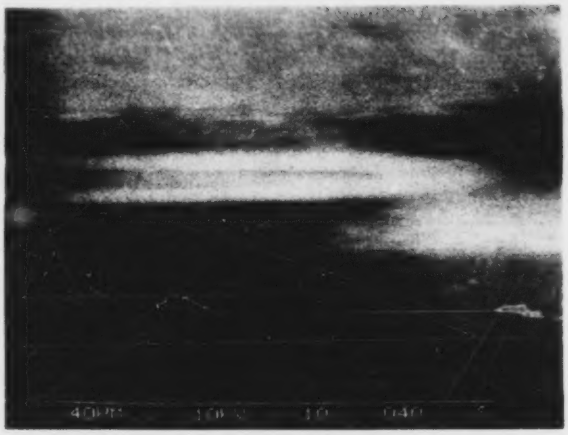

Fig. 5. Sharp crack in an unfilled epoxy resin.

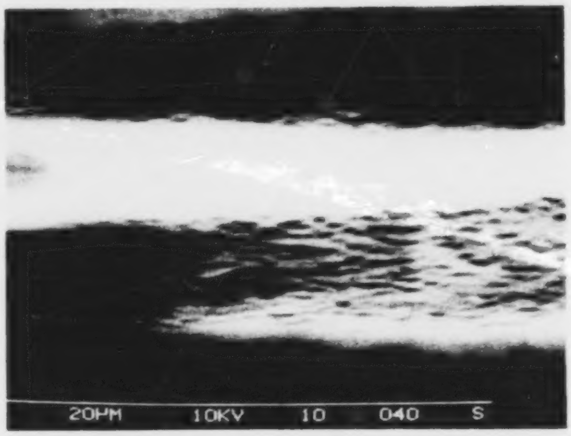

Fig. 6. Original sharp crack in unfilled epoxy resin progressively blunts.

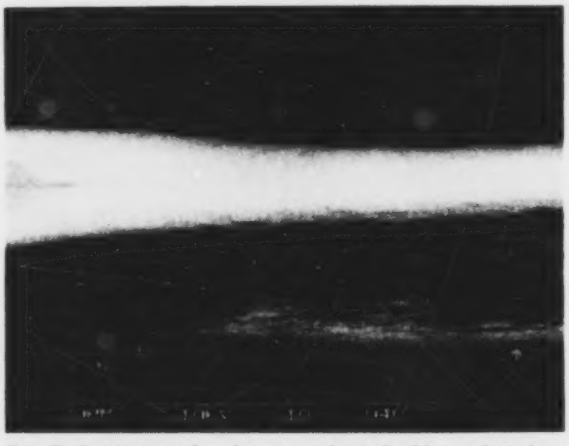

Fig. 7. Initiation of a sharp crack at the blunted tip (unfilled epoxy resin).

propagating and cause crack tip blunting. A higher stress is required to reinitiate a sharp crack and, hence, the value of K_{ci} is greater than K_{ca}. The magnitude of K_{ci} is dependent on the radius of the blunted crack. Data for a range of epoxy resins may be fitted to this theory, as shown by Kinloch and Williams (8).

The fracture tests conducted in the scanning electron microscope on unfilled resin A visualized directly this phenomenon of crack tip blunting. The process is shown in *Figs. 5* through *7*, which were taken from the video recording. In *Fig. 5* the crack tip is sharp; it progressively blunts (*Fig. 6*), and then the new sharp crack tip is initiated (*Fig. 7*). In these micrographs the cracking of the gold layer is evident; however, the plastic zone is clearly delimited by this effect. Pronounced shear lips may be seen that derive from the shear deformations occurring at constant volume; hence, the sample surface is sucked in. A more detailed photo of the plastic zone in such an unfilled epoxy is given in *Fig. 8*. It was clear from the video recording during the tests that, as the crack blunted, the plastic zone could extend further. Thus, after a certain extent of blunting, the plastic zone was considerably larger than when the crack tip was sharp. Under conditions of a sharp crack tip, the measured plastic zone size agreed quite well with predictions based on the Dugdale model.

Particulate-filled Resins

The fracture tests on the particulate-filled resin showed clearly the importance of the aspect ratio of the particles on the mechanisms of toughening. These mechanisms are reviewed in *Ref. 9*.

Glass-bead-filled Resins

An example of the crack tip zone in a composite prepared with 30% volume of silane-treated glass beads is shown in *Fig. 9*. In this system crack propagation occurred by the nucleation of voids at the pole of the next particle in the path of the crack. This void was not initiated at the interface but rather some 1 to 3 μm away from the resin-filler interface, as shown in *Fig. 9*. The resulting fracture surface showed that a thin layer of resin was still attached to the particles (see *Fig. 10*). The shear deformation of the resin between the crack tip and the nucleated void is clear from the presence of the shear lip in *Fig. 9*.

In contrast, for glass beads without any surface treatment, crack propagation was highly unstable and too rapid to be followed under the electron beam at high magnifications. In these systems, decohesion occurred at the interface ahead of the crack tip. This phenomenon also has been reported by Owen (10) and Su and Suh (11). It appears that this debonding of the particles gives rise to crack tip blunting and unstable crack propagation in this system. A typical fracture surface is shown in *Fig. 11*.

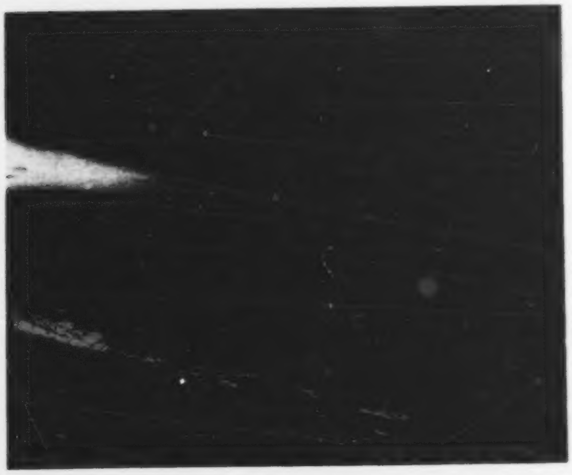

Fig. 8. Crack tip zone in an unfilled, unmodified epoxy resin.

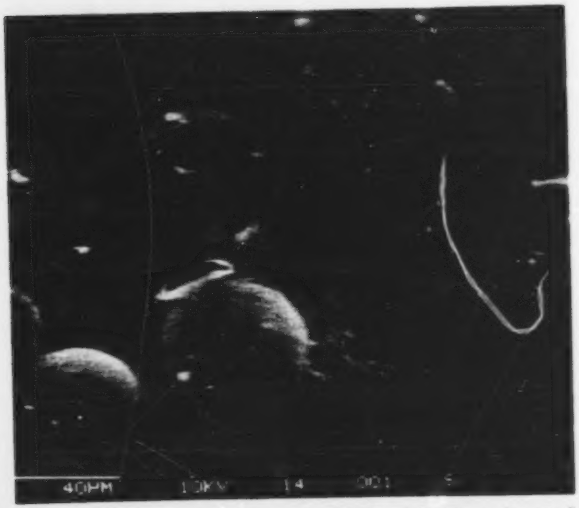

Fig. 9. Crack tip zone in a resin filled with silane-treated glass beads.

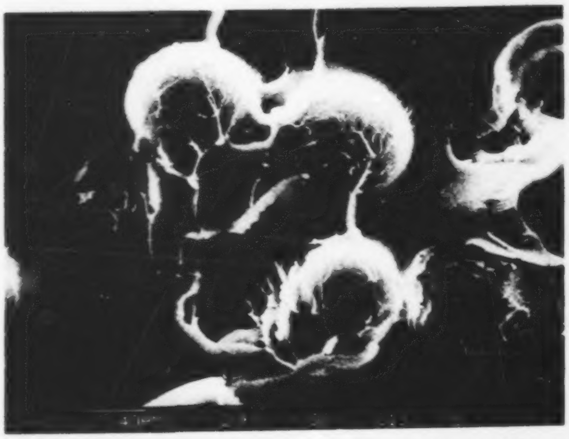

Fig. 10. Fracture surface of a resin filled with 30% volume of silane-treated glass beads.

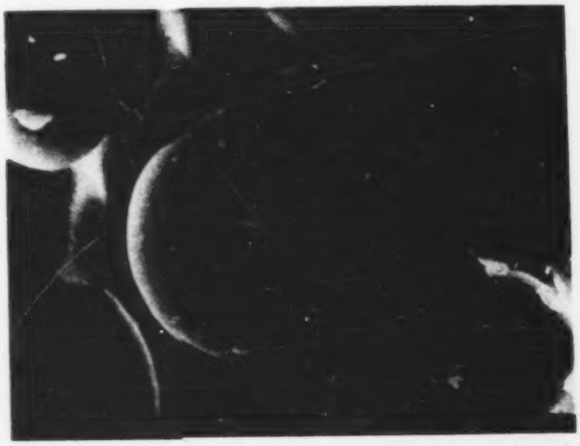

Fig. 11. Fracture surface of a resin filled with 30% volume of untreated glass beads.

Silicon-carbide-filled Resin

The crack tip zone in the composite prepared using 40% volume of silicon carbide particles is shown in *Fig. 12.* These particles are of irregular shape and the aspect ratio is approximately 4. In this system, the plastic zone was considerably larger than for either the unfilled resin or the glass-bead-filled resin. The fundamental mechanism of crack propagation appeared to be the same; that is, initiation of voids at the next particle ahead of the crack tip. However, because of the irregular shape of the particles, the crack path was more tortuous than in the case of the glass beads. The values of the stress intensity factor were also higher for the silicon carbide composites, as shown in *Fig. 13* (taken from *Ref. 9*).

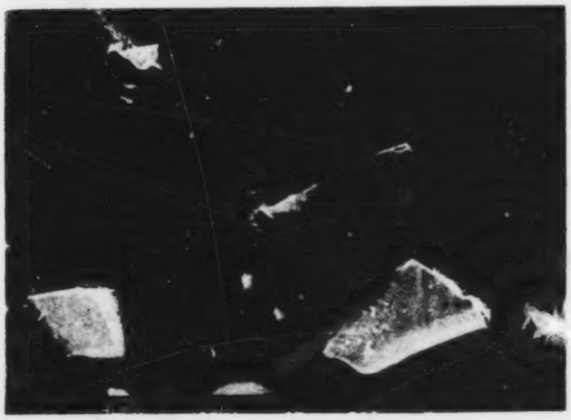

Fig. 12. Crack tip zone in a resin filled with silicon carbide particles.

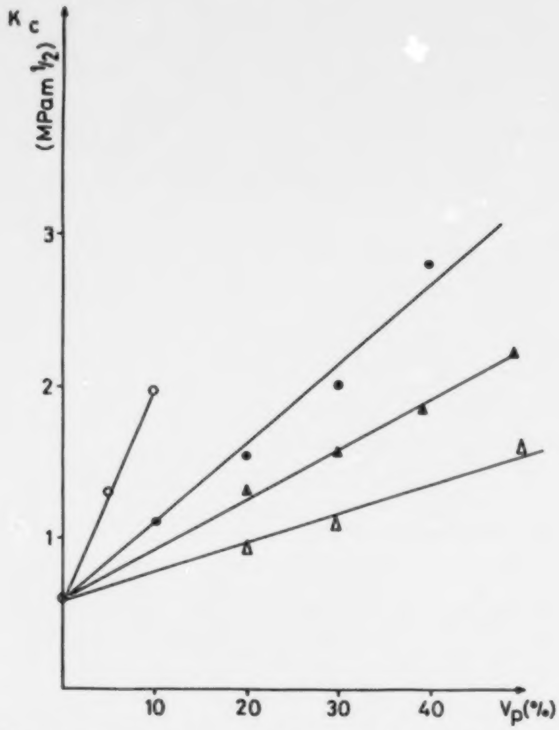

Fig. 13. Stress intensity factor as a function of volume fraction of filler: ▲, alumina and silica particles, △, silane-treated glass beads, ●, silicon carbide particles, ○, short glass fibers.

Resin-Filled with Short Glass Fibers

The video recording of the fracture tests of the composites prepared using 8% volume of short glass fibers indicated that for this system, the principal toughening mechanism is fiber pullout. This is difficult to reproduce with still photos, but during the recording it was possible to follow fibers near the surface pulling out from the surrounding matrix. The fracture surface morphology was also consistent with this mechanism, as shown in *Fig. 14*. The plastic zone in these composites was some 100 μm in size, deformation of the matrix being clearly visible along the fibers. Even at this low volume fraction the stress intensity factor was considerably higher than for the other particulate fillers (see *Fig. 13*). The aspect ratio of the fibers used was approximately 15.

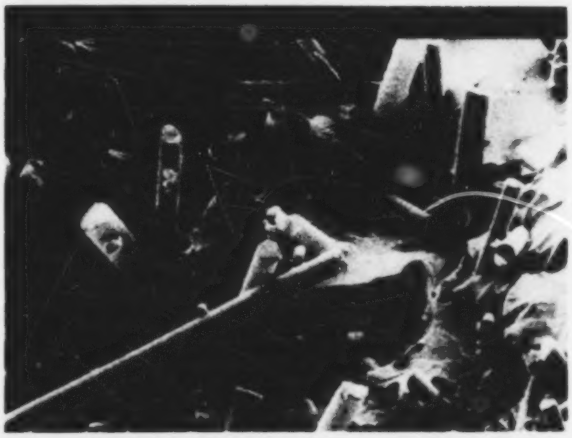

Fig. 14. Fracture surface of a resin filled with short glass fibers.

Rubber-modified Resin B

The fracture behavior of rubber-modified epoxy resins has been studied in detail in recent years. Considerable increases in fracture energy are observed, up to sixtyfold for some systems. A number of different mechanisms have been proposed such as deformation of the rubber particles across the crack tip (12), crazing of the matrix (13), or absorption of energy by the matrix (14). There is now, however, considerable evidence (15,16) that the high toughness derives from the blunting of the crack produced by cavitation of the rubber particles under the triaxial stress state at the crack tip. This cavitation lowers the local yield stress and provokes extensive shear yielding. The fracture surface of these rubber-modified resins is covered with holes, as shown in *Fig. 15*. The rubber in fact forms a lining in these depressions (16).

The plastic zone sizes and crack opening displacements (COD) are considerably larger than for the unmodified resins. From the fracture tests in the SEM, CODs were measured to be ~10 μm and plastic zones some hundreds of micrometers. The crack tip zone for a rubber-modified resin is shown in *Fig. 16*, which is for a sample fractured without gold coating and observed at low beam voltage (1.5 kV). The furrows derive from the shear deformation ahead of the crack and are the reason why the gold coating cracks, as can be seen by comparing *Figs. 16* and *17*. Furthermore, comparison with *Fig. 8* indicates the much larger plastic zone in the rubber-modified systems. Some isolated cases of material bridging the crack were observed (see *Fig. 16*). This is most probably epoxide rather than rubber because of the size of these bridges and the fact that after fracture, the broken moieties do not retract as would be characteristic of rubber. Such structures also have been observed in unmodified resins. Moreover, if the rubber deformation model were correct, a forest of deformed rubber particles would be observed at the crack tip.

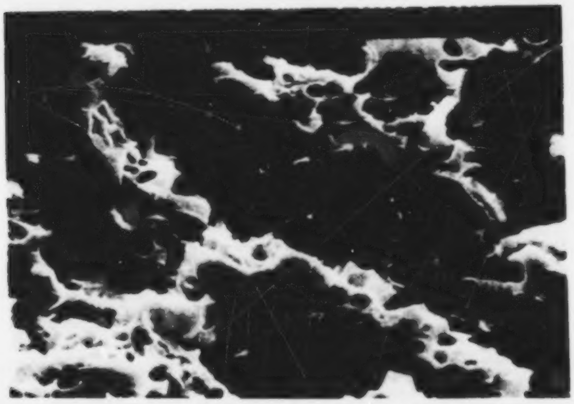

Fig. 15. Fracture surface of a rubber-modified epoxy resin.

Fig. 16. Crack tip zone in a rubber-modified epoxy under load in the SEM. The sample was not coated with gold and was observed at a beam voltage of 1.5 kV.

Fig. 17. Crack tip zone in a rubber-modified epoxy under load in the SEM. The sample was gold-coated before the test and observed at a beam voltage of 10 kV.

The video recordings confirmed the very strong tendency of these materials to crack tip blunting. In some instances, the extent of blunting was so great that, instead of the original crack continuing to propagate, a new void was initiated some tens of micrometers away from the original crack tip. The crack propagation was, however, slow and essentially continuous. This is in contrast to the effects of crack tip blunting in the unfilled, unmodified resin.

CONCLUSIONS

The technique of following fracture in situ in the scanning electron microscope is potentially a powerful means to study mechanisms of fracture. However, great care must be taken in interpreting the results since a number of sources of artifacts may be encountered. It should be used as a supplement to an extensive program of mechanical tests outside the microscope on the materials under investigation.

ACKNOWLEDGMENTS

The authors would like to thank Brian Senior and the Institut Interdepartmental de Microscopie (EPFL) for much help with scanning electron microscopy, Jean-Luc Roulin for technical assistance, and Dr. A. J. Kinloch for helpful suggestions and discussions. The financial support of Brown Boveri & Cie and the Commission pour l'Encouragement de la Recherche Scientifique is also gratefully acknowledged.

REFERENCES

1. A. J. Kinloch and R. J. Young, "Fracture Behavior of Polymers," Applied Science Publishers, London (1983).
2. S. Yamini and R. J. Young, *J. Mater. Sci.*, 15, 1823 (1980).
3. A. S. Holik, R. P. Kambour, P. G. Fink, and S. Y. Hobbs, *Microstruct. Sci.*, 7, 357 (1979).

4. A. C. Moloney and H. H. Kausch, *J. Mater. Sci. Lett.*, **4**, 289 (1985).
5. S. Banyopadhyay, V. M. Silva, H. Wrobel, and J. Nicholls, 6th Int. Conf. on Deformation, Yield and Fracture of Polymers, Plastics & Rubber Inst., Cambridge (April 1985).
6. N. Sato, T. Kurauchi, S. Sato, and O. Kamigaito, *Proc. ACS Polym. Mater. Sci. Eng.*, **49**, 1075 (1983).
7. S. Yamini and R. J. Young, *Polymer*, **18**, 1075 (1977).
8. A. J. Kinloch and J. G. Williams, *J. Mater. Sci.*, **15**, 987 (1980).
9. A. C. Moloney, H. H. Kausch, T. Kaiser, and H-R. Beer, *J. Mater. Sci.* (in press).
10. A. B. Owen, *J. Mater. Sci.*, **14**, 2523 (1979).
11. K. B. Su and N. P. Suh, *Soc. Plast. Eng.*, **27**, 46 (1981).
12. S. Kunz-Douglass, P. W. R. Beaumont, and M. F. Ashby, *J. Mater. Sci.*, **15**, 1109 (1980).
13. C. B. Bucknall, *Adv. Polym. Sci.*, **27**, 121 (1978).
14. J. N. Sultan, R. C. Raible, and F. J. McGarry, *Appl. Polym. Symp.*, **16**, 127 (1971).
15. A. F. Yee and R. A. Pearson, *J. Mater. Sci.*, **21**, 2462 (1986).
16. A. J. Kinloch, S. J. Shaw, D. A. Tod, and D. L. Hunston, *Polymer*, **24**, 1341 (1983).

DISCUSSION

S. Newman: I noticed that the rubber particles were rather small compared with the dimension of the crack. They are about 1 to 5 μm, and they really can not stop the crack. Since you are using carboxyl-terminated polybutadiene, which depending on the phase separation can give different size of dispersed particles, it may be interesting to add the rubber particles separately for better control of size. I am sure that there must be commercial products with particle diameters comparable with crack dimensions, and this system may have crack-termination capability.

A. C. Roulin-Moloney: The main fracture mechanism is by particle cavitation under the triaxial stresses at the crack tip which permits matrix shear yielding and gives rise to the large plastic zone.

S. Newman: Yes. This accounts for initiation. At the same time, there was a long argument that right sized rubber particles serve the second purpose; that is, the termination. Here we did not see any evidence of it at all.

A. C. Roulin-Moloney: One mechanism that we can rule out is the idea that the rubber particle bridges the crack.

A. Moet: We do not want a particle to stop the crack. The crack we saw looks like an earthquake. We want the particles to be of certain size and distribution that will be able to divide the crack. Below a certain size the particle is not able to provide the stress concentration capability. At a certain dispersion they may not interact; if they interact that may lead to failure. There is a balance between the particle size and particle size distribution. However, a particle is not a crack stopper. This is the toughening mechanism of acrylonitrile-butadiene-styrene resins, HIPS, and other engineering thermoplastics. The crack must run into a jungle of damage and not be stopped on a point.

A. C. Roulin-Moloney: These were shear bands here, not cracks.

A. Moet: It does not matter. It can be craze, crack, shear banding, fiber debonding, pullout, or breaking—anything that absorbs energy. They all help. Craze and shear banding are out when we discuss composites. You may see craze and shear band, and other defects on the same specimen. The wonder of composites is that the ingredients interact together and create a large energy dissipative system. The nice and simple mechanism of craze and crack, and of particles doing this or that is out.

Crack-Arrest Study in Mode II Delamination in Composites

T. VU-KHANH

Industrial Materials Research Institute
National Research Council of Canada
Boucherville, Québec, Canada J4B 6Y4

Procedures for measuring the crack initiation and arrest toughnesses in Mode II interlaminar fracture in composite materials were analyzed. Different techniques using flexural specimens were studied. The strain energy release rate, G, which is the energy available for crack propagation was calculated using simple beam theory. The calculation takes into account the transverse shear effect. Stable and unstable fractures are analyzed, and conditions required to measure the arrest toughness of interlaminar fracture are discussed. The methodology was applied to the measurement of fracture energy at the onset and arrest of delamination in glass/epoxy laminate.

INTRODUCTION

One of the most important hurdles to the application of advanced composites in load-bearing structures is the tendency of these materials to delaminate. Delamination represents a major damage in composites since it results in reduced stiffness, strength, and fatigue life of the structure. Basically, delamination is an interlaminar fracture problem. Because of high anisotropies of laminae, interlaminar stresses develop between layers of different fiber orientation (1–9). In the presence of these stresses and under some circumstances, delamination occurs. For instance, edge delaminations have been found to initiate at a cyclic stress level of about 30% of the static strength of a quasi-isotropic laminate. Delamination also occurs at existing defects, holes, or ply termination. Because of the complexity of interlaminar stresses developed, delamination is often three dimensional in nature.

Much work has been done to characterize the delamination resistance of composites in Mode I (10–15). However, in some common loading conditions, it has been shown that Mode II and Mode III can be dominant (16–19). The few reported investigations in shear Mode II delamination mainly focused attention on the initiation stage or slow crack growth in fatigue (13, 18, 20, 21). Under certain circumstances in service, catastrophic growth of delamination can occur. In that situation, the propagation of the crack is very fast and has an unstable character. The most direct approach to the evaluation of dynamic fracture is based on the measurements of the instantaneous dynamic stress field close to the propagating crack tip. However, such measurements are generally very difficult, particularly in opaque materials that are of most practical interest, because of the short time durations involved. For this reason, the procedure for measuring the crack-arrest toughness has received much attention in recent years. Crack-arrest toughness is a property that indicates the material's resistance to penetration by a running crack. This value is therefore essential to assess the structure integrity.

Computational and experimental methods for the analysis of dynamic crack propagation and arrest have been, so far, mainly developed for Mode I fracture of isotropic materials (22–24). No attention has been paid to the delamination problem in composites.

The purpose of this work was to investigate a technique to measure the crack-arrest toughness in Mode II interlaminar fracture of composite laminates, which is of great interest in helicopter applications. Since the most popular test for determining Mode II interlaminar fracture toughness is based on the use of the flexural specimen, the analysis was made for the case of cantilever beam specimens containing an initial delamination.

Stress singularities for a delamination crack in the composite laminate can be described by fracture mechanics parameters such as the stress intensity factor ($K_{I,II,III}$) or the strain energy release rate ($G_{I,II,III}$). While the stress intensity factor describes the details of an interlaminar crack-tip field, the strain energy release rate is of practical importance because it is physically measurable in the experiments and is also mathematically well defined. In this paper, the fracture energy release rate in flexural specimens is analyzed for Mode II delamination. The conditions for stable and unstable delamination growth are discussed in terms of specimen geometry and loading condition. The method for measuring the arrest toughness in Mode II delamination is presented.

STRAIN ENERGY RELEASE RATE

Two different types of initial crack in the cantilever beam specimen were analyzed: free-edge crack (*Fig. 1a*) and clamped-edge crack (*Fig. 1b*). The cantilever beam is not different from the three-point-bend specimen commonly used for Mode II delamination characterization. However, the initial-crack preparation is much simpler with the cantilever beam, especially in the case of embedded crack.

The strain energy release rate of a solid containing a crack may be determined by evaluating the elastic strain energy in the solid at a constant displacement of its boundary (25):

$$G = -dW/dA \qquad (1)$$

where G is the strain energy release rate, W is the elastic (potential) energy, and A is the crack surface. The strain energy is given by:

$$W = \frac{1}{2}\int_v \sigma_i \epsilon_j dv \qquad (2)$$

where v is the volume of the solid, σ_i and ϵ_j are stress and strain components respectively. The constitutive equations may be expressed by the generalized Hooke's law as

$$\sigma_i = Q_{ij}\epsilon_j \qquad (3)$$

where Q_{ij} is the modulus tensor.

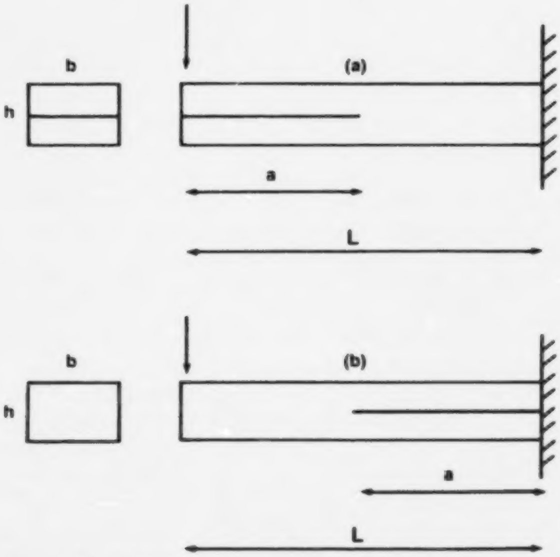

Fig. 1. Cantilever beam for Mode II delamination test: (a) free-edge crack specimen; (b) clamped-edge crack specimen.

Strain Energy in Bending

From bending theory, the relationship between curvature and bending moment of composite laminates can be expressed as (26)

$$k_i = d_{ij}M_j \qquad (4)$$

where d_{ij} is the flexural compliance tensor, k_i and M_j are curvature and moment components respectively.

From *Eqs 2* through *4*, the strain energy due to bending of the symmetric laminate beam can be derived ($M_2 = M_6 = 0$ and k_2 and k_6 are neglected):

$$W = \frac{1}{2}\int_v Q_{11}(d_{11}zM_1)^2 dv \qquad (5)$$

where z is the distance from the midplane of the laminate.

To calculate the strain energy in bending in the case of free-edge crack (*Fig. 1a*), the specimen was divided into three parts as shown in *Fig. 2*. The symmetry of the specimen and the conditions of equilibrium imply that:

$$\begin{aligned} F_1 = F_2 &= P/2 \\ M(3) &= Pa \end{aligned} \qquad (6)$$

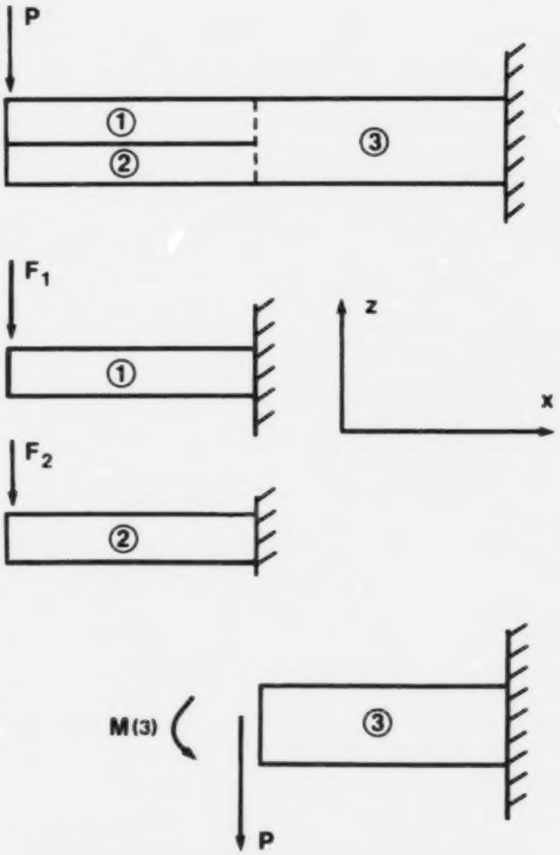

Fig. 2. Forces and moments in different portions of free-edge crack specimen.

If $W_{(1)}$, $W_{(2)}$, and $W_{(3)}$ are the strain energy in the portion 1, 2, and 3 respectively as labeled in *Fig. 2*, the strain energy in the beam is

$$W = W_{(1)} + W_{(2)} + W_{(3)} \qquad \text{(a)}$$

with

$$W_{(1)} = W_{(2)} = \frac{1}{2}\int_o^a \int_{-h/4}^{+h/4} \frac{1}{b} Q_{xx} \cdot \left(d_{xx} z \frac{P}{2} x\right)^2 dzdx \qquad \text{(b)} \qquad (7)$$

$$W_{(3)} = \frac{1}{2}\int_o^{(L-a)} \int_{-h/2}^{+h/2} \frac{1}{b} Q_{xx} \cdot [d_{xx} z P(x-a)]^2 dzdx \qquad \text{(c)}$$

Integration of the above equations becomes much simpler if the effective flexural modulus of the laminate is used. The effective flexural modulus along the x axis is defined as (26)

$$E_x^f = 12/h^3 d_{xx}. \qquad (8)$$

Using this effective modulus and considering the case in which E_x^f is the same for the three portions 1, 2, and 3 of the beam, the integration of *Eq 7* yields

$$W = P^2(2L^3 + 6a^3)/E_x^f bh^3. \qquad (9)$$

This equation gives the elastic strain energy in bending in the free-edge crack cantilever beam as a function of the load P and the crack length a.

For the case of clamped-edge crack specimen, the resultant forces and moments exerted on each part of the specimen are shown in *Fig. 3*. The action of portion 1 on portions 2 and 3 results in a shearing force $P/2$ and a moment M'. M' is the moment resulting from the distribution of internal normal stress on the upper half of portion 1 at the cross section AB, due to the bending moment produced by P. Under the action of the shearing force $P/2$, portions 2 and 3 cannot deform freely because of the condition of continuity at the cross section ACB. This continuity also creates a resisting moment M^* at AC and CB.

The strain energy in the specimen is thus

$$W' = W'_{(1)} + W'_{(2)} + W'_{(3)} \qquad \text{(a)}$$

with

$$W'_{(1)} = \frac{1}{2}\int_o^{(L-a)} \int_{-h/2}^{+h/2} \frac{1}{b} Q_{xx} \cdot [d_{xx} z P x]^2 dxdz \qquad \text{(b)} \qquad (10)$$

$$W'_{(2)} = W'_{(3)} = \frac{1}{2}\int_o^{a} \int_{-h/4}^{+h/4} \frac{1}{b} Q_{xx} \cdot \left[d_{xx} z \left(\frac{P}{2} x + M' - M^*\right)\right]^2 dxdz \qquad \text{(c)}$$

By using the effective modulus and considering the case in which E_x^f is the same in the three portions 1, 2, and 3 of the beam, M' and M^* are determined. The equilibrium condition gives

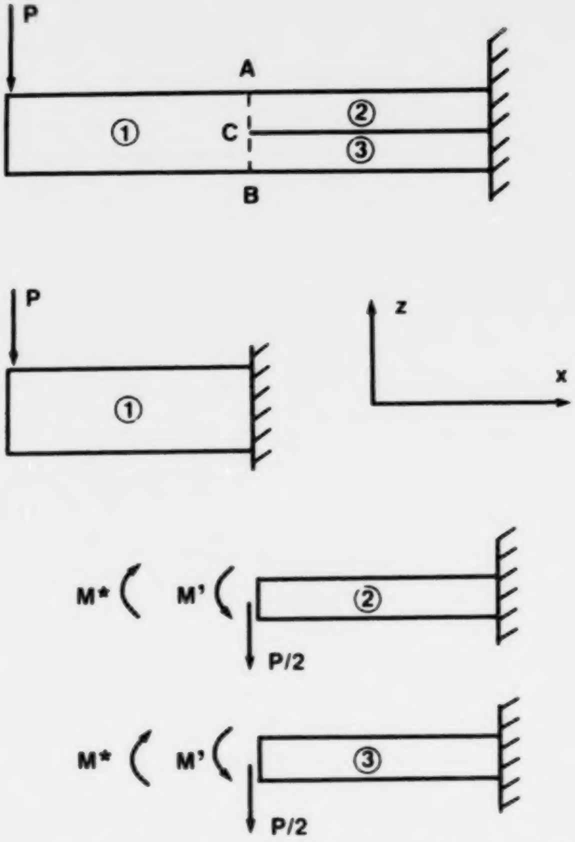

Fig. 3. Forces and moments in different portions of clamped-edge crack specimen.

$$M' = P(L-a)/8. \qquad (11)$$

The condition of continuity of the cross section ACB gives

$$M^* = 3Pa/16. \qquad (12)$$

Integration of *Eq 10* therefore yields the elastic strain energy in bending in the clamped-edge crack specimen:

$$W' = P^2(2L^3 + 3a^3/2)/E_x^f bh^3. \qquad (13)$$

Strain Energy Due to Shearing Force

Because of the low ratio of shear to longitudinal moduli of composites, the deflection of the beam due to shear forces may be significant. Although in a rigorous treatment bending and shear cannot be properly considered as separate components (27), it is useful to treat the shear effect separately. Shear strain is accounted for in elementary beam theory with the aid of a shear correction factor. It has been shown (27, 28) that inaccuracies are small if the shear correction coefficient is properly chosen, at least in the region outside the end effect region near the clamped end.

The elastic strain energy of shear therefore is

$$W_s = \frac{1}{k}\int [S(x)^2/2bhE_{st}]dx \qquad (14)$$

where $S(x)$ is the shearing force, E_{st} is the transverse shear modulus, and k is the shear coefficient.

The strain energy in shear, W_s, is calculated from shear force diagrams in different portions of the specimens. The computation shows that W_s is independent of the crack length, a, in both types of initial crack studied.

$$W_s = P^2L/2kbhE_{st}. \qquad (15)$$

Since shearing stresses do not change the energy due to tension or compression, energy due to shear can be added to the amount of energy due to tension and compression in bending. The total strain energy in the free-edge crack specimen therefore is

$$W = [P^2(2L^3 + 6a^3)/E_x^f bh^3] + [P^2L/2kbhE_{st}] \qquad (16)$$

and that of the clamped-edge crack specimen is

$$W' = [P^2(2L^3 + 3a^3/2)/E_x^f bh^3] + [P^2L/2kbhE_{st}]. \qquad (17)$$

The strain energy release rate is subsequently derived from *Eq 1*:

$$G_{II} = 18P^2a^2/E_x^f b^2h^3 \qquad (18)$$

for the free-edge crack specimen and

$$G_{II} = 9P^2a^2/2E_x^f b^2h^3 \qquad (19)$$

for the clamped-edge crack specimen.

EXPERIMENTAL

The experiments were carried out on glass/epoxy laminates. Two stacking sequences were used in this study: a quasi-homogeneous cross-ply laminate and a 28-ply $[90_3/0/90_6/0/90_3]_s$ laminate. The quasi-homogeneous cross-ply laminate was fabricated from a commercially available nonwoven cross-ply prepreg, SCOTCHPLY 1003. Sheets 250 mm by 250 mm were compression molded into different thicknesses and cured in accordance with the manufacturer's recommendations. The $[90_3/0/90_6/0/90_3]_s$ laminate was fabricated from FERRO-PREG CE-9000-9 continuous filament prepreg. The laminate was laid up by hand and fabricated in an autoclave according to the supplier's recommended cure procedures.

Beams 10-mm wide and different lengths were subsequently cut out from these sheets, parallel to the 0 degree direction. All the specimens contained an initial crack at midthickness. The initial crack was made by adding a thin Teflon film 50-μm thick during the prepreg lay-up step. For the quasi-homogeneous cross-ply laminate, the Teflon film was inserted between two adjacent layers of 0 degree fiber orientation. For the $[90_3/0/90_6/0/90_3]_s$ laminate, the crack direction was perpendicular to the main fiber orientation. The initial-crack length of the beams was varied by altering the position of the beam in the sheet. In the case of clamped-edge crack configuration, to prevent slippage between the upper and lower parts, a pin was inserted through the beam thickness at the extremity in the clamped region as shown in *Fig. 4*.

Bending tests were performed on an Instron testing machine, Model 1125. The tests were conducted at ambient temperature and 50% relative humidity, with a crosshead speed of 50 mm/min.

RESULTS AND DISCUSSION

To determine the effective flexural modulus, bending tests were carried out on cantilever beams without initial crack. The effect of shearing force on the flexural rigidity is shown in *Fig. 5* for the quasi-homogeneous cross-ply composite and in *Fig. 6* for the $[90_3/0/90_6/0/90_3]_s$ laminate. The effective flexural modulus was determined from simple beam theory, without accounting for shear effect, and is plotted as a function of the ratio of specimen length to thickness. These figures show that shear effect can be very important. The error due to shear in bending theory decreases when the specimen length is increased. When L/h is larger than about 10 in the case of $[90_3/0/90_6/0/90_3]_s$ and 18 in the case of quasi-homogeneous cross-ply laminates, the shear effect becomes negligible. E_x^f becomes independent of the specimen length.

The shear effect may be accounted for by using shear correction in beam theory as discussed above. From *Eqs 16* and *17*, the compliance of the specimen without initial crack can be obtained:

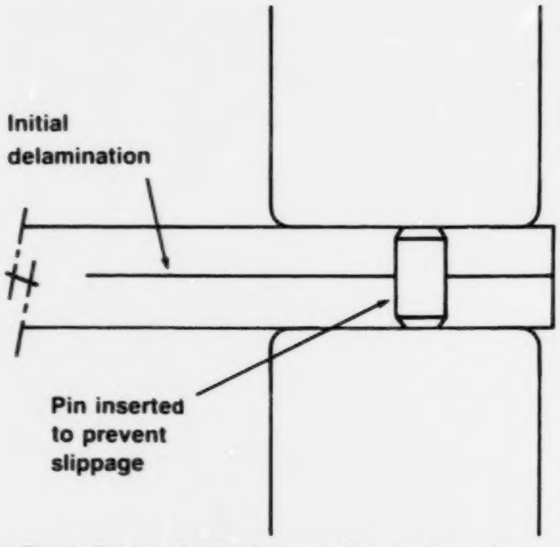

Fig. 4. Pin inserted in clamped-edge crack specimen.

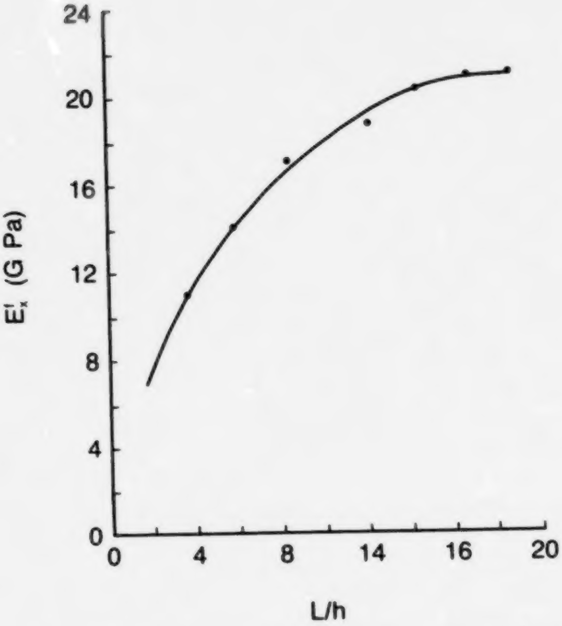

Fig. 5. Shear effect in quasi-homogeneous cross-ply laminate.

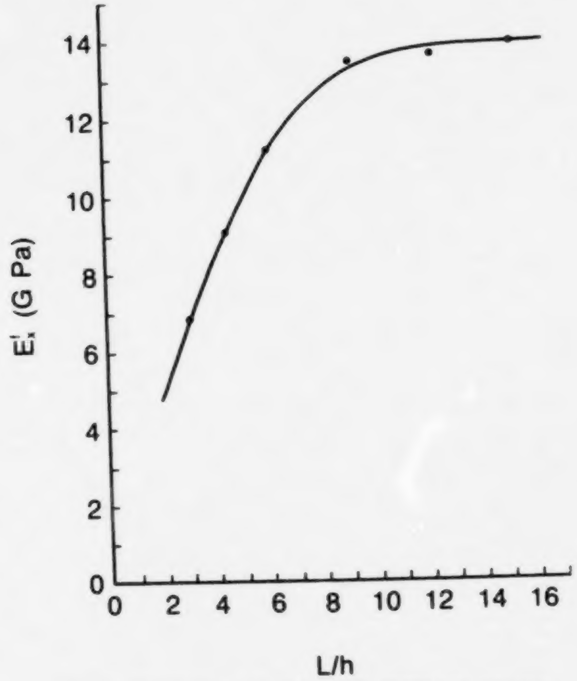

Fig. 6. Shear effect in $[90_3/0/90_6/0/90_3]_s$ laminate.

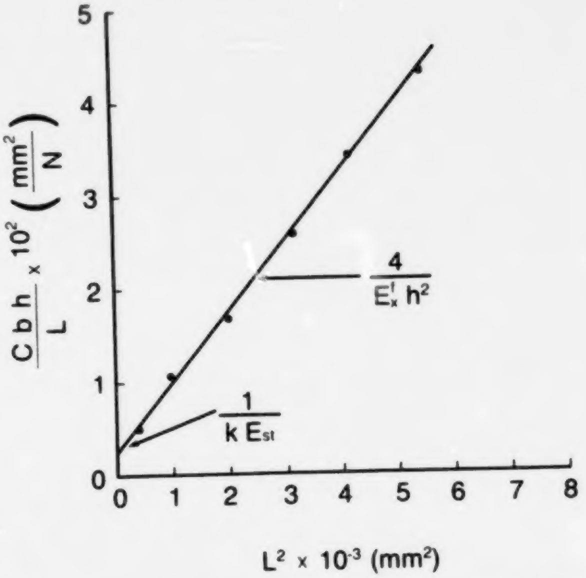

Fig. 7. Determination of effective flexural modulus and transverse shear modulus of quasi-homogeneous cross-ply laminate.

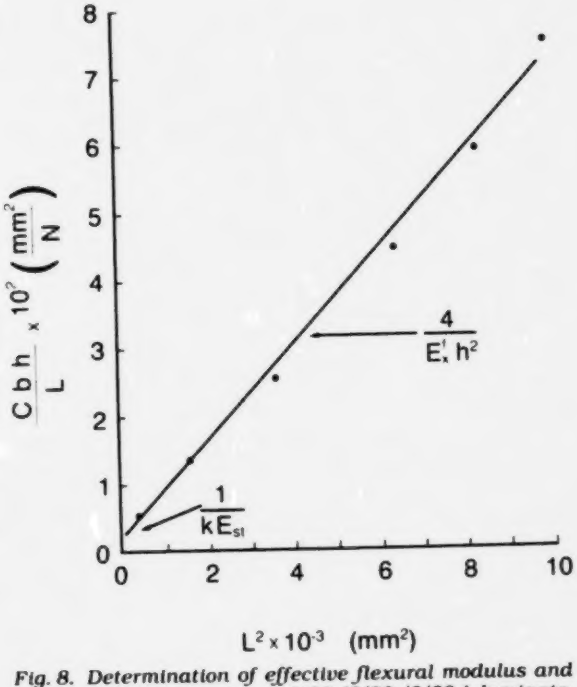

Fig. 8. Determination of effective flexural modulus and transverse shear modulus of $[90_3/0/90_6/0/90_3]_s$ laminate.

$$C = (4L^3/E_x^f bh^3) + (L/kbhE_{st}). \qquad (20)$$

From this equation, the plot of C/L vs. L^2 permits determination of E_x^f and E_{st}. *Figures 7* and *8* show the plots for the cases of quasi-homogeneous cross-ply and $[90_3/0/90_6/0/90_3]_s$ laminates respectively. The linear relationship between C/L and L^2 in these figures demonstrates the validity of shear correction in simple beam theory. From the slope of these curves, the effective flexural modulus can be determined. E_x^f was found to be 22 GPa for the quasi-homogeneous cross-ply laminate and 14 GPa for the $[90_3/0/90_6/0/90_3]_s$ laminate. From the intercept of C/L vs. L^2 curve, the value of kE_{st} can be deduced. The shear coefficient for laminated composites is discussed in *Refs. 29* and *30*. Since k contains also a material property (31), the value of kE_{st}, as determined from the intercept of C/L vs. L^2 curve, was used to calculate the shear effect in the discussion that follows.

To verify the accuracy of the present formulations for the elastic strain energy release rates in the specimens studied, the specimen compliance, derived from *Eqs 16* and *17*, was used for comparison with experimental measurements. It is worth noting that the strain energy release rate, G_{II}, is also directly related to the specimen compliance by

$$G_{II} = (P^2/2b)(dC/da). \tag{21}$$

Figures 9 through *12* show the comparison between the measured compliances and those derived from *Eqs 16* and *17* for two different specimen geometries and for the two studied laminates. Overall, the calculation is in good agreement with experimental measurements. To confirm the accuracy of the calculation based on simple beam theory, the results in the case of quasi-homogeneous cross-ply laminate were also compared with that of finite element analysis. The numerical computation was performed with the aid of the commercial finite element system ANSYS (32). The element used was a three-dimensional reinforced composite (STIF 65). The maximum number of elements was 110. The initial crack in the specimen was simulated by a three-dimensional interface ele-

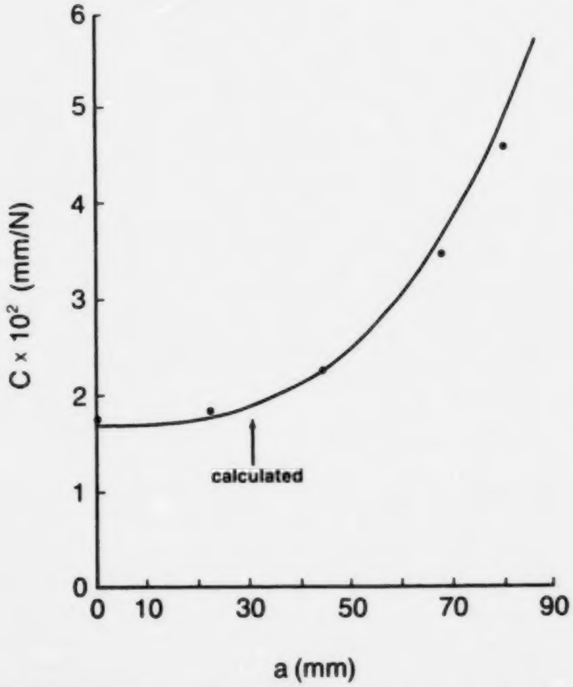

Fig. 9. Measured and calculated compliances of free-edge crack specimen as a function of delamination length (quasi-homogeneous cross-ply laminate, h = 6 mm, b = 10 mm, L = 90 mm).

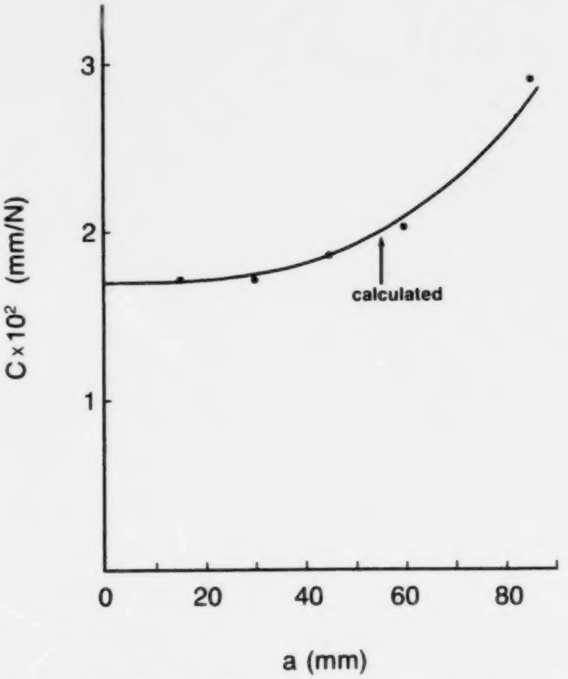

Fig. 10. Measured and calculated compliances of clamped-edge crack specimen as a function of delamination length (quasi-homogeneous cross-ply laminate, h = 6 mm, b = 10 mm, L = 90 mm).

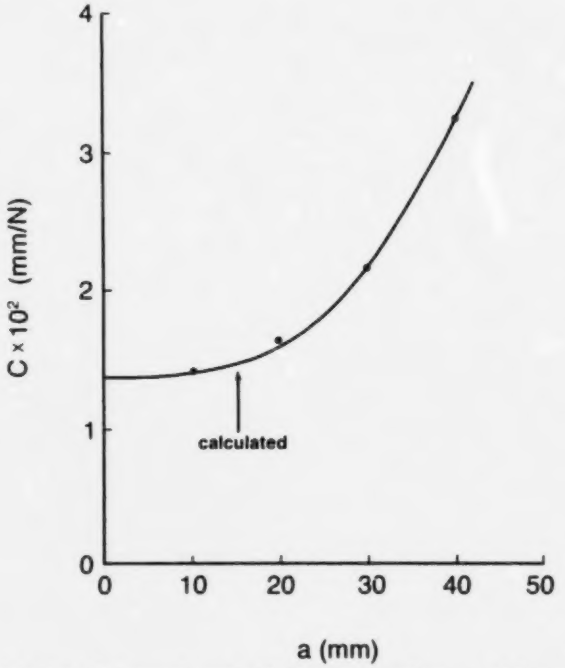

Fig. 11. Measured and calculated compliances of free-edge crack specimen as a function of delamination length ($[90_3/0/90_6/0/90_3]_s$ laminate, h = 7 mm, b = 10 mm, L = 50 mm).

ment (Gap, STIF 52). *Figures 13* and *14* show the comparison between analytical and numerical calculations. These results again confirm the validity of the simple beam theory used for Mode II delamination analysis.

Equations 16 through *19* permit definition of the conditions for stable or unstable delamination growth in Mode II in terms of the load-deflection diagram. Fracture occurs when the strain energy release rate in the specimen reaches a critical value ($G = G_c$). This means, from *Eqs 18* and *19*, that for a given fracture energy of the material G_c, delamination starts to grow at a given load level, P, and consequently at a given deflection, Δ, for each crack length a. The locus of fracture points represents a quasi-static equilibrium of fracture (33, 34) that defines the stable and unstable regions for delamination growth in the specimen. From *Eqs 16* and *18*, the locus of fracture points was computed for an arbitrary value of $G_c = 1$ kJ/m^2 for the case of free-edge crack specimen. The result is shown in *Fig. 15*. The same procedure was repeated using *Eqs 17* and *19* for the case of clamped-edge crack specimen, and the locus of fracture points is shown in *Fig. 16*. The loading paths corresponding to the cases of $a = 0$ and $a = L$ are also shown in these curves. Between these two loading-path limits, fracture occurs at the intersection between a given loading path and the fracture locus. In both cases, under load controlled conditions, delamination is always unstable since the loading path at a constant load level moves into the fracture region when the crack length increases.

Under displacement-controlled conditions, the nature of delamination growth in the two specimens is different. For the case of clamped-edge crack specimen, delamination growth is still unstable through the entire specimen length regardless of initial crack length, since

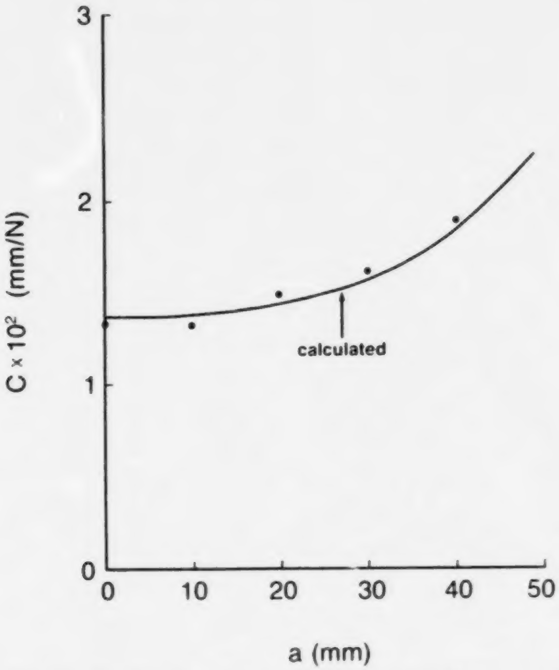

Fig. 12. Measured and calculated compliances of clamped-edge crack specimen as a function of delamination length ([90$_3$/0/90$_6$/0/90$_3$]$_s$ laminate, h = 7 mm, b = 10 mm, L = 50 mm).

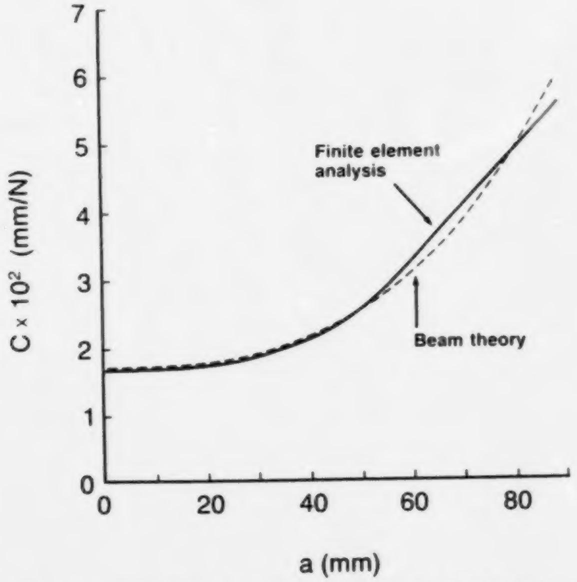

Fig. 13. Comparison between beam theory and finite element analysis in free-edge crack specimen (quasi-homogeneous cross-ply laminate, h = 6 mm, b = 10 mm, L = 90 mm).

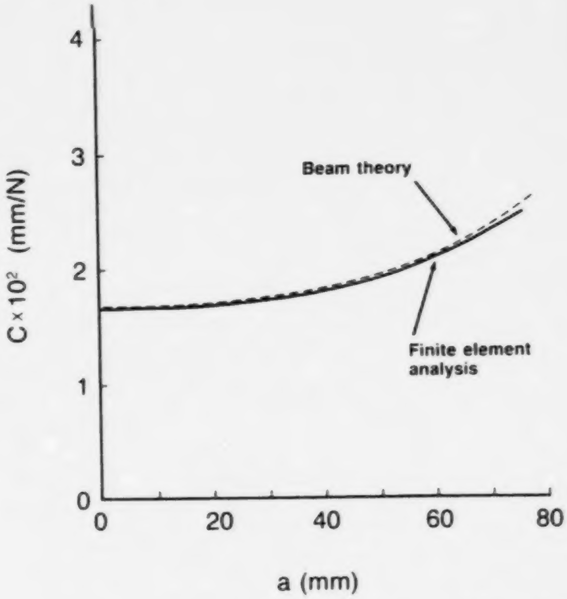

Fig. 14. Comparison between beam theory and finite element analysis in clamped-edge crack specimen (quasi-homogeneous cross-ply laminate, h = 6 mm, b = 10 mm, L = 90 mm).

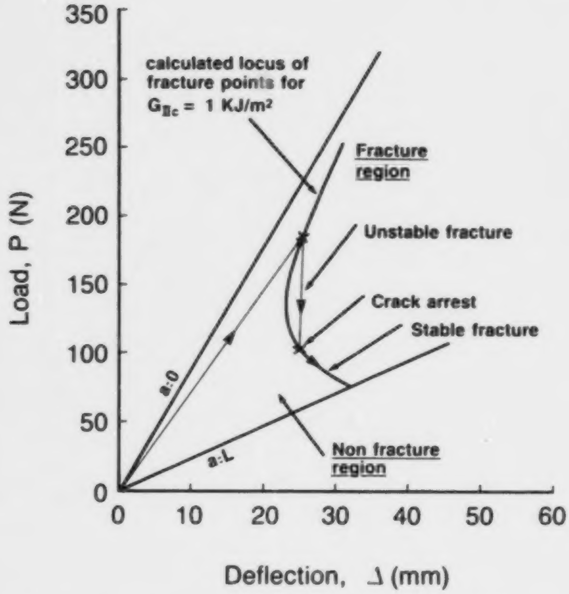

Fig. 15. Locus of fracture points for free-edge crack specimen with $G_{IIc} = 1$ kJ/m² (quasi-homogeneous cross-ply laminate, h = 6 mm, b = 10 mm, L = 90 mm).

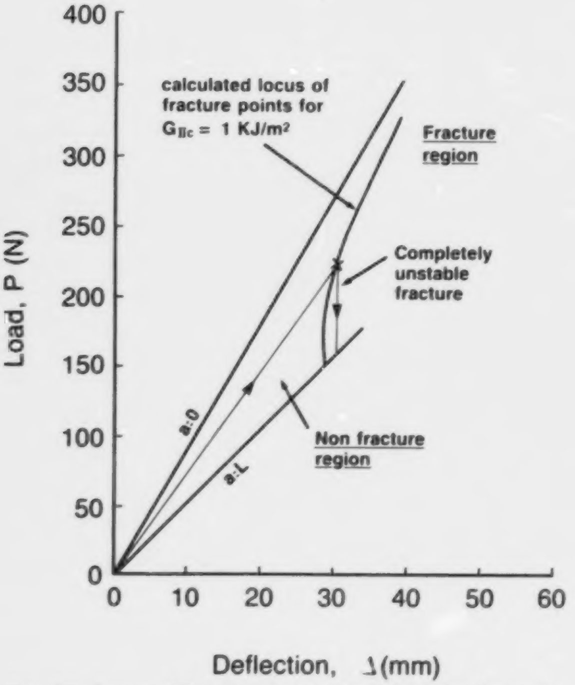

Fig. 16. Locus of fracture points for clamped-edge specimen with $G_{IIc} = 1$ kJ/m² (quasi-homogeneous cross-ply laminate, h = 6 mm, b = 10 mm, L = 90 mm).

the loading path at a constant deflection level is maintained in the fracture region during crack propagation. In the free-edge crack specimen, delamination can grow in an unstable or stable manner, depending on the initial crack length. With a long initial crack, the specimen compliance is large and the loading path meets the locus of fracture points at its lower region. At that point, the crack cannot propagate unless the deflection is increased because the loading path must move along the fracture locus.

With a short initial crack, at fracture point, the crack will propagate at a constant deflection level and will stop when the loading path meets the locus of fracture points at the lower region (*Fig. 15*). The crack will start growing again only if the deflection is increased. This specimen configuration therefore can be used to create an unstable fracture and a subsequent crack-arrest. The arrest toughness then may be determined in the same manner as in the initiation toughness measurement.

The determinations of G_{IIc} at initiation is given in *Figs. 17* and *18* for the $[90_3/0/90_6/0/90_3]_s$ laminate. *Figure 17* shows the plot of P^2 vs. $E^f_x b^2 h^3/18a^2$ for the case of free-edge crack specimen (*Eq 18*) and *Fig. 18* shows the plot of P^2 vs. $2\ E^f_x b^2 h^3/9a^2$ for the case of clamped-edge crack specimen (*Eq 19*). The linear relationship in these plots demonstrates the validity of the G_{II} formulations. Although the clamped-edge crack specimen gives a much more scattered result, the values of G_{IIc} obtained from the slope of these plots are equivalent. They are 0.60 kJ/m² for the case of free-edge crack and 0.63 kJ/m² for the case of clamped-edge crack.

Figure 19 shows the arrest toughness, G_{IIa}, of the $[90_3/0/90_6/0/90_3]_s$ laminate as a function of the crack length at arrest (after unstable

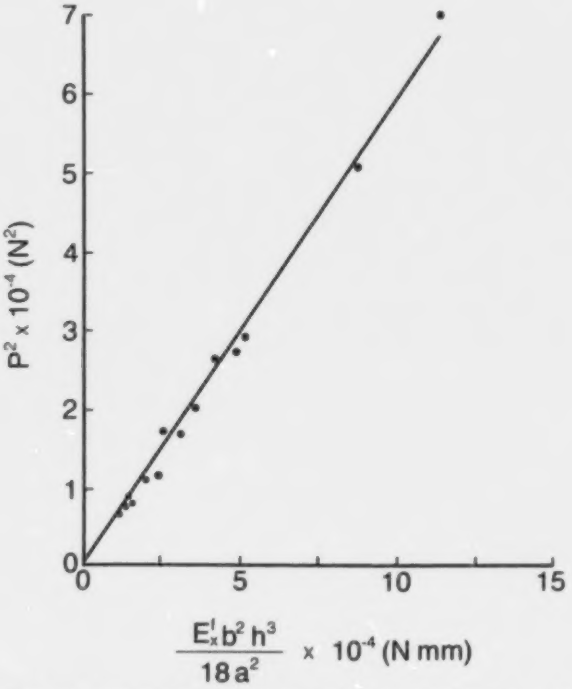

Fig. 17. Determination of initiation toughness (G_{IIc}) of $[90_3/0/90_6/0/90_3]_s$ laminate, with free-edge crack specimens.

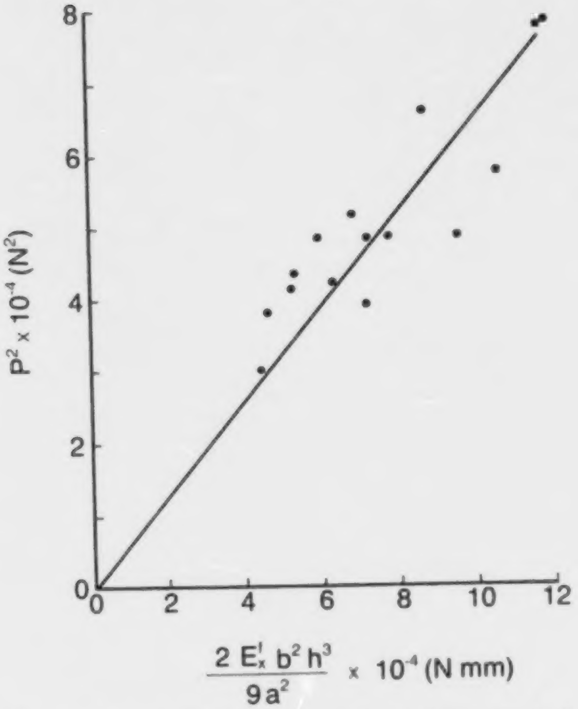

Fig. 18. Determination of initiation toughness (G_{IIc}) of $[90_3/0/90_6/0/90_3]_s$ laminate, with clamped-edge crack specimens.

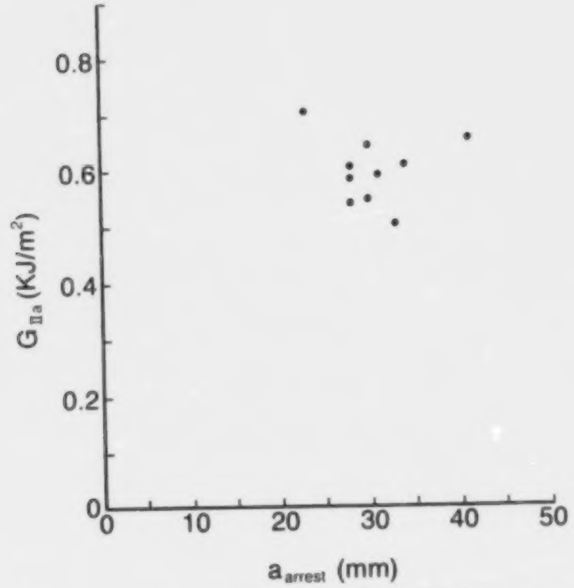

Fig. 19. Arrest toughness (G_{IIa}) in $[90_3/0/90_6/0/90_3]_s$ laminate.

growth). The shear Mode II arrest toughness was found to be equivalent to that at initiation for this laminate. However, the scatter of results was very large, and the control of the distance of unstable crack propagation was difficult. Further experimental data are needed to confirm the validity of this G_{IIa} value as a material characteristic.

SUMMARY AND CONCLUSION

The methodology to measure the arrest toughness in shear Mode II delamination of composites was presented in this study. The analysis of crack propagation was made for the cantilever beam specimen. Two configurations of delamination growth were investigated, embedded delamination and free-edge delamination. By use of simple beam theory, the strain energy available for crack propagation in these samples was calculated. The calculation results were in good agreement with experimental measurement and finite element analysis.

The calculated equilibrium of quasi-static fracture indicated that crack-arrest cannot occur in the clamped-edge crack specimen. Either under controlled load or controlled deflection conditions, after the initiation point, the strain energy release rate is large enough to make the crack propagate unstably through the entire length of the specimen. However, in the free-edge crack specimen, with appropriate initial crack lengths, unstable crack growth and subsequent crack-arrest can be created.

Measurements with both types of specimen give the same value of the shear Mode II delamination toughness. The measurement of the crack-arrest toughness in the $[90_3/0/90_6/0/90_3]_s$ glass/epoxy laminate showed that the arrest toughness value, G_{IIa} is equivalent to that at initiation. This is rather surprising because the arrest toughness represents the dynamic behavior of the material with a fast running crack. Measurements in Mode I crack propagation in both metals and plastics (22, 24, 35, 36) suggested that fracture energy during unstable, fast crack growth is much lower than that at initiation and during stable propagation. The arrest toughness found in this study suggests that the fracture energy of the material in shear Mode II delamination is not time dependent. This point needs to be elucidated by further investigation.

ACKNOWLEDGMENTS

This work is part of a joint project between the Industrial Materials Research Institute and Bell Helicopter Textron, a division of Textron Canada Ltd. The help of Miss M. Plourde in performing experimental tests is gratefully acknowledged.

NOMENCLATURE

a = crack length.
a_o = initial crack length.
a_{arrest} = crack length at arrest.
A = crack surface.
b = specimen width.
C = specimen compliance.
d_{ij} = flexural compliance tensor.

E_x^f = effective flexural modulus.
E_{st} = transverse shear modulus.
F = resultant force.
G = energy release rate per unit crack area.
G_{II} = G in shear Mode II.
G_{IIc} = value of G_{II} at crack initiation.
G_{IIa} = value of G_{II} at crack arrest.
h = specimen thickness.
k_i = curvature component.
L = specimen length.
M = resultant moment.
P = external load.
Q_{ij} = in-plane stiffness tensor.
v = volume.
W = strain energy.
$\left.\begin{array}{l}x\\y\\z\end{array}\right\}$ Cartesian coordinates.
ϵ = *strain.*
σ = *stress.*

REFERENCES

1. A. H. Puppo and H. A. Evensen, *J. Compos. Mater.*, **4**, 204 (1970).
2. R. B. Pipes and N. J. Pagano, *J. Compos. Mater.*, **4**, 538 (1970).
3. N. J. Pagano and R. B. Pipes, *J. Compos. Mater.*, **5**, 50 (1971).
4. J. M. Whitney, "Free-Edge Effect in the Characterization of Composite Materials," in "Analysis of the Test Methods for High Modulus Fibers and Composites," ASTM STP 521, J. M. Whitney, ed., p. 167 American Society for Testing and Materials, Philadelphia (1973).
5. R. B. Pipes, B. E. Kaminski, and N. J. Pagano, "Influence of the Free Edge upon the Strength of Angle-Ply Laminates," in "Analysis of the Test Methods for High Modulus Fibers and Composites," ASTM STP 521, J. M. Whitney, ed., p. 218 American Society for Testing and Materials, Philadelphia (1973).
6. N. J. Pagano, *J. Compos. Mater.*, **8**, 65 (1974).
7. A. S. D. Wang and F. W. Crossman, *J. Compos. Mater.*, **11**, 92 (1977).
8. J. T. S. Wang and J. N. Dixon, *J. Compos. Mater.*, **12**, 390 (1978).
9. R. R. Valisetty and L. W. Rehfield, "A New Ply Model for Interlaminar Stress Analysis," in "Delamination and Debonding of Materials," ASTM STP 876, W. S. Johnson, ed., p. 52 American Society for Testing and Materials, Philadelphia (1985).
10. J. M. Scott and D. C. Phillips, *J. Mater. Sci.*, **10**, 551 (1975).
11. F. X. de Charentenay, M. Bethmont, M. Benzeggagh, and J. F. Chrétien, in "Mechanical Behavior of Materials" (ICM 3), K. J. Miller and R. F. Smith, eds., Vol. 3, p. 241 (1979).
12. F. X. de Charentenay and M. Benzeggagh, in 4th Int. Conf. Comp. Mater., A. R. Bunsell, ed., Vol. 1, p. 186 (1980).
13. D. J. Wilkins, J. R. Eisenmann, R. A. Camin, W. S. Margolis, and R. A. Benson, in "Damage in Composite Materials," ASTM STP 775, K. L. Reifsnider, ed., p. 168 American Society for Testing and Materials, Philadelphia (1982).
14. A. J. Russell and K. N. Street, in "Progress in Science and Engineering of Composites" (ICCM IV), T. Hayashi, K. Kawata, and S. Umekawa, eds., p. 279 Japan Society for Composite Materials, Tokyo (1982).
15. F. X. de Charentenay, J. M. Harry, Y. J. Prel, and M. L. Benzeggagh, in "Effect of Defect in Composite Materials," ASTM STP 836, D. J. Wilkins, ed., p. 84 American Society for Testing and Materials, Philadelphia (1984).
16. A. S. D. Wang and F. W. Crossman, *J. Compos. Mater.*, **14**, 71 (1980).
17. S. S. Wang, *J. Compos. Mater.*, **17**, 210 (1983).
18. J. D. Whitcomb and I. S. Raju, "Analysis of Interlaminar Stresses in Thick Composite Laminates With and Without Edge Delamination," in "Delamination and Debonding of Material," ASTM STP 876, W. S. Johnson, ed., p. 69 American Society for Testing and Materials, Philadelphia (1985).
19. C. Bathias and A. Laksimi, "Delamination Threshold and Loading Effect in Fiber Glass Epoxy Composite," in "Delamination and Debonding of Materials," ASTM STP 876, W. S. Johnson, ed., p. 217 American Society for Testing Materials, Philadelphia (1985).
20. A. J. Russell and K. N. Street, in "Delamination and Debonding of Materials," ASTM STP 876, W. S. Johnson, ed., p. 349 American Society for Testing Materials, Philadelphia (1985).
21. E. A. Armanios, L. W. Rehfield, and A. D. Reddy, in "Composite Materials: Testing and Design," ASTM STP 893, J. M. Whitney, ed., p. 232 American Society for Testing Materials, Philadelphia (1986).
22. P. B. Crosby and E. J. Ripling, in "Fast Fracture and Crack Arrest," ASTM STP 627, G. T. Hahn and M. F. Kanninen, eds., p. 203 American Society for Testing Materials, Philadelphia (1977).
23. P. B. Crosley and E. J. Ripling, in "Fast Fracture and Crack Arrest," ASTM STP 627, G. T. Hahn and M. F. Kanninen, eds., p. 372 American Society for Testing Materials, Philadelphia (1977).
24. J. F. Kalthoff, J. Beinert, S. Winkler, and W. Klemm, in "Crack Arrest Methodology and Applications," ASTM STP 711, G. T. Hahn and M. F. Kanninen, eds., p. 109 American Society for Testing Materials, Philadelphia (1980).
25. J. G. Williams, "Fracture Mechanics of Polymers," Ch. 2, Ellis Horwood Ltd., Chichester, England (1984).
26. R. M. Jones, "Mechanisms of Composite Materials," Ch. 5, Scripta Book Company, Washington, D.C. (1975).
27. P. E. Sandorff, *J. Compos. Mater.*, **14**, 199 (1980).
28. T. R. Tauchert, *J. Compos. Mater.*, **9**, 207 (1975).
29. G. R. Cowper, *J. Appl. Mech.*, **33**, 335 (1966).
30. M. Z. Hu, H. Kolsky, and A. C. Pipkin, *J. Compos. Mater.*, **19**, 235 (1985).
31. S. Dharmarajan and H. McCutchen, Jr., *J. Compos. Mater.*, **7**, 530 (1973).
32. P. C. Kohuke, "Engineering Analysis System Theoretical Manual," Swanson Analysis System Inc., Houston (1983).
33. J. P. Berry, *J. Mech. Phys. Solids*, **8**, 194 (1960).
34. J. P. Berry, *J. Mech. Phys. Solids*, **8**, 207 (1960).
35. T. Vu-Khanh and F. X. de Charentenay, *Polym. Eng. Sci.*, **25**, 841 (1985).
36. T. Vu-Khanh, B. Sanschagrin, and B. Fisa, *Polym. Compos.*, **6**, 249 (1985).

DISCUSSION

A. J. Russell: In that cross-play laminate, was the delamination growing between two 90-degree plies?

T. Vu-Khanh: The initial delamination was created between two 90-degree plies but the crack jumped and propagated between 0 and 90 degrees.

L. A. Utracki: How did you calculate the locus of initiation curves both for the free and clamped edge? In *Fig. 15* of your preprint there are two points marked by *x*. Were these measured, calculated, or are they marked only for discussion purpose?

T. Vu-Khanh: The curve is theoretical, calculated from the unique relationship of the energy release rate, from the relation between compliance and deflection, *Eqs 16* through *19* in the text. The x-points represent the situation where the loading path crosses the fracture point. In the case of free edge the crack must stop when it meets the other part of the curve. They are experimental; only the locus of fracture points is theoretical.

A. Moet: Two questions about the same figure. You made these calculations assuming that the fracture energy is constant at 1 kJ/m^2. However, your data scatter so much that it could be half or twice this equally well. How would this affect your prediction?

T. Vu-Khanh: The intercept would only move to a lower load level, but the physical phenomenon would remain the same. The curve should be treated as a zone, not as a mathematical line.

A. Moet: The second question. The calculation was done for a straight crack, but in your own experiment, the crack jumped from one to another location. How does that affect the prediction?

T. Vu-Khanh: It should slightly affect the value of strain energy, but by how much I did not calculate as yet.

L. A. Utracki: If, as you said, the experimental points agree so well with the theory, the calculated deviation has to be indeed small.

Micromechanisms of Interlaminar Fracture and Fatigue

ALAN J. RUSSELL

Defence Research Establishment Pacific
Victoria, B.C., Canada V0S 1B0

The interlaminar fracture and fatigue properties of AS/3501-6 graphite/epoxy are discussed from a mechanistic point of view. Particular emphasis is placed on the interaction between the loading mode and the local geometry of the interlaminar zone and on how this affects the stresses close to the crack tip and the resulting failure path. Delamination growth under Mode I loading is shown to depend on the likelihood of fiber bridging occurring and on how effective these bridged fibers are at diverting strain energy away from the crack tip. The Mode II behavior is controlled by both the work required to shear the fibers from the matrix and the ease with which tensile failure of the matrix between the fibers can occur.

INTRODUCTION

One of the major limitations of the first generation of aerospace graphite/epoxy composite materials is the low fracture energy of the matrix. In structural applications, this manifests itself in a poor resistance to impact damage and in a low tolerance to delaminations. As a result, major efforts are presently under way both in resin chemistry to improve matrix toughness and in manufacturing technology to produce advanced composite structures with three-dimensional fiber reinforcement. For the user of the current materials, however, the delamination problem is limited to the need to assess defect criticality and predict fatigue crack growth rates so that appropriate repairs can be made in a timely manner. One approach to this requirement has been the development of a fracture mechanics methodology based on the strain energy release rate, G (1–3). An essential part of this work has been the generation of a material data base of fracture and fatigue properties for both tensile (Mode I) and shear (Mode II) loaded delaminations. This has required the development of novel test specimens and test procedures, particularly in the case of shear loading where few specimens existed and none was suited to thin laminates.

Although there have been numerous studies of the micromechanics of composite fracture both parallel and perpendicular to the fibers, this is not the case for delamination, where until recently relatively little work had been reported (4–6). In this paper, some previously reported results (7–10) showing the effects of temperature and moisture absorption on Hercules AS/3501-6 graphite/epoxy, along with some new results on the effect of fiber volume fraction, will be discussed from a mechanistic viewpoint with the aim of improving our understanding of the failure process. A detailed examination of the fractures surfaces also will help to clarify the precise location of the fracture path within the interlaminar zone as well as give an indication of the relative importance of the different energy-absorbing mechanisms such as matrix fracture, fiber/matrix debonding, and fiber breakage.

MODE I VS. MODE II LOADING

One of the most important findings concerning the delamination of brittle matrix composites such as AS/3501-6 is that the fracture energy is several times greater in Mode II than in Mode I (7, 8). This is shown in *Fig. 1* as a function of temperature and moisture content. It is somewhat surprising that hot/wet conditions should lead to an increase in G_{Ic} and, at the same time, to a marked reduction in G_{IIc}. Evidently, the softening of the matrix and the relaxation of the curing stresses that occur as the temperature and moisture content are raised have opposite effects depending on the nature of the loading. Similar data have been reported by Law and Wilkins (11).

Another major difference between tensile and shear loadings is that the resistance to fracture increases as the delamination extends under predominantly Mode I loading, but remains constant when Mode II dominates (8). The Mode I increase is caused by fiber bridging (7, 12), which occurs when the delamination fractures around a fiber, leaving it to bridge the gap between the fracture faces. As the crack contin-

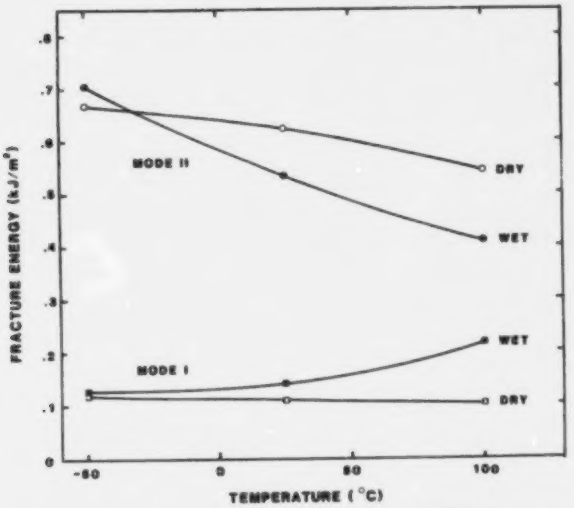

Fig. 1. Effect of temperature and moisture content on G_{Ic} and G_{IIc}. Each data point is the average of at least five measurements.

ues to advance, the gap widens and the bridged fiber becomes strained thereby diverting some of the available strain energy away from the crack tip. Previous work (13) has shown that a fracture model proposed by Wu (14) can correctly predict whether or not fiber bridging will occur for a given mixed-mode loading.

In *Fig. 2*, which shows the transition from a Mode I precrack to a Mode II fracture, it is apparent that the shear loading shifts the fracture path to one side of the matrix layer resulting in failure on or close to the fiber-matrix interface. Thus, in both modes of fracture, the fibers are directly involved in the failure process, and it is insufficient to think of delamination as simply the tensile or shear failure of a constrained layer of matrix. Instead, it is necessary to look in detail at the distribution of fibers and matrix within the interlaminar zone.

INTERLAMINAR ZONE GEOMETRY

Many factors influence the local geometry of the interlaminar matrix layer and, hence, have a direct effect on the fracture path of the delamination. These include the uniformity and resin content of the prepreg, the presence of stray fibers on the prepreg surface, the laminate stacking sequence, and the amount of resin bleed during curing. Of these, changing the number of bleeder plys is the easiest to accomplish, and the effect of this on the fiber distribution at the ply boundaries is shown in *Fig. 3* for four unidirectional laminates. An estimate of the thickness of the interlaminar matrix layer was made by comparing the areal density of fibers across the ply boundary with the density within the plys and attributing all of the missing fibers to a fiber-free zone of thickness, t_m. Despite this definition of t_m, it is important to note from *Fig. 3* that the interlaminar zone is by no means free of fibers. The average fiber volume fraction of the laminate, V_f, was also measured by an optical method (15), and both parameters are plotted against the bleeder ply to prepreg ply ratio in *Fig. 4*.

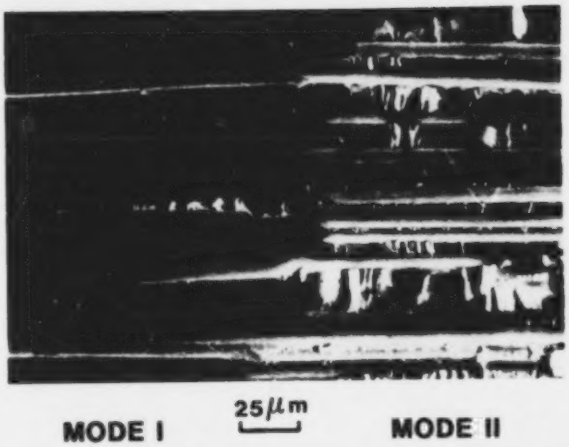

Fig. 2. Transition zone from a Mode I precrack to Mode II delamination.

Unidirectional laminates are generally used for measuring interlaminar fracture energies (with the exception of edge delamination), because they avoid the problem of transverse cracking and of the delamination leaving its initial plane. However, they have the disadvantage that the ply boundaries do not remain flat. This problem can be overcome by sandwiching the two 0-degree plys containing the delamination between two 90-degree plys in a cross-ply laminate as shown in *Fig. 5*. Values of t_m and V_f for the cross-ply laminate are also included in *Fig. 4*. The t_m value of the cross-ply laminate is less than that of the equivalently bled unidirectional laminate because the fibers do not nest together as well at the 0/90 interfaces. More resin is therefore required to fill the spaces between the 0-degree and 90-degree plys, leaving less for the 0/0 interface.

EXPERIMENTAL

The AS/3501-6 laminates were laid up by hand, autoclave-cured according to the manufacturer's recommended cure cycle, and then given an additional postcure of 8 h at 177°C. The laminates were all nominally 3-mm thick and void-free although the number of plys varied from 20 to 26 and the number of bleeder plys ranged from 1 to 15, depending on the fiber volume fraction required. Inserts of Teflon-coated glass fabric, 25-µm thick, were inserted between the two center plys of the laminates during lay-up to act as crack starters. Specimens to be tested dry were kept in a desiccator following postcure, while those to be tested wet were moisturized in distilled water at 75°C until saturation was achieved.

All of the specimen geometries and test pro-

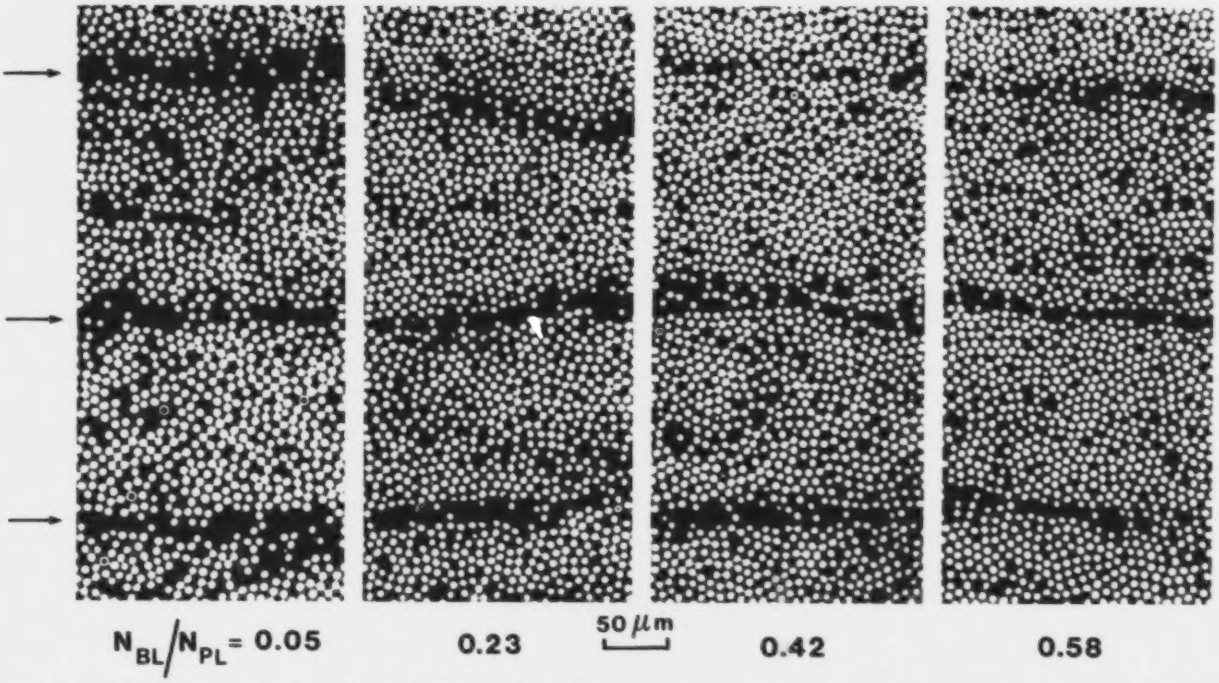

Fig. 3. Effect of bleeder ply/prepreg ply ratio (N_{BL}/N_{PL}) on the ply boundaries (indicated by arrows). Transverse sections through unidirectional lay-ups used for R-curves.

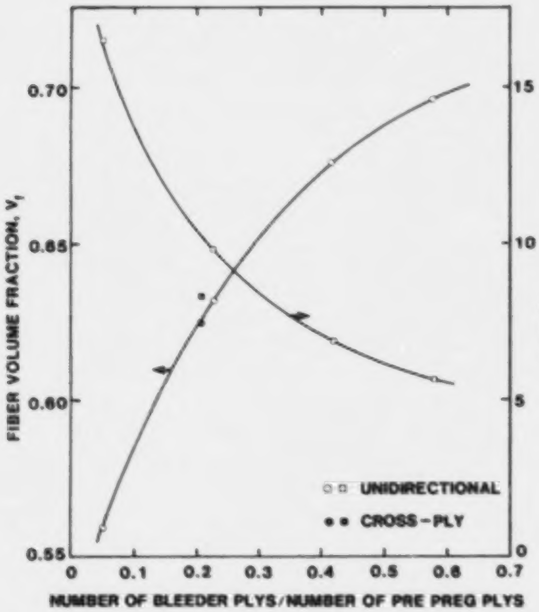

Fig. 4. Variation in V_f and t_m as a function of resin bleed.

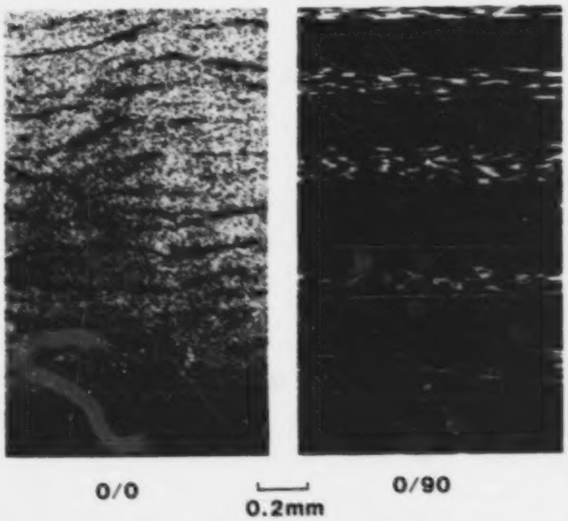

Fig. 5. Transverse section through the unidirectional and cross-ply laminates used for Mode I fatigue tests.

cedures have been described previously (8–10). All of the fracture specimens were 20-mm wide, 150-mm long, and had the delamination located at one end. The Mode I static tests were run directly on double cantilever beam (DCB) specimens having an initial crack length of 50 mm (8). Mode I fatigue testing was carried out under constant ΔG conditions so that any decrease in the fatigue crack growth rate resulting from fiber bridging would not be obscured by the effect of a changing ΔG. This was achieved by loading DCB specimens in series with an elastic spring under constant amplitude (10). The effect of the spring was to increase the compliance of the system, thereby reducing the load drop-off that accompanies crack growth in the DCB specimen. By carefully selecting the spring compliance and by making small periodic adjustments to the fatigue amplitude, it was possible to maintain ΔG constant.

End notched flexure (ENF) specimens having a total span of 100 mm and an initial crack length of 25 mm were used for the Mode II static tests (8). These specimens were precracked by clamping the specimen 2 mm beyond the end of the insert and wedging the crack open. Mode II fatigue tests were carried out on end notched cantilever beam (ENCB) specimens having a total span of 100 mm and an initial crack length of 30 mm (9). For all specimens, an expression for the compliance was derived from beam theory and verified experimentally by measuring the specimen compliance as a function of crack length. The strain energy release rate was then calculated from the relationship

$$G = \frac{P^2}{2b} \cdot \frac{dC}{da}$$

where P is the load, C the compliance, b the width, and a the crack length. Interlaminar shear strength was measured with four-point shear specimens as described by Browning, *et al.* (16).

RESULTS AND DISCUSSION

Mode I Static

Figure 6 shows examples of the Mode I resistance curves or R-curves (G_{IR} vs. crack growth) for the five laminates tested. In all cases, the fracture energy for initiation from the end of the insert, G_{Ic}, had a value close to 110 J/m^2 independent of the fiber volume fraction. For the unidirectional specimens, the fracture resistance was observed to increase linearly with crack growth over the initial 5 to 10 mm of delamination extension with the slope increasing with increasing V_f. Thereafter, the curves flattened out with the final values of G_{IR} being greater the higher the value of V_f. The fracture resistance of the cross-ply laminate also increased linearly at first, but after 6 mm, delamination growth became unstable and proceeded in a slip/stick fashion with regions of fast crack growth alternating with short increments of slow crack growth and load buildup.

The independence of G_{Ic} with V_f is consistent with findings that the Mode I critical fracture energy is simply equal to that of the matrix provided that the "plastic" zone size is not significantly affected by the presence of the fibers (17). It is intuitive that the closer the plys nest together the more likely fiber bridging will become and, hence, the greater the resulting fracture resistance. One method of measuring the extent of fiber bridging directly is to count the number of fiber ends, n_e on the fracture surface assuming that each fiber is eventually strained to failure. *Figure 7*, in which n_e is plotted against t_m, shows that fiber bridging does indeed increase as the plys are forced closer together. However, as shown by *Fig. 8*, the increase in fiber bridgings at the crack tip is not in itself sufficient to account for the increase in fracture resistance due to fiber bridging, G_{BR} ($=G_{IR} - G_{Ic}$). Clearly, the energy-absorbing ca-

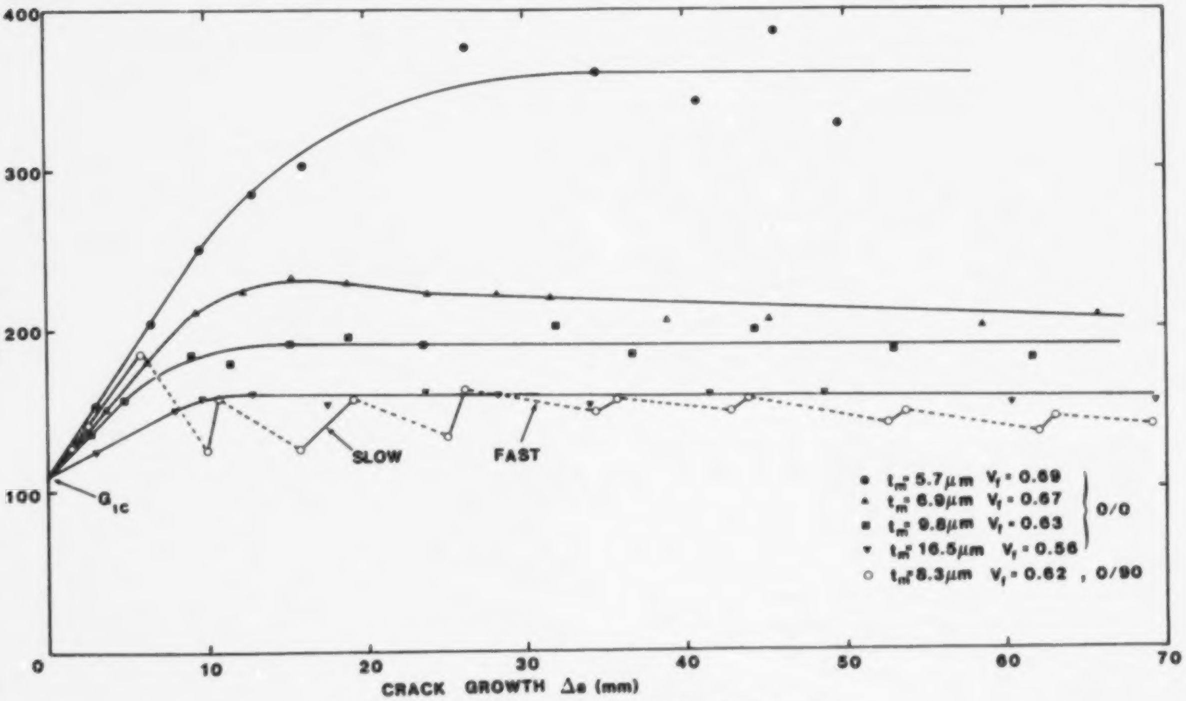

Fig. 6. Representative examples of Mode I R-curves.

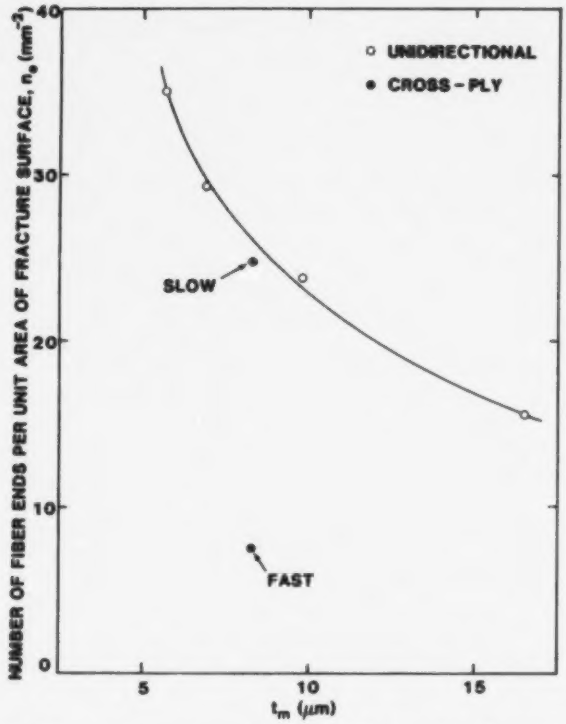

Fig. 7. Variation in areal density of fiber ends on fracture surface at Δa = 25 mm as a function of t_m.

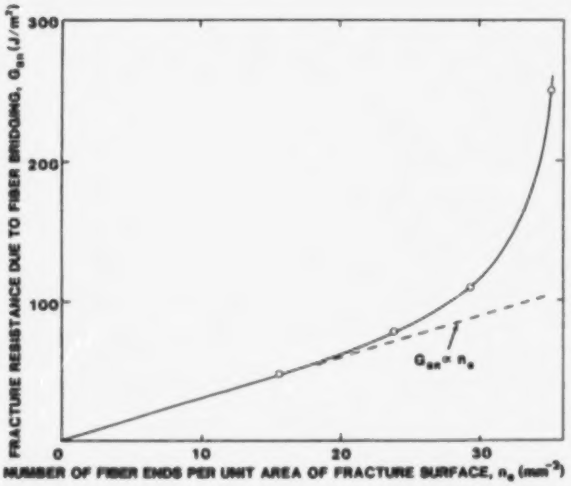

Fig. 8. Relationship between fracture resistance resulting from fiber bridging and the areal density of broken fiber ends on the fracture surface.

pacity of each bridged fiber also must be increasing.

Although several possible energy-absorbing mechanisms may be associated with fiber bridging, including debonding, two are by far the most important. These are matrix fracture, which takes place when the strain in the fiber peels it from the surface, and stored elastic energy, which is lost when the fiber breaks. Both of these energy contributions are proportional to the average free length of the bridged fibers at fracture, d_f. Evidence that d_f increases with decreasing t_m can be inferred from the shape of the R-curves. The leveling of the R-curves, which occurs as soon as the rate of bridged fiber fracture equals the rate of fiber bridging, can take place only after all of the initially bridged fibers fail. It is clear from *Figure 6* that it takes longer for this to happen as t_m becomes smaller and, therefore, d_f must increase. Presumably, as the thickness of the matrix layer decreases, it becomes easier for the fibers to peel from the surface and, hence, they persist longer before they fracture.

The slip/stick behavior of the cross-ply laminate demonstrates that t_m is not the only geometric factor influencing the Mode I fracture resistance. However, it is not obvious why reducing the ply waviness should result in unstable crack growth. One clue is given by the low number of broken fiber ends on the fast fracture surface as plotted in *Fig. 7*. Johnson and Mangalgiri (18) have suggested that fiber bridging occurs when areas of weakness on the opposite side of a fiber open up and grow as a result of the tensile strains ahead of the advancing crack tip. Such weaknesses can arise from microvoids, poor bonding at the fiber-matrix interface, or simply as microcracks within the matrix itself. For these defects to take over from the crack tip, they must not only extend forward but also fracture must occur around the fiber so that the new crack tip can open fully. During unstable crack growth less time will be available for this to happen, thereby reducing the likelihood of fiber bridging. Although this helps to explain the existence of sustained increments of rapid fracture, it does not account for the initial departure from slow stable crack growth after 6 mm of delamination extension.

Mode I Fatigue

Mode I interlaminar fatigue tests were carried out on a high fiber volume fraction unidirectional AS/3501-6 laminate (t_m = 5.5 μm) and a low fiber volume fraction cross-ply laminate (t_m = 12.7 μm). Extensive fiber bridging was observed for both lay-ups together with a rapid reduction in fatigue crack growth rate, da/dN, as the delamination extended. However, the effect of fiber bridging was different for the two laminates and also depended on the ΔG value as can be seen in *Fig. 9*. At high values of ΔG, da/dN was initially lower and dropped off more rapidly in the unidirectional laminate, which is consistent with more fiber bridging resulting from the lower value of t_m. However, at lower values of ΔG, da/dN dropped off faster in the cross-ply laminate. A possible explanation is that although there were fewer bridged fibers in the cross-ply laminate (as indicated by the greater initial crack growth rate), they were more deeply embedded in the matrix layer making it difficult for them to be peeled from the surface at the low ΔG values. As a result, they had a greater capacity for diverting the available strain energy away from the crack tip. This is shown schematically in *Fig. 10.*

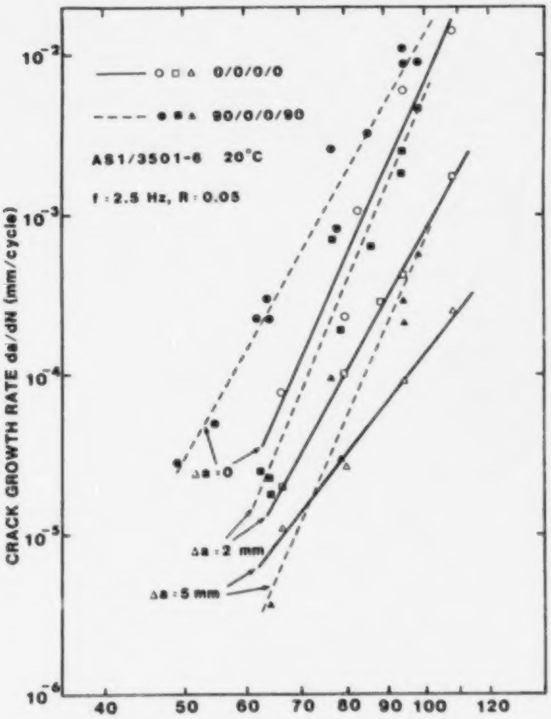

Fig. 9. Mode I da/dN vs. ΔG plots for unidirectional and cross-ply laminates at crack growth increments, Δa of 0, 2, and 5 mm.

Mode II Static

Figure 11 shows the effect of changing the thickness of the interlaminar zone on the Mode II fracture energy at −50°C and at 100°C. At both temperatures, G_{IIc} increases linearly with t_m. *Figure 11* also shows that the interlaminar shear strength is unaffected by t_m, indicating that the quality of the laminates was not degraded by varying the resin bleed. To understand the dependency of G_{IIc} on t_m as well as the

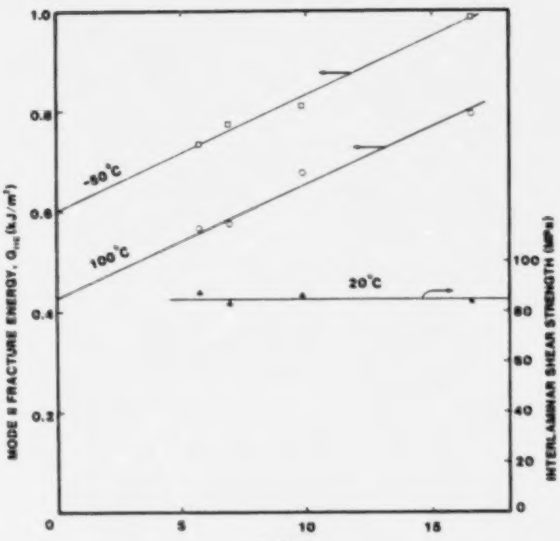

Fig. 11. Effect of t_m on the Mode II fracture energy at −50°C and 100°C and on the interlaminar shear strength at room temperature. Each data point is the average of at least five measurements.

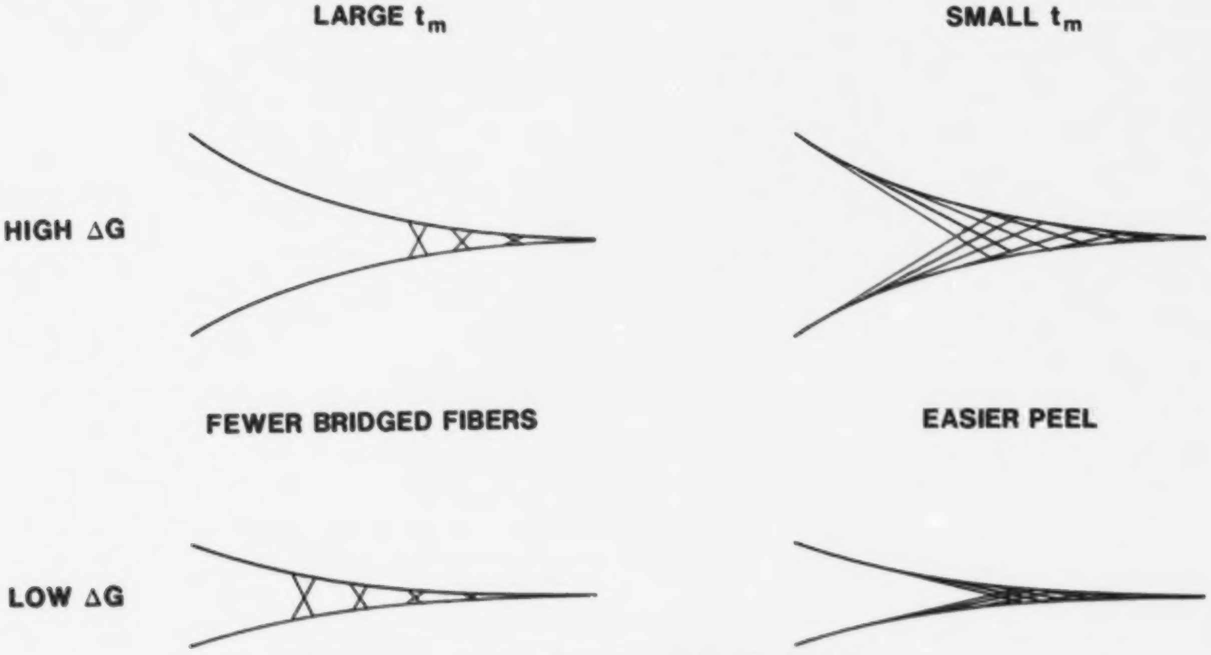

Fig. 10. Effect of t_m and ΔG on distribution of bridged fibers.

reason that the fracture energy for Mode II is several times greater than for Mode I, it is instructive to look at the fracture surfaces. *Figure 12* shows the matching faces of a shear mode fracture of a unidirectional laminate. The following features are of interest:

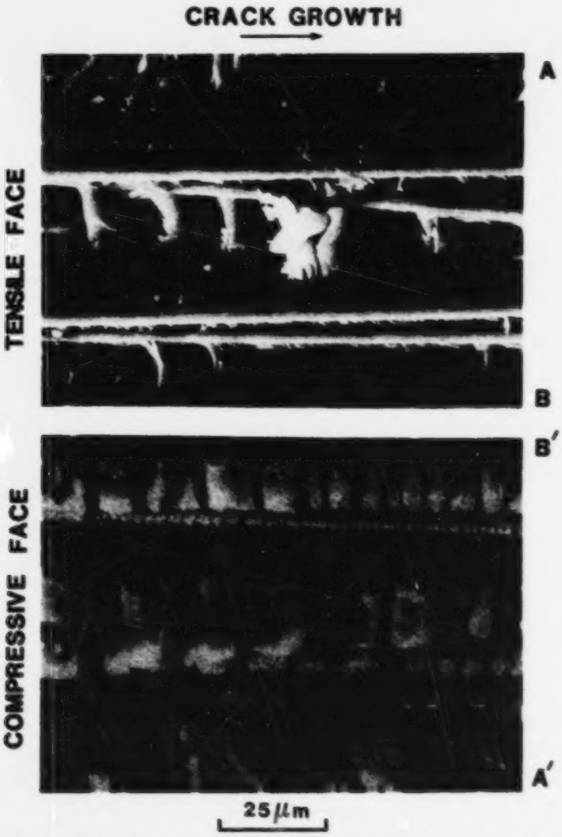

Fig. 12. Matching fractographs from opposite faces of a Mode II delamination. Arrows show examples of matrix fracture initiated along the edges of the hackles.

1. The compressive face contains predominantly fiber shear-out grooves, whereas the tensile face contains the mating fibers indicating that the fracture path is along the tensile side of the interlaminar matrix layer (see below for definition of tensile and compressive faces).
2. The matrix between the fiber shear-out grooves has failed in a series of parallel cracks known as hackles, transverse to the fibers and inclined at an angle to the interlaminar plane.

The origin of the hackles can be understood by considering the two-dimensional model shown in *Fig. 13* in which a thin layer of matrix of thickness t_m is sandwiched between two "fiber" layers of thickness t_f. To the left of the matrix, the upper fiber layer is subject to a tensile strain, ϵ_f, and will be referred to as the tensile side or face of the delamination. The lower layer is subject to a compressive strain, $-\epsilon_f$, and will be referred to as the compressive face. Shear transfer through the matrix results in a gradual decay in the fiber layer strains, while the resulting matrix shear strain can be resolved into a normal tensile strain and a normal compressive strain at an angle of 45 degrees to the plane as shown in *Fig. 14*. A close look at *Fig. 2* indicates that the initiation of matrix fracture under Mode II loading does indeed occur normal to the resolved tensile strain. Moreover, it has been shown (*Ref. 19, Eq 52*) that the shear stress is proportional to $1/\sqrt{t_m}$ and, hence, increasing the thickness of the interlaminar matrix layer will reduce the matrix strain, requiring a greater strain energy release rate to initiate fracture, in agreement with the data of *Fig. 11*.

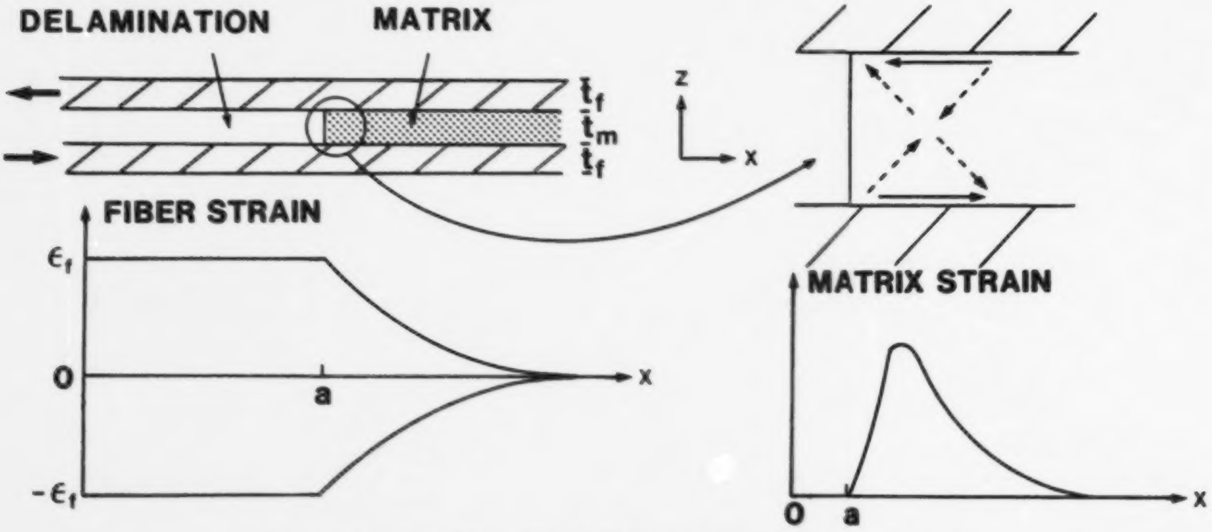

Fig. 13. Two-dimensional model of shear deformation at the crack tip.

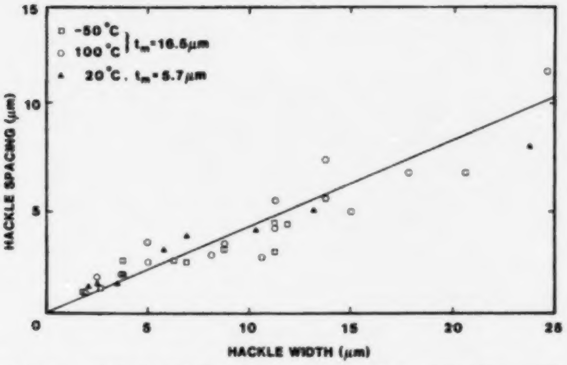

Fig. 14. Relationship between hackle spacing and hackle width.

After the first matrix crack has arrested, subsequent parallel cracks must initiate within the matrix presumably at a location of maximum tensile strain. From *Fig. 12* it appears that this occurs on the tensile side of the interlaminar matrix layer adjacent to the fibers. However, if the first crack to form lies too close to the previous hackle surface, the subsequent growth into a region of lower matrix strain may result in crack arrest. In fact, several incipient hackles may initiate and stop before a complete hackle is formed, as shown by the arrows in *Fig. 12*. Clearly, the buildup in matrix strain from the surface of the previous hackle to a value sufficient to allow the formation of the next complete matrix crack requires a greater distance as the distance between fibers increases. This is demonstrated graphically in *Fig. 14*, which shows a linear relationship between hackle width and hackle spacing independent of both t_m and temperature.

The effect of t_m on G_{IIc} also can be interpreted in terms of the microscopic area of matrix fracture. Although t_m does not affect the hackle spacing, the hackle height was observed to increase with increasing t_m. Moreover, as the parallel curves in *Fig. 11* indicate, the dependency of G_{IIc} on t_m is the same at −50°C as it is at 100°C, in agreement with the similar values of G_{Ic} at these two temperatures as shown in *Fig. 1*. Thus, the contribution of matrix fracture to the Mode II fracture energy depends on the thickness of the interlaminar matrix layer, but is relatively insensitive to temperature at least for dry specimens. The other major energy contribution to G_{IIc} is the work done in shearing the fibers out of the matrix. This is likely to be independent of t_m provided that the fracture path remains on the edge of the interlaminar matrix layer as was observed. It therefore seems probable that the major effect of increasing temperature on G_{IIc} is to reduce the work required for fiber shear-out. This is supported by the micromechanical analysis of Grimes and Adams (20) which showed that increasing the temperature and moisture content of AS/3501-6 resulted in a change in the normal residual stress at the fiber-matrix interface from compression to tension. This could be expected to have a major effect on the work of friction associated with shearing the fibers from the matrix.

Thus, the apparently inconsistent response to increasing moisture content and temperature of *Fig. 1* can be explained in terms of a change in matrix toughness for Mode I and a reduction in the interfacial fracture energy for Mode II. However, additional work is required to verify this for wet specimens.

Mode II Fatigue

The effect of fiber volume fraction on the Mode II fatigue properties is shown in *Fig. 15a*. By normalizing ΔG to the corresponding values of G_{IIc} as in *Fig. 15b*, the effect of V_f is eliminated, indicating that the same mechanism operates in both fracture and fatigue. *Figure 15b* also shows that changing the R ratio from 0 to −1 leads to a substantial increase in the Mode II interlaminar fatigue crack growth rates. Although the fatigued surfaces are somewhat obscured by the fretting that takes place, it is apparent from *Fig. 16* that the delamination lies close to the fibers on the tensile face when $R = 0$ but within the matrix when $R = -1$. Clearly, for $R = -1$ when the shear direction fully reverses in each cycle, there will be no preference for the delamination to move toward either side of the interlaminar zone. It is therefore possible that the enhanced da/dN values occurring at $R = -1$ result from the fact that only matrix failure is necessary instead of the higher energy-absorbing failure of the fiber-matrix interface and associated hackle formation.

SUMMARY AND CONCLUSIONS

By focusing attention on the local geometry of the interlaminar zone, several aspects of delamination behavior have been clarified. First of all, it has been shown that growth under

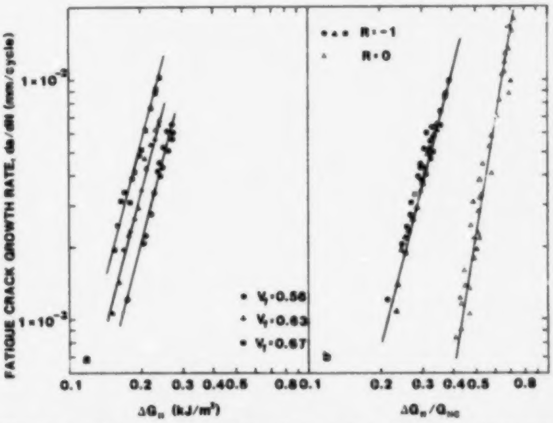

Fig. 15. Effect of V_f and R-ratio on the Mode II interlaminar fatigue crack growth rate.

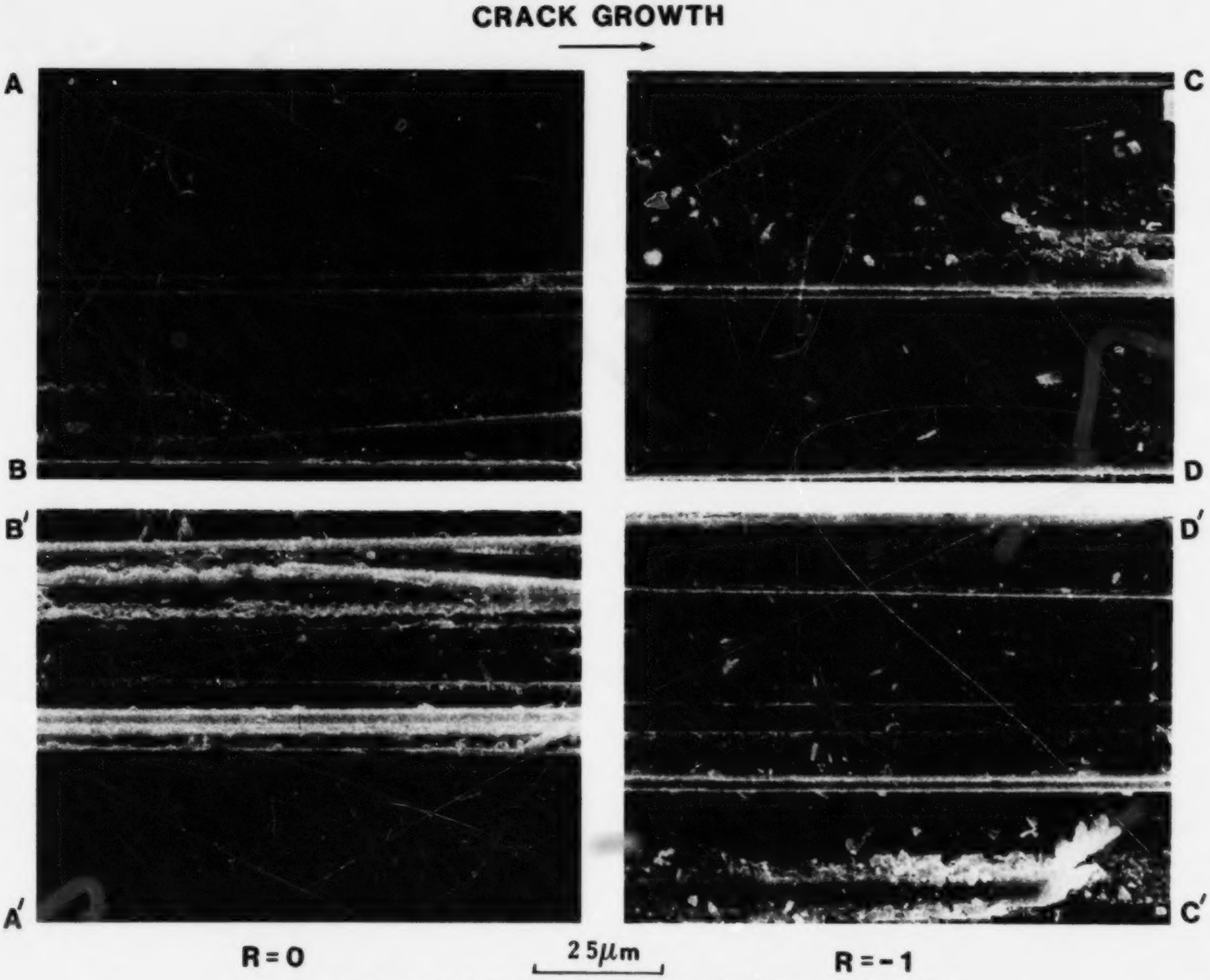

Fig. 16. Fractographs from Mode II fatigue cracks at R ratios of 0 and −1.

tensile opening is controlled not only by the extent to which fiber bridging occurs at the crack tip, but also by the ability of the bridged fibers to constrain the crack opening. For quasi-static growth, as well as for fatigue growth at high ΔG, maximum constraint is achieved if the fibers peel easily from the fracture surface since this delays fiber fracture and, hence, results in a more extended fiber-bridging zone. On the other hand, at low ΔG, where fiber fracture is less likely, the bridged fibers exert the greatest pull on the crack faces if peel is more difficult. It has been demonstrated also that slip/stick behavior will occur if the interlaminar plane is kept flat and that during fast fracture the likelihood of fiber bridging taking place is reduced.

Next, Mode II delamination involves both the shearing of the fibers out of the matrix as well as the tensile fracture of the matrix between the fibers. The energy required for matrix fracture increases as the thickness of the interlaminar zone increases and is typically several times G_{Ic}. The work required to shear the fibers out of the matrix is independent of the interlaminar geometry, but very sensitive to temperature and moisture content. Finally, there is evidence to suggest that during Mode II interlaminar fatigue, the crack growth depends on the failure path through the interlaminar zone. An R ratio of -1 results in a greater value of da/dN than does $R = 0$ at the same ΔG since the crack avoids failure along the fiber-matrix interface.

ACKNOWLEDGMENTS

This work is part of the program in support of the Department of National Defense data base requirements for damage tolerance analyses of advanced materials in high performance aircraft. The author is grateful to Dr. K. N. Street for many helpful discussions and encouragement and to Mr. E. Jensen for his expertise in carrying out much of the experimental part of this research.

NOMENCLATURE

a = crack length.
b = specimen width.

C = specimen compliance.
d_f = average free length of bridged fibers at fracture.
f = fatigue test frequency.
G_I = Mode I strain energy release rate.
G_{II} = Mode II strain energy release rate.
G_{Ic} = Mode I fracture energy.
G_{IIc} = Mode II fracture energy.
G_{IR} = Mode I fracture resistance.
G_{BR} = Mode I fracture resistance due to fiber bridging.
n_e = number of fiber ends per unit area of fracture surface.
P = specimen load.
R = fatigue stress ratio.
t_m = thickness of interlaminar matrix layer.
t_f = thickness of fiber layer.
V_f = fiber volume of fraction of laminate.
Δa = crack growth.
ΔG = strain energy release rate range for fatigue test.
ϵ_f = fiber strain.

REFERENCES

1. S. N. Chatterjee, "Composite Defect Significance," Naval Air Development Center Report 80048-60 (1982).
2. T. K. O'Brien, in "Damage in Composite Materials," ASTM STP 775, pp. 140–167, American Society for Testing and Materials, Philadelphia (1982).
3. D. J. Wilkins, in "Characterization, Analysis and Significance of Defects in Composite Materials," AGAARD Conf. Proc. 355, p 20 (1983).
4. W. M. Jordan and W. L. Bradley, "Micromechanisms of Fracture in Toughened Graphite-Epoxy Laminates," to appear in ASTM STP 937 on "Toughened Composites," American Society for Testing and Materials, Philadelphia.
5. S. M. Lee, "Failure Mechanism of Delamination Fracture," to appear in ASTM STP 972 on "Composite Materials: Testing and Design (8th Conf.)," American Society for Testing and Materials, Philadelphia.
6. D. Purslow, *Composites*, **17**, 289 (1986).
7. A. J. Russell and K. N. Street, Proc. ICCM IV, pp. 279–286, Japan Society for Composite Materials, Tokyo (1982).
8. A. J. Russell and K. N. Street, ASTM STP 876, pp. 349–370, American Society for Testing and Materials, Philadelphia (1985).
9. A. J. Russell and K. N. Street, "The Effect of Matrix Toughness on Delamination," accepted for publication in ASTM STP 937 on "Toughened Composites," American Society for Testing and Materials, Philadelphia.
10. A. J. Russell and K. N. Street, "A Constant ΔG Test for Measuring Mode I Interlaminar Fatigue Crack Growth Rates," accepted for publication in ASTM STP 972 on "Composite Materials: Testing and Design (8th Conf.)," American Society for Testing and Materials, Philadelphia.
11. G. E. Law and D. J. Wilkins, "Delamination Failure Criteria for Composite Laminates," Naval Air Systems Command Report NAV-GD-0053 (1984).
12. F. X. de Charentenay and M. Benzeggagh, Proc. ICCM III, pp. 186–197, Pergamon Press (1980).
13. A. J. Russell and K. N. Street, "Modelling Problems in Crack Tip Mechanics," pp. 307–315, Martinus Nijhoff (1984).
14. E. M. Wu, "Failure Modes of Composite Materials with Organic Matrices and Their Consequences on Design," pp. 2.1–2.25, AGAARD Conf. Proc. 163 (1975).
15. D. Purslow, *Composites*, **15**, 207 (1984).
16. C. E. Browning, F. L. Abrams, and J. M. Whitney, ASTM STP 797, pp. 54–74, American Society for Testing and Materials, Philadelphia (1983).
17. N. J. Johnston, NASA Conf Publ. 2321, "ACEE Composite Structures Technology," pp. 75–95 (1984).
18. W. S. Johnson and P. D. Mangalgiri, "Investigation of Fiber Bridging in DCB Specimens," NASA Tech. Memo 87716 (1986).
19. M. Goland and E. Reissner, *J. of Appl. Mech. Trans. ASME* 77, 17 (1944).
20. G. C. Grimes and D. F. Adams, "Investigation of Compression Fatigue Properties of Advanced Composites," Northrop Technical Report NOR 79-17 (1979).

Damage Tolerance in Graphite-Epoxy Composite: Comprehensive Monitoring Method

M. TASNON *and* C. ROY

Department of Mechanical Engineering
Université de Sherbrooke
Sherbrooke, Québec, Canada J1K 2R1

A failure model is proposed to calculate the minimum expected lifetime of a graphite-epoxy structure under cyclic loading conditions. The theoretical approach is based on the statistical theory of strength and the mechanical redistribution of stresses between plies of a damaged laminate. The use of the acoustic emission technique has permitted the development of internal damage to be monitored during cyclic loading of unidirectional laminates. The experimental results indicate that the composite can withstand greater damage at low level cyclic loading than observed during monotonic loading to failure. The theoretical modeling under development aims at predicting this behavior.

INTRODUCTION

Current civil aircraft composite structures are designed to a reduced set of strain requirements because of impact damage sensitivity, resin microcracking, and the unknown associated with the long-term environmental exposure. Therefore, tensile failure would not be expected in composite structures that have been designed to operate within the accepted strain limit of 4000 microstrain. To achieve additional weight saving in airframe construction, new advanced graphite composite materials have become available and are expected to raise the tensile design allowable strain limit to 6000 microstrain. The need for proven damage-tolerant design concepts for these materials has become of paramount importance. It is imperative to understand the development of damage and the mechanical behavior of laminates with defects if less conservative designs are to be considered by the manufacturers.

Engineers have conducted a large number of tests to establish a framework for damage-tolerant design for isotropic materials such as metals and polymers. Fong (1) estimated that close to one billion U.S. dollars a year is being spent worldwide on fatigue testing to provide the data base for fatigue design. Unusual compared with traditional engineering materials, composite laminates can be fabricated into an infinity of stacking configurations. The quantity of composite material available at the design stage is often limited because of its excessive cost. This precludes the rational establishment of a comprehensive data base on the fatigue behavior of composite laminates. Since full scale testing is also unlikely, it is of interest to develop a formulation for predicting the full scale structure damage tolerance based on coupon testing and analytical considerations.

The major objective of the research program is to develop a cumulative damage model for predicting the evolution of damage growth in composite laminates subjected to mechanical loading representative of that found in service. This paper will focus on the principles underlying an analytical cumulative damage model. Extensive experimental work will be required to assess fully the validity of the proposed model; however, limited experimental observations at the coupon level will be presented and the plausibility of the approach assessed.

THEORY

The Cumulative Damage Concept

The prediction of fatigue life of structures subjected to cyclic loading spectrum or the so-called "cumulative damage" (CD) remains a serious problem. Because of the disperse nature of the fatigue damage occurring in laminates, it is impossible to quantify the damage growth in them with the fracture mechanics approach. Consequently, the CD has been largely treated in composite materials following a phenomenological approach concerned with lifetime prediction of damaged laminates based on simple lifetime test data such as the *S-N* curves for constant amplitude loading without reference to the microstructural alteration associated with fatigue failure.

In this context, the fatigue damage level is presumed to be dependent only on the imposed stress level, σ, and the number, n, of fatigue cycles and is described by:

$$D = f(n, \sigma). \tag{1}$$

Assuming no initial damage in the material, damage is a continuous function that should satisfy the following initial and final boundary conditions:

a. For the case of constant amplitude loading,

$$\begin{aligned} D &= 0 \quad \text{when} \quad n = 0 \\ D &= 1 \quad \text{when} \quad n = N \end{aligned} \tag{2}$$

b. For the case of sequence loading, the fundamental principle underlying the phenomenological models is that for any intermediate locus in the life; a damage increment, $D\ (\Delta n_1, \sigma_1)$, is interchangeable with another "equivalent" damage, $D\ (\Delta n_2, \sigma_2)$. The fundamental property of D for two-stage loading is then

$$D(\Delta n_1, \sigma_1) = D(\Delta n_2, \sigma_2) \tag{3}$$

For the general case of sequence loading, the boundary conditions become

$$\begin{aligned} D &= 0 && \text{when } n = 0 \\ D &= \sum_{i=1}^{m} \Delta D_i = 1 && \text{pat failure} \end{aligned} \tag{4}$$

where m is the number of load sequences up to failure and ΔD_i is the amount of damage accumulation during fatigue at σ_i.

Many CD models based on this approach have been conceived on the premise that reasonable mathematical functions can relate the damage accumulation to the fatigue variables n and σ. The literature provides numerous examples whereby damage functional relations have been established by measuring various physical parameters during constant amplitude loading. As stated by Erismann (2) and Hashin (3), these models yield equivalent results since they are based on the same questionable hypothesis of damage equivalence.

It is the authors' viewpoint that a major shortcoming common to the CD models discussed above is the lack of direct relationship between the measured external parameters and the physical processes of damage and failure. For example, the equivalent damage principle expressed in *Eq 2* cannot be valid if the load history increment cannot be freely exchanged throughout the entire fatigue life, including the final stages. It is thus postulated that, on one hand, the specimen passes through exactly the same parameter configurations right to the end, thus being ruptured under constant conditions while, on the other hand, the same rupture may take place at different load levels. Therefore, the residual strength must be constant and variable at the same time, which is obviously paradoxical.

The primary point of departure of the proposed modeling effort from the ongoing work is then focused on defining models that are closely related to the micromechanisms of damage accumulation and failure.

The Modeling Approach

The microaspects of failure under cyclic loading are extremely complex for two technical reasons (4). The first is the enormous scale that separates atomic level (10^{-10} to 10^{-8} m), where understanding begins, from the component and structure level (10^{-2} to 10^{2} m) for which the prediction of the model is intended. For composite laminates, which are intrinsically inhomogeneous and in which the constitutive plies scale is comparable with the specimen scale, this size effect is especially important (5). The second reason is the impossibility of fabricating "identical" specimens with well-characterized microstructural constituents for controlled experimentation. For composite laminates, data reproducibility remains a major problem because of the numerous process variables related to the fabrication.

The proposed model considers that fatigue failure of a composite laminate is the end result of multiple physical and mechanical degradation processes interacting at different scales. Hence, a general description of the scenario can be as follows:

1. Define a general failure model based on the statistical distribution of strengths and stresses at the microscopic level of the materials.
2. Measure the parameters of the general model defined above for each substructure (e.g., plies and interfaces) of the laminate using the appropriate instrumentation. This will enable prediction of the fatigue life of each constitutive subelement undergoing fatigue damage.
3. Model the internal stress redistributions between degrading laminate subelements and anticipate strength and life of the entire laminate when these internal stress states are associated with the failure model of the critical load-bearing subelement.

General Tensile Failure Model

The statistical theory of strength of material considers that failure of any material is controlled by two probability functions (6). The first one is the distribution of strengths among the microscopic constitutive volume elements of the material. This is usually a Weibull distribution. The second one is the distribution of stresses applied to those volume elements. Under an applied tensile load, and considering for simplicity that the stress is uniformly distributed, the probability of failure of the microscopic element within the material is given by the Weibull distribution:

$$N_{(P)} = N_o[1 - \exp\{-(p - p_u)^{\delta}/P_o\}] \qquad (5)$$

where $N_{(P)}$ is the number of broken elements; N_o is the total number of elements in the volume; p is the load applied to each element; p_u and p_o are constants, and δ is the Weibull shape factor. Then the load applied to each volume element in order to break $N_{(P)}$ elements is

$$p_{(n)} = p_u + p_o[\ln\{N_o/(N_o - N_p)\}^{1/\delta}] \qquad (6)$$

and the load applied to the entire volume is

$$P = (N_o - N_p)[p_u + p_o(\ln\{N_o/(N_o - N_p)\}^{1/\delta})] \qquad (7)$$

This equation is schematically represented in *Fig. 1*. The work reported by Rosen (7) and Zweben (8) and more recently by Fuwa, *et al.* and Bunsell *et al.* (9, 10) demonstrates this characteristic failure behavior. If the material is to fail during fatigue cycling at a certain loading level P_1 inferior to P_{max}, damage growth must occur continuously from quasi-static damage level A_1 to final damage instability level at point B_1. It is believed that the evolving damage process is due to the stress redistribution within the microscopic volume elements.

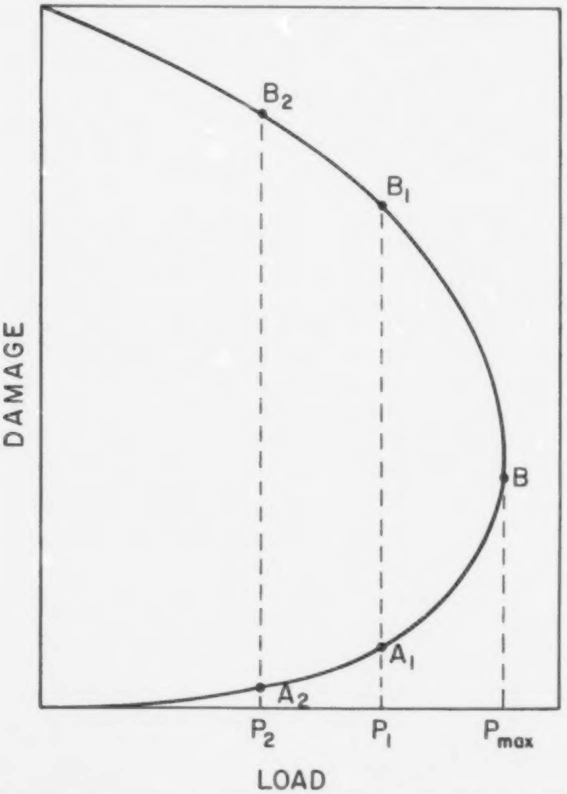

Fig. 1. The damage envelope predicted by the failure model. Critical damage for low load fatigue failure should be higher than the critical damage at maximum static load.

Hence, this model predicts that damage associated with constant amplitude, low-load, long-life failure is greater than damage associated with static failure. Indeed, the greatest possible damage state corresponds to the longest possible finite life. Final failure predicted by the model corresponds to an instability; therefore, the search for a unique sensitive damage parameter to describe the fatigue final stage might be elusive (11).

Direct Measurement of Damage

Major research efforts have been focused in recent years on the nondestructive quantification of damage during fatigue. Extensive use has been made of such methods as ultrasonic, X-ray radiography, acoustic emission, thermography, etc. Our experience with the acoustic emission (AE) technique over the last two years has demonstrated that even if many questions remain on how to relate AE to the micromechanisms of damage, AE is a technique that is very sensitive to any irreversible energy dissipating processes (12, 13). Therefore, AE was chosen as our principal technique to evaluate the damage function of various laminate elements.

Internal Stress Redistribution

Figure 2 is a schematic representation of the type of macroscopic damage commonly observed in a laminate at various stages during a tensile fatigue life. Elastic analyses such as those proposed by Reifsnider, *et al.* (14) enable us to compute the internal stress redistribution associated with those macroscopic damage modes. Computed local stresses in the critical load-bearing elements (e.g., 0-degree plies) then

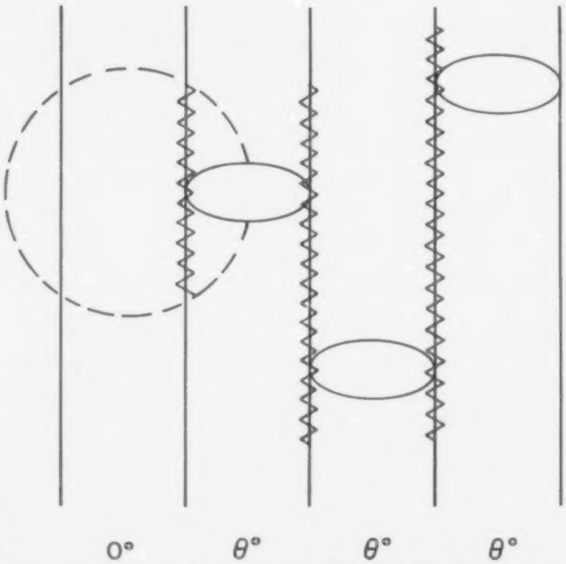

Fig. 2. Schematic diagram of local region of influence for matrix cracking and local delamination (after Reifsnider, et al., Ref. 14).

should be introduced into the corresponding cumulative damage model to predict the residual strength and life of the entire laminate.

EXPERIMENTAL

The samples used in this work were fabricated from Hercules IM6 high-strain graphite fibers preimpregnated with NARMCO 5245c bismalimide-modified epoxy resin. The finished plates were inspected by C-scan and cut with a fine grit diamond impregnated trim saw. Several specimen configurations are being studied, but the results and discussion in this paper will be limited to parallel-sided test samples from unidirectional 0°_8 and 90°_8.

All specimens were 25.4-mm (1.0-inch) wide and 1.0-mm thick. Fiberglass end tabs were bonded at each end. The thickness at the center section of the 0-degree specimens was reduced to 0.4 mm (≈ 3 plies) with a water-cooled grinding wheel. This geometry was chosen to reduce AE signals coming from the tabs region and to minimize the scale effect between the measurements and the behavior of the individual ply within the laminate. For practical reasons, 90-degree unidirectional samples were only reduced to 0.90 mm (≈ 7 plies).

The AE system is an AET-5000B microcomputer-based event analyzer. Three 175-kHz resonant transducers were fixed to each sample using silicone grease as a coupling medium. The two sensors mounted near the tab ends were used as guard sensors discriminating AE signals generated in the gripping areas from the valid AE signals detected by the third transducer mounted in the center of the sample. AE signals were recorded at a total gain of 80 dB and a threshold of 1 V in the detection unit. No background acoustic emission noise from the MTS testing machine was recorded.

RESULTS

Unidirectional 0-degree Tensile Properties

The properties of the unidirectional layers are shown in *Table 1*. Typical AE cumulative event counts for monotonic loading at different loading rates are represented in *Fig. 3*. The evolution of the cumulative damage as reflected by AE activity up to the final specimen fracture closely corresponds to the lower part of the damage envelope described before (see *Fig. 1*). As expected for this high-strain composite system, the first sign of damage appeared at a significantly higher strain level (0.4 to 0.5%) compared with the strain reported by Fuwa, *et al.* (9) for conventional CFRP in tension (0.15% to 0.3%). The noticeable strain rate effect observed demonstrates a time dependence of the mechanical breakdown phenomena.

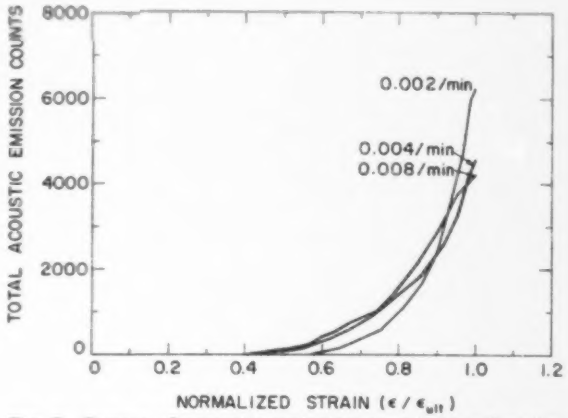

Fig. 3. Curves of acoustic emission counts as a function of load up to static failure for the on axis unidirectional. The effect of loading rate is noticeable.

Table 1. IM6-5245c Basic Mechanical Properties.

Loading Axis Θ	No. of Speci-men	Static Strength (MPa)	Ultimate strain με	Modulus (GPa)
0° (3 plies)	22	2595 (95)*	15560 (1080)	169 (14)
90° (8 plies)	10	59 (3.5)	11184 (869)	6.5 (0.12)

* The values in parentheses represent standard deviation of the measured quantity.

The fatigue tests carried out in tension-tension loading led unfortunately to premature failures of the specimens on the tabs region, thus invalidating any attempt to evaluate with AE the damage development in specimens of this orientation. The data obtained early in the tests clearly showed that the stress concentration near the gripping area contributed largely to local degradation. A test rig permitting testing of unidirectional composite in tubular form is being designed.

Unidirectional 90-degree Tensile Properties

Similar experiments conducted with 90-degree specimens enabled evaluation of damage development in this matrix and fiber-matrix interface dominated configuration. Transverse mechanical properties of the composite given in *Table 1* showed considerable scattering. Acoustic emission monitoring during the monotonic tests revealed relatively little damage development before final failure. Typical stress-strain curves obtained together with AE counts are shown in Fig. 4.

A series of tension-tension cyclic tests were performed on the 90_8-degree laminate for different maximum stress levels at a frequency of 1 Hz and a stress ratio ($\sigma_{min}/\sigma_{max}$) of 0.1. The *S-N* curve obtained with those few tests shows a large scatter band of results, as illustrated in *Fig. 5*. Acoustic emission was recorded to measure accumulation of damage during cycling between 60% and 90% of the fracture load. *Figure 6* shows curves of cumulative AE counts as a function of the number of cycles for these sample tests. Those curves provide a hint to the effect that the longest life results in greatest number of counts. We can also see that in most cases no significant increase of the rate of emis-

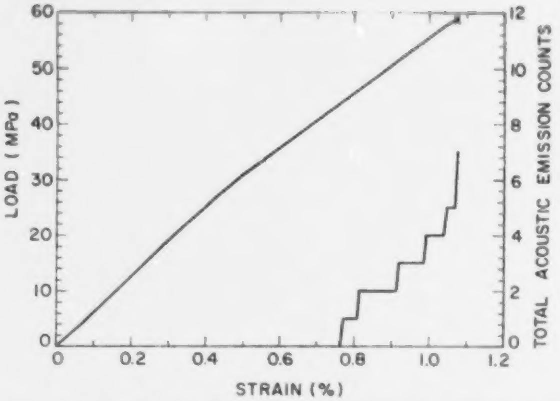

Fig. 4. AE counts and load-strain traces for transverse unidirectional loaded to failure. Very low acoustic emission activity was detected.

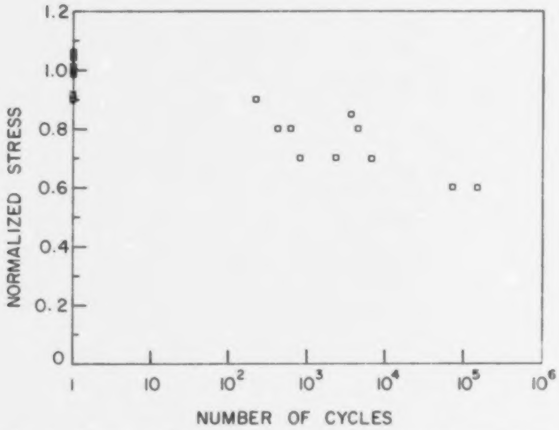

Fig. 5. Fatigue-life diagram for unidirectional composite under loading perpendicular to fibers.

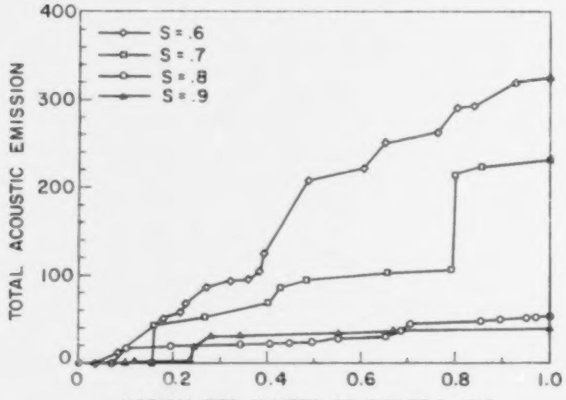

Fig. 6. Curves of acoustic emission count as a function of the number of cycles endured, n/N, for different maximum cyclic load levels $S = \sigma/\sigma_{ULT}$.

sion was observed before sudden failure. *Figure 7* shows an approximate damage envelope that has been generated from these results.

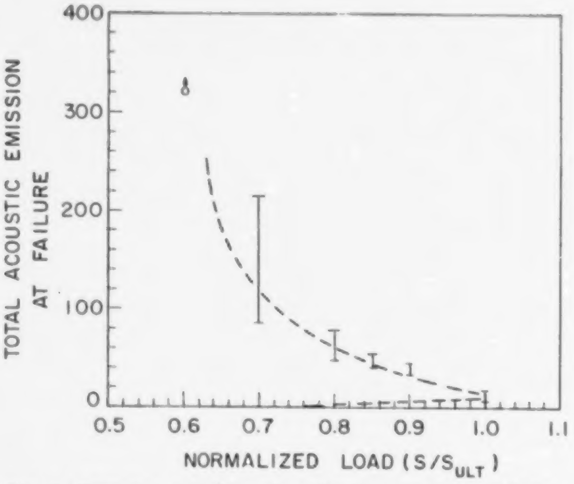

Fig. 7. Damage envelope for the transverse unidirectional as measured by acoustic emission.

Analysis of AE amplitude, duration, and rise time distributions suggests that there is no difference between the kind of damage incurred in a tensile test and that caused by cyclic loading. The large variability in tensile strength and fatigue *S-N* data resulting from microstructural differences between samples dictates that more results are required before completing the damage model.

CONCLUSIONS

The following conclusions are based on a cumulative damage model currently under development and therefore should be regarded as provisional findings:

1. A systematic modeling approach of fatigue damage at different scales has been described and its applicability was verified using the results of a unidirectional fatigue testing monitored with acoustic emission as a means of quantifying the damage evolution.

2. Preliminary results obtained during monotonic and cyclic loading support this model in such a way that failure occurs for a particular load at a critical damage level determined by the upper part of the damage envelope. The unidirectional composites under cyclic loading can clearly withstand greater damage at lower load levels before failure. A precise definition of the damage evolution at various load levels and also of the critical damage level at failure should provide a way to calculate the minimum lifetime of this type of specimen.

NOMENCLATURE

D = fatigue damage.
N = number of fatigue cycles to fracture.
$N_{(P)}$ = number of broken microscopic elements.
n = number of fatigue cycles.
P = load applied to the structure.
P_{max} = static strength.

p = load applied to each microscopic element.
P_u, P_o, δ = material constants.
σ = stress.

REFERENCES

1. J. T. Fong, "Fatigue Mechanisms," ASTM STP 675, J. T. Fong, ed., p. 730, American Society for Testing and Materials, Philadelphia (1979).
2. T. H. Erismann, *Eng. Fract. Mech.*, **8**, 115 (1976).
3. Z. Hashin, *Comp. Sci. Technol.*, **23**, 1 (1985).
4. J. T. Fong, "Damage in Composite Materials," ASTM STP 775, K. L. Reifsnider, ed., p. 243, American Society for Testing and Materials, Philadelphia (1982).
5. V. V. Bolotin, *Eng. Fract. Mech.*, **8**, 103 (1976).
6. C. Zweben and B. W. Rosen, *J. Mech. Phys. Solids*, **18**, 189 (1970).
7. B. W. Rosen, *AIAA J.*, **2**, 1985 (1964).
8. C. Zweben, *AIAA J.*, **6**, 2325 (1968).
9. M. Fuwa, B. Harris, and A. R. Bunsell, *J. Phys., D:*, **8**, 1460 (1975).
10. A. R. Bunsell, D. Larorche, and D. Valentin, "Long Term Behavior of Composite, ASTM STP 813, T. K. O'Brien, ed., p. 38, American Society for Testing and Materials, Philadelphia (1983).
11. P. C. Chou and R. Croman, "Composite Material: Testing and Design" (Fifth Conference), ASTM STP 674, p. 431, American Society for Testing and Materials, Philadelphia (1979).
12. A. Maslouhi, D. Proulx, C. Roy, M. Tasnon, and D. G. Zimcik, Proc. 2nd. Int. Symp. on Nondestructive Characterization of Materials, Montréal (July 20–24, 1986).
13. M. Fuwa, A. R. Bunsell, and B. Harris, *J. Mater. Sci.*, **10**, 2062 (1975).
14. K. L. Reifsnider, K. Schulte, and J. C. Duke, "Long Term Behavior of Composite," ASTM STP 813, K. L. Reifsnider, ed., p. 136, American Society for Testing and Materials, Philadelphia (1983).

DISCUSSION

S. Newman: The acoustic emission being generated during a damage—is it really a nondestructive test?

M. Tasnon: The acoustic emission (AE) technique is in itself nondestructive since it is a passive monitoring technique introducing no energy in the material under testing. It is the loading imposed to the structure that might be destructive or not. For example, when you test a structure to the service load level, you are not supposed to do a destructive test. Monitoring AE activity during this proof test is the best way to know if this load level is damaging or not.

F. G. Hamel: You said that there is an influence of strain rate on the total emission count during the unidirectional tensile loading. Don't you think that this may be due simply to a statistical effect? The acoustic events have certain duration and when the strain rate is increased the probability of having two events overlapping in time increases, and these will not be distinguished by the pickup.

M. Tasnon: Yes. With our computer system, two successive AE events can be discriminated if a minimum "time-out" interval of 32 μs separates the arrival of two signals. If not, the system will consider it as a single event of longer duration. Since our tests were conducted at very low strain rates, such "trains of events", characterized by a shift in the event duration statistical distribution, have not been observed for the most part of each test. Only at the very end of each test when fracture occurred did the counter saturate. Therefore, there is some statistical bias in the value of the last point of each curve in *Fig. 3*, but I believe that the viscoelastic properties of the matrix are mainly responsible for the different damage growth rates that we are observing.

F. G. Hamel: During the fatigue tests, there must be some events related to fiber breakup, fiber-fiber friction, delamination, and matrix creep, all of which may generate acoustic emission, but not all indicate critical damage.

M. Tasnon: Yes. For example, in unidirectional composites tested in tension, final failure is controlled by fiber breakage. It would be great if AE could count only the number of fibers breaking, but we all know that in real life many types of damage mechanisms occur simultaneously, all of them generating AE signals. Until signal analyses enable us to discriminate AE waveforms generated by different failure mechanisms, one can only consider AE as a global measure of the irreversible energy dissipated during the degradation of the material.

An additional problem arising during fatigue testing is the AE generated by the friction of the multiple crack surfaces. Since these AE signals are related not to damage creation but to previous damage, they should be rejected. Toward this aim we considered valid only the AE events generated during the top part (85% to 100%) of each load cycle. This is very arbitrary, but we found that even with more sophisticated computer analysis like those proposed by Awerbuck*, we obtained the same general trend as the one we reported in *Fig. 6*.

---

* J. Awerbuck, M. R. Gorman, M. Madhukar, Proc. First Int. Symp. on Acoustic Emission from Reinforced Composites, The Society of the Plastics Industry, New York (July 1983).

SI METRIC UNITS

The following list shows the names, symbols, and equivalence of the more common quantities allowed in the SI metric system. The prefixes and symbols for the more common multiple units are also shown. Neither list is complete. Full details are given by F. S. Conant, Polym. Eng. Sci., **17**, 222 (1977). A table of the more frequently needed conversion factors required to use the SI system is also shown. This journal prefers that SI metric units be employed in manuscripts submitted for publication.

Units and Symbols

Quantity	Name	Symbol	Equivalent to:
Length	metre	m	—
Time	second	s	—
	minute	min	—
	hour	h	—
Mass	kilogram	kg	—
Electric current	ampere	A	—
Plane angle	radian	rad	—
Capacity	litre	L	$10^{-3}m^3$
Frequency	hertz	Hz	s^{-1}
Force	newton	N	$m \cdot kg \cdot s^{-2}$
Pressure, Stress	pascal	Pa	$N \cdot m^{-2}$
Energy, Work, Heat	joule	J	$N \cdot m$
Power	watt	W	$J \cdot s^{-1}$
Viscosity, dynamic	pascal second	Pa·s	$N \cdot s \cdot m^{-2}$

(The following units should ***not*** be used: micron, angstrom, dyne, erg, calorie, poise, or stoke.)

Multiple Units

Prefix	Symbol	Equivalent to:
giga	G	10^9
mega	M	10^6
kilo	k	10^3
deci	d	10^{-1}
centi	c	10^{-2}
milli	m	10^{-3}
micro	μ	10^{-6}
nano	n	10^{-9}

Conversion Factors

Force: $1N = 10^5$ dynes $= 1.02 \times 10^{-1}$ kgf $= 2.248 \times 10^{-1}$ lbf.

Pressure, Stress: 1 Pa = 10 dyne $cm^{-2} = 7.5 \times 10^{-3}$ mm Hg $= 10^{-5}$ bar $= 1.02 \times 10^{-5}$ kg $cm^{-2} = 1.45 \times 10^{-4}$ psi.

Energy: 1 J $= 2.387 \times 10^{-1}$ cal.

Viscosity: 1 Pa·s = 10 poise.

Society of Plastics Engineers

Executive Office, 14 Fairfield Drive, Brookfield Center, CT 06805, U.S.A.
(203) 775-0471
Telex No. 643-712

MEMBERSHIP APPLICATION

I am applying for:

☐ Membership
☐ Reclassification (no charge)
☐ Reinstatement (initiation fee not required)

NAME: ______________________________
First Middle Last

DATE OF BIRTH: ______________________________
Month Day Year

ADDRESS:

Fill in both addresses and check your preferred mailing address.

☐ **COMPANY** (spell out name)
____
____
____
City State (Prov.) Zip

POSITION: ______________________________

☐ **HOME** ______________________________
____
City State (Prov.) Zip

Job Function

What is the *primary* end product manufactured or service performed at your company location?

Please Check your Primary job function (check one only)

- _____ 01 Production or Manufacturing Engineering
- _____ 02 Design or Design Engineering
- _____ 03 Purchasing
- _____ 04 Sales or Marketing
- _____ 05 Research or Development Engineering
- _____ 06 General or Corporate Management
- _____ 07 Other (Specify)

DIVISIONS

My free primary Division choice is ______________________________
check (✓) others below as secondary Divisions (cost -$4 each)

- _____ 21 Color and Appearance
- _____ 22 Extrusion
- _____ 23 Injection Molding
- _____ 24 Electrical and Electronic
- _____ 25 Thermoforming
- _____ 26 Engineering Properties and Structure
- _____ 27 Vinyl Plastics
- _____ 28 Thermoset
- _____ 29 Thermoplastics Materials & Foams (Nonvinyl)
- _____ 30 Blow Molding
- _____ 31 Plastics in Automotive
- _____ 33 Plastics Analysis
- _____ 34 Decorating
- _____ 35 Moldmaking and Mold Design
- _____ 36 Medical Plastics
- _____ 37 Marketing (in formation)
- _____ 38 Polymer Modifiers & Additives (in formation)

Grade	Requirements
Senior Member	Minimum of twelve (12) experience credits and current continuous membership in the Society for a minimum of two (2) years.
Member	Minimum of six (6) experience credits.
Affiliate Member	Less than six (6) experience credits.
Student Member	Regularly enrolled FULL-TIME student in a course of study in plastics.

Check below the membership grade for which you believe details of your experience in plastics qualifies you (see grades above).

☐ Student Member ☐ Member
☐ Affiliate Member ☐ Senior Member

Statement of Fees *(U.S. FUNDS ONLY)*

MEMBERSHIP YEAR: 7/1 thru 6/30

$10.00 INITIATION FEE MUST BE ATTACHED IN ORDER TO PROCESS YOUR APPLICATION. INITIATION FEE IS SEPARATE FROM ANNUAL DUES.

- **SENIOR MEMBER, MEMBER, AFFILIATE**
  - Annual Dues: 7/1-6/30 $55.00
  - If joining after 12/31 $27.50
  - If joining after 4/1 $10.00 (initiation fee only)
- **STUDENT MEMBER**
  - Annual Dues: whenever joining $14.00 (no initiation fee/not pro-rated)
- **REINSTATED MEMBER**
  - Annual Dues: whenever reinstated $55.00 (no initiation fee/not pro-rated)

I wish to join the ______________________________ Section.

REFERENCES The Bylaws require the names of three references who are familiar with your work. One of them should be a member of the Society. Assistance in providing member-references will be given on request. Signatures are not necessary.

1. (Member-Sponsor) ______________________________
2. ______________________________
3. ______________________________

STATEMENT OF COLLEGE WORK

Years attended		Institution	Major	Degree	Education Credits
From	To				

RECORD OF QUALIFYING EXPERIENCE IN PLASTICS

DATES				Give your title, name and location of employer. List in chronological order. Describe duties fully and state any important engineering work you have done in each position. If space is not sufficient, use separate sheet.	Time in years (a)	% in plastics (b)	Qualifying experience (a x b)
From		To					
Mo.	Yr.	Mo.	Yr.				
					yrs./mo.		yrs./mo.
						SUB-TOTAL	

Total education and experience credits. ▶ ________

I certify that the statements made in this application are correct. I agree, if elected, to be governed by the Constitution and Bylaws of the Society and to promote the objectives of the Society.

____
Signature in ink. Date

CREDENTIALS COMMITTEE APPROVAL ONLY	Approved Grade
(S)	Date
(S)	Date
Office use only:	Division
ID#	Job Class
Grade	Date Elected
Section	

If applying for Member or Senior Member, please complete *in detail:*

STATEMENT OF COLLEGE WORK

Years attended		Institution	Major	Degree	Experience Credits (see notes below)
From	To				

RECORD OF QUALIFYING EXPERIENCE IN PLASTICS

DATES				Give your title, name and location of employer. List in chronological order. Describe duties fully and state any important engineering work you have done in each position. If space is not sufficient, use separate sheet.	Time in years (a)	% in plastics (b)	Qualifying experience (a × b)
From		To					
Mo.	Yr.	Mo.	Yr.				
					yrs./mo.		yrs./mo.
						SUB-TOTAL	
						Total education and experience credits. ▶	

Grade	Requirements
Senior Member	Minimum of twelve (12) experience credits and current continuous membership in the Society for a minimum of two (2) years.
Member	Minimum of six (6) experience credits.
Affiliate Member	Less than six (6) experience credits.
Student Member	Regularly enrolled FULL-TIME student in a course of study in plastics.

CREDENTIALS COMMITTEE APPROVAL ONLY		Approved Grade
(S)	Date	
(S)	Date	

Experience Credits
Grade of Membership . . .

Membership grades are based on experience credits which are earned as follows:

1. **Experience credits earned for education.**
   Maximum credits allowable for education shall be six (6). Use highest degree credits ONLY.

Doctorate in science or engineering	**6 credits**
Masters in science or engineering	**5 credits**
Bachelors in science or engineering	**4 credits**
Any degree other than above	**2 credits**
Associate or Adjunct in Plastics	**2 credits**
Associate or Adjunct (awarded by Community College or equivalent for two-year course of studies, without specializing in plastics).	**1 credit**

When filling in the "Statement of College Work" above, place the corresponding number of credits earned in the right-hand column.

2. **Experience credits** are determined by the proportion of time involved in actual technical and engineering duties in plastics for each position held. For instance, if only three of the five years you worked for the XYZ Co. comprised technical or engineering duties, then three (3) years (60% of 5 yrs.) would constitute the "Qualifying Experience" you would enter in years and months in the right-hand column under "Record of Qualifying Experience in Plastics."

   Please detail carefully the engineering skill required for each position to help the Credentials Committee judge experience as "qualifying."

When you have determined the number of credits that you believe you have earned, consult the above member grade requirements. Indicate on the reverse side the grade of membership for which you believe you are qualified.

INFORMATION FOR AUTHORS

Submission of original and review articles is encouraged. There is no limit on length. Three copies of the manuscript should be submitted, which should be typed, one side only, double space, with at least a 2.5-cm (1-inch) margin. Submission will be taken to imply that the paper has not been previously published, that it is not being considered elsewhere for publication, and that if accepted it will not be published elsewhere in the same form, in any language, without the consent of the editor or publisher. Authors must agree to transfer copyright to the publisher when an article is accepted for publication. Unless notified to the contrary by the authors, the publisher assumes that the act of submitting the article signifies the author's agreement to such copyright transfer to the publisher. The journal carries a voluntary page charge. Each manuscript should include:

A separate title page, headed by a concise, meaningful title (no abbreviations). This page should provide:

- The name and affiliations of each contributing author at the time the paper was prepared.
- Indicate by asterisk any changes of address for each author since article preparation.
- Acknowledgment of any prior oral presentation and original source of the material.

A separate abstract page, consisting of a single paragraph, text only, of 100–200 words to include the title and the names and addresses of the authors. Define any abbreviations for substances or methods (such as ABS, SAXS, etc.).

A list of references, on a separate page at the end of the text, numbered in order of text citation. The references are to be abbreviated in the form used in Chemical Abstracts using the names of all authors preceded by initials; see Bibliographic Guide for Editors and Authors, American Chemical Society, Washington, D.C.

- Within the text, the reference citations are typed in parentheses in line with the main copy (no superscripts or subscripts), thus:

  According to Cohen, et al. (1) . . .

- In the list of references the general style is as follows:

For periodicals:

1. D. Cohen, A. Siegmann, and M. Narkis, *Polym. Eng. Sci.*, 27, 286 (1987).

The journal name and volume are to be underlined and the year is placed in parentheses. The issue number is given only when needed for identification. The article name is eliminated unless the reference is unclear without it.

For books: The title to be spelled out in full.

9. J. E. Q. Lipson and J. E. Guillet, in "Macromolecular Solutions," R. D. Seymour and G. Allen Stahl, Eds., Pergamon Press, New York (1982). (Include the state when the city is not identifiable.)

A list of nomenclature, identifying symbols and abbreviations, commonly desirable at the end of the text. Footnotes are to be avoided.

Equations, numbered and typed in the appropriate place in the text. Where symbols cannot be typed, write them neatly in ink.

Tables, each typed on a separate page, with a heading, and numbered with arabic numerals that correspond to the order in which they are cited in the text. The tables should be inserted in the manuscript after the references and before the figures.

Figures, assembled at the end of the manuscript and preceded by a separate typed list of captions that explain them. Please also supply a set of original figures or sharp glossy photos thereof, on 8½ × 11 paper or attached to sheets of this size, one sheet for each figure. Each should be identified on the front edge or on the back (photographs) with the name of the first author and the figure number (e.g., Smith, Fig. 1). Originals are to be prepared with high contrast India ink and to bear uniformly stencilled notations. Line drawings and photos should be of a quality suitable for good photographic reproduction and retained legibility upon size reduction to one quarter. Manuscript transmittal letter should indicate if the figures need be returned.

Send manuscripts to:
Roger S. Porter, Editor
POLYMER COMPOSITES
℅ Polymer Science & Engineering
University of Massachusetts
Amherst, Massachusetts 01003

For information concerning publication dates, page charges and reprint orders contact:
Editorial Department
Society of Plastics Engineers
14 Fairfield Drive
Brookfield Center, Connecticut 06805

Volume

2

Conseil national de recherches
Canada
Institut de génie des
matériaux
Boucherville (Québec)

National Research Council
Canada
Industrial Materials
Research Institute
Boucherville, Quebec

IGM86D-000-657-G
CNRC 28434

POLYMER COMPOSITES

VOLUME 8/NO. 6/DECEMBER 1987

Composites '86—Part 2

National Research Council of Canada
Industrial Materials Research Institute

CONTENTS

361 T. VU-KHANH and L.A. UTRACKI/Preamble

363 T. VU-KHANH/Survey of Current Status and Future Trends in Reinforced Plastics Composites

371 S. IABONI and R.T. WOODHAMS/Thermoforming of Ordered Polypropylenes

379 P.D. FRAYER/High Temperature Liquid Crystalline Copolyester Composites. Part 1: A Review and New Data for the Self-Reinforced Matrix Phase

396 J.C. KRAPEZ, P. CIELO, X. MALDAGUE, and L.A. UTRACKI/Optothermal Analysis of Polymer Composites

408 B. FISA, J. DUFOUR, and T. VU-KHANH/Weldline Integrity of Reinforced Plastics: Effect of Filler Shape

419 J.V. FOY and J.T. LINDT/Electrical Properties of Exfoliated-Graphite Filled Polyester Based Composites

427 P.W.K. LAM/The Characterization of Thermoset Cure Behavior by Differential Scanning Calorimetry. Part 1: Isothermal and Dynamic Study

437 L.A. UTRACKI/Panel Discussion on: Thermoplastics vs. Thermosets in Advanced Composites

442 Subject Index

444 Author Index

PUBLISHED BY THE SOCIETY OF PLASTICS ENGINEERS, INC.

POLYMER COMPOSITES

Published by the Society of Plastics Engineers

EDITOR—Roger S. Porter

℅ Polymer Science and Engineering
University of Massachusetts
Amherst, Mass. 01003

ASSOCIATE EDITORS—Richard E. Ball and Robert A. Weiss

℅ Western New England College
Springfield, Mass. 01119

℅ University of Connecticut
Storrs, Conn. 06268

ADVISORY BOARD

Lawrence J. Broutman
Illinois Institute of Technology
Anthony T. DiBenedetto
University of Connecticut
Nikolay Enikolopyan
USSR Academy of Sciences
David H. Kaelble
Arroyo Computer Center
John L. Kardos
Washington University
Lon Mathias
University of Southern Mississippi

Frederick J. McGarry
Massachusetts Institute of Technology
L. Nicolais
University of Naples
R. Byron Pipes
University of Delaware
N. S. Schneider
Army Materials and Mechanics Research Center
James C. Seferis
University of Washington
J. G. Williams
Imperial College of Science & Technology

PUBLICATIONS COMMITTEE

E. W. Rowan, Jr., Chairman
Parkway Plastics, Inc.

R. P. Braddicks, Jr.
Plastics Consultant
A. T. DiBenedetto
University of Connecticut
H. Finkel
Industrial Designer

R. D. Forger
Society of Plastics Engineers
J. L. Hull
Hull Corporation
M. A. Mendelsohn
Westinghouse Electric Corp.
R. S. Porter
University of Massachusetts

D. W. Riley
Extrusion Engineers
A. A. Schoengood
Society of Plastics Engineers
A. E. Whitney, Jr.
Plastics Consultant

Copyright by Society of Plastics Engineers, 1987. POSTMASTER: Send address changes to Polymer Composites, 14 Fairfield Dr., Brookfield Center, CT 06805. Telephone (203) 775-0471, TELEX 643-712. Reproduction in whole or in part without written permission is strictly prohibited.

Polymer Composites (ISSN 0272-8397) is published at Waverly Press, Easton, MD 21601. Address changes, undeliverable copies, and orders for subscriptions should be sent to Circulation Manager, Society of Plastics Engineers, 14 Fairfield Dr., Brookfield Center, CT 06805.

Published bimonthly (February, April, June, August, October, December). Second class postage paid at Brookfield Center, Conn., and additional entry offices. Accepted at special postal rate provided in P.M. Sec. 132.122.

Neither the Society of Plastics Engineers nor Polymer Composites is responsible for the views expressed by individual contributors either in articles published in Polymer Composites or in technical papers presented at meetings of the Society.

Subscription rates for 1987: SPE members, 1 year—$40. Nonmembers, 1 year—$100. Delivery outside North America, add $12 per year.

SOCIETY OF PLASTICS ENGINEERS
Business and Executive Offices, 14 Fairfield Dr., Brookfield Center, CT 06805

Daniel J. Domoff
Managing Editor

Marie J. Bruckenthal
Production Manager

Jeannette M. Piastuch
Copy Editor

Michael R. Cappelletti
Circulation Manager

OFFICERS OF THE SOCIETY

John R. Kretzschmar
President

Bruce A. Petersen
President-elect

Vivian E. Malpass
First Vice President

Leonard H. Drexler
Second Vice President

Jacques de Craene
Vice President for International Affairs

Kishor S. Mehta
Secretary

George W. Thorne
Treasurer

Robert D. Forger
Executive Director and Publisher

POLYMER COMPOSITES is indexed by:—Chemical Abstracts—Engineering Index, Inc.

PREAMBLE

After a period of sustained growth in plastics consumption, their volume now exceeds that of raw steel. However, since the beginning of the seventies, forecasts made by extrapolating from past data have proven too optimistic. The gap between capacity and sales of plastics in the Western world is widening. Pressure of competition forces companies to focus on materials offering higher performance.

The production of reinforced plastics has constantly increased since the Second World War. With a forecast annual growth rate of 8 to 12 percent over the next decade, composites are one of the fastest growing sector of the plastic industry. Advanced composites show the largest expansion, due mainly to a strong increase in demands in aerospace and military applications. Penetration of advanced composites into big-volume market has not occurred, but it is believed that advances in fiber and matrix performance as well as in the method of fabrication will accelerate the mass-production of these materials.

High-volume composites will see a less rapid growth but demands will continue to increase at a higher rate than that of matrix resin. Land transportation is and will remain the largest and fastest growing market for high-volume composites.

The next potential market for high performance plastics will be found in the area of substitution for metals in structural parts. In order to fulfill this function, the mechanical properties of plastics must be improved. The most attractive method seems to be through addition of stiffer and stronger reinforcements.

However, the bright future of reinforced plastics is impossible without sustained efforts in research and development as well as education of the user of the possibilities of these new materials. The composites offer unique properties which require imagination and ingenuity from scientists and engineers. Besides the technical problems, the particularity of composites necessitates an extensive training program on new approaches to design. These hurdles are many, but they will have to be overcome before composites can be used to their full potential.

The symposium "Composites-'86" of November 25 and 26 was the sixth one in a series on "Polymer Composites" and the sixteenth organized and sponsored by the Industrial Materials Research Institute of the National Research Council of Canada. The remaining symposia are part of the two other series on "Mathematical Modeling of Plastics Processing and Properties", and on "Polymer Blends".

Proceedings of these symposia have been published in the technical journals of the Society of Plastics Engineers: "Composites" in *Polymer Composites*, "Modeling" and "Polyblends" in *Polymer Engineering and Science*. In addition, the entire symposia are recorded and the tapes stored in the Institute library for two years, available to anyone interested in the subject. The meetings provide a source of the most recent information, an open forum for discussion and consultation, facilitate contacts between the academic and commercial competence, improve understanding, mutual respect, and cooperation between the participants.

In organizing this symposium, we tried to create a forum for discussions between people from different areas of both theory and practice. We hope that it was a fruitful meeting for those involved in the development of composites. Due to the diversity of composite materials, sharing the opinions and experiences constitutes a necessary and fertile element for the advancement.

The main topic of the meeting was the solid state behavior of advanced, fiber reinforced composites. Accordingly, the papers are grouped into two parts. The first starts with an invited review by M.R. Piggott on the influence of interface on composite properties followed by seven papers on interface characterization and mechanism of fracture and delamination in advanced composites.

The second part, starting with a review by T. Vu-Khanh on current status and future trends in reinforced plastics and ending with a transcript of discussion on the subject of thermoplastics *vs.* thermosets in advanced composites, deals primarily with analysis and performance of composites and composite-like materials.

It is our pleasant duty to express once again our gratitude and thanks to the authors and participants of the Symposium. As evidenced by the discussion transcripts the meeting was a lively one with a frank exchange of concepts and opinions. It made a small but important contribution toward better understanding of these materials.

T. Vu-Khanh and L.A. Utracki
Symposium Organizers

Survey of Current Status and Future Trends in Reinforced Plastics Composites

T. VU-KHANH

Industrial Materials Research Institute
National Research Council of Canada
Boucherville, Québec, Canada J4B 6Y4

The production of reinforced plastics has constantly increased since the Second World War. With a forecast growth rate of 8 to 12 percent annually over the next decade, composites are one of the fastest growing sectors of the plastics industry. Advanced composites will show the largest expansion, due to a strong increase in demands in aerospace and military markets. Penetration of advanced composites into big-volume markets has not occurred, but it is believed that advances in both materials and machinery will accelerate the mass-production of these materials. High-volume composites will see a less rapid growth rate but demands for these materials will continue to increase. Land transportation will remain the largest and will be also the fastest growing market for high-volume composites. Current status and future trends in the uses of various reinforcing fibers and matrix resins are presented. Hurdles to the expansion of reinforced plastics are also discussed.

INTRODUCTION

After a period of sustained growth in plastics consumption, the volume of plastics now exceeds that of raw steel. However, since the beginning of the seventies, forecasts made by extrapolating from past data have consistently proven too optimistic. The gap between capacity and sales of plastics in the Western world is widening. Pressure of composition compels companies to focus on materials offering higher performance. It is obvious that the next potential market for plastics will be found in the area of substitution for conventional metallic materials in structural parts. In order to fulfill this function, the mechanical properties of plastics must be improved. The most attractive idea for doing this has been through addition of stiffer and stronger reinforcements. Since the Second World War, the production of reinforced plastics has increased constantly. Today there is a bustle of activity in the plastic-composites industry.

This paper reviews the current status of reinforced plastics in various markets. The trends in the use of plastic composites for different applications are identified and the growth rates of demands predicted for these materials for the next decade are presented. The following points will be discussed:

- General survey of consumption and growth rate of the reinforced-plastics industry
- Present and future trends in the use of high-performance composites
- Present and future trends in high-volume composites
- Hurdles to the expansion of reinforced plastics

CONSUMPTION AND GROWTH RATE OF REINFORCED PLASTICS

Table 1 shows the 1985 consumption of reinforced and non-reinforced plastics for different geographical areas. At present, the world consumption of plastics is around 60 million metric tons in which reinforced plastics represent less than 5 percent. The United States alone accounts for 50 percent of the total world shipments of the plastics industry. The consumptions per capita of reinforced plastics and all plastics in different industrialized regions are shown in *Table 2*. It can be seen that the consumptions vary considerably. The U.S. is significantly ahead in plastics consumption, particularly reinforced plastics, with almost twice the amount consumed as Western Europe and Japan.

During the last decade, the average world annual growth rates of all plastics and reinforced plastics were about 6 and 8 percent respectively (*Table 3*). These growth rates have been considerably reduced compared to the healthy rate of growth of the plastics industry from 1950 to 1970. It must be noted, however, that the depression of demand for plastics and related products has been less severe than for other items after two consecutive energy crises. For the next decade, estimates are even more conservative. An annual growth of only about 4 percent is expected for all plastics consumption. This means that present consumption will not double by the end of the century. In this rather clouded perspective, forecasts for reinforced plastics nevertheless suggest a remarkable growth of between 8 and 12 percent per year until 1995.

The first factor contributing to the expansion of reinforced plastics is the ratio of performance to material density. Addition of reinforcing fibers increases the rigidity and strength of plastics. *Figure 1* shows a comparison between conventional metallic materials and common unidirectional composites with epoxy matrix. In terms of specific strength and stiffness (defined as the strength and modulus divided by the density of the material) polymeric composites can offer better performance.

Another factor that makes composite materials attractive is that they can be tailor-made to meet specific requirements. The performance of the final product can thus be optimized more efficiently. In addition, the behavior of anisotropic materials can be explored to achieve functions which are not accessible with conventional materials.

Reinforced plastics appeared in the very early development stage of the plastics industry and their production has been constantly increasing. The U.S. production of reinforced plastics since the Second World War is shown in *Fig. 2*. Due to advantageous properties, reinforced plastics find many applications in a variety of markets. The pattern of reinforced plastics consumption in the United States in 1985 is summarized in *Table 4*. The largest market for these materials is land transportation with more than 25 percent of the total consumption. The second market is construction which occupies 19.5 percent, followed by corrosion-resistant equipment with 14.4 percent. Consumption by these three industries accounts for 59 percent of the total.

In terms of matrix material, the most common resin used in composites is unsaturated polyester. This is due to low cost of the resin and also its adaptability to fabrication of large structures. *Figure 3* presents the share of the com-

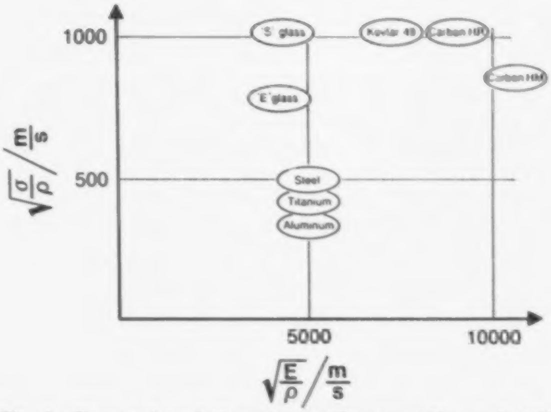

Fig. 1. Comparison between specific strengths and stiffnesses of conventional metallic materials and common unidirectional composites with epoxy matrix (13).

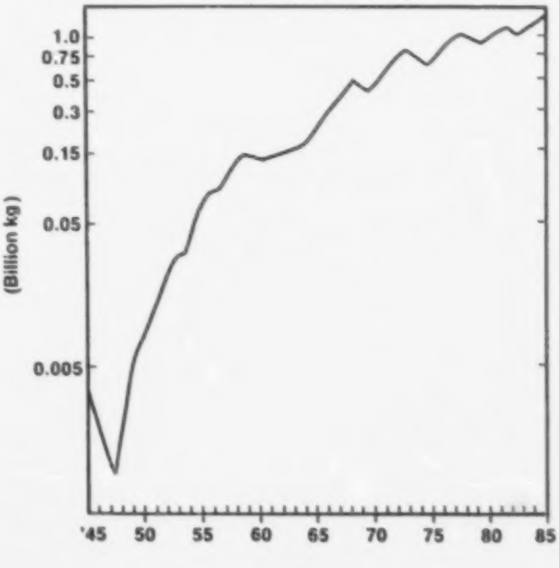

Fig. 2. U.S. production of reinforced plastics since the Second World War (9, 10).

Table 1. World Consumption of Reinforced Plastics and All Plastics in 1985 (1–3).

	Million Metric Tons		
	U.S.A.	Western Europe	Japan*
Reinforced Plastics	1.1	0.8	0.3
All Plastics	23	25	11

* Estimated.

Table 2. Consumptions Per Capita of Reinforced Plastics and All Plastics in Industrialized Regions in 1985 (kg).

	U.S.A.	Western Europe	Japan
Reinforced plastics	92	71	73
All plastics	4.3	2.2	2.5

Table 3. World Average Annual Growth Rates of All Plastics and Reinforced Plastics (4–8).

	1975–1985	1985–1995
All plastics	6%	4%
Reinforced plastics	8%	8 to 12%

Table 4. Pattern of U.S. Reinforced Plastics Consumption in 1985 (11).

Market	Millions Kg	Total %
Aircraft	18	1.6
Appliances/Business equipment	65	5.7
Construction	222	19.5
Consumer products	75	6.6
Corrosion-resistant equipment	163	14.4
Electrical/Electronic	102	9.0
Marine	162	14.3
(Land) Transportation	285	25.1
Others	43	3.8
Total	1135	100.0

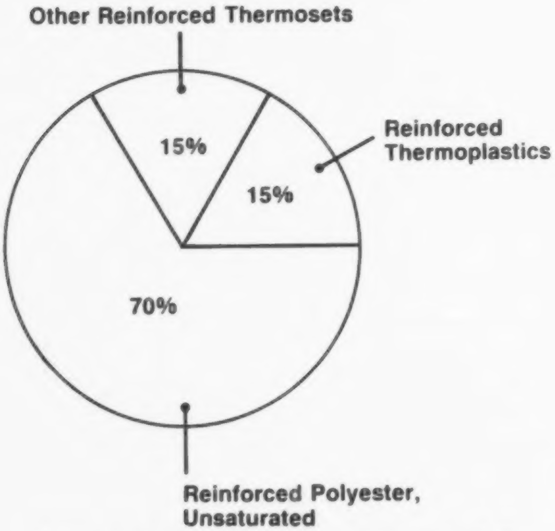

Fig. 3. Pattern of resins used in composites (2, 3).

posite market held by different matrix polymers. Unsaturated polyester represents about 70 percent of the total use while the other thermosets and thermoplastics evenly share the remaining part.

The pattern of 1985 U.S. consumption of composites based on unsaturated polyesters is shown in *Table 5*. As can be expected, these ratings are similar to those of reinforced plastics (see *Table 4*). However, some differences can be seen. For composites based on unsaturated polyester land transportation is only the fourth market, whereas marine along with corrosion-resistant products occupies the second place after construction.

As for reinforced thermoplastics, nylon and polypropylene are the most commonly used resins. They represent more than 50 percent of total production. Another 20 percent is occupied by polyester thermoplastics and the remaining production consists of other thermoplastics.

In terms of processing, about 64 percent of the total volume of reinforced plastics is made by open molding methods such as spray-up, hand lay-up, filament winding, pultrusion, etc. Closed molding such as injection, compression, resin transfer, etc., represents about 36 percent of total production.

Among the three common reinforcing fibers; glass, carbon, and aramid, glass is by far the most popular in terms of volume consumption (*Table 6*). This is due to the low cost and respectable performances offered. Their general characteristics are given in *Table 7*. The matrix and fibers are selected according to performance required and cost effectiveness.

The form of reinforcement is also an important factor. It determines the processing method and strongly influences the final product performance. *Figure 4* shows the effect of the form of continuous filament reinforcement on the mechanical properties of the composite. Taking the fiber performance as 100 percent, the roving form can impart 70 to 80 percent of the performance of the fibers to the composite, woven fabric 45 to 50 percent, and mat only 25 to 30 percent. In general, the fabrication cost of the composite is proportional to performance.

Reinforced plastics are often divided into two classes: high performance (advanced) and high volume composites. The term advanced composites is used for materials with specific rigidity and strength superior to conventional metallic materials. The particularity of this class of composite is that it is, in general, made with continuous fibers. "High volume composites" is used to designate other reinforced plastics. These materials are mainly used in large volume markets. Their performances are much lower than that of the former class. Here, the safety coefficient required in design is in general very large (>5).

ADVANCED COMPOSITES

Due to their high costs, low density and good mechanical performance, the main market for

Table 5. Pattern of Consumption of Composites Based on Unsaturated Polyesters in 1985 (1).

Market	Millions Kg	Total %
Aircraft/Aerospace	14	1.8
Appliances/Business equipment	42	5.2
Construction	200	24.9
Consumer	66	8.2
Corrosion-resistant products	160	20.0
Electrical	24	3.0
Marine	160	20.0
(Land) Transportation	110	13.7
Others	26	3.2
Total	802	100.0

Table 6. U.S. Sales of Reinforcing Fibers (12). Industry Estimates in Metric Tons.

Type	1984	1985	1986
Glass	300,000	315,000	320,000
Aramid	1,400	1,750	2,185
Carbon	1,200	1,560	2,000

Table 7. General Mechanical Characteristics of Common Fibers (13).

		Density (10^3 kg/m^3)	Filament Diameter (μm)	Strength (MPa)	Elastic Modulus (GPa)	Elongation at Fracture (%)
Glass	E	2.54	3.8–13	3200–3900	73	4.8
	S	2.48		4400–4900	86	5.4
Aramid	29	1.44	6–12	2700	60	4
	49	1.45			130	2.1
Carbon	High strength	1.78	8	2300–3100	210	0.9–1.2
	High modulus	1.87		1700–2200	350	0.5

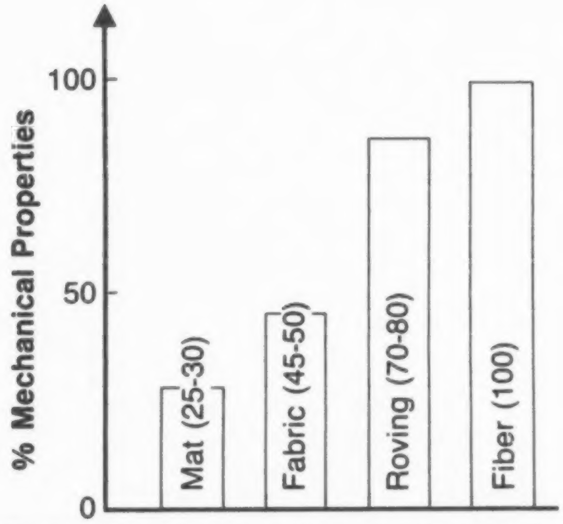

Fig. 4. Effect of reinforcement form on mechanical performance of composites (13).

Table 8. World Market for Advanced Composites (13).

Aircraft/aerospace	40%
Recreational uses	30%
Industrial products	20%
Automotive and others	10%

Table 9. Consumption of Advanced Composites in Industrialized Regions (13).

Use	Western Europe	U.S.A.	Japan
Aircraft/Missiles	80%	60%	10%
Recreational uses	10%	30%	80%
Others	10%	10%	10%

advanced composites is aerospace; about 40 percent of the total as shown in *Table 8*. Recreational uses are the second market with 30 percent, followed by industrial products (20 percent) and automotive parts and others (10 percent).

This pattern of consumption is not the same in all regions. It depends strongly on the military industry of the area. *Table 9* shows the uses of advanced composites in three main industrialized regions. It shows that aircraft and missile applications occupy 80 percent of the total consumption of advanced composites in Western Europe, 60 percent in the United States, and only 10 percent in Japan. On the other hand, only 10 percent of advanced composites in Western Europe is used in recreational application whereas this proportion attains 30 percent in the United States and 80 percent in Japan.

According to a recent study (14), the market for advanced polymer composites is projected to grow 16 percent per year throughout the next decade. A more moderate growth rate of 7 percent was forecast in another report (15). In both studies, the greatest opportunity is expected to occur in the aerospace market. The annual growth rates projected by these studies for aerospace applications were respectively 22 and 8.5 percent. Although these forecasts are dramatically different, both suggest that penetration of advanced composites into big volume production has not occurred yet and that aerospace application is still dominant. However, it is believed that this is just a question of time. Present advances in both machinery and materials will accelerate the mass-production of advanced composites. Acquisitions of established businesses in advanced composites by major plastics suppliers (16) are also the indications for the future.

The predicted expansion is due, in large part, to accelerated demands by civilian aircraft and helicopter industries (15). Currently, commercial aircraft such as the Boeing 757 and 767 contain only about 4 percent by weight of advanced composites. If the composites option is taken, it can be expected that within the next ten years, reinforced plastics will account for 65 percent of the materials. It is also projected that if the aluminum alloys option is taken, 25 percent of the market will nonetheless be occupied by the composites. Meanwhile, the applications in military aircraft will continue to increase. The next decade will see an acceleration in the applications of advanced composites in primary structural parts. An all-composite airframe is being developed by helicopter manufacturers. In addition to the benefits related to weight reduction, the use of composites can lower the fabrication costs. Processing routes such as filament winding are now being studied to produce an integrated fuselage using a small number of production steps.

The spin-off from technology developed in the aerospace industry is expected to enter the mass-production market. However, lower cost and high productivity technologies are needed to speed up the general acceptance of advanced composites in other markets. There have been many examples of application of high performance composites for automobile parts such as: leaf springs and steering columns made by filament winding, engine parts, etc. The all-composite car is also possible today, but the lack of equipment for mass-production makes it not cost competitive. Progress is being made in this area and automated fabrication processes (tape laying, pultrusion, resin transfer molding, filament winding, etc.) are believed to have very promising potential.

The most common reinforcing fibers used in advanced composites are S-glass, graphite, and kevlar. With a total world consumption of advanced composites of about 12,000 metric tons, S-glass occupies 42 percent, carbon 30 percent, and aramid 27 percent (14).

A variety of high-performance resins can be used as the matrix material for advanced composites, but still the most common by far is epoxy. *Figure 5* shows the proportion of world consumption of matrix resin in 1985. Epoxy represents 80 percent of the total consumption and thermoplastics and other thermosets occupy 8 and 12 percent respectively.

It is expected that the use of thermoplastics (such as polyetheretherketone, polysulphone, poly(phenylene sulphide), etc.) will significantly increase in the near future. These resins can impart lower fabrication cost, higher toughness, and damage tolerance which represent an important improvement since one of the most important weaknesses of advanced composites is brittleness. *Figure 6* shows the current delamination energy in advanced thermoset composites, in comparison with the fracture energies of some other commonly used thermoplastics. *Table 10* shows a comparison between selected thermoplastic and thermoset matrix resins used in advanced composites. With respect to epoxy and polyester, polyetheretherketone (PEEK) and polyethersulphone (PES) exhibit fracture elongation about ten times higher. In addition to the toughness improvement, thermoplastics can also offer higher solvent resistance, reduce fabrication costs, lower costs of materials storage, and reduce quality-control costs (19).

HIGH VOLUME COMPOSITES

After a period of strong expansion, sales figures for high volume composites have slowed down. For the next decade, the growth rate of this class of materials will not be comparable to that of high performance composites. The development of new materials exhibiting increased performance and the improvement of productivity are the main factors contributing to the sustained demand for these materials. New technologies and improved properties help

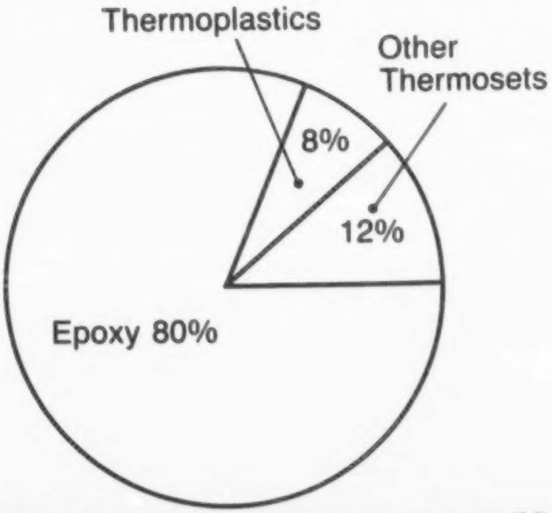

Fig. 5. Matrix resins used in advanced composites (14).

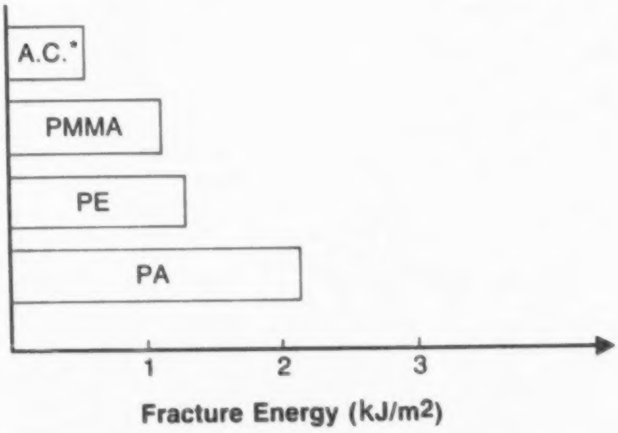

* Advanced Thermoset Composites: Common Delamination Energy

Fig. 6. Comparison between current delamination energy in advanced composites and fracture energies of common thermoplastics (28–31).

Table 10. Comparison Between Selected Thermoplastic and Thermoset Resins (17, 18).

Property	PEEK	PES	Conventional Epoxy	Conventional Polyester
Density (g/cc)	1.30	1.37	1.21	1.12
Tensile Strength (MPa)	93	84	59–74	55–70
Tensile Modulus (GPa)	3.8	2.8	2.8–3.5	3.4–3.9
Elongation at fracture (%)	>100	40–80	8	3

high volume composites to find new applications in existing markets. For example, in the marine segment, the sailboat market will continue to be sluggish, and further decline is anticipated. However, new applications in the power boat market are expected.

The design flexibility offered by novel resin/reinforcement combinations and new processing and machinery innovations enable high volume composites to compete with metals in more and more areas. Consequently, in declining markets such as corrosion-resistant equipment or construction, demands for reinforced plastics will continue to grow. For example, in appliances and business equipment, new plastics will favor innovative designs, while new processes will allow consolidation of large parts. Although production costs of reinforced plastic parts are still high, these materials can usually be molded or formed to be compatible with automated assembly. Automation forces new approaches to product design which tend to reduce assembly costs. This will be an important factor contributing to future expansion.

Among a very large number of markets, land transportation is the largest for high volume composites, and this situation will remain unchanged for the next decade. The continuing search by the automotive industry for less weight with greater strength and corrosion resistance, along with fewer steps during assembly, make reinforced plastics an attractive solution. *Table 11* shows possible weight reductions with composites in different automotive components. Besides other advantages such as better performance and lower production costs, weight saving is also a major parameter for automobile manufacturers since the direct result is reduction in energy consumption.

For the next five years, a leveling off in the number of cars made in North America has been forecast. Car and truck production is expected to grow only 2.8 percent per year until 1989. However, a strong surge in the growth rate of reinforced-plastics application is predicted. The use of reinforced plastics is no longer based on the question of choice but on the sophistication of design and on material selection. The growth of high-volume-composite application, however, will be uneven. Exterior panels and large structural parts will be the most promising areas of application.

Thermosets are still the preferred resins for high volume composites. *Table 12* shows the projected pattern of consumption of thermoset composites in automobiles for different manufacturing processes until 1989. Reinforced RIM (reaction injection molding) is expected to be one of the fastest growing processes. Compression molding will remain the dominant process for thermoset high volume composites but, as a percent of the total, it will decline from 83 to 72 percent through the forecast period.

Table 11. Possible Weight Reductions With Reinforced Plastics in Automotive Components (20).

	Reduction in Weight (%)
Internal engine components	30–70
Support structures	40–75
Miscellaneous	30–50

HURDLES TO THE EXPANSION OF REINFORCED PLASTICS

Even though forecasts appear to be optimistic, many hurdles have to be overcome to allow a rapid expansion of the use of composites. These can be related to technical aspects, industrial and economical reasons, or human and training problems. Depending on the market, the nature of the obstacle can be different.

In aerospace applications, the most important problems are related to technical aspects. Advanced composites offer high rigidity and strength, but their impact resistance is modest. Due to the poor toughness of matrices, advanced composites exhibit low interlaminar fracture energies. Although thermoplastics seem to offer better ductility, further development work is required. For a brittle matrix, an increase in the matrix ductility leads to a significant increase in the interlaminar fracture energy of the composite. However, with a ductile thermoplastic matrix it has been observed that increase in interlaminar fracture energy levels off as shown in *Fig. 7.* A great increase in matrix toughness improves the composite only slightly. More investigations on fracture mechanisms of advanced composites are needed to take full advantage of the ductility of thermoplastics. Another important hurdle is that designs of composite parts are based mainly on a trial and error approach, resulting in a costly procedure.

In industrial applications, heat resistance and fire retardance appear to be a limitation for the use of plastic composites in many areas. However, the major obstacle is probably related to a human problem. Design engineers are very reluctant to use new materials such as composites. Insufficient technological know-how and inadequate knowledge of the material behavior often result in rejection of reinforced plastics. The particularity of these materials requires combined knowledge of both the material and

Table 12. Projected Pattern of Consumption (in thousand metric tons) of Thermosetting Composites in North American Automobiles for Different Manufacturing Processes (21).

Process	1985	1987	1989
Compression	113	131	166
Injection	15	14	15
Low Pressure	9	9	9
Filament Winding	3	5	7
RRIM	16	32	35
Pultrusion	156	191	233

design aspect in order to obtain optimum use. In addition, the lack of simple calculation programs also limits development. An example of the need for a simple calculation program is shown in *Fig. 8*. For symmetric laminates containing identical ply orientations, interlaminar stress development in simple traction depends on the stacking sequence. As shown, it can change from tension to compression which will affect the strength of laminates. Therefore simple computer programs are essential in order to elucidate the particular behavior of composite materials.

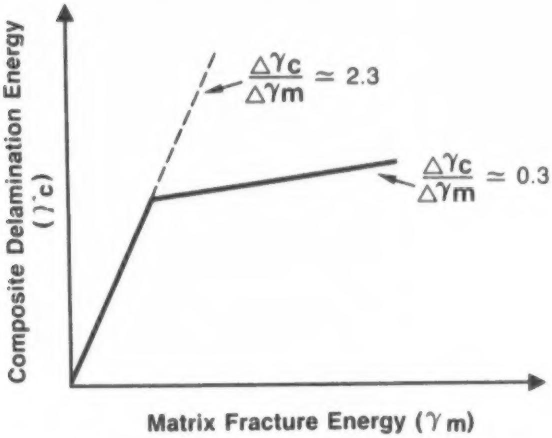

Fig. 7. Schematic drawing showing the effect of matrix toughness on interlaminar fracture energy of advanced composites (22).

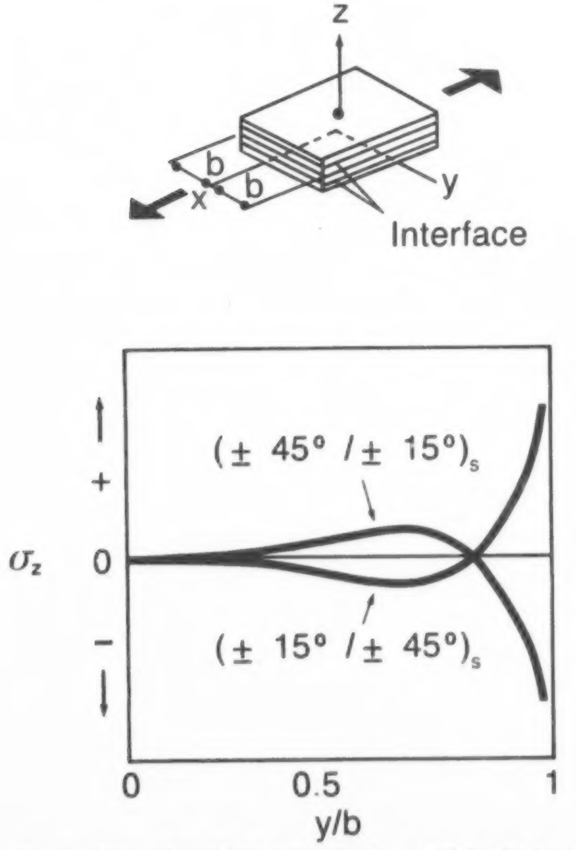

Fig. 8. Effect of stacking sequence on interlaminar normal stress (23–25).

In the mass production areas, cost is still a major factor in many applications. More equipment suitable for mass production is needed to reduce fabrication costs and to make composites more attractive. There is also a lack of experts and skilled labor. The education of designers and engineers should be one of the top priorities for the reinforced-plastics and composites industry. Much effort is needed for quality control. Training programs and quality standards and methods must be implemented to improve the quality level of composite materials. In impact-resistance characterization for instance, the Izod and Charpy tests are widely used. However, since the rigidity of plastics strongly increases with the addition of reinforcements, the measured impact energy often appears to be lower even if the true impact fracture energy of plastics is improved. An example is shown in *Fig. 9* for mica-reinforced polypropylene. The fracture toughness of polypropylene increased with addition of mica up to about 20 wt percent of loading (26) but in the same concentration range the Izod test showed a decrease in fracture energy (27).

Many more examples of barriers to the general acceptance of composites can be quoted.

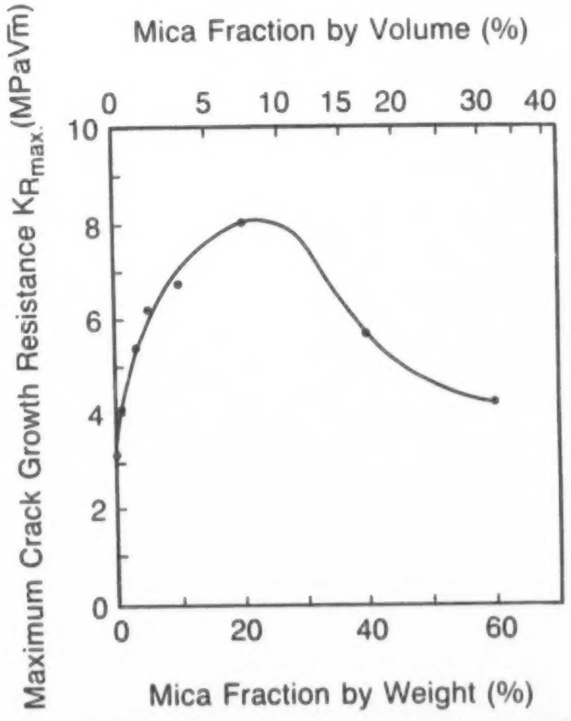

Fig. 9. Effect of mica concentration on maximum crack growth resistance of mica-reinforced polypropylene (26).

However, the purpose of the above discussion is only to illustrate the more common ones that contribute to numerous factors that prevent more rapid expansion of reinforced plastics.

SUMMARY AND CONCLUSION

With a forecast annual growth rate of 8 to 12 percent, reinforced-plastic composites will be one of the fastest growing sectors of the plastics industry through the next decade. The expansion of reinforced plastics is, however, uneven. Advanced composites hold the brightest performance future with a remarkable growth rate of about 16 percent per year. This is mainly due to a strong increase in demand in the aerospace and military markets. It is expected that the use of advanced composites in the aerospace industry will double by 1995. This expansion is due to an increase in new applications in civilian aircraft and helicopters. Although the penetration of advanced composites into the big volume market has not occurred, mass production is believed to be a question of time. Advances in both machinery and materials will accelerate the pace. The next potential big volume market for these materials is expected to be in the automotive industry.

The high volume composites will see a slower expansion. However, demands for these materials in some sectors will increase substantially. For instance, application of composites in automobiles will grow more than 10 percent annually, at least until the end of the eighties. This healthy growth will be a major factor for the development of high volume composites.

There are many hurdles that have to be overcome before a more rapid growth of reinforced plastics can be achieved. These hurdles are diverse and can be related to many causes. First of all, reinforced plastics have weaknesses. Their high rigidity and strength are often obtained at the expense of toughness. Heat resistance is a limitation in many applications. Because of their particular behavior, more data on properties of reinforced plastics are needed for confidence in their use. The lack of codes, standards, and simple calculation programs are further obstacles to their development. Besides technical problems, the reluctance of design engineers to utilize these materials is also a major factor. Training must be a priority in order to accelerate the acceptance of these materials.

REFERENCES

1. *Trends in End-Use Markets for Plastics*, January–December 1985.
2. "Modern Plastics International Special Report", *Mod. Plast. Int.*, **16**, 24 (1986).
3. "Materials '86", *Mod. Plast.*, **63**, 43 (1986).
4. "Industry news", *Plastics in Building Construction*, **8**, 2 (1985).
5. H. Rudolph, *Polym. J.*, **17**, 13 (1985).
6. *Mod. Plast.*, **53–63**, (1976–1986).
7. *Modern Plast. Int.*, **11–16**, (1981–1986).
8. Markets Newsletter; *Chem. Week*, **20** (11), 37 (1985).
9. M. Deitsch and V. Kollomitsh, Eds., "The Kline Guide to the Plastics Industry", C. H. Kline & Co. Inc., Fairfield, N.J., (1982).
10. "Business Outlook", *Plast. World*, **43**, 6 (1985).
11. "Reinforced Plastics", *Trends in End-Use Markets for Plastics*, March, 0606 (1985).
12. A. S. Wood, *Mod. Plast. Int.*, **15**, 52 (1985).
13. C. Bord, J. P. Durand, M. Reyne, and M. Weiss, "Matériaux Composites, Evolution, Aspects Technico-Economiques", Etude 123221, Ministère de la Recherche et de l'Industrie, France, N° 80-2-37-0239 (DICTD).
14. D. Prown "Advanced Polymer Composites", C. H. Kline & Co. Inc., Fairfield, N.J., (1985).
15. "High Performance Composites", Frost & Sullivan Inc., New York, N.Y., (1985).
16. A. S. Wood, *Mod. Plast.*, **63**, 44 (1986).
17. C. K. Hall, "Continuous fibre reinforced thermoplastics in new generation radomes", Int. Conf. Fibre Reinforced Composites '84, pp. 19.1–19.12, Liverpool, England, 3–5 April (1984).
18. "Advances in fibre reinforced plastics", *Reinfor. Plast.*, **28**, 154 (1984).
19. "Advanced Composites News", *Plast. Technol.*, **32**, 13 (1986).
20. K. R. Berg, "Advanced composite materials compete in the automotive market", in "Fibrous Composites in Structural Design", E. M. Lenoe, D. W. Oplinger, and J. J. Burke, Eds., New York (1980).
21. "Plastics/Market Trends", *Plast. World*, **43**, 106 (1985).
22. D. L. Hunston, W. D. Bascom, R. J. Moulton, and N. J. Johnston, "Matrix Resin Effects in Composite Delamination: Mode-I Fracture Aspects", ASTM Symposium on "Toughened Composites", Houston, TX, March 13–15, (1985).
23. A. H. Puppo and H. A. Evensen, *J. Compos. Mater.*, **4**, 204 (1970).
24. R. B. Pipes and N. J. Pagano, *J. Compos. Mater.*, **4**, 538 (1970).
25. N. J. Pagano and R. B. Pipes, *J. Compos. Mater.*, **5**, 50 (1971).
26. T. Vu-Khanh, B. Sanschagrin, and B. Fisa, *Polym. Compos.*, **6**, 249 (1985).
27. C. Busigin, R. Lahtinen, G. M. Martinez, G. Thomas, and R. T. Woodhams, *Polym. Eng. Sci.*, **24**, 169 (1984).
28. D. J. Wilkins, J. R. Eisenmann, R. A. Camin, W. S. Margolis, and R. A. Benson, in *Damage in Composite Materials*, ASTM STP 775, K. L. Reifsnider, Ed., American Society for Testing and Materials, 168 (1982).
29. A. J. Russell and K. N. Street, in *Progress in Science and Engineering of Composites* (ICCM IV), T. Hayashi, K. Kawata, and S. Umekawa, Eds., 279 (1982).
30. F. X. de Charentenay, J. M. Harry, Y. J. Prel, and M. L. Benzeggagh, in *Effect of Defects in Composite Materials*, ASTM STP 836, American Society for Testing and Materials, 84 (1984).
31. J. G. Williams, "Fracture Mechanics of Polymers", Ellis Horwood Ltd., Chichester, West Sussex, England (1984).

Thermoforming of Ordered Polypropylenes

S. IABONI and R. T. WOODHAMS

Department of Chemical Engineering and Applied Chemistry
University of Toronto, Toronto, Canada M5S 1A4

Uniaxial molecular ordering of polyolefin billets by a process of roll-drawing produces clear, transparent sheets having greatly increased strength and modulus in the draw direction whereas the strength and modulus in the transverse direction remain essentially unaltered. Such sheets may be laminated together by means of ultrasonic welding, electromagnetic induction heating or simple pressure lamination using adhesive tie layers to produce multiply laminates with controlled biaxial properties. These self-reinforced laminates have mechanical properties which compare favorably with advanced aramid or carbon fiber composites. Conventional thermoforming techniques may be employed to convert these highly ordered sheets into shaped products having potential commercial value. In these investigations examples are presented to illustrate the methods of laminating and thermoforming of ordered polypropylene sheets. Examples are also presented to demonstrate the feasibility of pressure forming of ordered polypropylene laminates into more complex three-dimensional shapes without loss of their mechanical properties. The techniques described in this paper may be applied to other crystalline polymers to create a new spectrum of self-reinforced plastics capable of approaching the limits of performance.

INTRODUCTION

In a previous publication a process referred to as "roll-drawing" was employed to manufacture highly ordered polypropylene (isotactic) sheets having predominantly uniaxial orientation in the draw direction (1). Roll-drawing is a novel method of orienting polymer chains by solid phase deformation at temperatures slightly below the crystalline melting transition. The limiting draw ratio is predetermined by the number of chain entanglements, a value which is normally related to molecular weight and chain flexibility. Commercial extrusion grade polypropylenes have a limiting draw ratio near 20. At such draw ratios the uniaxial ordered sheets generally attain a Young's modulus of 20 GPa and a corresponding tensile strength of 0.5 GPa in the draw direction while the properties in the transverse direction are virtually unaffected. The mechanical properties in any direction may be predicted from composite mechanics for anisotropic sheets (2–4). Simple lamination of these ordered sheets should produce biaxially strengthened laminates with specific properties comparable to those of many advanced fiber composites derived from aramid or carbon fibers.

The objective of this research project is to seek appropriate methods of laminating ordered plastics without loss of orientation and to examine the thermoforming characteristics of ordered laminates. Reported here are the preliminary findings for these unusual high performance materials.

ROLL-DRAWING PROCEDURE

The roll-drawing equipment is comprised of four sets of heated rolls with heavy duty bearings as illustrated in *Fig. 1*. The extruded polymer billet (Trovador 500 Series stress-relieved polypropylene sheet manufactured by Dynamit Nobel; $\bar{M}_n = 70{,}900$, $\bar{M}_w = 377{,}000$) was preheated to 158°C in a circulating air oven. The billets were 15 cm wide and 9.91 mm thick, tapered at one end to facilitate feeding each billet into the first set of working rolls. The leading edge was then manually inserted into the second, third, and fourth set of rolls. The working rolls were preset at a gap of approximately 1 mm and this gap largely determined the final thickness of the drawn sheet, functioning as a non-passive slit extrusion die. The working rolls were maintained at 158°C by

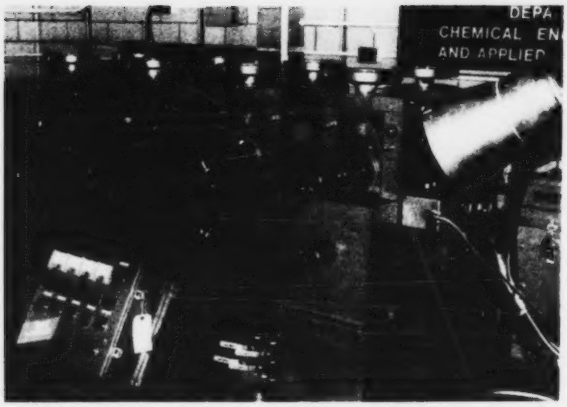

Fig. 1. The four-stand plastics roll-drawing mill is shown with an extruder sheet die feeding the heated working rolls. Maximum draw ratios of twenty are obtained in a single pass.

heated circulating oil whereas the remaining rolls provided tension and cooling of the drawn sheet. Although draw ratios near 20 were attainable by careful manipulation of the drawing conditions, the sheets used in the following thermoforming experiments had draw ratios of 10 to 11. The sheets were cut into rectangular test specimens and grid lines were drawn on the surfaces in order to measure the deformation after thermoforming. Small sections of the thermoformed grid were removed for measuring the dynamic modulus with a Rheovibron instrument.

LAMINATION PROCEDURES

Three methods of ply lamination were employed in order to fabricate multiply laminates with biaxial orientations. The simplest technique involved ultrasonic welding. A second method employed induction heating with a 10 MHz electromagnetic welding unit using the patented Hellerbond process (5). A third technique involved laminating the ordered polypropylene sheets together with an adhesive tie layer (Shell Development 8010 ethylene-butene copolymer, melting point 140°C).

THERMOFORMING PROCEDURE

A simple aluminum mold was constructed for attachment to a hydraulic press as shown in *Fig. 2*. The polypropylene sheet was clamped in a circular retaining ring which could be separately placed in an oven and removed for insertion in the mold just prior to thermoforming. The heated ring assembly was placed over the female cavity mold which was fitted with a vacuum port and then the press was immediately closed, causing the Teflon plug to force the softened sheet into the cylindrical cavity, assisted by vacuum and pressure as indicated. Each specimen was preheated in a circulating air oven for 20 min at temperatures between 160 and 180°C. The preferred temperature of the female cavity mold was 140°C with the upper Teflon plug section near 100°C. The recovered thermoformed specimens were analyzed for retention of mechanical properties, flow profiles, and wall uniformities over the drawn sections.

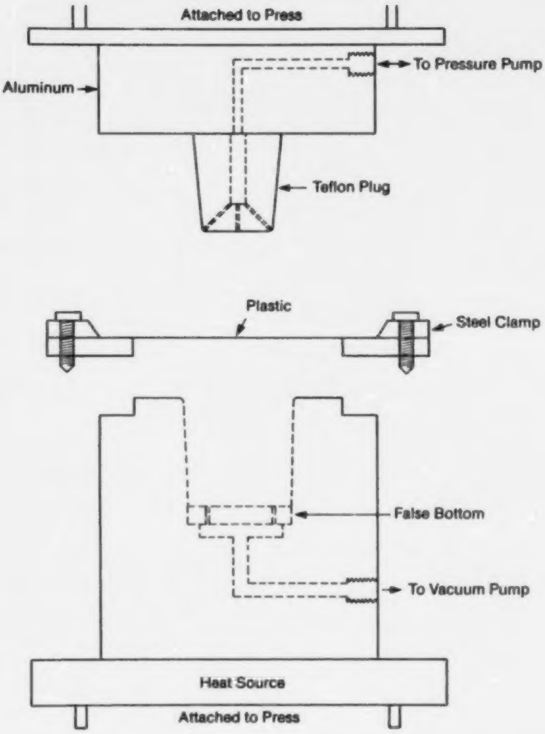

Plug Assist Die Used in Thermoforming

Fig. 2. The ordered thermoplastic is firmly gripped in a circular retaining ring and thermoformed in a heated cylindrical cavity with plug assist.

COMPRESSION MOLDING OF ORDERED LAMINATES

An aluminum mold having a V-shaped cavity was constructed in order to examine the mold filling characteristics of ordered polypropylene laminates. The flat mold was open at each side as shown in *Fig. 3*. The mold was placed in a heated 50 ton press between two flat plates. Samples of laminated, ordered polypropylene were then placed in the mold cavity and compressed at various temperatures to determine whether the laminates could be satisfactorily pressure formed into complex shapes without loss of their mechanical properties. The recovered specimens were tested in a 3-point bending mode to detect any loss of stiffness during the molding cycle.

RESULTS

Figure 4 shows the ordered polypropylene sheet firmly clamped in the retaining ring prior to thermoforming. The square grid pattern was

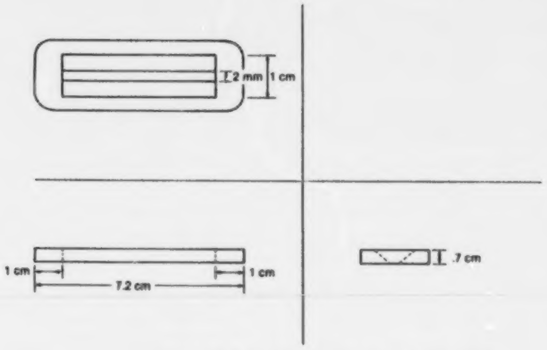

Fig. 3. A simple V-shaped cavity mold was fashioned from an aluminum plate in order to evaluate the forming characteristics of ordered laminates.

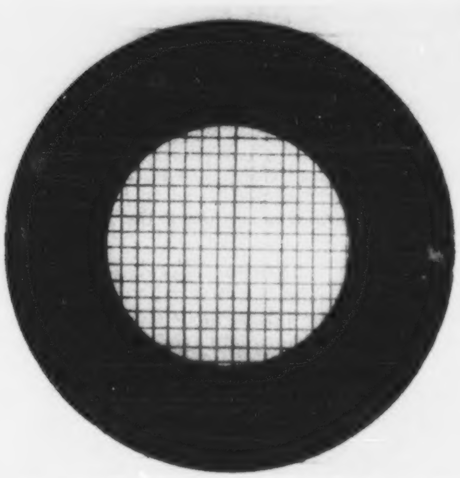

Fig. 4. A top view of the transparent sheet of ordered polypropylene with impressed grid lines clamped securely in the retaining ring just prior to thermoforming.

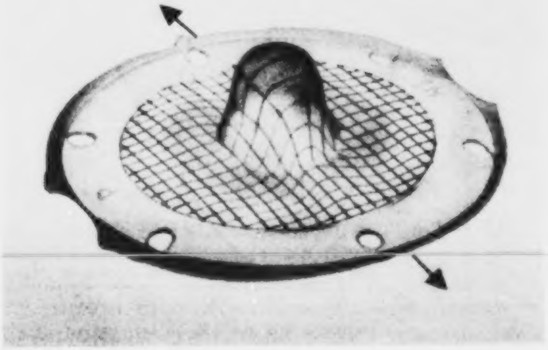

Fig. 5. After thermoforming the grid lines reveal the extent of biaxial drawing in each segment. Note the much larger extent of deformation in the direction perpendicular to the draw direction (the latter indicated by arrows).

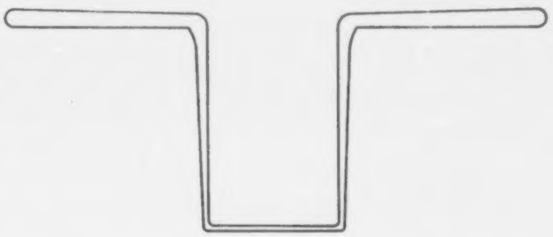

Fig. 6. The thermoformed cross section of the cylindrical cup shows a gradual reduction in thickness to the bottom of the draw zone.

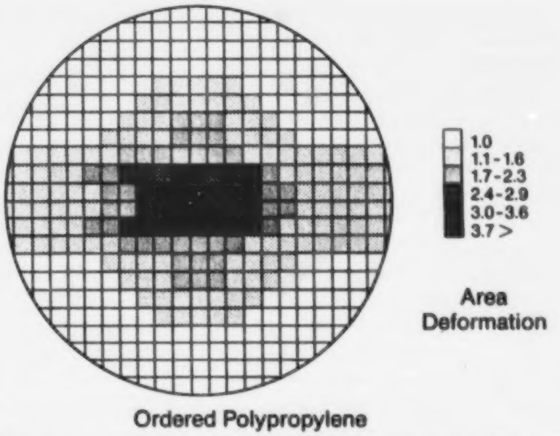

Fig. 7. A topographical map of the thermoformed sheet reveals the anisotropic nature of the area deformation (reciprocal of thickness) which reflects the unidirectional ordering of the polymeric molecules.

impressed onto the surface of the test sheet so that the strain profile could be measured after thermoforming. A typical thermoformed specimen is shown in *Fig. 5*. Note that the grid pattern indicates a much smaller deformation in the draw direction than in the transverse direction. An examination of the cross sectional thickness in *Fig. 6* illustrates the relative uniformity of draw, especially at the corners, with the wall thickness diminishing gradually towards the extremities at the bottom of the draw zone. The thickness profile is shown in *Fig. 7* for a sample sheet with an original sheet thickness of 1.0 mm which reduces to 0.27 mm or less in the middle of the drawn section. The draw profile is noticeably anisotropic with the grid lines indicating considerable plastic flow perpendicular to the draw direction whereas in the longitudinal direction the deformation is restrained.

Dynamic mechanical measurements of small sections cut from the bottom section of the thermoformed cup were determined over the temperature range from 0 to 140°C with a Rheovibron instrument. The tan δ values plotted in *Fig. 8* show two distinct features. First, the ratio of the loss modulus E'' to the storage modulus E' (tension mode) at 30 Hz decreases signifi-

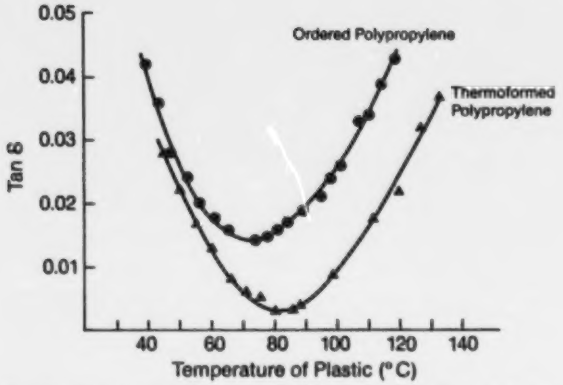

Fig. 8. The loss tangent of ordered polypropylene shows a minimum near 77°C which increases to 82°C after thermoforming (section taken from maximum draw zone). The decrease in Tan δ after thermoforming is attributed to a reduction in the loss modulus and an increase in the real modulus as a result of increased ordering.

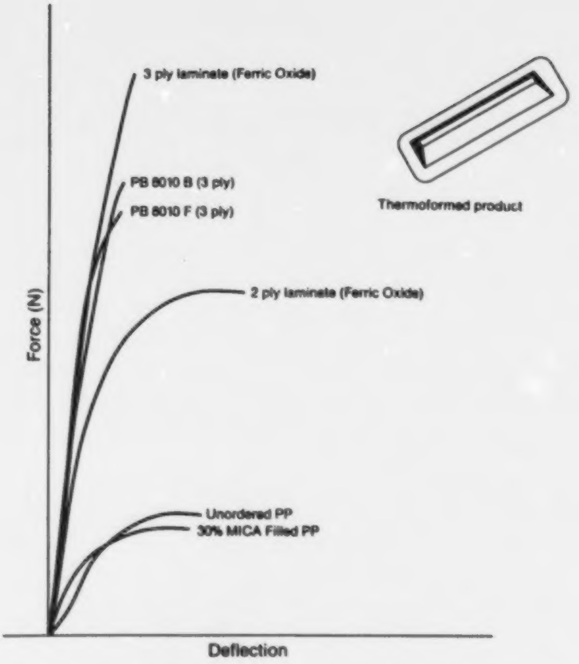

Fig. 9. Three-point bending deflections of compression molded laminates revealed large differences in the strengths and stiffness according to the method of preparation.

cantly after thermoforming, confirming that the actual draw ratio and degree of ordering has increased after thermoforming in this region. There has been no evident loss of ordering despite heating the preform to 180°C for 20 min or longer in the oven, and in fact the modulus actually increased due to the additional superimposed strain after thermoforming. The stress retention of ordered plastics at elevated temperatures is still under investigation but these preliminary observations indicate the remarkable retention of ordering even at temperatures several degrees above the melting transition of polypropylene where the sheet is in a transparent amorphous rubbery state.

The second observation is the shift in the tan δ minimum from about 72 to 83°C, indicating an apparent 10 degree increase in the melting temperature of the polypropylene after thermoforming. Such increases in the melting point of ordered plastics have been reported by several other investigators and are characteristic of ordered crystalline polymers. These changes in dynamic mechanical properties after thermoforming may be attributed to two factors. One factor is the increased draw ratio imparted by the thermoforming process and the other is the period of annealing during the thermoforming operation. It is likely both factors contribute to the increased storage modulus implied by the observed tan δ responses.

Pressure Forming

The press-formed laminates produced 5.2 cm oblong specimens having the rectangular shape shown in *Fig. 9*. Excess material was placed in the mold cavity, so that some flashing was inevitable. Near perfect replication of the mold contours was achieved despite the simplicity of the mold design, thus indicating the feasibility of molding complex parts from preordered billets or laminates. The miniature beams were subjected to three point bending in an Instron Tester in order to qualitatively compare the stiffness of the press formed parts with normal polypropylene. Included for reference was a commercial extruded polypropylene sheet and a polypropylene composite containing 30 percent mica. It is apparent from the force-displacement curves in *Fig. 9* that the ordered specimens were markedly stiffer and stronger than conventional molded polypropylene samples. The laminates were employed for the purpose of controlling the biaxial properties and providing preforms of the required thickness in order to fill the mold cavity. The molding process can be compared to the molding of glass fiber reinforced sheet molding compounds (SMC) in which the heated material is forced to flow under an applied pressure, thereby filling the mold cavity. The three-ply laminates with two plies aligned longitudinally in the mold cavity were particularly rigid and strong as shown in *Fig. 9*. It is apparent that the mechanical properties of the ordered polypropylene laminates can be retained at 160°C if pressure is applied and that the material can also be caused to flow under such conditions. In a separate series of experiments, cross-plied sheets of ordered polypropylene were laminated with an ethylene-butene-1 copolymer (Shell Development 8010 resin). The mechanical properties of the laminated sheets were sensitive to the time, temperature, and the applied pressure during lamination as indicated in *Figs. 10* to *15*. Since it was suspected that

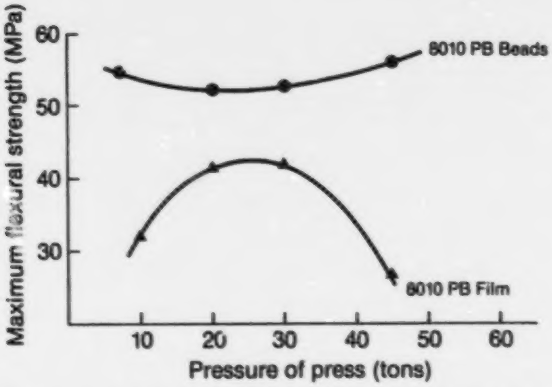

Fig. 10. The flexural strengths of ordered polypropylene laminates prepared with ethylene-butene copolymer tie layers (8010 PB) were sensitive to lamination pressures.

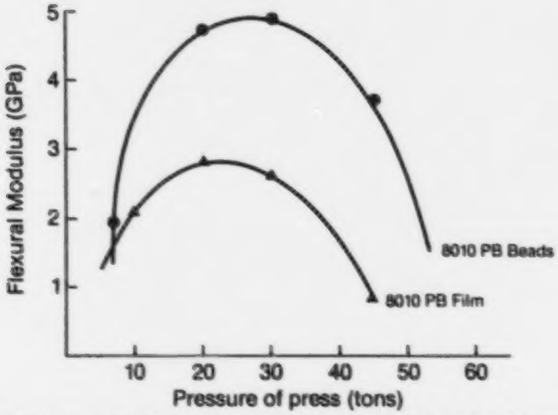

Fig. 11. The flexural modulus values of ordered polypropylene laminates attained maximum values at lamination pressures near 30 tons at 160°C.

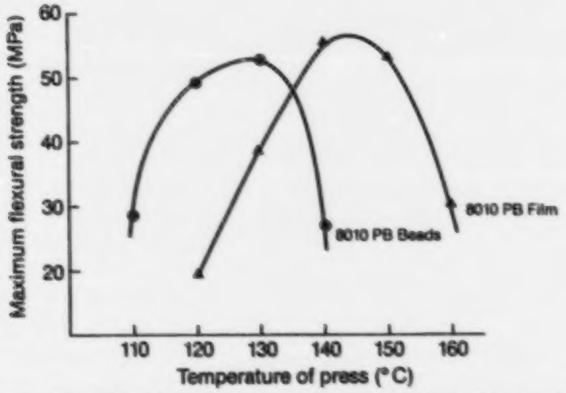

Fig. 12. The optimum lamination temperature of ordered polypropylene laminates was sensitive to the nature of the ethylene-butene (8010 PB) tie layer. Antiblocking agents in the extruded 8010 PB film may have accounted for the different response in this series.

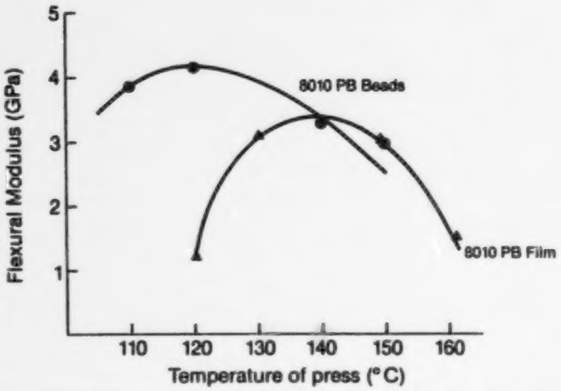

Fig. 13. Both the flexural modulus and the flexural strength appear to follow the same trend with respect to lamination temperature when the lamination pressure and lamination time are held constant.

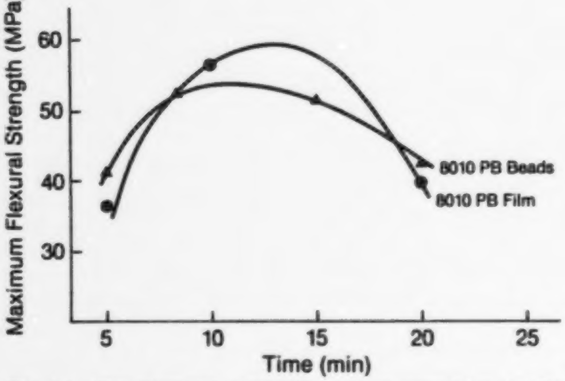

Fig. 14. The flexural strength is also sensitive to the heating time, reaching a maximum after 10 to 15 min.

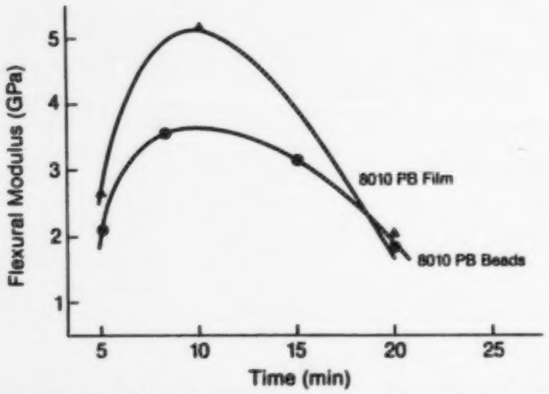

Fig. 15. The flexural modulus values of the ordered polypropylene laminates attain maximum values after 10 min lamination time at constant pressure and temperature during lamination.

the extruded ethylene-1-butene copolymer film was contaminated with an anti-blocking agent, films were also prepared from unadulterated ethylene-1-butene pellets by pressing the resin between heated flat plates. Results are presented for both types of adhesive films, those prepared in-house by pressing were designated as "8010 BP Beads". The extruded 8010 PB film was used as supplied by the Shell Development Company in Houston, Texas. It is unclear why the flexural properties of the laminates should show a maximum when plotted against the platen pressure (*Figs. 10* and *11*). The same type of dependence is apparent when the flexural properties of the laminate are plotted *vs.* time in the press and *vs.* platen temperatures. It is apparent that the conditions of time, temperature, and pressure must be controlled within a narrow range to ensure proper retention of the mechanical properties of these laminates.

Under certain conditions of heat and pressure Hwa-Lee and Schultz (6) found that highly oriented films of polypropylene could be successfully laminated together without the use of adhesives. These authors also observed a maximum in the ply adhesion when plotted *vs.* the molding pressures. Adhesion was attributed to interpenetration of the amorphous segments in the surface of the films while in contact at elevated temperatures and pressures.

DISCUSSION

These preliminary experiments were designed to explore the feasibility of joining and laminating ordered polypropylene sheets and subsequently shaping them by conventional thermoforming methods or compression molding. It was found that the ordered polypropylene sheets could be readily laminated using ultrasonic welding, induction heating (Hellerbond process) or hot press lamination with adhesive films without any significant loss of performance. Cross plied laminates exhibit the usual planar star-shaped tensile strength profiles with maximum tensile values of 220 MPa in the orthogonal directions (*Fig. 16*). When the densities of these laminates are taken into consideration, their weight performances exceed those of many high performance fiber-reinforced composites (*Fig. 17*).

The thermoforming experiments demonstrated that uniaxial ordered polypropylene can be formed into simple shapes having a draw ratio of at least 1. These studies will be extended to multiply laminates in the future.

In many respects, the uniaxial ordered sheets resemble the behavior of wood or unidirectional fiber composites and the mechanical properties can be predicted from fiber composite theories and anisotropic sheet mechanics (1–3). Their major difference with respect to fiber-reinforced thermosets (whether polyester or epoxy based) is the thermoplastic nature of ordered plastics and their dimensional stability at elevated temperatures or under prolonged stress. Consequently the creep properties of ordered thermoplastics may limit their use in certain structural applications. Additional research is required to define the performance envelope of ordered polymers and compare the short and long term properties with those of other more established materials of construction.

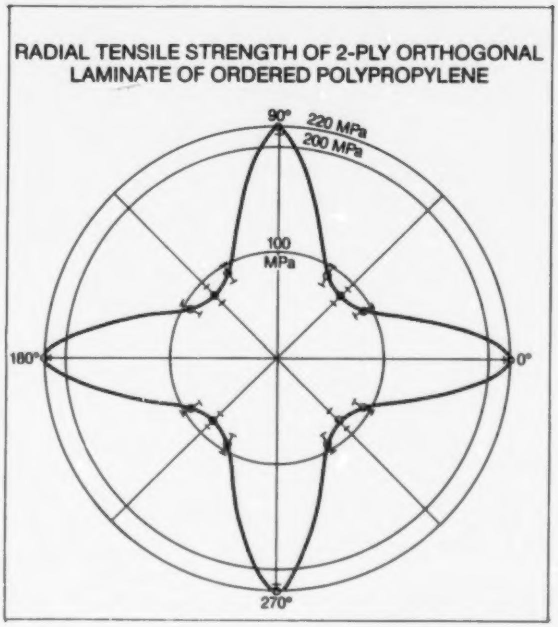

Fig. 16. The two-ply orthogonal laminates show the typical star-shaped tensile strength behavior characteristic of laminated fiber composites.

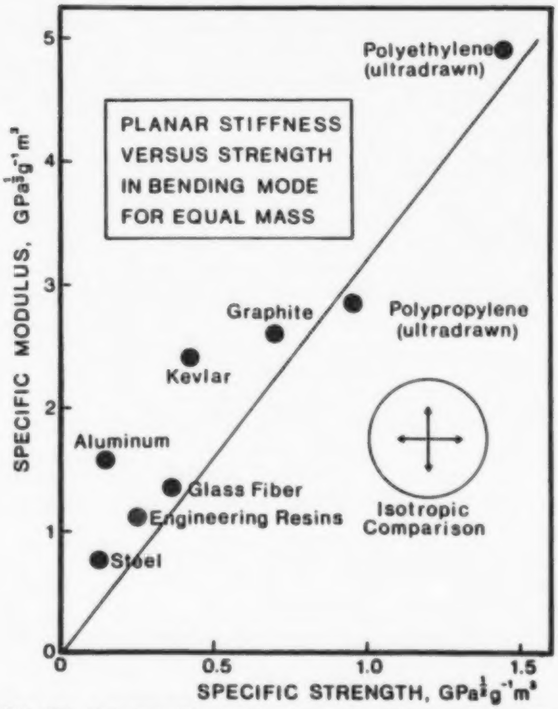

Fig. 17. A comparison of the two-ply orthogonal specific tensile strength and specific flexural modulus properties of ordered laminates reveals the remarkable performance of ordered polyolefins vs. other common materials of construction when weight or density is taken into consideration.

It should be noted that the success of lamination resides more in the choice of the adhesive tie layer than in the method of bonding (whether by heat, ultrasonics or induction heating). In each bonding method the tie layer softens and fuses with the ordered polymer surface without causing substantial relaxation of the ordered polymer chains except at the interface. These bonding techniques may be extended to the lamination or welding of ordered plastics with other unlike thermoplastics, thermosets, metals or ceramics, and permit joining with almost any type of surface. In some situations it may be necessary to surface treat polyolefin materials (eg. corona oxidation) to enhance their ability to be painted, decorated or bonded with similar or dissimilar materials.

CONCLUSION

Many linear polymers are prevented from achieving full orientation and parallel alignment of their molecules due to inherent chain entanglements. However, normal extrusion grade polypropylenes may be roll-drawn to nearly 25 percent of their ultimate properties thereby attaining a maximum modulus of 20 GPa and a corresponding tensile strength of 0.5 GPa. These unidirectional self-reinforced sheets possess some of the desired characteristics of uniaxial oriented fiber composites and may be laminated together to form biaxially strengthened laminates. Suitable methods of lamination include ultrasonic welding, electromagnetic induction welding (Hellerbond process) or simple thermal lamination with an adhesive film. The mechanical properties of the resulting laminates compare favorably with those of many high performance composite materials. The roll-drawn polypropylene sheets may be readily thermoformed at temperatures near 180°C or compression molded at temperatures near 160°C. Such simple fabrication techniques may be employed without significant loss of the outstanding mechanical properties. With further development it seems probable that ordered plastics can be molded into any structure now produced by thermoforming, compression molding or injection molding with full retention of their strength and modulus. Further gains in performance can be expected when the techniques of ordering approach the limits of performance imposed by the atomic bonds in polymer chains. Such limits have already been attained in the case of certain ultradrawn fibers and films.

ACKNOWLEDGMENTS

The authors are particularly grateful to Dr. R. Neil Campbell of the Shell Development Company, Houston, Texas, for providing the experimental ethylene-1-butene copolymer resins and films used in this investigation. Appreciation is expressed to Alcan International Limited for donating research funds in support of the solid phase processing program at the University of Toronto. This research was also supported by the Natural Sciences and Engineering Research Council of Canada, Grant No. A4873.

REFERENCES

1. P. E. Burke, G. C. Weatherly, and R. T. Woodhams, *Polym. Eng. Sci.* (in press); ibid "Roll-Drawing of Polypropylene", SPE Tech. Papers (ANTEC), **32**, Boston, Mass., April 28, 1986.
2. M. R. Piggott, "Load Bearing Fibre Composites", pp 72–77, Pergammon Press, (1980).
3. I. M. Ward, "Mechanical Properties of Solid Polymers", Second Edition, pp 314–325, John Wiley and Sons, (1983).
4. A. Peterlin, "The Strength and Stiffness of Polymers", Inc., A. E. Zachariades and R. S. Porter, Eds., Chapter 3, pp. 107–117, Marcel Dekker, (1983).
5. A. Leatherman, *Plast. Eng.*, **37**, 27 (1981).
6. I. Hwa-Lee, and J. M. Schultz, *Polymer*, **27**, 1219 (1986).

S. IABONI AND R. T. WOODHAMS, DISCUSSION

R. C. Fews: How much will these materials cost when they reach commercial applications?

R. T. Woodhams: At the moment I would guess that the cost of roll-drawing is comparable to the cost of extrusion since the two processes are quite similar. The rolling process for steel and the rolling process for plastics differ in several respects. We have found for example that adiabatic heating in the roll nip tends to limit the draw rate for plastics materials. For sheet thicknesses of one millimeter the maximum draw rate is about 4 meters per minute.

R. C. Fews: So it will be less expensive than, say, graphite-epoxy composites?

R. T. Woodhams: Judging from the known material cost of polypropylene and assuming normal processing costs the total cost should be slightly greater than that of an extruded sheet of the same material.

S. Newman: You are neglecting the cost of lamination. The lamination step may be difficult on a production basis. When laminating (or bonding) at elevated temperatures followed by cooling, severe stresses may be generated due to differential shrinkage of the neighboring plies. The differential shrinkage can be quite large and the tie layers must absorb these stresses. That may be why you prefer to use an elastomeric tie layer. If you subject the laminate to a wide temperature variation do you observe any distortion or delamination?

R. T. Woodhams: The cross-plied (two-ply) laminates do tend to warp as you might expect. This is avoided if odd numbers plies are laminated together. The isotactic poly(butene-1) tie layers are non-elastomeric crystalline thermoplastics with melting transitions near 135°C.

A. Moet: It seems that the material exists under excessive residual stress. Did you make any attempt to measure the recovery of residual stresses?

R. T. Woodhams: At the present time there are students investigating the stress relaxation and strain recovery characteristics of these ordered polymers both in the longitudinal and transverse directions as a function of the temperature. The preliminary results indicate that ordered polymers resist stress relaxation even at temperatures above their melting transitions (when constrained) but quickly contract near their melting point if unconstrained.

A. Moet: What would happen if instead of polybutene you used polypropylene to laminate the sheets?

R. T. Woodhams: Polypropylene films have been successfully used as tie layers using the electromagnetic (induction) welding process or the ultrasonic welding process. In the case of hot press lamination the lower melting transition of the polybutene (135°C) permits satisfactory adhesion without exceeding the melting point of the ordered polypropylene layers (170°C).

J. A. Radosta: Can you say more about the biaxial orientation process?

R. T. Woodhams: Although the process has not yet been disclosed, a biaxial rolling method has been reportedly developed in Japan.

R. Gauvin: Did you say that these rolled sheets retain their shape even above the melting point?

R. T. Woodhams: Of course these ultradrawn materials quickly retract at temperatures near their melting point. What is perhaps unusual is their tendency to retain order and resist stress relaxation when constrained at elevated temperatures (ie. constant strain), even at temperatures above their melting points.

R. Gauvin: This surprises me. We have been forging UHMWPE and if one heats the material, say a former gear, to 150°C it deforms rapidly.

R. T. Woodhams: Certainly the unrestrained sheet will deform above its melting point, retracting as would a stretched rubber band; but if the material is not permitted to retract (ie. at constant strain) the mechanical properties will be retained for very long periods of time (hours or days).

S. Newman: I thought that these materials would have a higher melting point (T_m). This follows from simple thermodynamics: $\Delta H - T\Delta S = 0$ at $T = T_m$, therefore $T_m = \Delta H/\Delta S$. Consequently, if the sheets are ordered then the entropy term will be smaller causing the melting point to increase.

M. R. Piggott: This being oriented material under stress it may be more easily attacked by solvents. Have you examined the behavior of these sheets when exposed to solvents? Are they subject to crazing for example?

R. T. Woodhams: Although this aspect has not yet been investigated it seems quite possible that these ordered structures may be more sensitive to solvent crazing and environmental attack in general. The unusual characteristics of these new materials may warrant a great deal further study.

S. Newman: Solvent stress cracking is well known for many polymers including polyethylene. However normal polypropylenes are not subject to stress cracking induced by solvents. However, after rolling it is likely that the normal spherulitic structure will have been disturbed.

High Temperature Liquid Crystalline Copolyester Composites.
Part I: A Review and New Data for the Self-Reinforced Matrix Phase

PAUL D. FRAYER

Dartco Manufacturing Inc.
Div. of Premark International
Augusta, Georgia 30906

Our work concerns structure-processing-morphology-property (SPMP) relationships in fibrous composites where the polymeric matrix may be self-reinforced. Composites have been made using a commercially available thermotropic liquid crystalline polymer (TLCP) with nematic and isotropic transitions at 693 and 738 K, respectively. To understand the behavior of such composites one must first understand the composite nature of the matrix resin. Thus, this article covers the SPMP relationships for the self-reinforced matrix phase alone. A review and new data are presented on the molecular dynamics of wholly aromatic copolyesters in the solid state to help clarify the nature of the temperature dependence of mechanical properties. Subsequent papers concern short (Part II) and continuous (Part III) fiber reinforced composites.

INTRODUCTION

Scope

This article concerns the thermotropic liquid crystalline polymers (TLCP's), such as the wholly aromatic copolyester based on p-hydroxybenzoic acid (PHBA), terephthalic acid (TPA), and biphenol (BP) (XYDAR®, Dartco Mfg. Inc.) and other TLCP's which have been made in large enough quantities to study the structure-processing-morphology-property (SPMP) relationships. Here "structure" is defined as the physical state on the scale of molecular dimensions.

The literature is reviewed concerning structure determined by X-ray diffraction and spectroscopic methods, processing by extrusion and molding, and morphology observed by microscopy. Self-reinforcement, anisotropy, and the temperature dependence of structure and properties, especially modulus, are discussed for the TLCP matrix phase without the complications of other fibers in the system.

Matrix Resin Developments

Increased understanding of SPMP relationships in conventional polymers led to improved product performance, reduced costs, large volume growth, and broader market applications. TLCP's represent a new class of resins that may be used as the matrix phase in composites, but their SPMP characteristics, differing from those of amorphous and semi-crystalline polymers, are not well understood.

Although more than 400 TLCP's have been described in the literature (1), only a few have been made in large enough quantities to study SPMP relationships. This paper mainly concerns those few materials. The ultimate objective is to understand how to attain their full performance potential.

Composite Materials Developments

Increased understanding of composite materials and the availability of computer aided design and manufacturing are leading to a "revolution" in structural applications for polymers both as the matrix and reinforcing phase (2, 3). Major resin producers have acquired composites businesses and technologies or entered into joint ventures to take advantage of the opportunity (4).

While engineering design and manufacturing experiences have been dominated by more isotropic materials, our opportunity is "to combine anisotropic materials with imaginative design and to vary the properties across a single structure at the points and directions desired" (2).

New Views of Polymeric Composites

Our concepts of composite materials are still evolving. Whereas previously we viewed a composite as containing two or more chemically distinct materials on a macroscale with a distinct interface (5), we now include interphase regions (6), surface treatments which may alter the interphase chemical composition (7), control of interfacial/interphase morphologies (8), compositional/structural gradients (9), "self-structured composite" polymers (10), and molecular composites (11–15). Also, polymeric fibers (16–18), as well as carbon and graphite fibers (19, 20), are self-structured composites where the polymeric "reinforcement" phase dominates the properties.

TLCP General Literature Reviews

Brown and Crooker (21) recently published a general review on low molecular weight liquid crystals. Monnerie (22) reviewed spectroscopic methods to determine local orientation, molecular motions, and phase transitions. Dobb and McIntyre (23), White (24), Jackson (25), Noel (26), Huynh-Ba and Cluff (27), Chung (28), Koide (29), and Varshney (30) recently reviewed the TLCP literature, which is rapidly expanding.

Jin, et al. (31) reviewed some patent literature related to chemical composition. Lenz, *et al.* discussed characterization of TLCP's (32) and TLC model compounds (33), structure-order (34) and structure-thermal property relationships (35) for some main chain TLCP's.

Composition and Processing Variations

Lenz (36) recently reviewed TLCP synthetic routes. It is likely that different routes yield different compositions and structures as well as different molecular weight distributions.

Chen and Lenz (37) reported crystallization-induced structural reorganization from random to blocky comonomer sequence distributions by ester interchange reactions both in the solid and nematic phases for a family of main chain copolyesters with flexible spacer groups.

Lenz (38) reported that a copolyester with 60/40 mol percent ratio PHBA/PET consists of serveral fractions of different composition. Quach, *et al.* (39) reported different DSC behavior for soluble and insoluble fractions for "old" and "new" samples of the "same" polyester. Joseph, *et al.* (40) observed by ESCA and chemical etching experiments a PHBA-rich skin region and a PET-rich core region.

Recently, Gochanour and Weinburg (41) reported time-dependent melt rheology for both a TLCP and the isotropic copolyester Kodar® PETG (Eastman). The "melt" state is metastable due to the presence of crystallites whose fraction may increase with time. Similarly, Wunder, *et al.* (42) report different rheological behavior as a function of temperature depending on the melt structure (partially melted solid, anisotropic melt, biphasic melt, and isotropic melt).

Conventional Polymers as Self-Structured Composites

Keller (10) recently reviewed the structure and morphology of conventional polymers. He noted the hierarchical nature of semi-crystalline polymers which can be called "self-structured composites." Enhancing the properties of some conventional polymers by controlling the composite nature has been a topic of increasing interest over the past 10 to 15 years (10, 43, 44). A few examples are cited below.

Samuels (44) reviewed some methods to characterize the "structural state" at various levels of organization. He refers to semi-crystalline polymers as the "ideal composite" because the two phases (amorphous and crystalline) usually have the same chemical composition and are chemically connected.

Mead and Porter (45) used "different morphologies of polyethylene as the matrix and as the reinforcement." They used pullout tests to measure "interfacial shear strength of these single polymer composites."

Janssen, Boetes, and Smith (46) described a process for making "self-reinforcing" polypropylene by *in-situ* formation of strong, highly crystalline fibers in the polymeric matrix. Sakellarides and McHugh (47) produced oriented structures in polyethylene during film extrusion by introducing needles into an elongational flow path. Ehrenstein and Maertin (48) injection molded self-reinforced polyethylene using a baffle in the flow path to create the well-known shish-kebab morphology aligned in the flow direction.

Gohil and Petermann (49) reported on the use of short fiber-reinforced composite theory for poly(butene-1) films containing shish-kebab structures. They refer to these materials as "inherently reinforced polymer composites."

Burton, *et al.* (50) reported that chain extended sheets of shish-kebab structures can form in a short carbon fiber-reinforced semicrystalline thermoplastic. It is more widely known that the transcrystalline morphology may form at the fiber-matrix interface. Such interfacial morphologies and structural gradients may impair composite performance in the presence of chemicals when adhesion to the reinforcing fibers is poor, even though enhanced crystallization in some polymers results in significant increases in the heat distortion temperature, strength, and modulus.

Highly drawn fibers with more extended chains, such as Allied's gel spun SPECTRA® fibers made from high molecular weight polyethylene (51), are clear examples where the "reinforcement" phase of the polymer dominates the properties. Stiffness values over 200 GPa have been reported (52, 53); the theoretical limits are about 300 GPa modulus and 25 GPa strength. The main requirements for "composite-like properties" are extended chain orientation, ordered lateral packing, and a low concentration of axial defects (53).

RESULTS AND DISCUSSION

Morphological Observations

Although reinforcement efficiency is normally judged by comparing the reinforced with the non-reinforced resin processed under the same conditions, with TLCP's we must consider their composite nature and the effect of adding fibers on their self-reinforced morphology. Also, processing under the same conditions may not be possible. Thus, this paper (first of 3 parts) establishes the reference state for understanding SPMP relationships in fiber-reinforced, self-structured matrix composites. Next we review the literature on the morphology of TLCP's and compare them with XYDAR*.

Skin-Core Morphologies Without Transverse Core Orientation

Jackson and Kuhfuss (54) and Jackson (55, 56) suggested that the observed changes in mechanical properties as a function of chemical composition and processing conditions reflect changes in average chain orientation for many different TLCP's, especially the PHBA/PET resin series, but did not present any evidence other than mechanical properties. Extensive studies by others (57–59) using microscopy and X-ray diffraction of microtomed sections on the same family of resins show a highly oriented skin and less oriented core for various molding conditions and thicknesses.

Many papers have been written on the rheology of main chain TLCP's (57–72). These works include many different polymer types and different processing conditions. All suggest the same conclusion of a highly oriented skin and less oriented core, but this may be a result of the flow geometry and relatively thin samples. Those papers which gave X-ray data (57–59, 69) show either that the core material is less oriented but still aligned on the average along the flow direction or that no preferred orientation exists.

Similarly, many papers have been written on morphological studies separate from rheological measurements (73–82). Most concern thin samples or highly oriented fibers where the chances for transverse core orientation are small.

Thapar and Bevis (73) reported on the micromorphology of an injection molded experimental TLCP made by ICI, a 70/30 mol percent ratio PHBA/ANA (acetoxynaphthoic acid). In the skin they observed a preferred orientation parallel to the flow direction. Their X-ray data showed no preferred orientation in the core for a standard ASTM type IV tensile bar. The sample consisted of fibrils, the diameter increasing from the skin to the core, and the number decreasing from the skin to the core until no fibrils are seen in the core. Thus, even for these relatively thick moldings no transverse orientation was observed in the core for their polymer and molding conditions.

Transverse Core Orientation Observations

Ophir and Ide (80) reported on injection molding a TLCP made from 60/20/20 mol percent ratio acetoxybenzoic acid (ABA)/terephthalic acid (TPA)/naphthylene diacetate (NDA). They noted the tendency for TLCP's to behave like conventional glass reinforced thermoplastics in that a diverging flow, as can occur when molding thicker samples, may cause the glass fibers to orient transversely in the core. The proportion of transverse core in their TLCP is said to depend on molding conditions. From their micrograph the core appears to be only a few percent of the total thickness.

Weng, Hiltner, and Baer (81) reported on the hierarchical structure of an injection molded sample with higher naphthoic content (42 mol percent) than used by Thapar and Bevis (73), who observed no preferred orientation in the core with a wide range of molding conditions. Weng, *et al.* (81) reported the core to be about 1/3 of the sample thickness. The core also had no structural hierarchy, but tended to have the chains aligned transversely to the flow direction, especially down the centerline of the rectangular plaque (203 mm by 51 mm by 3 mm).

Sawyer and Jaffe (82) of Celanese reported not only a hierarchical structure based on microfibrils (50 nm), fibrils (500 nm), and macrofibrils (5000 nm), but also a defect hierarchy superimposed on the structural hierarchy. The defects are said to be due to the regular meander of the chains with localization of defects within the microfibril at about 50 nm periodicity. The structure of the chemical repeats probably affects the meander of the chains and the resulting morphology.

Duska, *et al.* (83, 84) observed the chain orientation at 90° to the flow direction in the core of injection molded XYDAR* resin. He reported *skin* structures which make up 16, 38, and 58 percent of the total molded thickness for tensile bars with thicknesses of 3.2, 1.6, and 0.8 mm, respectively. At least seven distinct layers were observed. The skin layers were defined as the outermost four layers (two per side) since X-ray diffraction showed that these layers have similar chain packing and orientation with the polymer chain axes aligned in the flow direction. Two thin boundary layers separated the skin layers from the transversely oriented core and exhibited nearly random orientation by X-ray diffraction. Each of these layers is about 0.125 mm thick and may consist of many sub-layers which together form a quasi-isotropic planar structure.

Analogous to work by others (54–56), our work has shown that for XYDAR®, molding conditions and sample thicknesses can be chosen to maximize the flow direction properties. Duska, *et al.* (83, 84) showed that the skin contributes most to the mechanical properties when molded bars are tested in the flow direction. He also showed that when 50 percent by weight glass and mineral filled compounds are molded and tested under similar conditions as the base resin, the tensile and flexural strengths and moduli are all reduced. It is intriguing that the reduction in strength properties is not as great as for comparably filled amorphous or semi-crystalline polymers and that the moduli decrease rather than increase.

How Fillers Affect Self-Reinforcement Is Unclear

Most thermoplastics have moduli which are lower than those of fillers such as glass or minerals. Thus, one expects the moduli to increase with increasing filler volume fraction (85, 86). This is not the case at least for filled XYDAR® resin.

Analysis of the generalized equation for relative modulus given by Nielsen (86) suggests two possible conclusions. Either the glass or mineral fillers are lower in modulus than that fraction of the TLCP resin which was replaced or the average orientation is reduced since the properties are largely controlled by the more oriented material.

Similarly, the strength of filled polymers is known to decrease with increasing particulate filler volume fraction (87). From known empirical relations one would predict the filled composite tensile strength for 50 weight percent of glass or mineral filler (33 to 35 volume percent) to be less than 40 percent of the resin strength. However, Duska, *et al.* (83, 84) reported tensile strengths for molded bars with 50 percent by weight glass and mineral fillers in XYDAR® of 70 to 90 percent of the unfilled, molded resin for thicker samples and 50 to 60 percent in thinner samples. Since the development of a skin-core structure in highly filled molded parts is less obvious by microscopy, the mechanism for how fillers affect self-reinforcement is unclear.

Introducing glass or graphite fibers with a significant aspect ratio has been found to reinforce XYDAR® when properly compounded and molded. The commercial glass-reinforced compound is called XYDAR® RC-210. However, unlike some other glass-reinforced thermoplastics, the degree of reinforcement is not dramatic, although significant. This is apparently a general phenomenon for TLCP's. Interpretation of the effects of adding fillers and short fibers to TLCP's is the main subject of Part II to be published.

An Important Research Contribution to Understanding TLCP's

Perhaps the most significant paper on SPMP relationships is that of Alderman and Mackley (78) from 1985. They studied a wide range of main chain TLCP's. They observed that with increasing shear rate a sharp transition occurs at a critical shear rate for the onset of a dense disclination texture, but that on cessation of shear the relaxation process (the decrease in the number of disclinations and the increase in domain size) occurs more slowly, in about one minute. That domains diminish in size with shearing has been incorporated in theoretical models of TLCP rheology (65, 66).

Alderman and Mackley (78) showed that the skin-core structure in fibers is directly related to the change in velocity profile at the die exit. Two polymers were shown to behave as power law fluids and the modulus *vs.* draw ratio was shown to be directly related to the well-known power law velocity profile equations. "As draw ratio increases the amount of oriented skin increases and the amount of 'disoriented' core decreases." Disorientation in the core was shown to be related to deceleration in the core which results in axial compression.

They also found that as the draw ratio increased, the modulus rose to a critical point where it reached a plateau. The relative positions for the critical draw ratios for a flexible-rigid and a rigid polymer were predicted from the velocity profile equations, but the absolute values were low.

Although the actual mechanisms are not clear, the excellent work of Alderman and Mackley has brought us one step closer to clarifying the interdependence of rheological and morphological phenomena and their relationship to properties. While the ultimate strength and elongation properties may be determined more by super-molecular level organization and defects (1, 82), non-destructive properties such as stiffness *vs.* temperature may be determined by molecular level phenomena.

Aromatic Polymer Conformations, Packing, and Transitions

This section concerns the molecular dynamics of wholly aromatic polymer molecules in the solid state. First, we consider phase and relaxation transition processes followed by polymorphism in macromolecules. Next we discuss micro- and macro-order parameters in TLCP's followed by a description of the nature of the crystallites. Then we consider the effects of polydispersity, defects, conformations and chain packing. Finally, we review transitions observed in aromatic polymers and draw some conclusions on the nature of the "glass transition" temperature in wholly aromatic copolyesters.

Phase and Relaxation Transition Processes

Solid state "transitions" may be divided into relaxation and phase transition processes. The former occur at a temperature dependent on test frequency; the latter occur at a specific temperature independent of frequency.

In polymers a relaxation process (the beta transition) occurs below but *usually* near the glass transition process (the alpha transition) (88). The beta process is thought to be related to motion of *one or two* monomeric units and is viewed as a precursor to the alpha process. The alpha or glass transition is believed to be related to the motion of *dozens* of monomeric units and to involve "long range" cooperative motions (88).

In contrast, phase transitions can be explained by either cooperative molecular motions resulting from 1) "statistics," or 2) interactions, or 3) both, where the latter is most common (89). As noted above, the cooperative motions in a phase transition should occur independent of test frequency.

Dobb and McIntyre (23) noted that some thermotropic copolyesters may be quenched into a more dense form than when slow-cooled and/or annealed. A kinetically favored stress state which is thermodynamically a metastable state might occur when the phenyl rings are forced into a more coplanar conformation and the frozen-in stresses overcome steric repulsions. However, the axial correlations may be poor. Thus, longer range cooperative motions by annealing could result in a 1-dimensional (only orientational order) quenched nematic liquid crystalline *phase transition* to a 2-dimensional liquid crystalline state (orientational plus positional order resulting from axial correlations).

Polymorphism In Macromolecules

Polymorphism is common in semi-crystalline polymers, and thermal expansion can lead to a "rotary phase" as occurs when an orthorhombic crystal form converts to a hexagonal phase (10). Thus, polymorphism involves a phase transition in which the cooperative motions are long range and span the size of the crystalline domain. Polymorphism is also common in liquid crystals (22).

In the formation of fibrillated polypropylene, the existence of liquid crystalline domains on cooling the melt has been proposed with hexagonal packing like the crystalline beta modification (90). Such a form may facilitate orientation during stretching before converting to the monoclinic crystalline alpha form. In this case the polymorphic phase transition is from a liquid crystalline to a crystalline form. Corradini, *et al.* (91) more recently analyzed the quenched mesophase structure in polypropylene by X-ray diffraction compared with the Fourier transforms of various models of chain aggregates with disorder. It appears that the quenched form may have a conformation like the monoclinic form while packing in a pseudo-hexagonal but axially disordered manner.

That for the crystalline fraction in the core material of injection molded XYDAR® at room temperature we observed mainly orthorhombic chain packing which, as temperature increases, converts into an expanded orthorhombic form, then to a pseudo-hexagonal form, and finally to a regular hexagonal form was not surprising. However, the highly oriented, fiber-like X-ray pattern with nearly 3-dimensional crystalline order was unexpected since analysis of the data (92, 93) suggests that XYDAR® is a random copolyester.

Details of our X-ray diffraction studies for XYDAR® SRT 300 as a function of temperature will be published separately (92, 93). Field, *et al.* (94) highlighted some of our results. A brief summary is given here only as related to the temperature dependence of properties.

Below about 400 K two orthorhombic polymorphic forms coexist in the *core* material. One form converts to the other above about 400 K. In the same temperature region the more stable form changes its conformation such that one of the two crystal axes in the plane perpendicular to the chain axis contracts slightly (rather than expanding with increasing temperature) while the axis at 90° expands more than expected for the change in the temperature. Thus, actually two polymorphic transitions occur. All forms have orthorhombic packing below about 575 K.

In the 400 K temperature region where we have observed polymorphic transitions in the crystalline fraction of the core material, some authors have suggested that a "glass transition" also occurs in highly aromatic TLCP's. For wholly aromatic copolyesters the actual molecular dynamics may involve processes which are not in truly amorphous regions where by definition no order exists. At a minimum these rod-like molecules will have at least 1-dimensional order, i.e. orientational order. Thus, what may appear as a relaxation process may actually be a polymorphic phase transition wherein the axial positional order of the chains is improved as well as the chain packing. More will be said later about the dimensionality of the order.

In XYDAR® we have observed different conformations and packing for the skin and core materials. The solid state properties for molded parts which are skin-core composites appear to reflect these differences and changes in structure as a function of temperature. The nature of the molecular motions in the quenched, oriented skin and in the core fraction which does not contribute to the crystallinity by X-ray scattering is considered further below.

It is widely known that TLC copolyesters can be annealed below their solid-to-nematic phase transition. However, the mechanism for the annealing process is unclear. In what follows we will review the literature concerning other factors (micro- *vs.* macro-order, chain packing and conformations of aperiodic macromolecules, the nature of crystallites and the regions between crystallites) in an attempt to better understand the temperature dependence of the structure and properties.

TLCP Micro- and Macro-Order Parameters

Lenz (32), reviewed TLCP phase changes by DSC and the general structural features by wide and small angle X-ray diffraction, electron diffraction and microscopy, small angle light scattering, refractive index, NMR, ESR, dielectric and magnetic susceptibilities.

Two levels of order parameters appear to be related to some properties: 1) the micro-order parameter for describing orientation within "domains," and 2) the macro-order parameter for describing the alignment of domains. Thus, an unoriented sample may have a high micro-order parameter and zero macro-order parameter. Aligning domains by processing may yield a product where both micro- and macro-order parameters are high.

Blundell's Model for the Nature of the "Crystallites"

In 1982 Blundell (95) studied quenched, annealed and slow cooled, unoriented and oriented samples of two "rigid chain" TLCP's; one contained some aliphatic sequences. He proposed that the *quenched material* contains microcrystals that are too small to give X-ray lines. He estimated the crystal size in the chain packing direction from an (hk0) reflection to be only 10 nm for the slow cooled sample and 5 nm for the quenched oriented sample. He noted that for microcrystals to be mistaken for "amorphous" material their size would have to be only 3 nm.

In conventional polymers the fold surface energy dominates surface energy effects. Blundell indicates that for extended chain polymers without folds one cannot attribute the low heats of fusion to surface energy effects for the solid-nematic transition, but rather one may attribute them to the copolymers' non-regular structure, which introduces imperfections within the crystal lattice. On the other hand, the low entropies are shown to be a consequence of the chain rigidity in the nematic state.

Perhaps low X-ray percent crystallinities are observed because of the small and imperfect crystals, some of which are mistaken for "amorphous" material. Blundell's model resembles the fringed micelle model without chain folds where neighboring crystallites are molecularly interconnected (tie molecules). Such a fringed micelle model was also recently proposed for a strictly alternating, flexible-rigid chain polymer which is proposed to exhibit a continuous rather than a polydomain LC phase with various defects or disclinations (79).

It is unclear how the solid state models can be related to recent observations of banded textures in sheared nematic melts which by microarea electron diffraction are thought to be caused by a serpentine trajectory of the molecules (96, 97). Banded structures have been observed in lyotropic polymers and occur in sheared melts of TLCP's (98). The banded structures may be related to some stage in the relaxation process of the sheared melt prior to freezing in the molecular packing.

Molecular Weight Distribution and Defects

Works on defect structures concern the nature of domain walls (the "transitional region between adjacent microstructural domains") (96, 99–103), models for aggregation of chain ends (104, 105), changes in the number and the positions of disclinations during flow to explain rheological behavior and the relative proportions of skin and core during fiber spinning (78), as well as "localization of defects within a microfibril at about a 50 nm periodicity" (82).

It is clear that the molecular weight distribution is important for the behavior in both the melt and solid phases. The lower the average molecular weight, the higher the number of chain ends which can aggregate or individually can form point defects by co-crystallization in crystallites or form defects in the quenched, ordered state.

Also, segregation of the low molecular weight tail may occur in the walls or vein structures and alter the processing and properties (96–103). Flory (106) and Flory, *et al.* (107–113) have shown theoretically that polydisperse systems tend to fractionate with a biphasic equilibrium being established between the isotropic and anisotropic (nematic) phases, the higher molecular weight components residing in the anisotropic phase (106). Furthermore, "the anisotropic phase approaches the selectivity of a pure crystal in its rejection of a foreign component" (111).

The existence and segregation of oligomers in condensation polymers are well known (e.g. (113–115). In flexible chain polymers the oligomers may also be cyclic and hence may be "incompatible" with the polymer and not cocrystallize (116). For extended chain rod-like polymers, co-crystallization is possible, but an additional driving force for segregation may exist as a result of the chemistry of the chain ends.

Although the segregation process is thermodynamically driven, it may be kinetically limited because of the high rigidity of the system. Heat treatment at lower temperatures may induce further segregation except when the oligomeric species are locked into a crystallite lattice. As noted later, such molecular mobility would obfuscate the interpretation of spectroscopic data aimed at detecting polymeric chain motions.

It is significant to note that as few as three consecutive para repeat units linked by ester groups are sufficient for liquid crystalline behavior with a nematic range on the order of 400 to 550 K, depending on composition (55). Also, the average molecular weight for many rigid chain TLCP's is thought to be approximately 20,000 to 30,000 g/mol, which translates to only about 100 to 150 nm length.

Relatively short rigid chains may take on some polymeric behavior, but the end groups can affect chain packing (117, 118). Khanna and Pearce (119) recently showed that thermal stability does not increase beyond about 10 to 15 repeat units in some aromatic polyamides.

Packing and Conformations in Aromatic Polymers

Poly(p-phenylene) has no known glass or melting transition, but can be processed by solid phase sintering (120). Thus, some molecular motions can occur in the solid state. Oriented, annealed poly(p-phenylene) (PPP) has orthorhombic packing at room temperature, but "is paracrystalline like the nematic structure in liquid crystals" (121). Thus, computer simulations of chain conformations at room temperature can explain the X-ray and electron diffraction data by assuming rigid extended chains with regular lateral packing but with axial shift disorders.

The orthorhombic packing is controlled by the chain conformation wherein adjacent phenyl rings cannot be coplanar because of steric hindrance between neighboring phenyl ring hydrogens. The phenyl rings can rotate clockwise or counter-clockwise along the chain axis with equal probability, i.e. a double potential well exists on either side of the higher energy coplanar conformation. The unit cell contains two chains, one shifted relative to the other to balance intermolecular attraction and repulsion forces between and along the chains. Similar results were obtained for other aromatic homopolymers such as poly(2,5-benzoxazole) and poly(2,6-benzothiazole) (122).

In poly(p-benzamide), poly(p-phenylene terephthalamide), and poly(p-p′-benzanilidene terephthalamide) the amount of disorder again depends on the balance of attraction and repulsion forces, where preferred conformations depend not only on strong intermolecular hydrogen bonding and normal steric interactions, but also on intramolecular steric and resonance effect associated with the adjacent amide and phenyl groups (123–126).

Polymorphism is known for poly(p-xylylene) (127) and poly(p-hydroxybenzoate) (128, 129) where in the latter case probable conformations have been discussed. Disordered conformations can exist since formation of the thermodynamically favored state is kinetically limited.

Aromatic polymers like poly(ether ether ketone) which have much greater flexibility due to the ether linkages and which also have nonlinear links, i.e. 120° bond angle, can form a true amorphous phase. For example, PEEK has a glass transition between 423 and 430 K depending on the isothermal crystallization temperature (130), and may have little or no packing disorder in the crystalline phase (131). Such polymers with *periodic* repeating units are crystallizable, but crystallization may be kinetically limited.

In the examples given above, good X-ray data are partly a result of the periodic nature of the polymer chains. This has not been the case in general for TLCP's with aperiodic chain repeating units made by random copolymerization. Introducing more imperfections in chain packing can improve processability (131–143). As Blackwell, *et al.* (141) noted recently for a highly oriented, melt spun fiber of a PHBA/HNA copolyester, we have also seen evidence for almost 3-dimensional order in XYDAR®, which also exhibits aperiodic meridional reflections (92, 93). Apparently, the dimensionality of molecular order in rigid chain polymers may be fractional and not restricted to 1, 2, or 3 dimensions.

Transitions vs. Temperature In Aromatic Polymers

Copolymerization and altering the orientation and number of linking groups between the rings can reduce the temperature for phase transition and relaxation processes by adding conformational mobility and altering both the thermodynamically and kinetically favored chain packings. Adding non-linearity and/or ring substituents can increase the average lateral packing distance and give some rings greater latitude of movement about the chain axis for the same temperature.

Phenyl rings in the backbone of polymers have been observed to undergo 180° flips, but the crystalline regions can add constraints that inhibit free flipping in the amorphous regions (144). The number of rings that can flip "cooperatively" to alter chain packing is a function of temperature and of chemical composition, especially the balance between intermolecular attraction and repulsion forces which are also affected by the local stress state.

Ring flip motions in TLCP's have been reported (145, 146). Introducing enough flexible chain segments into the backbone of a rigid chain polymer can yield a material which contains a truly amorphous (0-dimensional order) phase. On reducing the temperature below the "melting" temperature in a *partly flexible chain* polymer, the micro-order in the nematic state is retained and the intermolecular motions are frozen in place so that below the glass transition temperature only intramolecular motions such as trans-gauche and ring flip conformational motions were detected by deuteron magnetic resonance spectroscopy (145).

For three rigid chain polymers containing 2,6-naphthylene groups in which the bordering ester is linked to the naphthylene in different ways (146), dielectric and mechanical loss processes correlate with the directionality of the ester group near 323 K. Thus, it appears that such loss processes may be associated with 180° ring flips and combined carbonyl-ring flips. However, at such a low temperature these "beta loss processes" most likely involve cooperative motions of only a few monomer units.

These same authors (146) also observed another process near but above the beta transition that they called an alpha process, the normal nomenclature for the glass transition in truly amorphous polymers. As noted previously, other explanations are possible for such a loss peak.

Dielectric loss measurements at frequencies of 0.03 to 300 kHz and temperatures from 113 to 573 K on a series of flexible chain polymers with $—O—(CH_2)_m—O$ sequences for $m = 5$, 6, or 10 reacted with 1 mol of PHBA and 1 mol of TPA showed two low temperature loss peaks at 326 to 358 K and 363 to 393 K attributed to relaxation processes related to "localized ester group motions" (147). Several high temperature loss peaks in the range from 413 to 553 K were said to involve both ester and phenyl motions resulting in chain ordering in the solid state.

Mitchell and Ishii (148) reported NMR work on semi-flexible and rigid chain copolyesters for temperatures of 293 to 473 K for samples with preferred orientation. The polymers included PHBA/PET 60/40 mol percent ratio and PHBA/HNA (hydroxynapthoic acid) with 75/25 and 58/42 mol percent ratios. The rigid chain polymers showed greater interchain interactions and some longitudinal correlations consistent with X-ray data.

For the PHBA/PET system (148) one data point at 128 K suggests a transition below 293 K. (NOTE: A low temperature "beta relaxation" observed by dielectric spectroscopy in a rigid rod polymer was shown to be due to water dipole motions (149).)

By 353 K in the PHBA/PET polymer the ethylene protons are rotating freely. Up to 473 K no loss of correlations of the phenyl rings was seen along the chain axis (i.e., no axial translation), also in agreement with X-ray data. The results are complicated by a mobile fraction which may be attributed to free rotation of end groups.

For the PHBA/HNA systems (148) a decrease in interchain interactions with temperature results in localized rotational motions in the 323 to 373 K range. A small mobile fraction appears around 423 K and may be attributed to a low molecular weight impurity or rotation of end groups.

Takase, *et al.* (150) recently reported three transitions for the PHBA/PET 60/40 mol percent polymer at 233, 338, and 453 K. The lowest temperature transition is said to be due to local segmental motion while the high temperature transitions involve "significant interchain cooperative motions." This system is said to exhibit two-phase behavior.

The PHBA/HNA 75/25 mol percent polymer (151) also shows a low temperature transition (activation energy only 5 kcal/mol) associated with local segmental motion of the ester groups. At 348 K the increase in intrachain motion is said to "involve several segments of the *same chain* in some cooperative motion." The high temperature transition at 523 K may involve the onset of cooperative *interchain* motions of the aromatic segments and sterically related ester mobility.

Clements, *et al.* (152) reported broad-line NMR results for the PHBA/HNA 74:26 mol percent polymer which was melt spun into a highly drawn, thin tape and then annealed for 4 h at 523 K followed by 15 h at 553 K. They described the resulting polymer as "not crystalline" although highly ordered. As noted earlier, "not crystalline" does not imply "amorphous" since these polymers should have at least 1-dimensional (orientational) order rather than no order at all.

Rigid and mobile lattice calculations were made. In the first case, single chain and interchain interactions were modeled. In the second case, rotating monomer units and coherent rotating chains were modeled.

Their experimental and calculated results provide possible explanations for three transitions (about 213, 273, and 353 K) observed by dynamic mechanical analysis at low frequencies relative to NMR. The transition at 213 K can be explained by a rigid hexagonal lattice of chains rather than a single rigid chain. The transition at 273 K is best explained by motions of the PHBA monomeric units. The transition at 353 K is best modeled by a lattice of hexagonally packed chains in which both the PHBA and the HNA monomeric units are mobile. Thus, the HNA units apparently do not rotate about the chain axis alone.

No data were reported at higher temperatures even though a lattice of coherently rotating chains was modeled. Since the sample was annealed for 15 h at 553 K, it is unlikely that complete rotation of chains or long range cooperative motions in regions between crystallites would occur until above this temperature.

Next we consider further the nature of the molecular dynamics in the solid state. However, we will begin by considering the molecular motions in the nematic melt prior to solidification.

Can Rigid Chain TLCP's Have a Glass Transition Temperature?

The molecular dynamics in the melt phase can be viewed as the precursor to the solid state structure. Cooling the sample at a fast rate would be like taking a high speed snapshot of a fast moving object.

McFarlane, *et al.* (153) reported melt phase NMR spectra for mainly PHBA or PHBA/HQ (hydroquinone) modified poly(ethylene terephthalate). They showed that in the nematic melt phase the chain molecules are freely rotating about the chain axis and translating in three dimensions. This is consistent with the model of the nematic melt of low molecular weight liquid crystals.

At the same time, they speculated that the reason for a lower viscosity in the nematic phase than in the isotropic phase may be due to the orientation of domains of molecules and not individual molecules. Thus, relaxation of induced orientation in the nematic state by thermal energy would involve a larger effective mass than in isotropic polymer melts. Consequently, both the molecular packing within a domain and the relative orientations of the domains that will exist when a snapshot is taken will depend on the rate of cooling compared with the relaxation time.

With this veiw in mind, Stamatoff (154) has suggested that sufficiently rapid cooling can result in "a polymeric glass with nematic structural order." Annealing would then increase the structural order from 1-dimensional to approaching 3-dimensional order, limited only by the sequence distribution within the polymer chains and how they can pack and, of course, by the time and temperature. Thus, in many practical situations, where heat transfer is limited, a range of cooling rates will yield many intermediate degrees of order.

Windle, *et al.* (155) reported the existence of preferred long range correlations even for random copolyesters with aperiodic repeating chains. Thus, "lateral growth of ordered entities does not necessarily require regular sequences." They discuss the probabilities of pre-defined sequences and their lateral aggregation with the possibility of "longer-range sorting and fractionation" creating larger crystals during annealing in the solid state. Small non-periodic liquid crystals can form with biaxial optical properties.

Such microstructural order in the solid state is consistent with Blundell's model (95) and explains the existence of "some form of crystallinity" observed by thermal analysis, while by X-ray diffraction little evidence was found in the PHBA/HNA type random copolymers for "crystallinity" as normally seen in polymers with periodic repeat units.

In the PHBA/HNA 70/30 mol percent polymer with a degree of polymerization between 150 and 200 and with a solid-to-nematic transition at 553 K, as studied by Windle, *et al.* (155) by optical microscopy, "microstructural mobility" begins at 463 K. Although the transition to the nematic melt is at about 553 K, "global molecular orientation" begins to decay with time above 523 K. Above 553 K the microstructural mobility occurs on a time scale of about 1 s. Optical biaxiality exists within the temperature range from about 523 to 553 K, indicating that the micro-order parameter remains high even though "global molecular orientation" (or macro-order parameter) is decaying significantly below the transition to the nematic melt state. Later we discuss the effect of these phenomena on mechanical properties as function of temperature.

Cao and Wunderlich (156) reported the transitions by DSC above room temperature for the PHBA/HNA series with mol percent ratios 100/0, 75/25, 58/42, 30/70, and 0/100. The samples were pellets with "clear skin-core effect" and *only the surface layers* were analyzed. The "glass transition temperatures" for the series were in the range of 377 to 434 K by DSC, but the only way the authors could interpret these transitions as "normal" based on heat capacity changes (31 to 34 J/Kmol) was to assume that "extraordinary broadening" occurred over a 200 K range!

They call the higher temperature transitions (520 to 620 K) "disordering transitions" or what was referred to above by Windle, *et al.* (155) as decay of "global molecular orientation." Cao and Wunderlich (156) describe these polymers as "intermediate between the liquid-crystalline and condis-crystalline state with a *small* amount of crystallinity," i.e. for the *quenched* skin layers.

"Condis" (conformationally disordered) crystals have been described in the literature (157) for a number of periodic repeating polymer chains. The "condis crystal" is characterized ~~by~~ "cooperative motion between various conformational isomers." A CD (conformationally disordered) glass supposedly has these motions frozen into the solid phase. Polymorphic transitions may result from increased mobility in CD crystals.

For polymorphic transitions "large scale" motions are required, i.e. a crystallite of one polymorph changes to a crystallite of another polymorph. Cao and Wunderlich's DSC data strongly suggest that a continuum of cooperative motions may exist as a function of temperature. As the thermal energy increases, the number of cooperating segments increases, which agrees with a fringed micelle model having a distribution of sizes of microcrystals connecting regions of highly aligned (locally anisotropic) chains with various degrees of order or disorder in the molecular packing as well as varying lengths between the more ordered crystallites.

From all of the above discussions, one is forced to conclude that *a classical glass transition does not exist* for the wholly aromatic copolyesters. "Long range" cooperative motions required for a glass transition probably do not occur until higher temperatures. Also, these polymers could only exist in a truly amorphous or zero order state if they could be quenched rapidly enough from their *isotropic* state. In commercial practice processing in the nematic state appears to be preferred for obtaining the maximum performance and best processability.

At lower temperatures "long range" cooperative motions can occur by polymorphic phase transitions in crystallites which have a higher degree of dimensional order than in the regions between crystallites. Changes in conformational disorder probably involve "shorter range" motions similar to beta relaxations. More work is needed to understand these processes, especially their frequency dependence.

For completeness it should be noted that flexible-rigid chain TLCP's (26, 158), including side chain TLCP's (26, 159), can exhibit classical glass transition temperatures and in some cases other polymorphic LC transitions (such as crystal-smectic, smectic-smectic, and smectic-nematic phase transitions) as well as ordered glassy states. Rehage and Frenzel (159) summarized the pressure-volume-temperature data for some side-chain TLCP's with flexible main chains compared with isotropic polymers. Nonrandom or block copolyesters may also give TLCP's with a glass transition (26).

TLCP Mechanical Properties vs. Temperature

For the wholly aromatic TLC copolyesters some authors have expressed concern that the lower temperature transitions below about 400 K are like glass transitions with the implication that TLCP's will have limited use above this temperature. Recently, elevated temperature use (500 to 535 K) has been demonstrated by the success of ULTRA 21® dual-oven cookware for the consumer market by the Tupperware Div. of Premark International. This product is based on XYDAR® resin made by Dartco Mfg., Inc. Clearly this lower transition in these polymers is not limiting the usefulness of these materials.

Later we show that below 500 K the increase in properties with decreasing temperature is common for other highly aromatic polymers. Above 500 K the changes in properties are similar for aromatic polymers, but the "disordering transitions" occur at different temperatures.

Log Modulus vs. Temperature for Conventional Polymers

For unoriented, uncrosslinked, amorphous polymers the modulus usually falls at least 1000-fold above the glass transition temperature (160). Although crystallinity and orientation can increase the glass transition and decrease the magnitude of the modulus drop to one or two orders of magnitude, semi-crystalline polymers are usually limited in their use to applications below their glass transition. This is especially true if a product is placed under a load since distortion or creep would occur.

That wholly aromatic copolyesters do not exhibit a classical glass transition temperature is further supported by the excellent creep resistance of XYDAR® at elevated temperatures (161). Also, the UL (Underwriter Laboratories) continuous use temperature rating for XYDAR® resin is above 500 K.

In addition to fiber reinforcement to enhance the use temperature of polymers, it is well known to introduce rigidity by intra-chain (aromatic or aliphatic ring) sequences and interchain (crosslinking) groups as ways of increasing the glass transition temperature and minimizing the change in properties with temperature. It is also known that these methods are generally more effective than increasing orientation or crystallinity in conventional thermoplastics.

Log Modulus vs. Temperature for Some TLCP's

From earlier discussions regarding the nature of the changes in structure with temperature for wholly aromatic TLCP's, the short term properties may be limited by the temperature where the "disordering transitions" occur, i.e. where the macro-order parameter is changing significantly with time.

It is clear that at lower temperatures short range cooperative motions such as ring flips may occur, that polymorphic transitions may also take place, and that both of these can affect the mechanical properties as a function of temperature well below the temperature where major structural changes can occur. The reversibility of properties with temperature is an area that needs further study.

Figure 1 compares the moduli by dynamic mechanical analysis (DMA) for injection molded XYDAR® SRT 300 ("self-reinforced thermoplastic") with other injection molded TLCP's. The PHBA/PET polymer (formerly known as Eastman Chem. Co.'s X7G) has some flexible chain segments in the polymer backbone. The ABA/TPA/NDA polymer data was reported by Ophir and Ide (80). For the wholly aromatic polymers the transitions below 500 K are less than one order of magnitude. The moduli for these TLCP's are about 5 to 10 times higher than for most conventional thermoplastics because of the high degree of orientation combined with the high chain rigidity.

Figure 2 compares a compression molded (CM) XYDAR® SRT 300 with injection molded (IM) SRT 500 and IM PEEK sample. The latter is semi-crystalline and has a glass transition

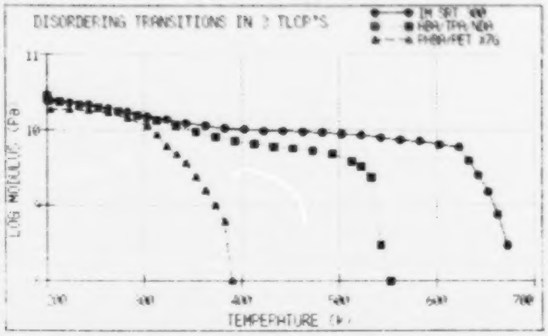

Fig. 1. The DMA log modulus vs. absolute temperature for three injection molded (IM) TLCP's: 1) XYDAR SRT 300, 2) the 60/20/20 mol percent copolyester of acetoxybenzoic acid (ABA), terephthalic acid (TPA) and naphthylene diacetate (80), and the 70/30 percent mol copolyester of p-hydroxybenzoic acid (PHBA), and poly(ethylene terephthalate) PET (54).

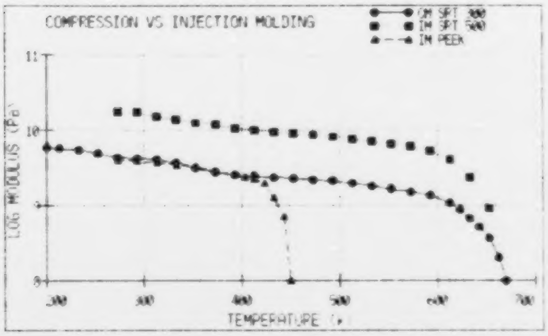

Fig. 2. The DMA log modulus vs. absolute temperature for compression molded (CM) SRT 300, injection molded (IM) SRT 500, and injection molded poly(aryl ether ether ketone) (PEEK).

temperature of about 425 to 430 K. The compression molded XYDAR® sample with no orientation has a modulus comparable to that of injection molded PEEK which has some orientation.

SRT 500 resin differs from the SRT 300 in that it is modified for easier processing. By comparing *Figs. 1* and *2* one notes that the loss of "global orientation" occurs at a slightly higher temperature for injection molded SRT 300 relative to injection molded SRT 500.

In our work with short fiber reinforced composites, we noted that, as with other polymers, the matrix phase dominates the thermal performance. Although Part II of our work covers this topic, we compare in *Fig. 3* some injection molded, glass fiber reinforced TLCP's. RC 210 is based on XYDAR® while the other two are based on two different resins made by Celanese. All three contain 30 percent by weight glass fibers.

From *Figs. 1, 2*, and *3* one sees that RC-210 has a higher modulus than either SRT 300 or 500. Although the increase in modulus is not dramatic, it is significant. Only above the disordering temperature (about 610 K for RC-210) is the glass fiber reinforcement effect lost.

Log Modulus vs. Temperature for Other Aromatic Polymers

Bessenov and Kuzetsov (162) reported on a series of aromatic polyimides (PI) without and with various "hinge" groups. We have selected modulus data for unoriented films of four of their polymers to compare with XYDAR® and poly(p-phenylene) (PPP) (data from Gale (120)) as shown in *Fig. 4*. Our codes PI A, B, C, and D correspond to their codes 1A, 1B, 1C, and 2D. They use the term "softening" temperature (*ST*) for glass transition temperature.

PI A (*ST* = 850 K) has 45 percent crystallinity (melting point *MP* = 1130 K) and is based on the pyromellitimide sequence joined to a biphenyl sequence; it has no hinge groups.

PI B (*ST* = 685 K) has 50 percent crystallinity (*MP* = 915 K) and contains one ether hinge in the dianhydride and none in the biphenyl group.

PI C (*ST* = 550 K) has 20 percent crystallinity (*MP* = 835 K) and is like PI A, but with one phenyl of the biphenyl substituted with two ether-phenyl sequences.

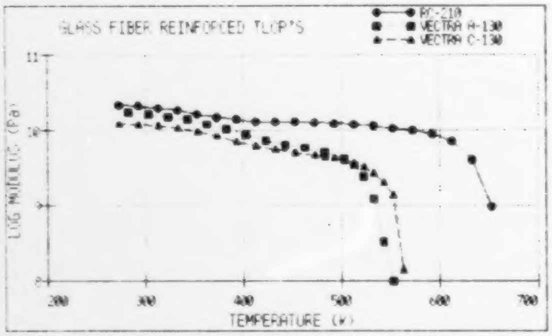

Fig. 3. The DMA log modulus vs. absolute temperature for three 30 percent glass fiber reinforced TLCP's: 1) XYDAR RC-210 made by Dartco Mfg. Inc., 2) VECTRA A-130, and 3) VECTRA C-130 both made by Celanese Specialty Operations.

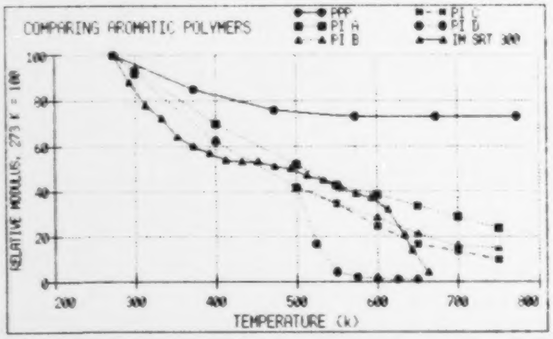

Fig. 4. The relative modulus normalized to 100 units at 273 K vs. absolute temperature for poly(p-phenylene) (120), four polyimides (PI A, B, C, and D) (162), and injection molded SRT 300. See text for details on the polyimides.

PI D (*ST* = 500 K) has 30 percent crystallinity (*MP* = 665 K) and has the ether hinge in the dianhydride like PI B plus the two ether-phenyl sequences as in PI C.

Degradation and crosslinking probably occur before the melting points for all polyimides and probably before the glass transition in PI A. The glass transitions are generally small because of the high rigidity of the aromatic polyimide rings. None of these polymers has a glass temperature below 500 K.

Even PPP has an increasing modulus below 500 K. Ring flips are the only mechanism for small scale cooperative motions in PPP. The absolute value of the modulus (about 3.5 GPa) is about 20 percent of the modulus for SRT 300 at 273 K and about 30 percent at 500 K. The similarity in the molecular chain packing was discussed earlier. Note that the modulus tends toward a plateau for both PPP and SRT 300.

The increase in the modulus for a copolyester may be greater than the PPP modulus perhaps because the ring flip motions apparently include carbonyl groups directly attached to the rings (95), i.e. the ester carbonyl dipole-dipole interactions (directional bonds) are weakened. Alternatively, the difference could be due to the fact that the PPP was compression sintered and has no orientation while the SRT 300 was injection molded.

Figure 5 compares injection molded *vs.* compression molded SRT 300 and the ABA/TPA/NDA polymer (80) where 500 K is taken as the reference temperature. Above about 300 K the IM and CM SRT 300 samples are equivalent despite differences in orientation. Below 300 K the phenyl ring flipping motions are decreased. The larger increase in the modulus for the ABA/TPA/NDA polymer may be due to the presence of the more bulky naphthylene rings whose crankshaft motions would be frozen in at a higher temperature than the para phenyl rings in SRT 300. Also, recall that the amount of skin to core may be higher for the injection molded ABA/TPA/NDA polymer compared to the IM SRT 300.

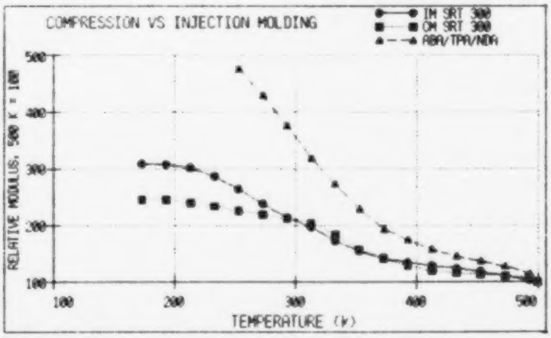

Fig. 5. The relative modulus normalized to 100 units at 500 K vs. absolute temperature for injection molded (IM) SRT 300, compression molded (CM) SRT 300, and the 60/20/20 mol percent copolyester of acetoxybenzoic acid (ABA), terephthalic acid (TPA), and naphthylene diacetate (80).

From *Figs. 1* and *2* it is clear that the effect of orientation on absolute property values is lost above the disordering transition (about 610 K in SRT 300). In PPP it appears that degradation occurs before the disordering transition.

Relative Moduli for TLCP's Compared to Some Polyimides

Figures 6 and *7* compare the relative moduli for the TLC copolyesters with the unoriented polyimides described previously. Below 500 K PI A (the most rigid) shows the least increase in modulus with decreasing temperature. PI B, C, and D all have the same relative increase in modulus with decreasing temperature. Above 500 K the decrease in the relative moduli with increasing temperature corresponds to the relative rigidity. PI D has its glass transition temperature at 500 K.

The relative modulus of injection molded SRT 500 is similar to the polyimides up to the TLCP disordering transition near 600 K. Below 500 K the ABA/TPA/NDA polymer shows a larger increase in the relative modulus. On the other hand, near 500 K this TLCP is near its disordering temperature. Its relative modulus slope between 400 and 500 K is comparable to the

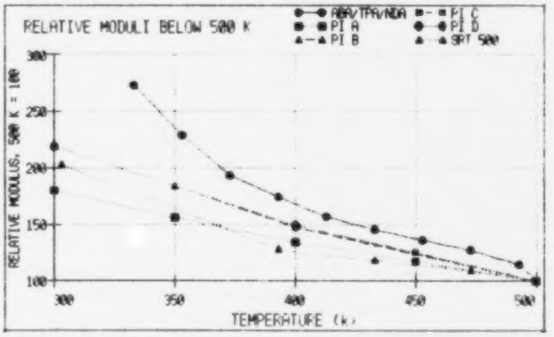

Fig. 6. The relative modulus normalized to 100 units at 500 K vs. absolute temperature below 500 K for the 60/20/20 mol percent copolyester of acetoxybenzoic acid (ABA), terephthalic acid (TPA) and naphthylene diacetate (80), four polyimides (162), and injection molded SRT 500.

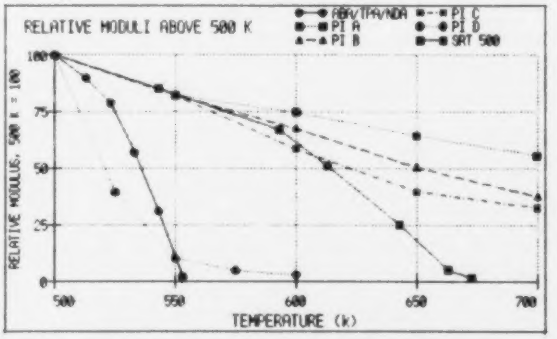

Fig. 7. As in Fig. 6, but above 500 K.

other polymers. The increase in the modulus below 400 K may actually be due to a combination of freezing-in the naphthylene ring crankshaft motions plus the effect of orientation.

The Lower Temperature Transitions in XYDAR®

As in most of the other TLC copolyesters, PHBA is a main component in SRT 300, a random copolymer of 50/25/25 mol percent ratios of p-hydroxybenzoic acid, terephthalic acid, and biphenol (i.e. PHBA/TPA/BP).

Figure 8 gives the storage and loss modulus curves by dynamic mechanical analysis (DMA) on an expanded scale (i.e. not logarithmic) for injection molded SRT 300. *Figure 9* gives the corresponding loss tangent curve.

In contrast to the copolyesters containing naphthylene units, not three but two loss peaks are observed. Based on the recent work of Clements, *et al.* (151, 152) described earlier, the main lower temperature loss peak might correspond to localized ring flip motions of the PHBA units. However, the TPA units in XYDAR® would not be expected to be that different in the volume swept out during rotation. Thus, the main loss peak may be due to the combined motions of both the PHBA and TPA units.

The smaller loss peak near 350 K might be assigned to motions of the biphenyl rings or to the polymorphic phase transitions of the more ordered material in the core. More work is needed before a definite assignment can be made. For example, the effect of frequency on the loss peak positions should be studied. Also, since the sample we used was from a molded test bar, it is of interest to study samples with different amounts of skin and core.

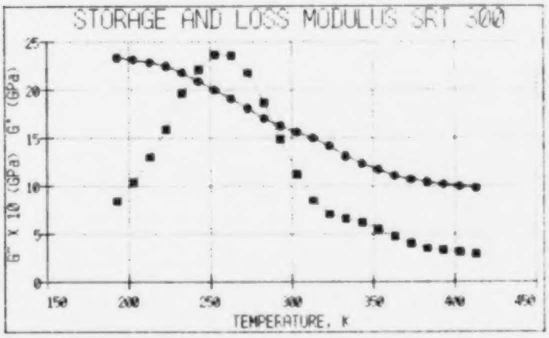

Fig. 8. The DMA storage and loss modulus plotted on an expanded linear scale vs. absolute temperature to show the lower temperature transitions in injection molded SRT 300.

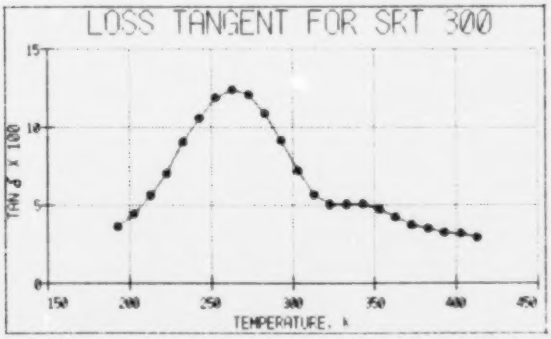

Fig. 9. The loss tangent curve corresponding to Fig. 8.

Clements, et al. (151) reported a five-fold drop in modulus for the PHBA/HNA polymer they studied over the same temperature range as shown in *Fig. 8* where we observed a 2.3-fold drop. This difference is likely caused by the relative amount of highly oriented *and* ordered material since they used oriented tapes annealed at 523 to 543 K up to 70 h while our samples were injection molded test bars, were not annealed, and contained transversely oriented core material.

The Higher Temperature Transitions in XYDAR®

Figure 10 gives the log storage and loss modulus curves over a broader temperature range. In addition to the disordering transition loss peak above about 610 K, we observed a loss peak shoulder on the lower temperature side in this sample. The nature of this transition requires further study since in this temperature range a polymorphic transition from an othorhombic to a pseudo-hexagonal packing occurs in the core material. Also, it is well known that solid state polymerization and annealing of less ordered material can occur in this temperature range. Recall that the UL continuous use temperature rating for SRT 300 is around 515 K and that the solid-to-nematic melt phase transition is around 700 K.

CONCLUSIONS

1. Thermotropic liquid crystalline polymers are self-reinforced composites which often exhibit skin-core morphologies that are complex and depend on flow geometry, processing conditions, and polymer type.

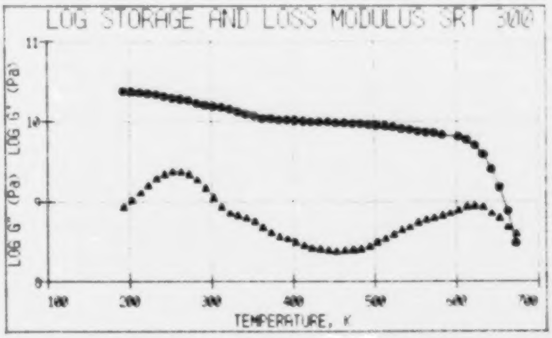

Fig. 10. The DMA log storage and loss modulus vs. absolute temperature for injection molded SRT 300 to compare the lower and higher temperature transitions.

2. New theories may be needed for understanding filled and fiber-reinforced TLCP's because of changes in the self-reinforced phase morphology.

3. To understand the behavior of fiber-reinforced TLCP's, one must first understand the composite nature of the resin. Thus, we have reviewed the literature and provided new data on structure-morphology-processing-property relationships.

4. The molecular dynamics of wholly aromatic copolyesters in the solid state have been reviewed to help clarify the nature of the temperature dependence of mechanical properties. We have shown that a classical glass transition temperature should not exist in rigid chain TLCP's since at least 1-dimensional or nematic structural order can exist rather than a truly amorphous or zero order state.

5. The structural order that can be present in highly aromatic, random copolyesters can range anywhere from one to three dimensions, limited only by the sequence distribution within the polymer chains (i.e. chain packing) and the time-temperature-deformation history of the material.

REFERENCES

1. V. V. Tsukruk, V. V. Shilov, and Y. S. Lipatov, *Acta Polym.*, **36**, 403 (1985).
2. R. C. Forney, *Brit. Plast. Rubber*, **6**, 41 (1986).
3. M. H. Naitove, *Plast. Technol.*, **3**, 13 (1986).
4. A. S. Wood, *Mod. Plast.*, **3**, 44 (1986).
5. J. A. Manson and L. H. Sperling, "Polymer Blends and Composites," Plenum Press, New York (1976).
6. Y. S. Lipatove, *J. Adhesion*, **10**, 85 (1979).
7. H. Ishida, *Polym. Compos.* **5**, 101 (1984).
8. R. H. Burton and M. J. Folkes, *Plast. Rubber Process. Applic.*, **3**, 129 (1983).
9. M. B. Bever and P. E. Duwez, *Mater. Sci. Eng.*, **10**, 1 (1972).
10. A. Keller, "Polymers, Liquid Crystals and Low-Dimensional Solids," N. March and M. Tosi, Eds., Ch. 1 to 5, Plenum Press, New York (1984).
11. T. E. Helminiak, C. L. Benner, and F. E. Arnold, *ACS, Div. Polym. Chem. Polym. Prep.*, **16**, 659 (1975).
12. T. E. Helminiak, ACS, Nat. Symp. on Polymers in Service of Man, **16**, 86 (1980).
13. D. R. Wiff, W. F. Hwang, C. L. Benner, and T. E. Helminiak, *Bull. Am. Phys. Soc.*, **27**, 290 (1982); *Ibid.*, **28**, 390 (1983).
14. W. F. Hwang, D. R. Wiff, C. L. Benner, and T. E. Helminiak, *Macromol. Sci. (Phys.)*, **B22**, 231 (1983).
15. S. J. Krause, T. Haddock, G. E. Price, G. Lenhart, T. E. Helminiak, and W. W. Adams, *J. Polym. Sci., Part B: Polym. Phys.*, **24**, 1991 (1986).
16. S. L. Kwolek (DuPont), U.S.Pat. 3,671,542 (1972).
17. P. W. Morgan, *Macromolecules*, **10**, 1381 (1977).
18. M. G. Northolt, "Recent Advances in Liquid Crystalline Polymers," R. L. Chapoy, Ed., Elsevier Appl. Sci. Publ., New York (1985).
19. C. J. Atkinson, J. R. Lander, and H. Marsh, *Brit. Polym. J.*, **3**, 1 (1981).
20. M. Guigon, and A. Oberlin, *Comp. Sci. Technol.*, **25**, 231 (1986).
21. G. H. Brown and, P. P. Crooker, *Chem. Eng. News*, **1**, 24 (1983).
22. L. Monnerie, *Pure Appl. Chem.*, **57**, 1563 (1985).
23. M. G. Dobb, and J. E. McIntyre, *Adv. Polym. Sci.*, **60/61**, 63 (1984).
24. J. L. White, *J. Appl. Polym. Sci., Appl. Polym. Symp.*, **41**, 3 (1985).
25. W. J. Jackson, *J. Appl. Polym. Sci., Appl. Polym. Symp.*, **41**, 25 (1985).
26. C. Noel, "Polymeric Liquid Crystals," A. Blumstein, Ed., p. 21, Plenum Press, New York (1985).
27. G. Huynh-Ba and E. F. Cluff, "Polymeric Liquid Crystals," A. Blumstein, Ed., p. 217, Plenum Press, New York (1985).
28. T. S. Chung, *Polym. Eng. Sci.*, **26**, 901 (1986).
29. N. Koide, *Mol. Cryst. Liq. Cryst.*, **139**, 47 (1986).
30. S. K. Varshney, *Rev. Macromol. Chem. Phys.*, **C26**, 551 (1986).
31. J. S. Jin, S. Antoun, C. Ober, and R. W. Lenz, *Brit. Polym. J.*, **12**, 132 (1980).
32. R. W. Lenz, *Pure Appl. Chem.*, **57**, 977 (1985).
33. R. W. Lenz, and G. L. Grune, *Mol. Cryst. Liq. Cryst.*, **106**, 383 (1984).
34. R. W. Lenz, *Pure Appl. Chem.*, **57**, 1537 (1985).
35. R. W. Lenz, *J. Polym. Sci., Polym. Symp.*, **72**, 1 (1985).
36. R. W. Lenz, "Recent Advances in Liquid Crystalline Polymers," L. L. Chapoy, Ed., Ch. 1, p. 3, Elsevier Appl. Sci. Publ., New York (1985).
37. G. Chen and R. W. Lenz, *Polymer*, **26**, 1309 (1985).
38. R. W. Lenz, IUPAC Meeting on "Non-Crystalline Order in Polymers," Naples (May 28, 1985).
39. L. Quach, W. Volksen, R. Herbold, and J. Economy, *ACS, Div. Polym. Chem. Polym. Prep.*, **27**, 307 (1986).
40. E. G. Joseph, G. L. Wilkes, and D. G. Baird, *Polym. Eng. Sci.*, **25**, 377 (1985).
41. C. R. Gochanour and M. Weinberg, *J. Rheol.*, **30**, 101 (1986).
42. S. L. Wunder, S. Ramachandran, C. R. Gochanour, and M. Weinberg, *Macromolecules*, **19**, 1696 (1986).
43. R. J. Samuels, "Structured Polymer Properties," Wiley-Interscience, New York (1974).
44. R. J. Samuels, *Polym. Eng. Sci.*, **25**, 864 (1985).
45. W. T. Mead and R. S. Porter, *J. Appl. Polym. Sci.*, **22**, 3249 (1978).
46. L. P. B. M. Janssen, R. Boetes, and J. M. Smith, The Plastics and Rubber Institute, Polymer Extrusion II, *Conference Proceedings*, p. 25.1, London (May 1982).
47. S. L. Sakellarides and A. J. McHugh, *Polym. Eng. Sci.*, **25**, 1179 (1985).
48. G. Ehrenstein and C. Maertin, *Kunststoffe*, **76**, 524 (1986).
49. R. M. Gohil and J. Petermann, *J. Mater. Sci.*, **18**, 1719 (1983).
50. R. H. Burton, T. M. Day, and M. J. Folkes, *Polym. Commun.*, **26**, 361 (1985).
51. J. Smook, M. Flinteman, and A. J. Pennings, *J. Mater. Sci.*, **19**, 31 (1984).
52. P. A. Irvine and P. Smith, *Macromolecules*, **19**, 240 (1986).
53. W. W. Adams, *ACS Polym. Prep., Div. of Polym. Chem.*, **26** (2), 306 (1985).
54. W. J. Jackson, Jr., and H. F. Kuhfuss, *J. Polym. Sci., Part A: Polym. Chem.*, **14**, 2043 (1976).
55. W. J. Jackson, Jr., *Brit. Polym. J.*, **12**, 154 (1980).
56. W. J. Jackson, Jr., *J. Appl. Polym. Sci., Appl. Poly. Symp.*, **41**, 25 (1985).
57. E. G. Joseph, G. L. Wilkes, and D. G. Baird, *Polymer*, **26**, 689 (1985).
58. E. G. Joseph, G. L. Wilkes, and D. G. Baird, *Polym. Eng. Sci.*, **25**, 377 (1985).
59. G. G. Viola, D. G. Baird, and G. L. Wilkes, *Polym. Eng. Sci.*, **25**, 888 (1985).
60. B. P. Griffin and M. K. Cox, *Brit. Polym. J.*, **12**, 147 (1980).
61. K. F. Wissbrun, *Brit. Polym. J.*, **12**, 163 (1980).
62. F. N. Cogswell, *Brit. Polym. J.*, **12**, 166 (1980).
63. K. F. Wissbrun, *J. Rheol.*, **25**, 619 (1981).
64. T. Asada and S. Onogi, *Polym. Eng. Rev.*, **3**, 323 (1983).
65. K. F. Wissbrun, *Faraday Discuss. Chem. Soc.*, **79**, 161 (1985).
66. G. Marrucci, *Pure Appl. Chem.*, **57**, 1545 (1985).

67. A. E. Zachariades and J. A. Logan, "Recent Advances in Liquid Crystalline Polymers," L. L. Chapoy, Ed., p. 177, Elsevier Appl. Sci. Publ., New York (1985).
68. H. Sugiyama, D. N. Lewis, J. L. White, and J. F. Fellers, *J. Appl. Polym. Sci.*, **30**, 2329 (1985).
69. J. L. White, *J. Appl. Polym. Sci., Appl. Polym. Symp.*, **41**, 241 (1985).
70. G. G. Viola and D. G. Baird, *J. Rheol.*, **30**, 601 (1986).
71. A. E. Zachariades, A. Fox, and P. Navard, *SPE ANTEC Tech. Papers*, **32**, 721 (1986).
72. D. Dove and D. G. Baird, *SPE ANTEC Papers*, **32**, 715 (1986).
73. H. Thapar and M. Bevis, *J. Mater. Sci. Lett.*, **2**, 733 (1983).
74. A. M. Donald, C. Viney, and A. H. Windle, *Polymer*, **24**, 155 (1983).
75. A. M. Donald and A. H. Windle, *Polymer*, **25**, 1235 (1984).
76. A. E. Zachariades, P. Navard, and J. A. Logan, *Mol. Cryst. Liq. Cryst.*, **110**, 93 (1984).
77. A. M. Donald and A. H. Windle, "Recent Advances in Liquid Crystalline Polymers," L. L. Chapoy, Ed., p. 187, Elsevier Appl. Sci. Publ., New York (1985).
78. N. J. Alderman and M. R. Mackley, *Faraday Discuss. Chem. Soc.*, **79**, 149 (1985).
79. E. L. Thomas and B. A. Wood, *Faraday Discuss. Chem. Soc.*, **79**, 229 (1985).
80. Z. Ophir and Y. Ide, *Polym. Eng. Sci.*, **23**, 792 (1983).
81. T. Weng, A. Hiltner, and E. Baer, *J. Mater. Sci.*, **21**, 744 (1986).
82. L. C. Sawyer and M. Jaffe, *J. Mater. Sci.*, **21**, 1897 (1986).
83. J. J. Duska, N. D. Field, and F. Scardiglia, Polymer Processing Society Conference, Montreal (April 1986).
84. J. J. Duska, *Plast. Eng.*, **12**, 39, 1987.
85. M. Narkis, *J. Appl. Polym. Sci.*, **22**, 2391 (1978).
86. L. E. Nielsen, "Mechanical Properties of Polymers and Composites," Vol. 2, Ch. 7, p. 388, Marcel Dekker, Inc., New York (1974).
87. M. Schrager, *J. Appl. Polym. Sci.*, **22**, 2379 (1978).
88. V. A. Bershtein, V. M. Egorov, A. F. Podolsky, and V. A. Stepanov, *J. Polym. Sci., Part C: Polym. Lett.*, **23**, 371 (1985).
89. R. B. Stinchcombe, "Polymers, Liquid Crystals and Low-Dimensional Solids," N. March and M. Tosi, Eds., Ch. 13, Plenum Press, New York (1984).
90. M. Zverev and S. Pankov, *Khim. Volokna*, **2**, 30 (1984).
91. P. Corradini, V. Petraccone, C. DeRosa, and G. Guerra, *Macromolecules*, **19**, 2699 (1986).
92. P. D. Frayer, N. D. Field, R. Layton, F. Scardiglia, and R. Baldwin, to be published, journal not chosen.
93. J. Blackwell, H. M. Cheng, A. Biswas, N. D. Field, P. D. Frayer, and R. Layton, Polymer Processing Soc., Third Annual Meeting, Stuttgart, W. Germany (April 7–10, 1987).
94. N. D. Field, R. Baldwin, F. Scardiglia, J. Duska, R. Layton, and P. Frayer, Div. Polym. Chem., Inc., Am. Chem. Soc., Topical Workshop on "Flow Deformation and Molecular Reorganization in Polymers with Crystalline and Liquid Crystalline Order," Montreal (April 1986).
95. D. J. Blundell, *Polymer*, **23**, 359 (1982).
96. A. M. Donald and A. H. Windle, "Recent Advances in Liquid Crystalline Polymers," L. L. Chapoy, Ed., Ch. 12, Elsevier Appl. Sci. Publ., New York (1985).
97. S. Hu, M. Xu, J. Li, B. Qian, X. Wang, and R. W. Lenz, *J. Polym. Sci., Part B: Polym. Phys.*, **23**, 2387 (1985).
98. A. M. Donald, C. Viney, and A. H. Windle, *Polymer*, **24**, 155.
99. A. M. Donald and A. H. Windle, *Polymer*, **25**, 1235 (1984).
100. A. M. Donald and A. H. Windle, *J. Mater. Sci. Lett.*, **4**, 58 (1985).
101. A. M. Donald, C. Viney, and A. H. Windle, *Phil. Mag. B*, **52**, 925 (1985).
102. C. Viney, G. R. Mitchell, and A. H. Windle, *Mol. Cryst. Liq. Cryst.*, **129**, 75 (1985).
103. A. M. Donald, *Polym. Commun.*, **27**, 18 (1986).
104. M. Kleman, *Faraday Discuss. Chem. Soc.*, **79**, 215 (1985).
105. G. Magelet and M. Kleman, *Polymer*, **27**, 714 (1986).
106. P. J. Flory, *Ber. der Bunsen-Gesellschaft*, **81**, 885 (1977).
107. P. J. Flory and A. Abe, *Macromolecules*, **11**, 1119 (1978).
108. A. Abe and P. J. Flory, *Macromolecules*, **11**, 1122 (1978).
109. P. J. Flory and R. S. Frost, *Macromolecules*, **11**, 1126 (1978).
110. R. S. Frost and P. J. Flory, *Macromolecules*, **11**, 1134 (1978).
111. P. J. Flory, *Macromolecules*, **11**, 1138 (1978).
112. P. J. Flory, *Macromolecules*, **11**, 1141 (1978).
113. A. L. Cimecioglu, S. H. Zeronian, K. W. Alger, and M. J. Collins, *J. Appl. Polym. Sci.*, **32**, 4719 (1986).
114. G. C. East and A. M. Girshap, *Polym. Commun.*, **23**, 323 (1982).
115. P. G. Kosky and E. A. Guggenheim, *Polym. Eng. Sci.*, **25**, 1145 (1985).
116. P. D. Frayer, J. L. Koenig, and J. B. Lando, *J. Macromol. Sci.: Phys.*, **B3**, 329 (1969); *Ibid.*, **B6**, 129 (1972).
117. H. R. Kricheldorf and G. Schwarz, *Makromol. Chem.*, **184**, 475 (1983).
118. W. Volksen, R. Geiss, and J. Economy, *J. Polym. Sci., Part B: Polym. Phys.*, **24**, 2117 (1986).
119. Y. P. Khanna and E. M. Pearce, *J. Polym. Sci., Part A: Polym. Chem.*, **24**, 2377 (1986).
120. D. Gale, *J. Appl. Polym. Sci.*, **22**, 1955 (1978); *Ibid.*, **22**, 1971 (1978).
121. A. Kawaguchi and J. Peterman, *Mol. Cryst. Liq. Cryst.*, **133**, 189 (1986).
122. A. V. Fratini, E. M. Cross, J. F. O'Brien, and W. W. Adams, *J. Macromol. Sci.: Phys.*, **B24**, 159 (1985–86).
123. M. G. Northolt, "Recent Advances in Liquid Crystalline Polymers," L. L. Chapoy, Ed., Ch. 20, Elsevier Appl. Sci. Publ., New York (1985).
124. T. Ii, K. Tashiro, M. Kobayashi, and H. Tadokoro, *Macromolecules*, **19**, 1809 (1986).
125. M. Takase and W. R. Krigbaum, *J. Polym. Sci., Part B: Polym. Phys.*, **24**, 1115 (1986).
126. T. Ii, K. Tashiro, M. Kobayashi, and H. Tadokoro, *Macromolecules*, **19**, 1772 (1986).
127. D. E. Kirkpatrick and B. Wunderlich, *J. Polym. Sci., Part B: Polym. Phys.*, **24**, 931 (1986).
128. G. Lieser, G. Schwarz, and H. R. Kricheldorf, *J. Polym. Sci., Part B: Polym. Phys.*, **21**, 1599 (1983); G. Lieser, *Ibid.*, **21**, 1611 (1983).
129. J. Economy, W. Volksen, and R. H. Geiss, *Mol. Cryst. Liq. Cryst.*, **105**, 289 (1984).
130. S. Z. D. Cheng, M. Y. Cao, and B. Wunderlich, *Macromolecules*, **19**, 1868 (1986).
131. A. J. Lovinger and D. D. Davis, *Macromolecules*, **19**, 1861 (1986).
132. J. Blackwell and G. A. Gutierrez, *Polymer*, **23**, 671 (1985).
133. G. A. Gutierrez, R. A. Chivers, J. B. Stamatoff, and H. Yoon, *Polymer*, **24**, 937 (1983).
134. J. Blackwell, G. Lieser, and G. A. Gutierrez, *Macromolecules*, **16**, 1418 (1983).
135. R. A. Chivers, J. Blackwell, and G. A. Gutierrez, *Polymer*, **25**, 435 (1984).
136. J. Blackwell, G. A. Gutierrez, and R. A. Chivers, *Macromolecules*, **17**, 1219 (1984).
137. J. Blackwell, G. A. Gutierrez, and R. A. Chivers, *J. Polym. Sci., Part B: Polym. Phys.*, **22**, 1343 (1984).
138. J. Blackwell, A. Biswas, and R. C. Bonart, *Macromolecules*, **18**, 2126 (1985).
139. G. A. Gutierrez, J. Blackwell, and R. A. Chivers, *Polymer*, **26**, 348 (1985).
140. R. A. Chivers and J. Blackwell, *Polymer*, **26**, 997 (1985).
141. J. Blackwell, A. Biswas, G. A. Gutierrez, and R. A.

Chivers, *Faraday Disc. Chem. Soc.*, **79**, 73–84 (1985).

142. R. A. Chivers, J. Blackwell, G. A. Gutierrez, J. B. Stamatoff, and H. Yoon, "Polymeric Liquid Crystals," A. Blumstein, Ed., p. 153, Plenum Press, New York (1985).
143. J. Blackwell, G. A. Gutierrez, and R. A. Chivers, "Polymeric Liquid Crystals," A. Blumstein, Ed., p. 167, Plenum Press, New York (1985).
144. J. J. Dumais, A. L. Cholli, L. W. Jelinski, J. L. Hedrick, and J. E. McGrath, *Macromolecules*, **19**, 1884 (1986).
145. K. Mueller, B. Hisgen, H. Ringsdorff, R. W. Lenz, and G. Kothe, *Mol. Cryst. Liq. Cryst.*, **113**, 167 (1984).
146. D. J. Blundell and K. A. Buckingham, *Polymer*, **26**, 1623 (1985).
147. T. I. Borisova, N. A. Nikonorova, A. Y. Bilibin, and S. S. Skorokhodov, *Vysokomol. Soedin., Ser. A*, **28**, 584 (1986).
148. G. R. Mitchell and F. Ishii, *Polym. Commun.*, **26**, 34 (1985).
149. S. Smigasiewicz and B. Kowalski, *J. Polym. Sci., Part B: Polym. Phys.*, **24**, 1961 (1986).
150. Y. Takase, G. R. Mitchell, and A. Odajima, *Polym. Commun.*, **27**, 76 (1986).
151. J. Clements, G. R. Davies, R. Jakeways, M. J. Troughton, and I. M. Ward, ACS Polymeric Mat. Sci. Eng. Div. Proc., **54**, 8 (1986).
152. J. Clements, J. Humphreys, and I. M. Ward, *J. Polym. Sci., Part B: Polym. Phys.*, **24**, 2293 (1986).
153. F. E. McFarlane, V. A. Nicely, and T. G. Davis, "Contemporary Topics in Polymer Science," E. M. Pierce and J. R. Schaefgen, Eds., Ch. 2, p. 109, Plenum Press, New York (1977).
154. J. B. Stamatoff, *Mol. Cryst. Liq. Cryst.*, **110**, 75 (1984).
155. A. H. Windle, C. Viney, R. Golombok, A. M. Donald, and G. Mitchell, *Faraday Discuss. Chem. Soc.*, **79**, 55 (1985).
156. M. Cao and B. Wunderlich, *J. Polym. Sci., Part B: Polym. Phys.*, **23**, 521 (1985).
157. B. Wunderlich and J. Grebowicz, "Polymeric Liquid Crystals," A. Blumstein, Ed., p. 145, Plenum Press, New York (1985).
158. C. Noel, C. Friedrich, L. Bosio, and C. Strazielle, *Polymer*, **25**, 1281 (1984).
159. G. Rehage and J. Frenzel, *Brit. Polym. J.*, **12**, 173 (1982).
160. A. Rudin, "The Elements of Polymer Science and Engineering," p. 419, Academic Press, Inc., Orlando, Florida (1982).
161. "XYDAR® High-Performance Engineering Resins—Technical Information Bulletin," Dartco Mfg. Inc. (1985).
162. M. I. Bessenov and N. P. Kuznetsov, "Polyimides—Synthesis, Characterization, and Applications," K. L. Mittal, Ed., Vol. 1, p. 385, Plenum Press, New York (1984).

P. D. FRAYER: DISCUSSION

L. P. Hubert: Have you tried to weld or laminate these LCP's?

P. D. Frayer: It is difficult to weld this particular material. However, we have an extrusion grade which can be made into films and heat laminated. Ultrasonic welding of the injection molding grade is difficult in part because the melting point is above 400°C.

S. Newman: You talked about a melting point which is molecular weight independent, and you used the term "fold length." Did you mean fold period?

P. D. Frayer: Yes, for conventional semi-crystalline polymers which exhibit chain folding. The rigid chain TLCP's do not chain fold, but are extended chains.

S. Newman: So, how do you rationalize the relationship between the melting point and molecular weight?

P. D. Frayer: For folded chains the melting point is proportional to the fold period. For rigid, extended chain polymers the isotropic melting point may increase with increasing molecular weight. At very high molecular weight these polymers become infusible. The nematic transition probably depends on the size of the crystallites where a higher degree of order exists. For comparison, Teflon is believed to have some extended chain crystals so that the as-polymerized material has a melting point of about 347°C. However, after melting out the extended chain form, the new melting point is about 327°C. For extended, rigid chain TLCP's the order is lost along the chains in the nematic state. Thus, there exists axial disorder, but interactions still occur between the aligned chains. Making them longer would increase these interactions. Thus, the longer the chains the harder it is to separate them by thermal energy and the higher the isotropic melting point.

A. Moet: When dealing with LCP laminates, what is the nature of the interphase, of the inter-laminar weld regions?

P. D. Frayer: I do not know the answer. Between two laminates oriented in different directions the molecular layers in contact would have shifted orientations. So the mechanism is not clear. How that occurs during the molding process in the boundary layer between the skin and core is also unclear. It may be that whole sheets of layers get rotated rather than slight shifts of individual molecular layers, but still the bonding mechanism is unclear.

A. Moet: This material is particularly suitable for extrusion, not molding?

P. D. Frayer: Our main interest has been with filled and fiber-reinforced, injection molded composites. There are only a few specialized applications where you would want to have the anisotropy that exists in the unfilled injection molded resin. Fillers drastically modify the anisotropy and the nature of the skin and core. Neither the injection molding resin nor the filled compounds will extrude well. They are best formed in a closed cavity. Our extrusion grade resins can be processed at lower temperatures, for example 365 *vs.* 425°C for the injection molding grades.

L. A. Utracki: Your LCP's are copolymers. Do you have any idea what is the randomness of the monomeric placement?

P. D. Frayer: Some details on the molecular structure will be presented at the Polymer Processing Society meeting in Stuttgart, W. Germany in April of 1987. These materials are so chemically resistant that they do not dissolve. They are most noted for their high temperature properties. Many techniques for characterizing solid polymers have not given any useful information regarding the sequence distribution. The only uselful method thus far was developed by Professor John Blackwell at Case Western Reserve University in which he can model the aperiodic meridional X-ray reflections. Based on models of our materials and the experimental X-ray data, as far as he can determine, there are no significant block lengths of the p-hydroxy benzoic acid units. By his method he cannot detect block lengths less than about four equivalent units. Separate from the aperiodic meridional reflections, if one measures the periodicity of the layer line spacings, one finds that the average repeat distance is about 7.6 Angstroms. Thus, this layer line spacing corresponds to a copolymer having a repeating sequence of the 50/25/25 mol percent ratios of the p-hydroxybenzoic acid, terephthalic acid, and biphenol monomer units where the 7.6 Angstroms corresponds to the average length of four monomers in the repeating sequence.

Optothermal Analysis of Polymer Composites

J. C. KRAPEZ, P. CIELO, X. MALDAGUE, *and* L. A. UTRACKI

National Research Council Canada
Industrial Materials Research Institute
Boucherville, Québec, J4B 6Y4 Canada

A number of thermographic techniques under optical-radiation heating are described for the nondestructive evaluation of different kinds of fiber-filled polymer-based composites. Shallow delaminations within carbon-fiber reinforced laminates can be detected by this method under wide-area surface heating to 5 or 10° above ambient. A number of image-processing algorithms are described for improving the visibility of subsurface defects. Spot-heating techniques are presented for the characterization of fiber concentration, distribution, and orientation in carbon or steel fiber-filled composites. Particular emphasis is given to the possibility of mapping fiber-orientation properties at gradually deeper layers below the surface. These optothermal techniques appear to be a convenient tool for the inspection of opaque composites in terms of rapidity, lack of sample preparation requirement, and simplicity both in its implementation and in the interpretation of results.

INTRODUCTION

Optothermal techniques, using radiative heating and temperature monitoring by infrared (IR) sensors, are being increasingly used in industry for various inspection tasks. Examples are the nondestructive testing (NDT) of layered structures (1–3), reversible stress-pattern analysis (4), and material anisotropy investigations in stretched polymers (5, 6) as well as in fiber-filled composites (7, 8). These methods are attractive because of noncontact nature, rapidity of implementation, ability of scanning over large surfaces, and relative independence of the workpiece surface morphology.

In this paper we describe a number of applications of the optothermal techniques to the nondestructive evaluation of polymer composites. Thermographic techniques with extended surface heating are described for the NDT of carbon-fiber-reinforced-plastics (CFRP) laminates, with particular emphasis on image-processing methods which are shown to enhance the visibility of subsurface defects. Spot-heating thermographic methods will subsequently be described for the characterization of a number of properties of fiber-filled thermoset and thermoplastic composites including fiber concentration, distribution, and orientation investigations. It is shown that thermography can provide information on fiber orientation not only near the surface of the material, but also at gradually deeper layers below the surface.

THERMOGRAPHIC NDT OF CFRP LAMINATES

Heat-flow analysis

A typical apparatus for thermographic NDT of industrial materials is shown in *Fig. 1*. The surface of the inspected structure is subjected to transient thermal excitation by a pulsed heat source such as an array of heating lamps. An IR camera is used to monitor the surface temperature during and after heating, watching for hot spots which are related to subsurface defects.

Heat flows from the heated surface within the material producing, in the case of a homogeneous material surface-heated by an infinitely short heat pulse covering an area much wider than the thickness, l, of the sheet and for observation times much smaller than the thermal propagation time, $l^2/4\alpha$, across the sheet, a temperature field given by the one-dimensional expression (9):

$$T(z, t) = Q(K\rho c\pi t)^{-1/2}\exp[-z^2/4\alpha t] \qquad (1)$$

where T is the temperature, z is the depth below the surface, t is the time since the heat pulse, Q is the absorbed energy density, K, ρ, and c are respectively the thermal conductivity, the mass density, and the specific heat of the inspected material, and $\alpha = K/\rho c$ is its thermal diffusivity. If a defect is present below the heated surface, the thermal parameters of the material will change leading to a modification of the surface temperature which indicates the presence of a subsurface flaw. *Equation 1* shows that the presence of a defect at a depth, z, below the surface will be most visible after a time delay of the order of the thermal propagation time:

$$t_m = z^2/4\alpha \qquad (2)$$

making possible a rough evaluation of the defect depth, z, if the thermal diffusivity α of the material is known.

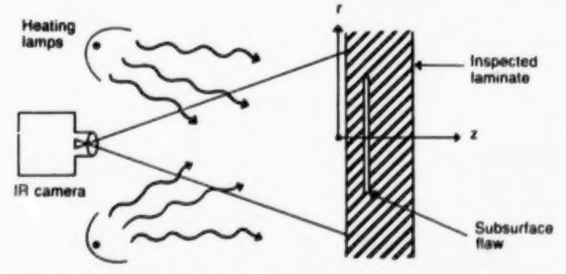

Fig. 1. Schematic for thermographic nondestructive testing of industrial materials.

More specifically, a CFRP sheet may contain a subsurface delamination of given diameter as shown in *Fig. 1*. The simplified one-dimensional expression given by *Eq 1* is no longer valid in this case. Although more sophisticated analytical solutions of the heat flow in materials of finite thickness under a heating pulse of finite duration have been obtained (10), finite-difference numerical simulations provide the most versatile tool when three-dimensional heat flow in anisotropic materials of complex geometry and in the presence of nonlinear surface losses is to be modeled. An example of such a simulation is presented in *Fig. 2*. The upper row represents the temperature distribution across a section r–z of the heated material, as shown in *Fig. 1*, at three successive times after the heating pulse. The model is based on the explicit interative approach for the solution of the heat diffusion equation (11), it is cylindrically symmetric, and the assumed material parameters roughly corresponding to a 0–90° CFRP sheet with a 2 cm-diameter delamination 2 mm below the surface are summarized in *Table 1*.

It can be seen from *Fig. 2* that the thermal

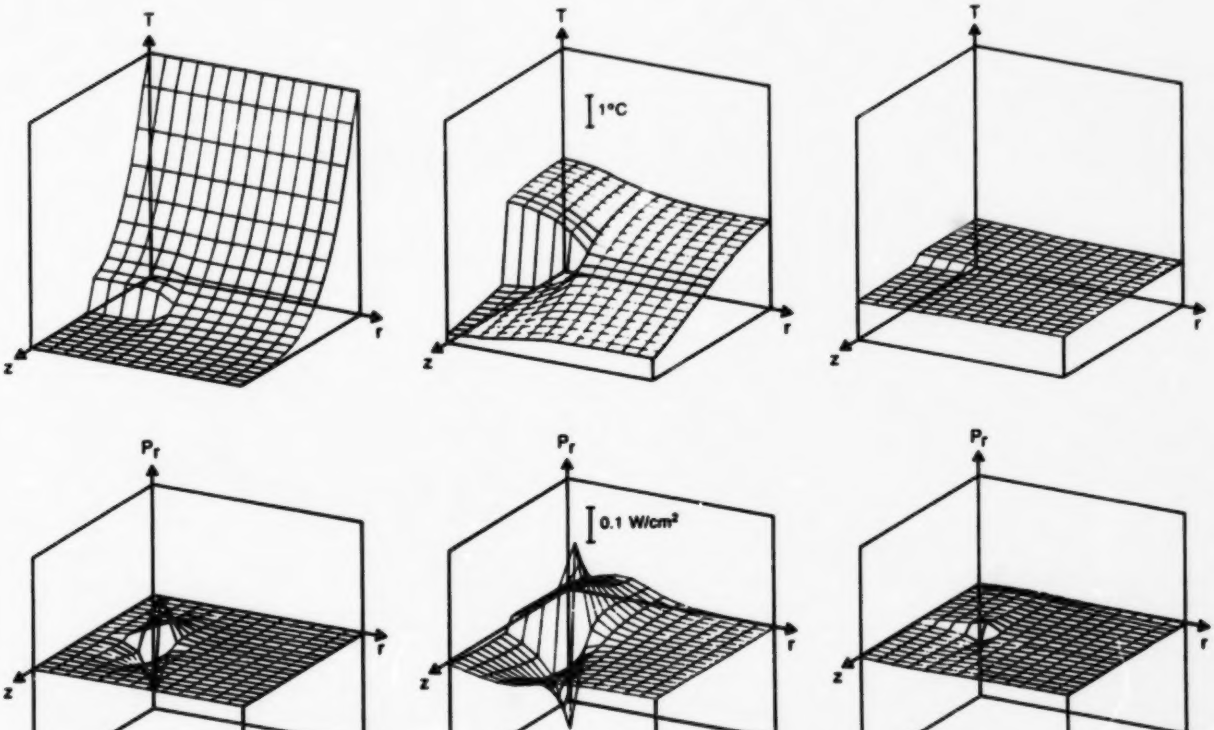

Fig. 2. Three-dimensional finite-difference plots showing the computed distributions of temperature (top row) and radial heat-flow (bottom row) across the r-z plane shown in Fig. 1, respectively after 1.6 s (left), 6.3 s (middle), and 25 s (right) after starting heating.

Table 1. Material Parameters for the Finite-Difference Model Shown in Fig. 2.

Parameter	Value	Units
Mass density	2000	kg/m^3
Specific heat	1000	J/kg/K
Bulk thermal conductivity:		
—parallel to the surface	10	W/m/K
—normal to the surface	1	W/m/K
Thermal conductance of the delaminated interface (corresponding to a 200 μm-thick air-filled gap)	120	W/m^2/K
Absorbed surface heat power	10^4	W/m^2
Heat-pulse duration	2	s
Radiative surface losses (T = surface temperature, T_a = ambient temperature in K)	$5.67 \cdot 10^{8} \cdot (T^4 - T_a^4)$	W/m^2
Convective surface losses	$10 \cdot (T - T_a)$	W/m^2

front has hardly reached the delamination defect after 1.6 s, so that the presence of the defect still does not affect the surface temperature distribution (intersection of the plotted temperature surface with the z = 0 plane). After 6.3 s a much larger temperature differential develops across the delaminated interface, leading to a larger surface temperature over the delaminated area which indicates the presence of the subsurface defect. Even for a very high thermal resistance of the delaminated interface, the surface temperature differential which develops over the defect is limited by the radial thermal flow which is mainly responsible for the temperature uniformization obtained after 25 s. As can be seen in the lower plots of *Fig. 2*, the radial thermal flow, positive above and negative below the defect, is first localized in the vicinity of the defect border, spreading over a progressively wider volume as time advances. The result is a smoother thermal distribution on the surface (z = 0) as compared to the thermal distribution immediately over the defect, as the upper row, second column plot of *Fig. 2* shows. Such a smoothening effect, which decreases the defect visibility, becomes increasingly important with a decrease of the defect diameter/depth ratio and of the ratio between the axial and the radial thermal conductivities in the material.

Thermographic Inspection of Implanted Defects in CFRP Laminates

The above conclusions were verified on a number of weaved CFRP samples with simulated subsurface delaminations (50 μm-thick Teflon double-tape implants inserted in the multi-ply sheet prior to curing) which were prepared by Dassault Aviation, Paris, France and by Canadair, Montréal, Canada. The nondestructive inspection of adhesively-bonded laminates at the various stages of manufacture as well as during service is an important requirement in the aircraft industry and represents a substantial fraction of the manufacturing costs. The development of fast and readily implemented procedures for such inspections would greatly contribute to the required increase in productivity.

Figure 3 shows some thermal images of a nearly 5 by 5 cm^2 area over the implanted defects as obtained with an IR camera after radiative heating from 5 parabolic-mirror backed, 1 KW lamps positioned at nearly 0.7 m from the surface to generate a heat input of nearly 1

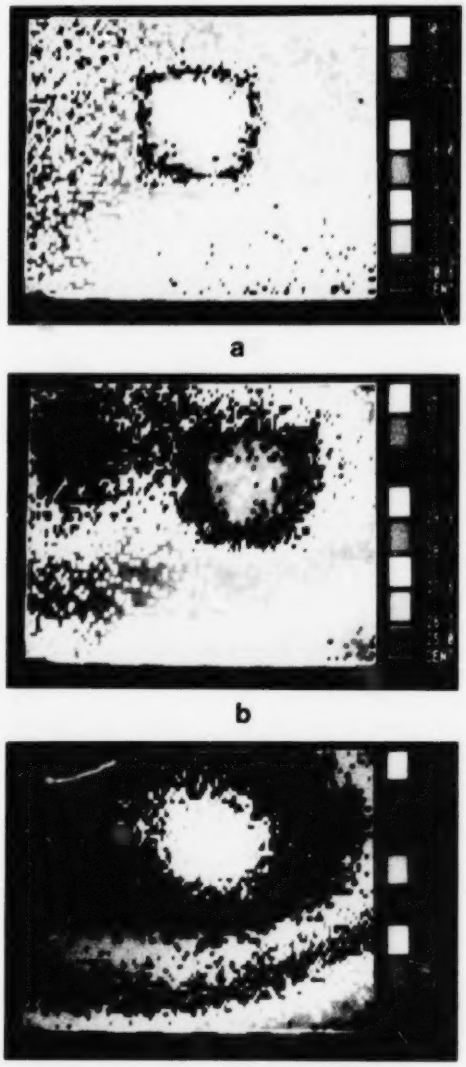

a

b

c

Fig. 3. Untreated thermal images of samples with 2 by 2 cm^2 size Teflon implants inserted at depths of (a) 0.3 mm, (b) 1.12 mm, and (c) 2.25 mm below the surface.

W/cm^2 on the surface. The IR camera is an AGEMA 782 SW having a temperature sensitivity of 0.2°C at ambient temperature. The three thermographs, displaying color isotherms of the heated surface, show three regions of the 5 mm-thick plate with 2 by 2 cm^2 implants inserted at depths of 0.3, 1.12, and 2.25 mm respectively under the surface. Heating periods of 0.1, 0.5 and 4 s were respectively used in the three cases, and the displayed thermograms were taken after 1.2, 3.7, and 6.1 s respectively after starting heating.

The effect of the three-dimensional heat flow analyzed in *Fig. 2* is readily apparent in the experimental thermographs shown in *Fig. 3*. The edges of the square-shaped implanted defect became more and more blurred as the depth of the defect increases, while the thermal contrast over the defect area decreases. This is a direct consequence of the three-dimensional spread of the thermal front around the defect as shown in *Fig. 2*. Such a spread results in poor defect visibility when the thermal path to the depth of the delaminated interface is of the order of the thermal path corresponding to the radius of the delamination. In isotropic materials, only defects of diameter two or three times larger than their depth can normally be detected by thermal techniques. The thermal anisotropy of graphite-epoxy laminates, where the thermal diffusivity α_L in a direction parallel to the fibers is typically larger by an order of magnitude than the thermal diffusivity α_T in the normal direction (3), further increases such a minimum ratio by a factor $(\alpha_L/\alpha_T)^{1/2}$, as can be inferred from *Eq 2*. Only defects of diameter 5 to 10 times larger than their depth can thus be detected by thermal methods in such materials.

Image-Processing Techniques for Improving Defect Visibility

The 2 by 2 cm^2, 2.25 mm-deep defect corresponding to *Fig. 3c* is not easily discernible from the noise visible in this image, in spite of a diameter/depth ratio of 9 which is within the above mentioned defect-visibility limits. This is confirmed by the finite-difference simulation of *Fig. 2*, which for a diameter/depth ratio of 10 indicates that a temperature differential of almost 1°C should be present along the surface between the center of the delaminated area and the surrounding defect-free area. This is substantially higher than the detection limit of nearly 0.1°C which can be reached with our camera.

The main obstacle to the resolution of small temperature differentials across the imaged area is related to nonuniformity of the heat distribution across the irradiated area. Each lamp produces a roughly gaussian projected heat pattern, and even by carefully aligning the five heating lamps to produce a roughly uniform intensity over the center of the irradiated plane, heat-input variations of 10 to 20 percent across the inspected area are unavoidable in practice. Such a noise source is however repetitive, and thus can be corrected by a proper choice of image-processing techniques (3).

An example of a space-domain technique to correct for the nonuniformity of the heat input is shown in *Fig. 4*. *Figure 4a* shows the thermal image obtained over the 20 by 20 mm^2, 2.25 mm-deep implant which was shown in *Fig. 3c*. Some of the thermal features visible in this image are related to the subsurface defect, while others are due to the nonuniformity of the radiation source. The effect of such a noise unrelated to the presence of defects may be eliminated by subtracting from the recorded image the reference image *4b* obtained under similar conditions over a defect-free area of the sample.

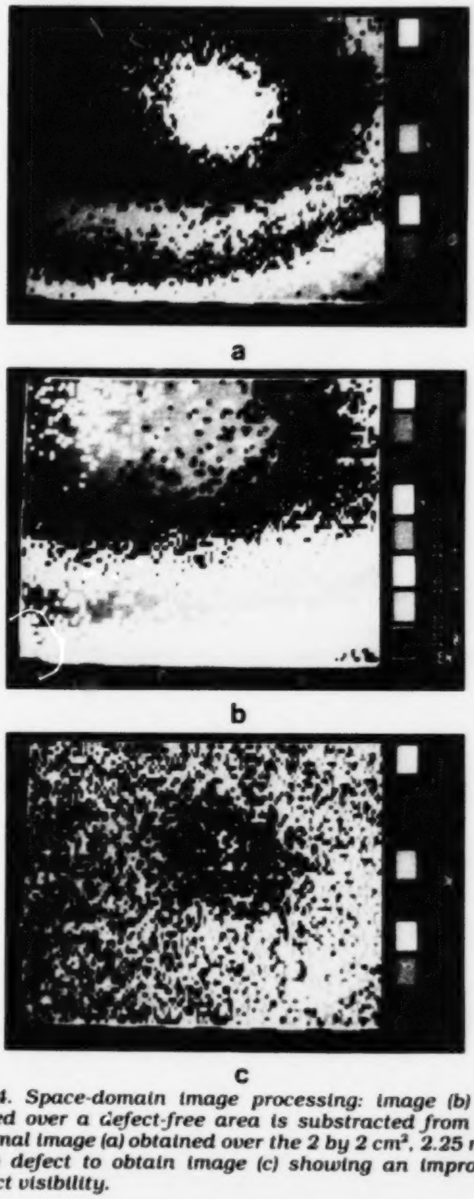

Fig. 4. Space-domain image processing: image (b) obtained over a defect-free area is substracted from the thermal image (a) obtained over the 2 by 2 cm^2, 2.25 mm-deep defect to obtain image (c) showing an improved defect visibility.

The differential image *4c* shows more clearly the position of the subsurface defect.

When thermal-noise features in the recorded image are not repetitive, such as when the surface emissivity of the sample varies in an unpredictable manner or when reflections from an a-priori unknown background are present, time-domain image processing methods may be effectively applied to the identification of subsurface flaws. Such methods are based on the variations of the logarithmic thermal-evolution slope in the presence of a subsurface defect, independently of the absolute value of the surface-temperature rise, as shown in *Fig. 5* (12).

An example of such an approach is shown in *Fig. 6*. In this case, a sample with a 10 by 10 mm^2, 0.5 mm-deep implanted defect was imaged in transmission after (a) 3 s and (b) 5 s from the start of step-heating with a 1.5 KW linear lamp on the back of the 3 mm-thick graphite-epoxy sheet. Strong reflective noise is here introduced by an IR-radiating torch in the background behind the camera. The high-contrast diagonal pattern which is visible in *Figs. 6a* and *b* is related to the different reflectivity across the surface of the woven composite. As the surface structure is exactly the same in these two images, such a reflective noise is eliminated in the difference image, *Fig. 6c*, which shows vividly the position of the subsurface defect. Such an image effectively represents a map of the temperature *vs.* time variation slope over the defect area, a slope which may change by a factor of two or more when a defect is present, as *Fig. 5* shows for the case of the pulse heated side.

Thermographic Inspection of Impact Damage in CFRP Sheets

Impact damage in composite sheets is a combination of both fiber fracture and interlaminar defects. It may be produced by a variety of in-service accidents from the simple dropping of a tool to artillery damage. The impacted surface often presents only a slight indentation to visual inspection while the opposite surface, which is normally unaccessible in the assembled part, may be completely fractured. Thermography is particularly well suited to the detection of impact damage in laminates because such a technique is quite sensitive to shallow interlaminar flaws while being applicable *in-situ*, without contact and with access from the external side only of the assembled part, as is required in the case of in-service inspection.

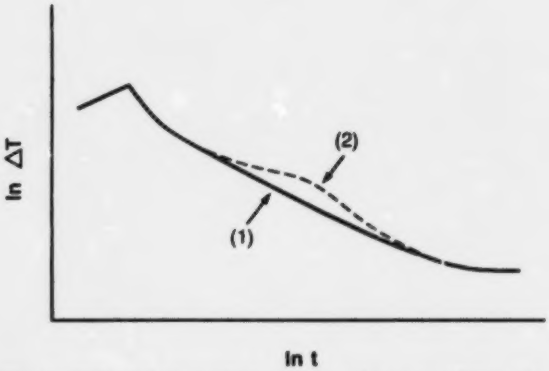

Fig. 5. Calculated surface temperature evolution of a sheet of homogeneous material (curve 1) or of a sheet containing a delamination defect (curve 2) after the absorption of a square-wave surface heat pulse.

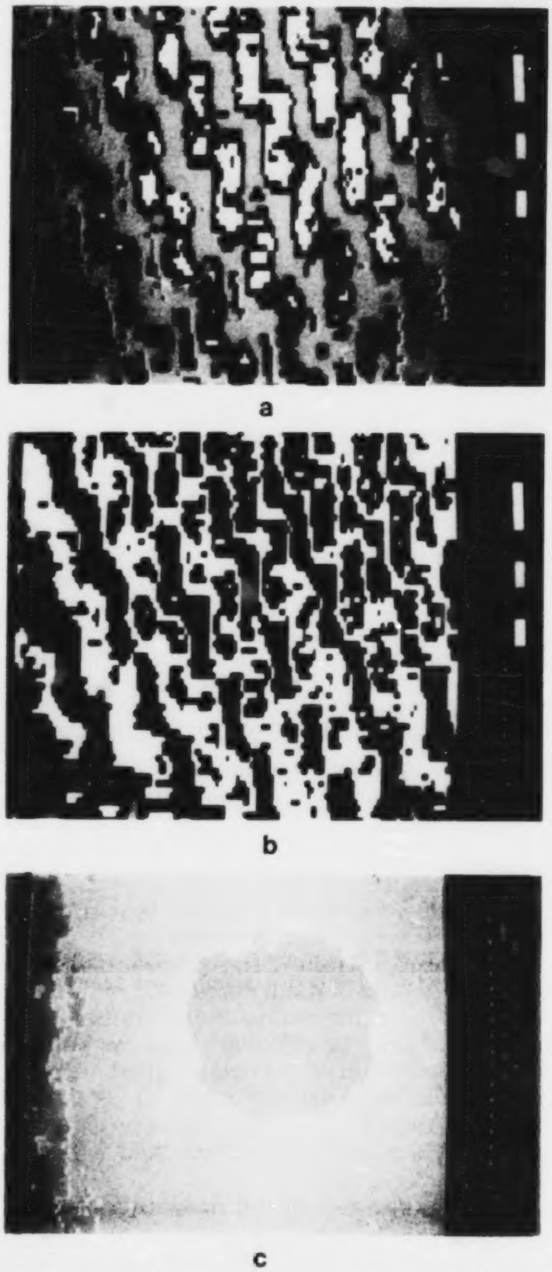

Fig. 6. Time-domain image processing: images (a) and (b) of the same area over a 10 by 10 mm, 0.5 mm-deep defect are obtained under conditions of strong reflective noise after 3 and 5 s respectively, after starting of heating. Image-subtraction (c) gives a much clearer defect visibility.

A number of impact tests were performed on NARMCO 5217 graphite-epoxy specimens of different thickness and ply lay-up order. Impact damage was produced using a DYNATUP 8200 drop-weight impact tester with an ETI 630 instrumented test system. This system used a drop weight of 2.6 kg with an instrumented striking tup of a diameter of 1.27 cm. A flag trigger positioned just above the striking surface on the drop weight starts the data-acquisition system and also measures the velocity history of the drop weight. The instrumented tup measures the striking force history from which the energy absorbed by the specimen is calculated. Typical energies were in the order of 50 J/cm of specimen thickness.

Wide delaminations with small impact energies were produced on unsupported thin sheets, as shown in *Fig. 7*. Two thermal images are shown of 8-ply graphite-epoxy sheets, 1.14 mm-thick, with (a) $(0, \pm45, 90)_s$ and (b) $(0, 90)_{2s}$ fiber orientation lay-up, backed by a soft-foam layer, after absorption of a nearly 6 J impact. A surface area of nearly 5 by 5 cm^2 was raised in temperature to approximately 15°C above ambient by a single tungsten-hallogen lamp equipped with parabolic back-reflector and IR-cutting front windows to eliminate self-emission noise. The displayed thermographs were obtained with our IR camera with high-temperature filter, after a 1 s heating time. Strong interlayer damage is clearly visible on both sides of the impacted point, with a preferential orientation along the direction of the graphite fibers in the first ply, which runs from top to bottom in *Fig. 7*. In some cases, damage far from the surface may also be produced, as in *Fig. 7b* where a long crack is visible on the opposite surface at a 90° orientation. Less extensive damage is normally suffered in thicker or solidly-supported sheets.

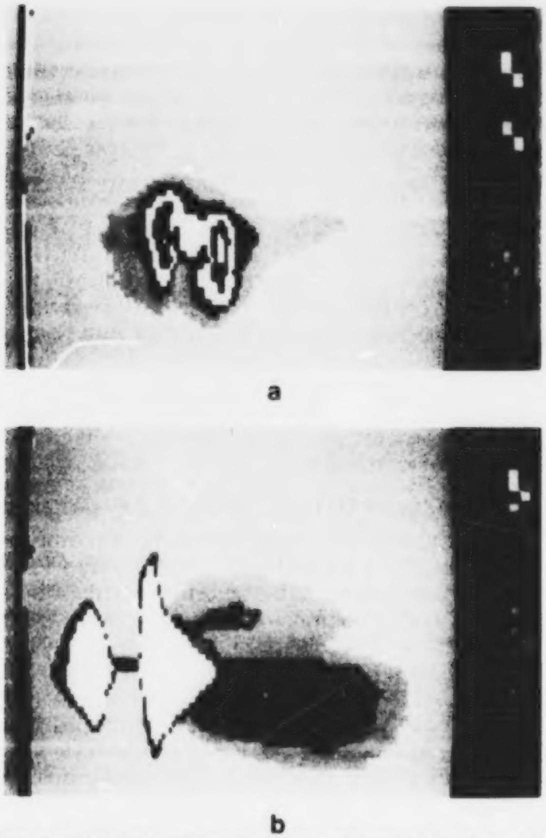

Fig. 7. Thermal images of impact-damaged 8-ply graphite-epoxy sheets with (a) $(0, \pm45, 90)_s$ and (b) $(0, 90)_{2s}$ lay-up. The impact energy was nearly 6 J. The imaged area measures 5.5 by 5.0 cm.

THERMOGRAPHIC EVALUATION OF FILLER CONCENTRATION IN POLYMER-BASED COMPOSITES

An interesting application of thermal methods is the rapid and nondestructive evaluation of phase or molecular orientation in stretched polymer films or in composites by an analysis of the thermal propagation pattern (5–8). A typical configuration is shown in *Fig. 8*. The inspected part is spot-heated by a narrow laser beam or other point heat source, and the heat-propagation pattern is analyzed by an IR camera. If the material is oriented, such as a unidirectional graphite-epoxy sheet, an elliptical thermal pattern will be observed, with the ratio between the two principal axes (b/a) being related to the square root of the thermal diffusivities in the longitudinal and transverse directions. This may be used to evaluate the orientation of extruded or molded parts, or the relative thermal conductivities of the filler and the matrix in a composite.

Analysis of Graphite-Epoxy Composites

This thermal approach was evaluated for possible application to a typical quality control requirement for graphite-epoxy materials, the evaluation of the filler-matrix proportions in the cured part. Inadequate temperature or part-assembly conditions may produce excessive squeezing of the epoxy material out of the composite, resulting in epoxy-starved regions whose mechanical properties may be affected.

A finite-difference simulation of thermal propagation in the graphite-epoxy material was performed assuming uniform fiber-to-fiber spacing to determine the suitability of thermographic techniques to the detection of epoxy-starved conditions (13). The eccentricity (b/a) of

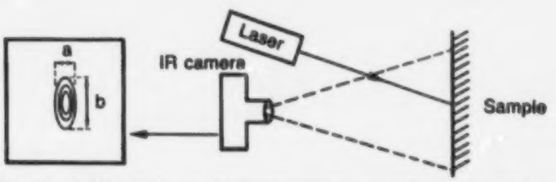

Fig. 8. Schematic of thermographic analysis of phase orientation in composite materials.

the simulated thermal pattern was calculated for different graphite-fiber volume concentrations and for different ratios of the fiber thermal conductivity, K_f, over the matrix conductivity, K_m, as shown in *Fig. 9*. Such calculations indicated that the eccentricity is a relatively unsensitive parameter for the evaluation of fiber contents when the fiber concentration is in the 30 to 50 percent range by volume, which corresponds to typical fiber-concentration values of graphite-epoxy materials. As shown in *Fig. 10*, the absolute value of the thermal propagation distance in the transient thermal field is more sensitive to fiber concentration.

The evaluation of such a parameter may be performed independently of variations in the absorbed heat power by thermal imaging the spot-heated area under transient heating conditions and comparing the recorded thermograph with a reference thermograph obtained on a sample with known fiber concentration.

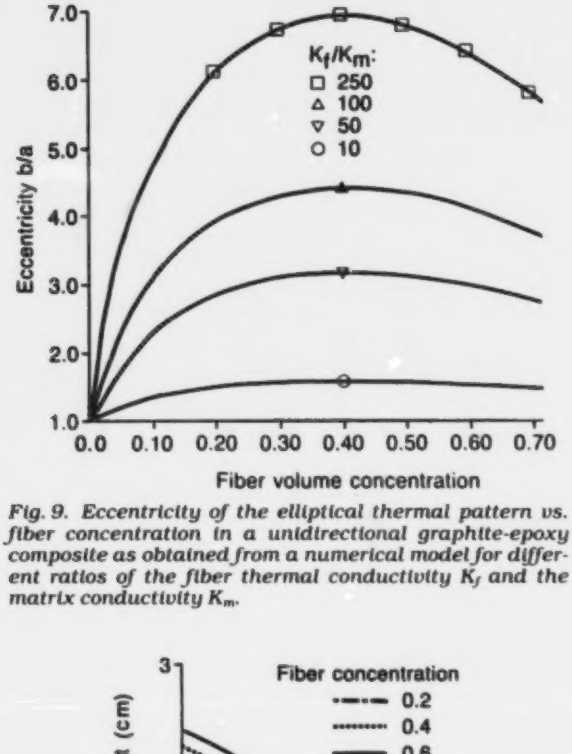

Fig. 9. Eccentricity of the elliptical thermal pattern vs. fiber concentration in a unidirectional graphite-epoxy composite as obtained from a numerical model for different ratios of the fiber thermal conductivity K_f and the matrix conductivity K_m.

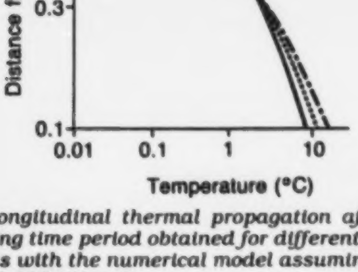

Fig. 10. Longitudinal thermal propagation after a 1 s spot-heating time period obtained for different fiber concentrations with the numerical model assuming $K_f = 0.5$ and $K_m = 0.002$ W/cm K.

Analysis of Steel-Polypropylene Samples

A similar analysis can be performed on short-fiber-filled composites, such as steel-polypropylene materials which are increasingly used as electrically and thermally conductive plastics (8, 14). The fibers were preferentially oriented in a two-step operation: 1) extrusion of precompounded grains using a Werner-Pfleiderer twin screw extruder with a single rod die (convergence ratio 10) and 2) hand layout of the extruded rods and compression molding at 180°C. The fibers were 3 mm long and 60 μm in effective diameter. The conductivity of such materials varies sharply when a relatively low concentration, typically 5 to 15 percent in weight of fibers is added to the polymer matrix. The evaluation of such a concentration-dependent conductivity is conveniently performed by non-contact thermal techniques, using double-side (laser-flash) or single-side (8) techniques. Preliminary results of fiber concentration evaluation, dispersion uniformity and orientation, as performed for experimental convenience by a spot-heating thermographic method, will be discussed.

A number of temperature profiles along the longitudinal axis (parallel to the average fiber orientation) as obtained under spot-heating for steel-polypropylene black-painted sheets, 1.9 mm-thick, with fiber concentrations of 5, 10, and 15 weight-percent respectively, are shown in *Fig. 11*. In order to reduce the relatively extended dynamic range of the temperature excursion under diverging-wave conditions, the followed procedure consisted in reaching the stationary regime under continuous wave surface spot heating with our 0.1 W, 0.7 mm beam-diameter laser and then shutting off the laser beam. The curves obtained in *Fig. 11* were recorded after 6 s from the instant of laser shut-off. The temperature values are normalized following the expression:

$$T_N(x) = (T(x) - T_B)/(T_C - T_B) \qquad (3)$$

where $T_N(x)$ is the plotted normalized temperature along the longitudinal x axis, $T(x)$ is the actual temperature, T_B is the temperature at the left border of the thermograph (40 pixels from the center) and T_C is the temperature at the center of the thermal pattern. The different thermal patterns were thus directly comparable independently of variations in the amount of absorbed heat, surface emissivity, or reflectivity. It can be seen that the temperature profile obtained with the 5 percent concentration sample is sharper than those obtained with higher fiber concentrations, indicating that the longitudinal diffusion of the thermal perturbation is slower with this sample.

An alternative approach to evaluate fiber concentration in an oriented sample is to record the ellipticity of the thermal pattern obtained under spot heating conditions and to deduce the local concentration from calculations of the kind shown in *Fig. 9*. As such a diagram shows, the ellipticity value is relatively insensitive to fiber concentration in the 30 to 60 percent volume concentration, but it is strongly dependent on such a parameter for steel-fiber concentrations of 0 to 15 weight percent, or less than 2 volume percent.

Figure 12 shows the results obtained with the steel-polypropylene sheets. The error bars in the data are related to the eccentricity variations recorded at different positions over the thermal pattern. Such random variations are related to the statistical fluctuations in the local concentration of the 1 mm-average-length fibers across the nearly 15 mm-diameter heated pattern. These variations, both in fiber concentration and orientation, are strikingly evident in the comparison between the data 1 and 2 recorded at two different positions of the same 10 percent-average-concentration sample. A combination of both thermal diffusivity and pattern anisotropy measurements must be done to evaluate both the local fiber concentration and orientation when the fibers are not known a priori to be perfectly aligned.

Finally, it should be noted that the surface thermal pattern is little affected by the quality of the fiber-matrix interface. Even the presence of a uniform air layer completely surrounding each fiber in a steel-polypropylene composite results in hardly noticeable thermal features when the surface of the polymer matrix is spot-heated. A finite-difference simulation for 15 percent volume fraction of fibers gave an eccentricity variation of less than 3 percent for an interface fiber-matrix as large as 5 percent of the fiber volume.

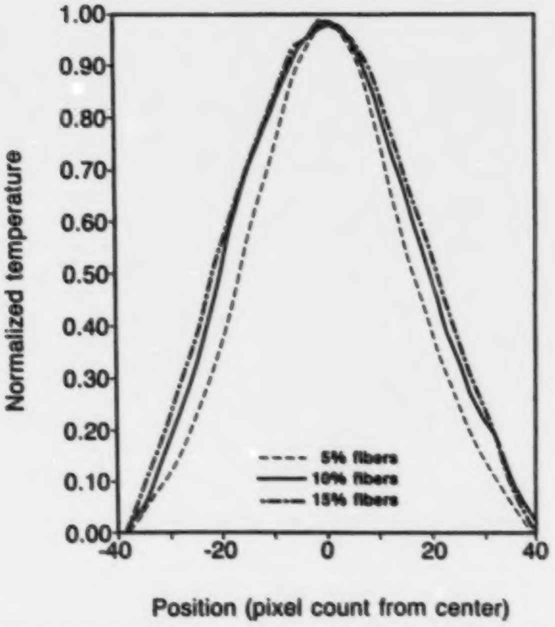

Fig. 11. Temperature profiles of steel-polypropylene samples with different fiber weight concentration under spot-heating conditions.

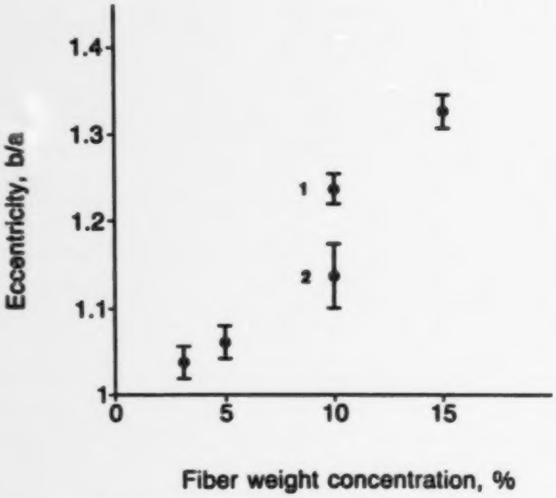

Fig. 12. Eccentricity of the elliptical thermal pattern vs. fiber concentration as measured on preferentially oriented steel-fiber/polypropylene samples. The data dispersion is related to the statistical fluctuations of the fiber distribution at different positions in the samples.

THERMOGRAPHIC EVALUATION OF FILLER DIRECTIONALITY IN POLYMER-BASED COMPOSITES

In several cases, the average concentration of short-fiber filler in polymer composites is relatively well known, while the local orientation of nominally random-oriented fibers may present important fluctuations. Such behavior, which is often related to molten flow during the molding process, has long been known to considerably affect the local physical properties of fiber-filled composites (15). Spot-heating thermographic inspection has recently been reported as a convenient and noninvasive technique for the rapid evaluation of fiber orientation at different sampling locations close to the surface of a molded component (7). In this work, we analyze in particular the three-dimensional analytical capabilities of thermographic fiber-orientation evaluation at different depths below the surface.

Theoretical Analysis

The basic principle of our approach is the following. If a laser beam is focused on the surface of a composite sheet, the ellipticity of the thermal pattern which is observable by an IR camera around the heated spot will be determined by the anisotropy of the material situated in the immediate vicinity of the heated spot. As the thermal front propagates deeper and deeper within the material, the appearance of the pattern will be affected by successive layers situated deeper and deeper within the sample. This makes it possible to obtain three-dimensional filler orientation information on the inspected sheet.

The capabilities of such an approach are illustrated in *Fig. 13*. A double sheet composed of two layers, each 2 mm-thick and containing (0°, 90°) mutually perpendicular fibers, is assumed to be surface heated by a focused, step-heating source. After a short heating time period, $t \le l^2/\alpha_T$, where l is the sheet thickness and α_T its transverse thermal diffusivity, only the first layer interacts with the heat flow, so that the eccentricity tends to the square root of the assumed value 2 of the ratio between the longitudinal and the transverse (i.e., in the plane normal to the fiber direction) thermal conductivities in the composite material. (The eccentricity which is referred to is the ratio b/a between the principal axes of the isotherms). The lower eccentricity value observed at shorter distances from the heated spot (along the longitudinal axis) is related to the presence in the model of an isotropic surface film, nearly 200 μm-thick on each layer, representing the average thickness of polymeric material which is normally encountered above the fibers. At longer heating periods a strong eccentricity is still visible at a distance from the heated spot smaller than the sheet thickness. At larger distances, however, the eccentricity tends toward the unity value which is expected for the average pseudo-isotropic properties of the (0°, 90°) sheet. Consequently, a plot of the eccentricity *vs.* radial distance at the surface of an unknown sample makes it possible to evaluate the directional properties of the material at different depths below the surface.

Experimental Results

The viability of this basic concept was verified on a number of samples comprising two sheets of nominally unidirectional, 2 mm-thick each, steel-polypropylene samples with respectively 10 and 15 percent steel concentration bonded in a (0°, 90°) configuration. The samples were held in a horizontal plane in order to avoid thermal-pattern distortions related to air-convection effects above the nearly 0.5 mm-diameter area of the black-painted sheet surface heated by the 0.1 W Argon laser beam. Moreover, time-domain image-subtraction methods before and after heating were used to compensate for reflectivity and camera-response non-uniformities across the imaged field.

A typical plot of the thermal-pattern eccentricity *vs.* radial distance, as obtained under stationary spot-heating conditions, is shown in *Fig. 14*. The eccentricity observed with the unidirectional (single-sheet) sample assumes a relatively constant value of the order of 1.2 typical of the 10 percent steel concentration, as shown in *Fig. 12*. The lower values of the eccentricity at distances closer to the heating spot may be explained in part by the existence of a thin

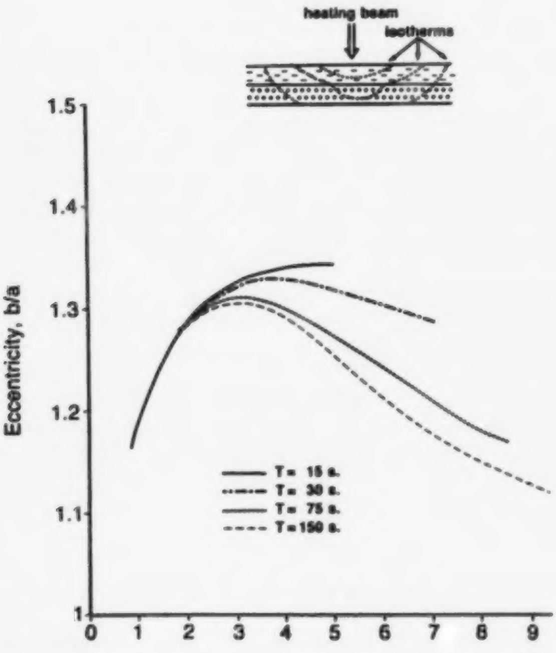

Fig. 13. Finite-difference simulation of the surface-pattern ellipticity in a double sheet containing mutually perpendicular fibers, as a function of the radial distance from the heated spot.

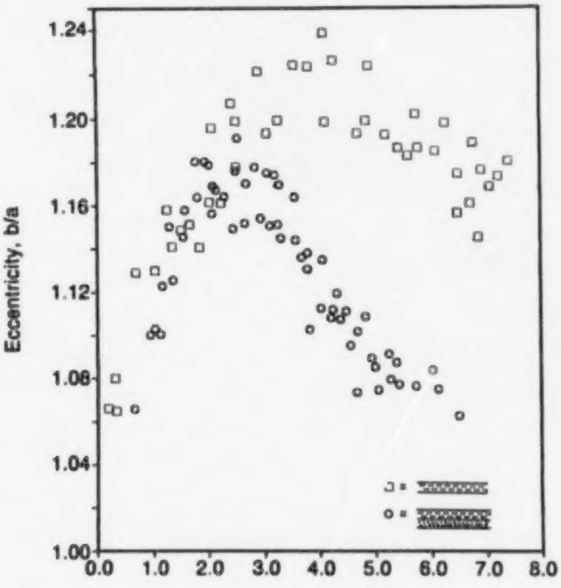

Fig. 14. Experimental plots of thermal-pattern eccentricity vs. radial distance as obtained on a unidirectional single-sheet and on a (0°, 90°) double-sheet steel-polypropylene sample.

isotropic layer on top of the fibers, as discussed in reference to *Fig. 13*, and in part by the finite diameter of the heating beam, whose effect was evaluated to an error of 4 percent at a distance equal to three times the heating source radius (16). Statistical effects related to the fractal behavior of the steel-fiber cluster (17) may also partially affect such a distribution.

When a second sheet of perpendicular orientation is bonded on the bottom of the inspected sheet, the eccentricity values recorded near the heated spot are hardly affected, while the values far from the center gradually drop to agreement with the theoretical model shown in *Fig. 13*. Such an approach thus appears to provide a rough evaluation of the average degree of fiber orientation at different depths from the surface, in spite of the strong dispersion of the data which is mainly related to the statistical fluctuations of the fiber distribution within the material.

Similarly encouraging results are obtained with CFRP laminates, as *Fig. 15* shows. The spot-heating technique was here applied to a double-sheet sample, each sheet 2 mm-thick, of long-fiber graphite-filled epoxy. The difference between the unidirectional and the (0°, 90°) sample is very clear, and corresponds closely to the theoretical computations for the case of an anisotropy ratio close to 8. The dispersion of the data is much smaller for this relatively regular graphite-fiber network, as compared to the steel-polypropylene fibers shown in *Fig. 14*.

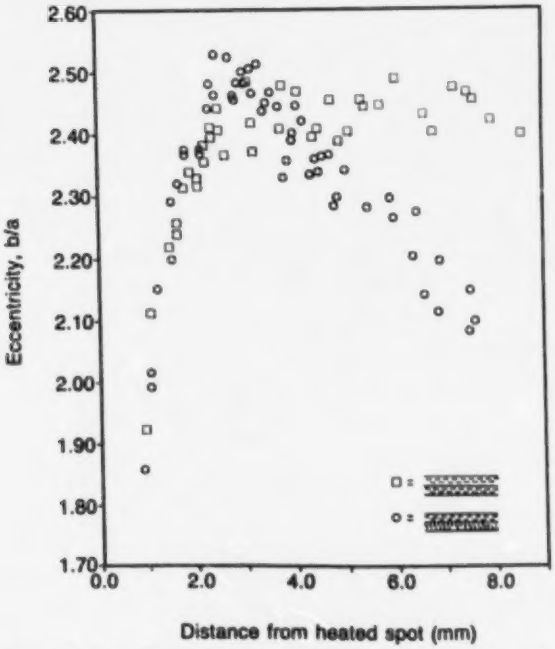

Fig. 15. Experimental plots of thermal-pattern eccentricity vs. radial distance as obtained on a unidirectional and a (0°, 90°), 2 mm/sheet graphite-epoxy laminate.

COMPARISON OF DIVERGING-WAVE AND CONVERGING-WAVE TECHNIQUES FOR ANISOTROPY EVALUATION

The converging-wave technique (8) is quite convenient for single-side thermal-diffusivity evaluation because of the lower temperature excursion as compared to the diverging-wave approach, resulting in a reduced surface overheating. The applicability of such an approach for anisotropy analysis was thus taken into consideration.

The temperature evolution $T_0(t)$ at $x = y = z = 0$ in an anisotropic medium of thermal conductivities K_x, K_y, and K_z along the three axes heated by a Dirac pulse of energy Q at the point (x, y, z) at $t = 0$ can be written (9):

$$T_0(t) = (Q/8)^{\bullet}[\rho c/(\pi^3 t^3 K_x K_y K_z)]^{1/2} \cdot \exp\{-\rho c(x^2/K_x + y^2/K_y + z^2/K_z)/4t\} \tag{4}$$

which for $z = 0$ in a semi-infinite volume, with $\alpha_L = K_x/\rho c = A\alpha_T$ being the longitudinal thermal diffusivity and α_T the transverse diffusivity, and (R, θ) being the polar coordinates of (x, y), becomes:

$$T_0(t) = (2QA/\rho c)^{\bullet}(4\pi t\alpha_L)^{-3/2} \cdot \exp\{-R^2(\cos^2\theta + A\sin^2\theta)/4\alpha_L t)\} \tag{5}$$

By integrating such an expression for all the values of θ from 0 to $\pi/2$, and normalizing the temperature evolution curves with respect to their maxima, the set of curve shown in *Fig. 16* is obtained. For a given value of α_L, the half-rise time first tends to increase as the transverse diffusivity, α_T, decreases, then drops back to the limit value of a two-dimensional heat flow when the anisotropy ratio tends to infinity. In

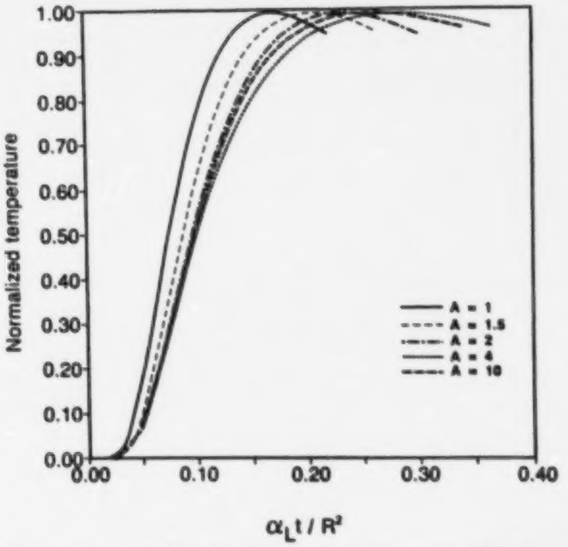

Fig. 16. Calculated temperature in a converging-wave configuration for an anisotropic material with different values of the ratio A between longitudinal and transverse thermal conductivities.

order to obtain a parameter which is related to the anisotropy ratio rather than to the absolute values of the axial diffusivities, the shape, rather than the absolute response time of the thermograms, should be considered. One such parameter is the normalized slope in the middle of the thermogram, given by the ratio $t_{2/3}/t_{1/3}$ between the time periods required to reach $2/3$ and $1/3$, respectively, of the peak temperature. This parameter, as shown in *Fig. 17*, varies nonmonotonically by less than 10 percent with the anisotropy ratio. It can be concluded that the converging-wave technique, although being appropriate for thermal diffusivity evaluation of materials which are isotropic in the plane of the heated surface, is not convenient for a reliable evaluation of the anisotropy.

The alternative approach, spot heating with simultaneous recording of the temperature evolution at a distance R along the two 0°, 90° principal directions (or along three 0, 45, 90° directions if the principal axes are unknown a priori) appears to be better suited for anisotropy evaluations. By taking the ratio between the half-rise time values along the principal axes, one obtains a parameter varying monotonically and simply equal to the inverse anisotropy ratio. To limit surface overheating, one can increase the diameter of the heated area, at the expense of a deformation of the thermal response curves along the longitudinal or the transverse directions, as shown in *Fig. 18*. The corresponding percent of error on the anisotropy ratio, shown in *Fig. 19* as a function of the fraction of the peak temperature at which the rise times are recorded, is relatively low and can be further reduced by an a priori calibration if heat and surface absorptivity distributions across the heated area are known.

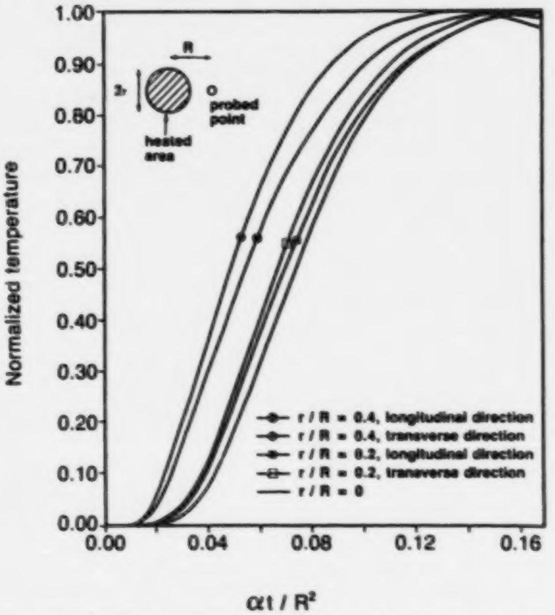

Fig. 18. Variation of the temperature evolution at a distance R from the center of the area pulse-heated over a disk of radius r as a function of the r/R ratio.

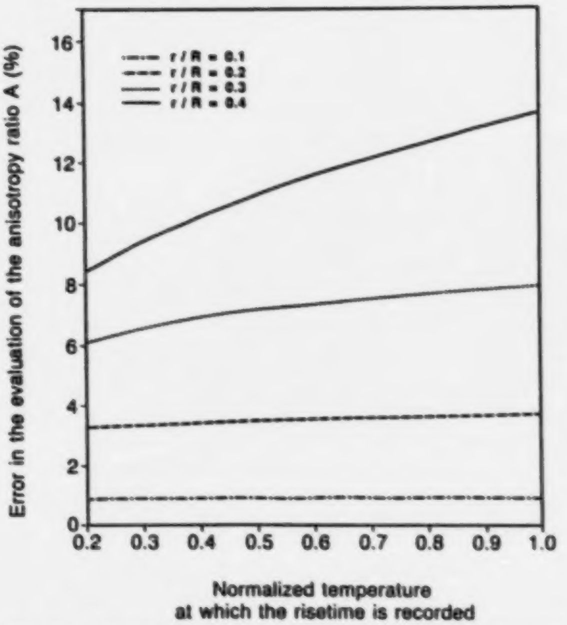

Fig. 19. Percent error in the anisotropy ratio (supposed to be equal to 4) for different r/R ratios as a function of the normalized temperature (see Fig. 19) at which the risetime is recorded.

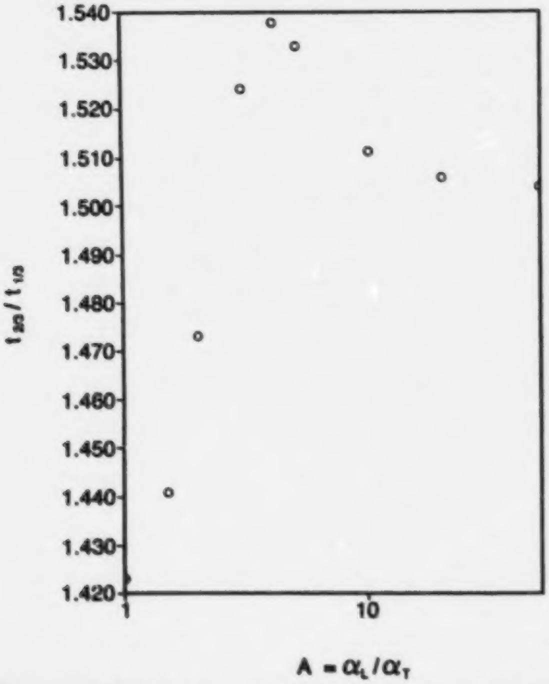

Fig. 17. Variation of the normalized central slope of the thermograms shown in Fig. 17 for different values of the anisotropy ratio.

One possible approach for conveniently evaluating the anisotropy ratio over a surface of uniform emissivity in a diverging-wave configuration would be to scan the probed point in a circular path around the heated spot by using, for example, a rotating wedge in front of the detector. The AC component at a frequency rate equal to twice the rotation rate would be related to $(\alpha_T^{-1/2} - \alpha_L^{-1/2})$. More complex approaches using an IR camera as described in the previous section, but with the heating beam slowly scanned over a convenient path, such as a spiral, could be chosen to order to provide both short-term, high spatial resolution features and long-term, wide-area features for larger-depth inspection with limited surface overheating.

CONCLUSION

A number of thermographic techniques were described for the nondestructive evaluation of fiber-filled polymer-based composites. The optothermal approach appears to be convenient for the inspection of opaque to visible and IR radiation composites because of its rapidity, lack of sample preparation requirements, and simplicity both in terms of its implementation and the interpretation of results. Appropriate signal-processing procedures are shown to extend the information available from such an analysis to progressively deeper layers below the surface.

ACKNOWLEDGMENT

The authors wish to thank G. Dziub of Canadair, Montreal and H. Tretout of Dassault, Paris, for the supply of the CFRP samples with implanted defects, as well as P. Sammut and M. Lamontagne of IMRI for their skillful technical assistance.

NOMENCLATURE

α = Thermal diffusivity.
α_L, α_T = Longitudinal and transverse diffusivities, respectively.
A = Anisotropy ratio.
C = Specific heat.
K = Thermal conductivity.
Kx, Ky, Kz = Principal thermal conductivities.
l = Sample thickness.
Q = Absorbed energy density in *Eq 1*, or absorbed energy in *Eqs 4* and *5*.
R = Radius of the annulus in the C.W. technique or distance between heated area center and probed point in the D.W. technique.
r = Radius of the heated area in the D.W. technique.
t = Time.
$t_{1/3}$, $t_{2/3}$ = Time when temperature reaches ⅓ (respectively ⅔) of its peak.
T = Temperature.
T_N = Normalized temperature.
T_B = Temperature at the left image border.
T_C = Temperature maximum.
z = Depth below the heated surface.

REFERENCES

1. V. P. Vavilov and R. Taylor, "Research Techniques in NDT", R. S. Sharpe, Ed., **5**, 239, Academic Press, London (1982).
2. W. N. Reynolds and G. M. Wells, *Brit. J. NDT*, **26**, 40 (1984).
3. P. Cielo, R. Lewak, and D. L. Balageas, "Thermosense VIII", H. Kaplan, Ed., **581**, 47, SPIE, Bellingham, WA (1985).
4. L. R. Baker, "Optical Techniques for Industrial Inspection", P. Cielo, Ed., **665**, 2., SPIE, Bellingham, WA (1986).
5. H. G. Kilian and M. Pietralla, *Polymer*, **19**, 664 (1978).
6. E. Piorkowska, A. Galeski, and M. Kryszewski, *Colloid Polym. Sci.*, **260**, 735 (1982).
7. J. D. Aindow, M. F. Markham, K. E. Puttick, J. G. Rider, and M. R. Rudman, *NDT Int.*, **19**, 24 (1986).
8. P. Cielo, L. A. Utracki, and M. Lamontagne, *Can. J. Phys.*, **64**, 9 (1986).
9. H. S. Carslaw and T. C. Jaeger, "Conduction of Heat in Solids" Ch. 10, Oxford University Press, Oxford (1959).
10. D. L. Balageas, J. C. Krapez, and P. Cielo, *J. Appl. Phys.*, **59**, 348 (1986).
11. P. Cielo, Proc. 14th Symp. on NDE, D. W. Moore and G. A. Matzkanin, Ed., p. 418, NTIAC—Southern Res. Inst., San Antonio, TX (1983).
12. P. Cielo, *J. Appl. Phys.*, **56**, 230 (1984).
13. P. Cielo, X. Maldague, J. C. Krapez, and R. Lewak, "Optics-based techniques for the characterization of composites and ceramics", 2nd Int. Symp. on Nondestructive Characterization of Materials, Montreal, July 21–23, 1986. To be published by Plenum Press, 1987.
14. T. Katsura, M. R. Kamal, and L. A. Utracki, *Polym. Compos.*, **6**, 282 (1985).
15. R. H. Knibbs and J. B. Morris, *Composites*, **5**, 209 (1974).
16. M. Pietralla, *Colloid Polym. Sci.*, **259**, 111 (1981).
17. H. Nakanishi, *Mater. Sci. Forum*, **4**, 129 (1985).

DISCUSSION

S. Newman: Can you tell us what the resolution would be for defect detection by the thermo-optic technique? What would be the smallest defect you can detect?

J. C. Krapez: In isotropic materials, in order to be certain to detect a defect, its diameter has to be at least 2 to 3 times larger than the depth. In case of nonisotropic materials, the diffusivity in radial direction is larger and one has to increase this minimum ratio. For example for graphite/epoxy sample with fibers parallel to the surface the diameter of defect has to be 5 to 10 times larger than depth.

Further studies are carried on to quantify simultaneously the defect's depth, diameter, and thermal resistivity.

By eliminating the noise effects continuously during the thermal evolution, the minimum ratio between diameter and depth is expected to be further decreased.

Weldline Integrity of Reinforced Plastics: Effect of Filler Shape

B. FISA

Ecole Polytechnique de Montréal
Montreal, Quebec, Canada H3C 3A7

and

J. DUFOUR *and* T. VU-KHANH

Industrial Materials Research Institute
Boucherville, Quebec, Canada J4B 6Y4

The paper is a preliminary report on glass fiber and glass flake orientation in the weldline zone of injection molded reinforced polypropylene. Two types of weldlines were studied using simple shape molds: one where two melt streams meet head-on and become immobilized, the other where the weldline formation is followed by additional flow. In the weldlines of the first type, which are characteristic of current standard molds used to test weldline strength, the anisometric particles are almost perfectly oriented perpendicular to flow. As a result, the weldlines of this type tend to be weak and brittle. In the second case when the weldline is formed by merging of melt streams separated by an insert, particle orientation in the weldline area remains different from other areas of the sample for long distances from the insert. It is shown that in molds where the weldline formation is followed by laterally expanding flow the change of particle orientation is faster than for unidirectional flow.

INTRODUCTION

Weldlines represent a potential source of weakness in both injection molded and extruded parts. In injection molding, weldlines are generated when two separate melt streams join either in multigated molds or as a consequence of flow around obstacles in the mold (pins, inserts, etc.). Different thermal history and molecular orientation in the weldline area lead to morphological heterogeneities which may cause loss of strength. The subject of weldlines in unfilled plastics has been reviewed by Moslé, *et al.* (1) and by Malguarnera (2). In brittle thermoplastics such as polystyrene or styrene-acrylonitrile copolymer, the weldline produces a rather severe reduction in tensile strength (50 percent for a double-gated standard tensile bar mold). In semi-crystalline (polyacetal, nylon) or ductile, amorphous (polycarbonate) polymers, the effect of weldline on mechanical properties is minor or negligible principally due to the material's ability to yield (1). In addition, in unfilled polymers, the effect can be reduced by modifying processing conditions, e.g. increasing melt temperature, injection speed, or pressure (2). In general, weldlines are much weaker in multiphase systems including incompatible polymer blends (3).

There is relatively little data on weldline behavior of filled polymers. Salvadori, *et al.* (4) studied the weldline strength of polypropylene filled with calcium carbonate, talc, glass fibers, and glass spheres. With low aspect ratio fillers (glass spheres and calcium carbonate) a more moderate drop in strength occurs compared to talc and glass fibers. Similar conclusions were also reached by Cloud, *et al.* (5). For example, these authors reported a 50 percent loss in strength for Nylon 66 containing 40 percent of glass fibers. This was attributed to the fact that fibers tend to orient parallel to the weldline.

Recently, as the papers from different sources indicate (6–9), there has been a growing interest in the weldline properties of plastics reinforced with high aspect ratio mica. Mica together with glass flakes represent a group of planar reinforcements which may be used when flow generated anisotropy from fibrous reinforcement is not acceptable (10). One significant drawback of mica filled plastics is that they exhibit very low weldline strength further decreased by delamination of mica flakes themselves (5, 11). Effects of coupling agents, flake size, and annealing were also reported. Most of the results published on weldlines in reinforced plastics were obtained using standard double-gated tensile bar mold (ASTM-D647). With this mold, flakes (or fibers) become oriented almost perfectly in the direction perpendicular to the flow. This type of weldline where two melt streams flowing in opposite directions meet head-on and become almost immediately immobilized is sometimes unavoidable. However, the other type of weldline generated when the melt stream is divided as it flows around an insert is by far more common although very little is known about fiber or flake orientation in weldlines of this type (12). For example, in an injection molded dashboard made from fiber reinforced ABS polymer, seven weldlines of varying lengths were identified (13).

The objective of this work is to study both types of weldlines using relatively large particle size fillers of different shapes. Glass spheres, fibers, and flakes were used. As pointed out by Utracki in a recent review (14) data on flow generated orientations in flake filled polymer melts is often contradictory. For this reason, the choice was made to examine in a qualitative manner relatively large number of filler and mold shapes as opposed to a deeper study of one particular aspect of the problem.

EXPERIMENTAL

Materials

Polypropylene

An injection molding grade having a melt index of 12g/10 min. (Profax 6301, Himont Canada Inc.), was used. This polymer is in powder form.

Glass Spheres

An uncoated grade of glass beads (No 3000, Potters Industries, Laprairie, Quebec) was selected for this work, it has a particle size range of 4 to 44 μm.

Glass Fibers and Flakes

Milled glass fiber ($^1/_{32}$ in.) and glass/flakes (Hammermilled Flake Glass $^1/_{64}$ in.) were obtained from Owens Corning Fiber Glass, Toledo, OH.

Processing

Molds

A two-cavity experimental mold with interchangeable cavities was used. The cavity/runner configuration is shown in *Fig. 1*. Five different cavities, all vented in the center, were used. These are illustrated in *Fig. 2*. Since only one of each of cavities 2C, 2D, and 2E were available, molding was carried out with cavity 2A in the other half of the mold. Two two-gated moldings were molded simultaneously.

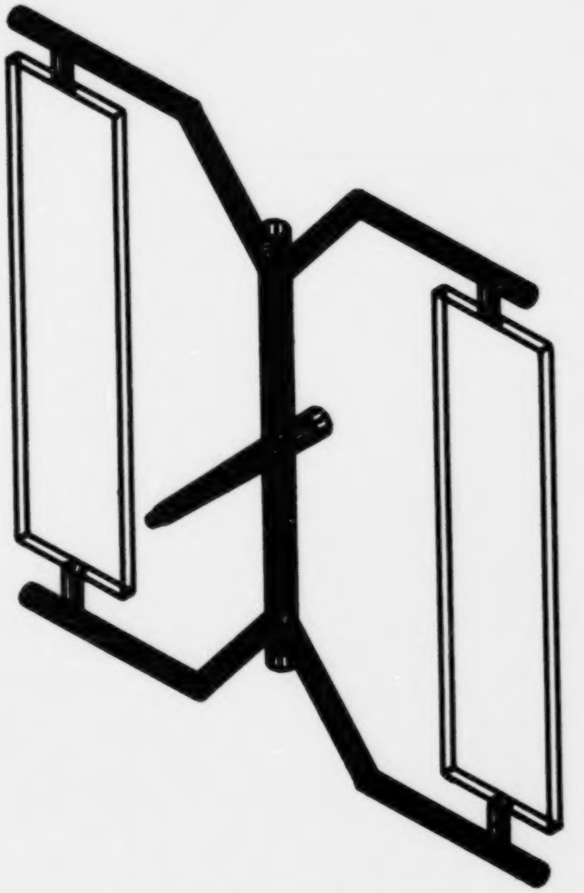

Fig. 1. Mold and runner configuration.

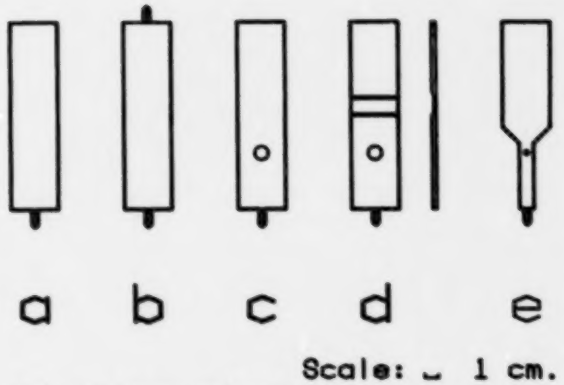

Fig. 2. Interchangeable mold cavities. A: rectangular single gated, B: rectangular two-gated, C: rectangular with a round pin, D: rectangular with a round pin and a thinner zone, E: cavity where the flow around insert is followed by lateral expansion.

Injection Molding

Polypropylene powder and filler were dry blended using high intensity powder mixer (Welex 35M). The dry blend was used directly to feed the injection press (Engel Es 150–170). Processing conditions are summarized in *Table 1*.

RESULTS AND DISCUSSION

Double-Gated Mold

The surface appearance of moldings in the weldline area is shown in *Fig. 3*. In all cases, using a double-gated mold, a well defined V-notch resulting from the compression of air in the mold is observed. The existence of V-notch seems to be a general feature of samples molded using this type of mold (2) including the standard ASTM D-647 double-gated mold (7). In pure polypropylene, the notch is smooth and regular. For filled samples, the notch becomes wider and deeper as one goes from spheres to fibers to flakes. For spheres and fibers the filler particles protruding from beneath the surface are also present in the V-notch. In the initial stages of this work, the polypropylene filled with glass spheres was investigated in some detail. In particular, we were interested to determine whether filler concentration gradients develop in or close to the weldline. The conclusion was that no such gradients can be attributed to the weldline as such. With spherical filler the weldline could not be even detected, except for the V-notch.

Table 1. Processing Conditions.

Zone temperature #1	170°C
Zone temperature #2	180°C
Zone temperature #3	200°C
Nozzle temperature	207°C
Mold temperature	60°C
Injection speed	26.7 ml/s
Screw speed	high
Back pressure	1.03 MPa (hyd.)
Holding pressure	4.8 MPa
Holding time	22 s
Cooling time	80 s

With fibers and flakes, the weldline region is very different from the material away from the weldline. First, as shown in *Fig. 4*, the trans-

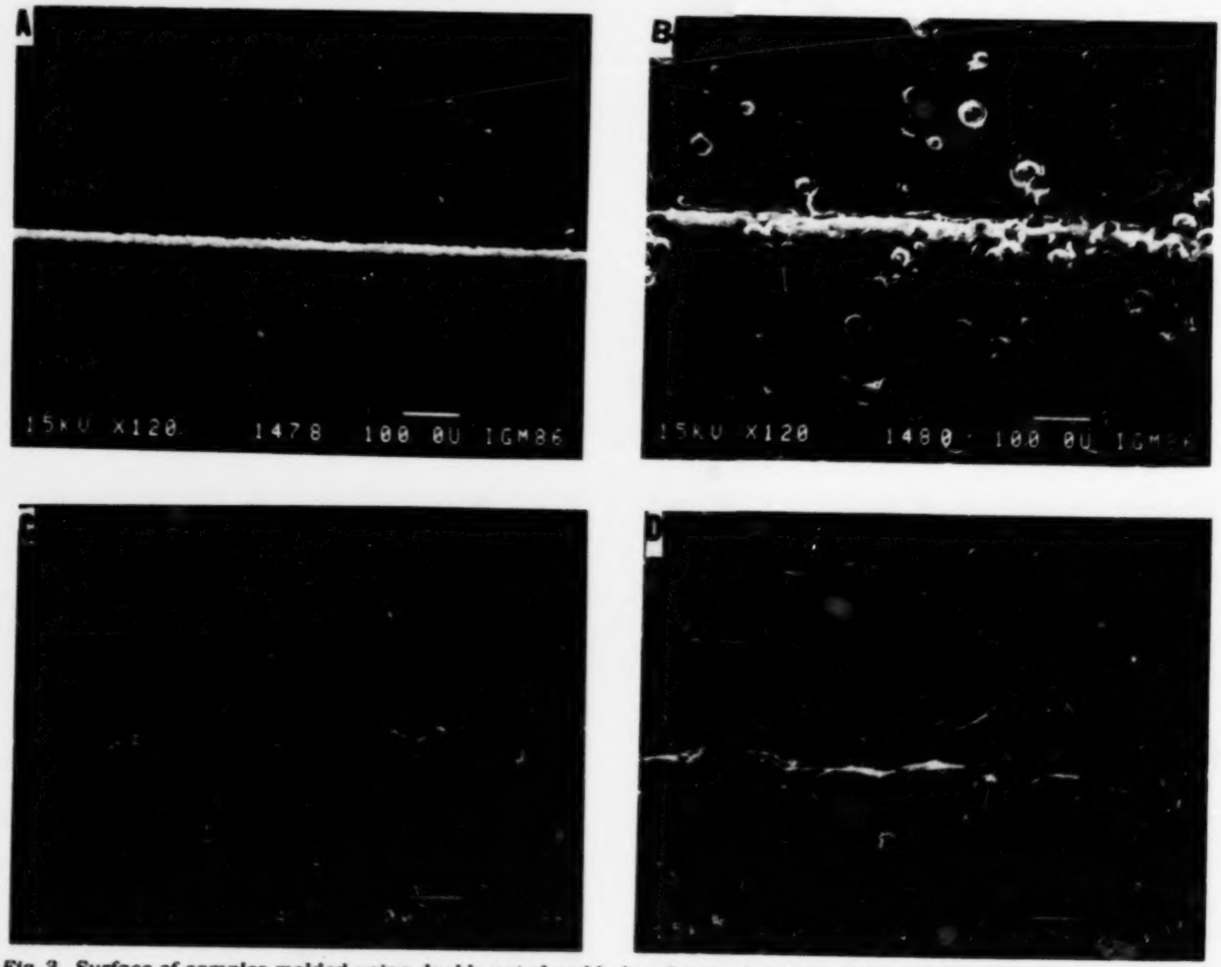

Fig. 3. Surface of samples molded using double-gated mold. A: polypropylene (PP), B: PP + glass spheres, C: PP + glass fibers, D: PP + glass flakes. Filler concentration: 35 wt. percent.

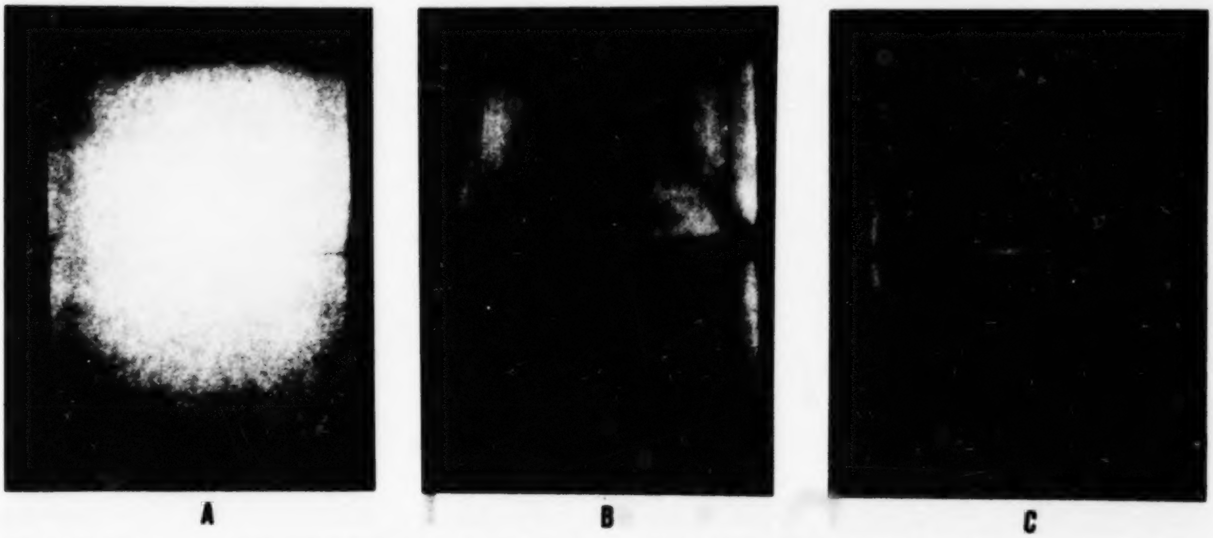

Fig. 4. Transmission photographs of weldline area of samples molded using the double-gated mold: A: PP + glass spheres, B: PP + glass fibers, C: PP + glass flakes. Filler concentration: 35 wt. percent.

mission of light in the weldline is similar to that in the edge of the molding. This is an indication of a similar particle orientation. Secondly, the part is visibly thicker in the weldline than in other areas of the molding. This can be attributed to differences in shrinkage resulting from orientation variations (see Table 2).

The fiber and flake orientation in samples with and without weldline is shown in *Fig. 5*. In the weldline-free moldings the well known complex fiber or flake distribution is observed. Close to the skin, the filler is oriented essentially parallel to the skin and to the flow direction whereas in the middle layer, the orientation is less pronounced (*Fig. 5A* and *C*). In the weldline zone an almost perfect orientation of fibers and flakes parallel to the weldline plane (perpendicular to the flow, *Fig. 5B* and *D*) was observed. Reducing the fiber and flake aspect ratio to less than 10 by grinding does not significantly affect the flake orientation.

These results which are similar to what was already reported for glass fibers (5), mica flakes (7), and for talc (15) invite two comments. First, while it may be possible to improve somewhat the weldline strength of double-gated moldings by controlling the filler aspect ratio or adhesion at the filler-matrix interface (8, 9, 11) the weldline will always be much weaker than other areas of the part as long as differences in filler orientation remain. Even in the most favorable case of the strong filler matrix interface, the local elastic modulus in the weldline zone will be much lower than elsewhere in the part (16). If such part is subjected to a load the local strain will be higher in the weldline area, leading to a rapid fracture at low elongations.

Second comment is about the general usefulness of the double-gated mold for testing of weldline characteristics of plastics reinforced with anisometric particles. This mold may be appropriate for evaluation of weldline strength in unreinforced plastics where the loss of strength can be attributed to factors such as lack of chain interpenetration at the interface of the two melt fronts. In such cases, the effect of parameters such as melt temperature, molding pressure, etc. on the bond strength, can be conveniently investigated.

Table 2. Increase of Thickness in the Weldline Area.

Mold	Distance from Insert (mm)	Difference in Thickness* (%)	
		Fibers	Flakes
2B		1.65	2.5
2C	20	0.3	1.9
	70	0	1.6
2D	20	0.3	1.9
	70	0	0.9
2E	20	0	1.2
	70	0	0.9

* The sample thickness at the weldline and 8 mm from the weldline. Nominal thickness of the part is 3.2 mm. Averages of 10 readings. Standard deviation was less than 0.2 percent in all cases.

In reinforced thermoplastics weldlines of this type (i.e. head-on meeting of two melt streams flowing in opposite directions with no additional flow) are much less frequent than weldlines resulting from flow around inserts, pins, etc. where, after the melt streams recombined, there is additional flow. The following section of this paper deals with these weldlines.

Molds with an Insert

Mold filling process is affected by the presence of the pin in the mold. This is particularly true for melts containing fibers and flakes. *Figure 6*, which shows stacked "short shots" of

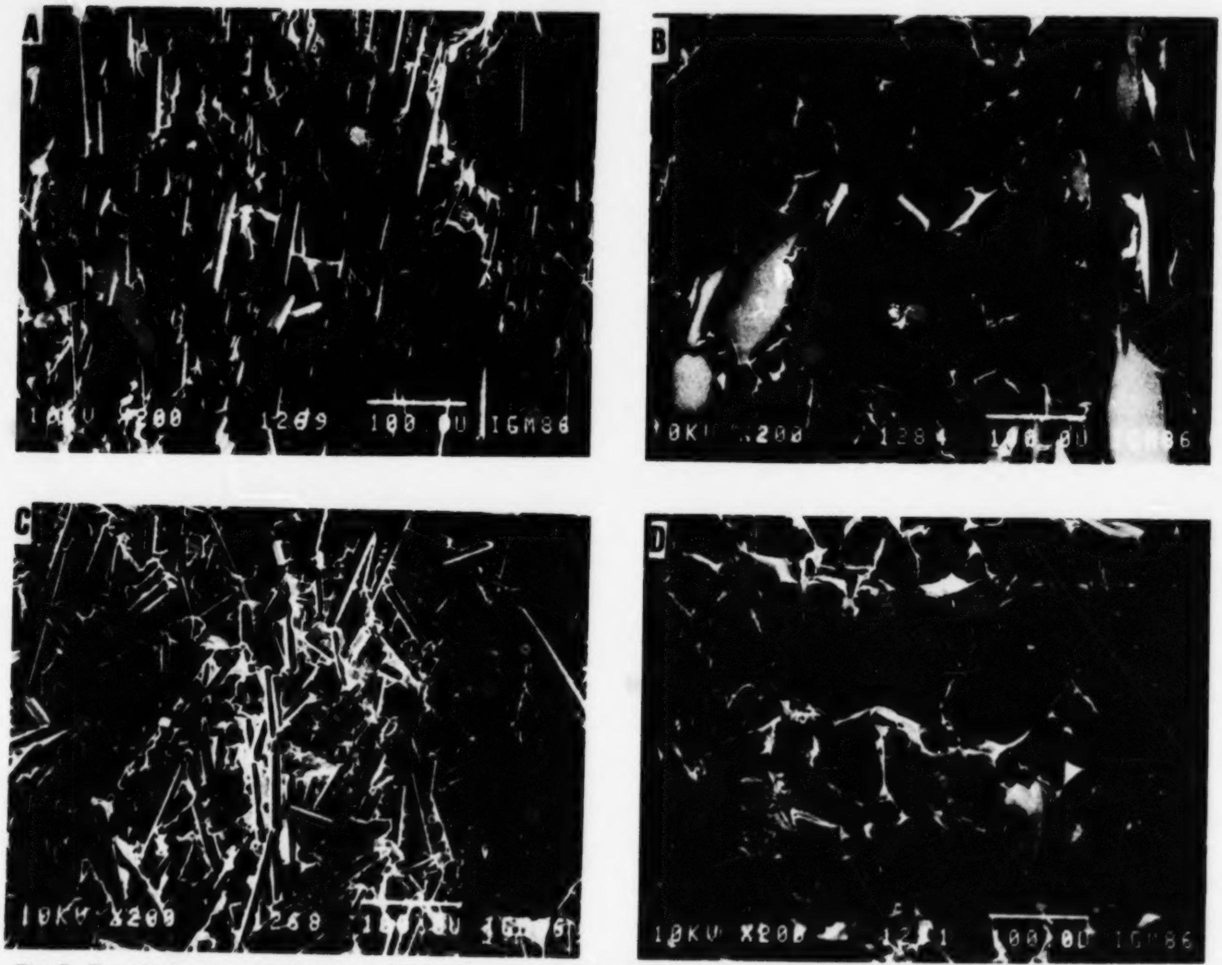

Fig. 5. Tensile fracture surfaces for filled polypropylene with and without the weldline. A and B: center of the plaque molded with a single gated mold (Fig. 2A), fibers and flakes respectively; C and D: equivalent areas, double-gated mold.

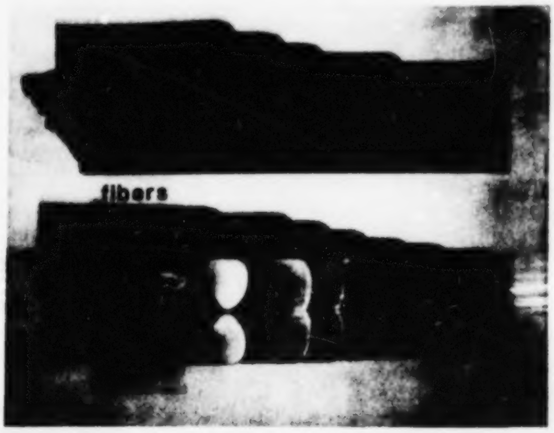

Fig. 6. Short shots of polypropylene filled with glass fibers and flakes.

polypropylene containing 35 wt. percent of fibers or flakes (mold 2C), illustrates how the two melt streams retain their separate identities long after merging. In fact, a clearly visible weldline extends along the plaque centerline. This is shown in the *Fig. 7*. For glass sphere filled polypropylene (*Fig. 7A*) the weldline is not detectable: even the V-notch is absent from the surface. With glass fibers without a weldline (mold 2A) the fiber orientation is quite similar to what was reported by several authors (16–19). Moving from the skin (*Fig. 8A*) to the plaque core, the proportion of fibers oriented parallel to the flow gradually decreases. In the center (*Fig. 8B*), random-in-plane orientation prevails. Such clear change in fiber orientation is not detectable in samples with weldlines (*Fig. 8C* and *D*). In these micrographs all fibers seem to be well oriented in the flow direction throughout the fracture surface and no change in fiber orientation with the distance from the pin could be detected. With flake filled resin the change in flake orientation is easier to follow as illustrated in *Fig. 9*. In the absence of weldline (*Fig. 9A*) two surface layers consisting of flakes oriented parallel to the skin represent more than two thirds of the sample thickness. In the core a central layer having flakes oriented perpen-

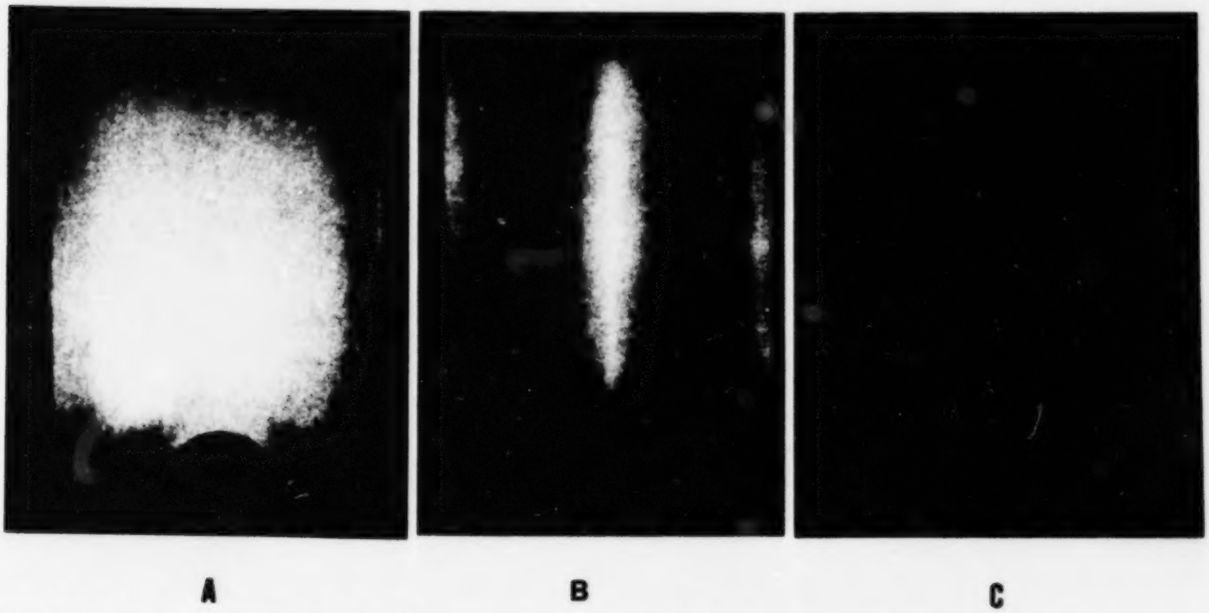

Fig. 7. Transmission photographs of weldline areas for samples molded using the mold 2C. A: PP + glass spheres, B: PP + glass fibers, C: PP + glass flakes. Filler concentration: 35 wt. percent.

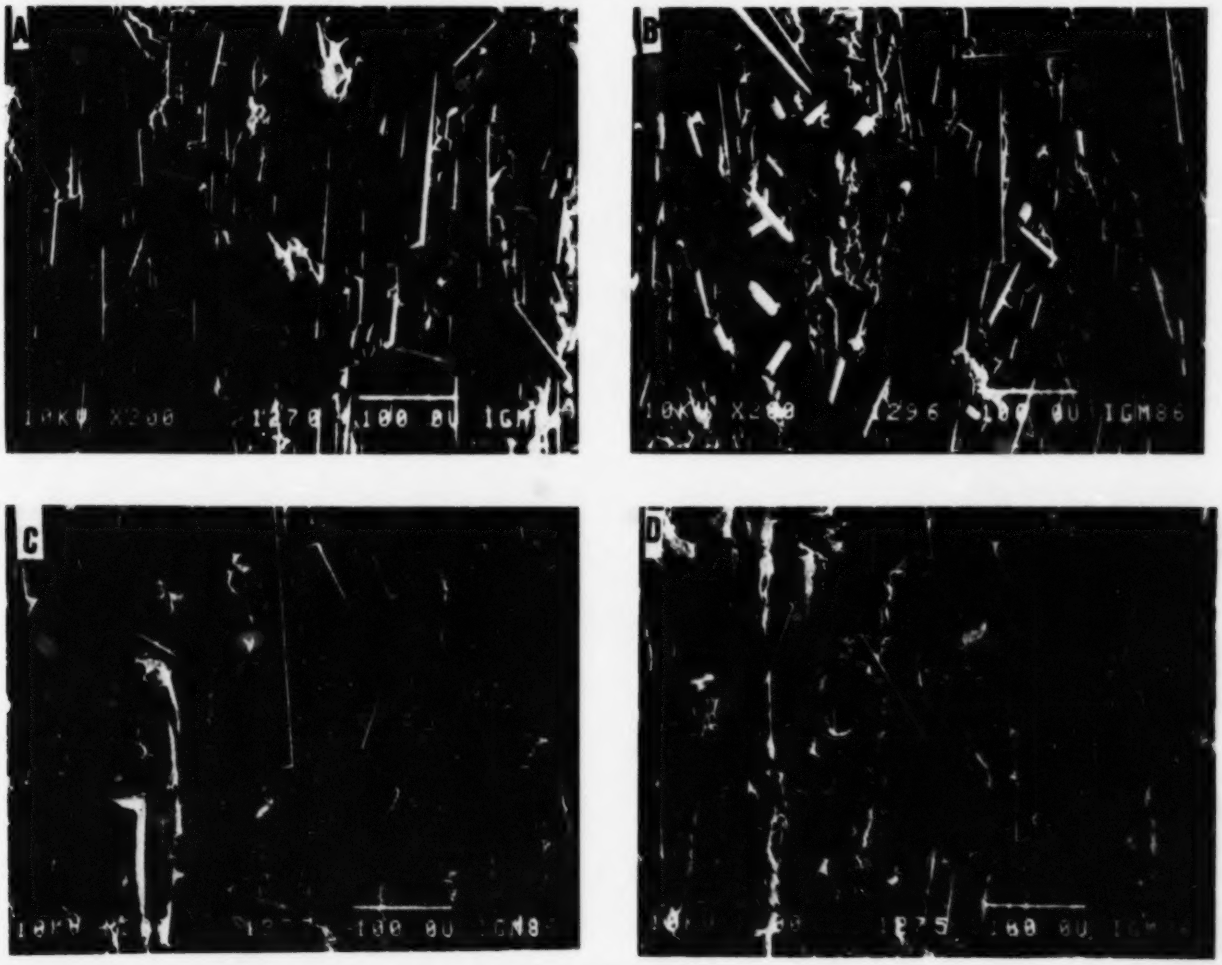
A
10KV X200
100 0U
B
10KV X200
296
100 0U
IGM86
C
100 0U
D
1275
100 0U

Fig. 8. Effect of the insert on fiber orientation. A and B: single gated mold: skin and core respectively. C and D: mold with insert: skin and core respectively. Tensile fracture surfaces, 20 mm from the pin. Flow direction from top to bottom.

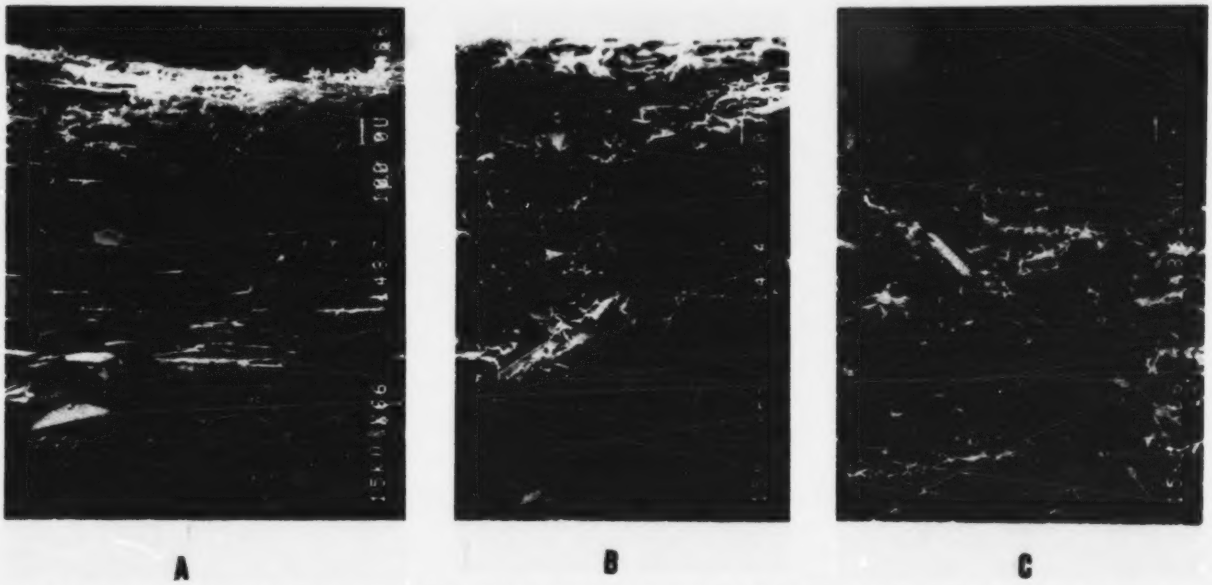

Fig. 9. Effect of the insert on flake orientation. A: mold without insert; B and C: mold with insert 20 and 70 mm from the pin. Tensile fracture surfaces. Half of the sample thickness is shown with skin on top of micrographs.

dicular to the skin is less than 1 mm thick. In samples, at weldline 20 mm from the pin (*Fig. 9B*) the thickness of the surface layer with flakes oriented parallel to the surface is only 300 μm. This means that only about 20 percent of the sample thickness will have flakes oriented parallel to the surface in the weldline area. *Figure 9C* shows the flake orientation in the weldline 70 mm away from the pin. The thickness of the surface layer increased to about 450 μm. At this rate of change in orientation one can estimate that with glass flakes with this plaque thickness (3.2 mm) and flake concentration (35 wt. percent), it would take between 20 to 40 cm of flow, after the two melt streams recombined, to eliminate the effect of the pin. Other experiments where parameters such as pin diameter, injection speed, melt viscosity, flake, or fiber concentration were varied gave similar results.

Complementary experiments at flake concentrations of 5 and 10 wt. percent—well below the maximum volume packing fraction of these glass flakes (10) gave similar orientation pattern. This suggests that the principal reason why the filler keeps the orientation imposed by the flow around the pin for such long distance is not related to steric hindrance effect where flakes would be prevented from rotation by its neighbors. The "fountain flow" model of mold filling (20) can be used to interpret the three layer structure of flake filled moldings. The skin material originates from the expanding melt front where elongational flow orientates the particles and polymer chains parallel to the surface of the melt front. The center layer formed as a result of shear flow of the melt which flowed into the mold behind the melt front. However, shear forces are lower in the center for these materials which basically exhibit plug flow. Although some orientation occurs also in shear flow, the periods of rotation observed in suspensions of fibers (19) or estimated for polypropylene filled with mica flakes (21) are long compared to the mold fill time. In any case, in shear flow the axis of particle rotation is perpendicular to the flow direction (19): given the initial orientation (i.e. just after the pin) flakes would rotate along their edges. What is desired, however, is to change the flake orientation in the core of the weldline from perpendicular to parallel to the skin. With the end-gated rectangular mold this requires long flow from the insert.

Let us now examine flake orientations in molds for other shapes than a simple rectangle. The mold illustrated in *Fig. 2D* has a narrow section: the melt passes from 3.2 to 1.6 mm before expanding back to 3.2 mm. In the mold shown in *Fig. 2E*, the melt expands laterally shortly after weldline formation. Tensile fracture surfaces of samples from these molds are shown in *Fig. 10*. For comparison, fracture surfaces of a sample with no weldline (mold 2A) and with the longitudinal weldline (mold 2C) are also included. In the mold with narrow section the thickness of the outside layer with flakes oriented parallel to the skin is about 800 μm (*Fig. 10C*). This is 50 to 60 percent more than in the sample without narrow section (*Fig. 10B*). In laterally diverging flow (mold 2E-*Fig. 10D*) the flakes adapt an orientation which appears to be similar to that observed in samples without weldlines (*Fig. 10A*). Another view of the flake orientation development is shown in *Fig. 11*. These micrographs were obtained by

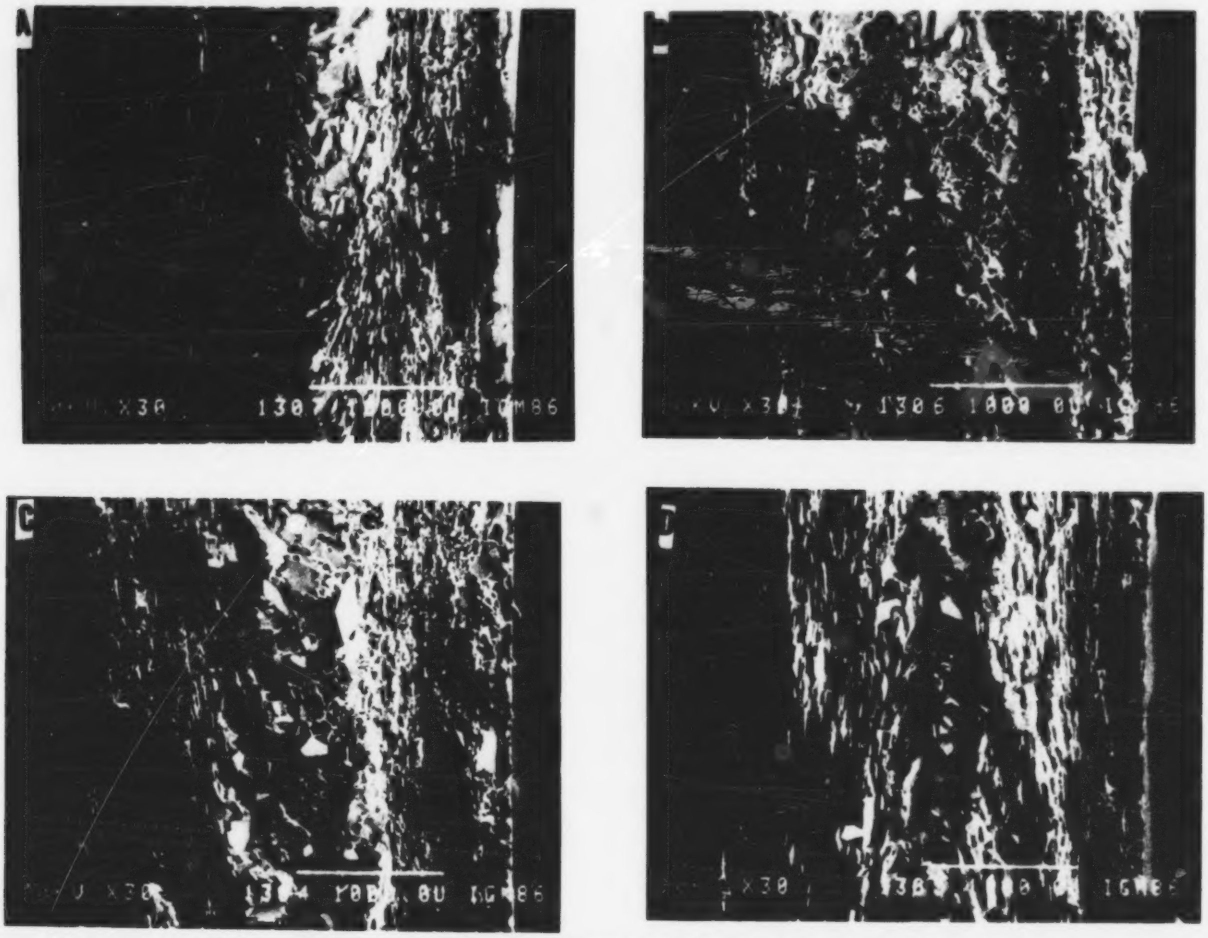

Fig. 10. Effect of mold shape on flake orientation. A: rectangular mold without insert (Fig. 2A). B: rectangular mold with insert (Fig. 2C). C: rectangular mold with a narrow section (Fig. 2D). D: laterally expanding flow mold (Fig. 2E). Tensile fracture surfaces (see Fig. 12 for sample dimensions and position). Distance from the insert 50 mm (equivalent for mold without insert).

cutting the samples perpendicular to the weldline. Immediately after the two melt streams merged (*Fig. 11A*), there is a line of flakes oriented perpendicular to the skin throughout the sample thickness. At a distance of 50 mm from the pin the flake orientation has already changed significantly in all three samples. Again relative thickness of layers oriented parallel to the sample skin increases, going from rectangular mold (*Fig. 11B*) to the mold with narrower section (*Fig. 11C*); the laterally expanding mold (*Fig. 11D*) clearly produces best flake orientation.

Another method can be used to characterize the differences in particle orientation between the weldline and the rest of the sample. It consists of measuring sample thicknesses on and at a short distance from the weldline. The degree of shrinkage depends on the coefficient of thermal expansion which in turn is a function of particle orientation. Results obtained with spheres, flakes, and fibers (*Table 2*) can be summarized as follows:

a) There are no measurable variations in thickness for polypropylene containing glass spheres.
b) With the double-gated mold the moldings are significantly thicker in the weldline area for both fibers and flakes.
c) In moldings where the weldline was formed by flow around the insert, samples containing fibers do not show measurable differences. The change of orientation from random-in-plane away from the weldline to parallel to flow in the mitochondria should not induce significant changes in thermal expansion coefficient. With flakes significant differences are observed, and as *Table 2* indicates, the thickness differences decrease gradually as the distance from the pin increases. The effect of the convergent—divergent flow mold (2D) and lateral flow expansion mold (2E) on flake orientation is detected by this method.

Finally, although the study of mechanical

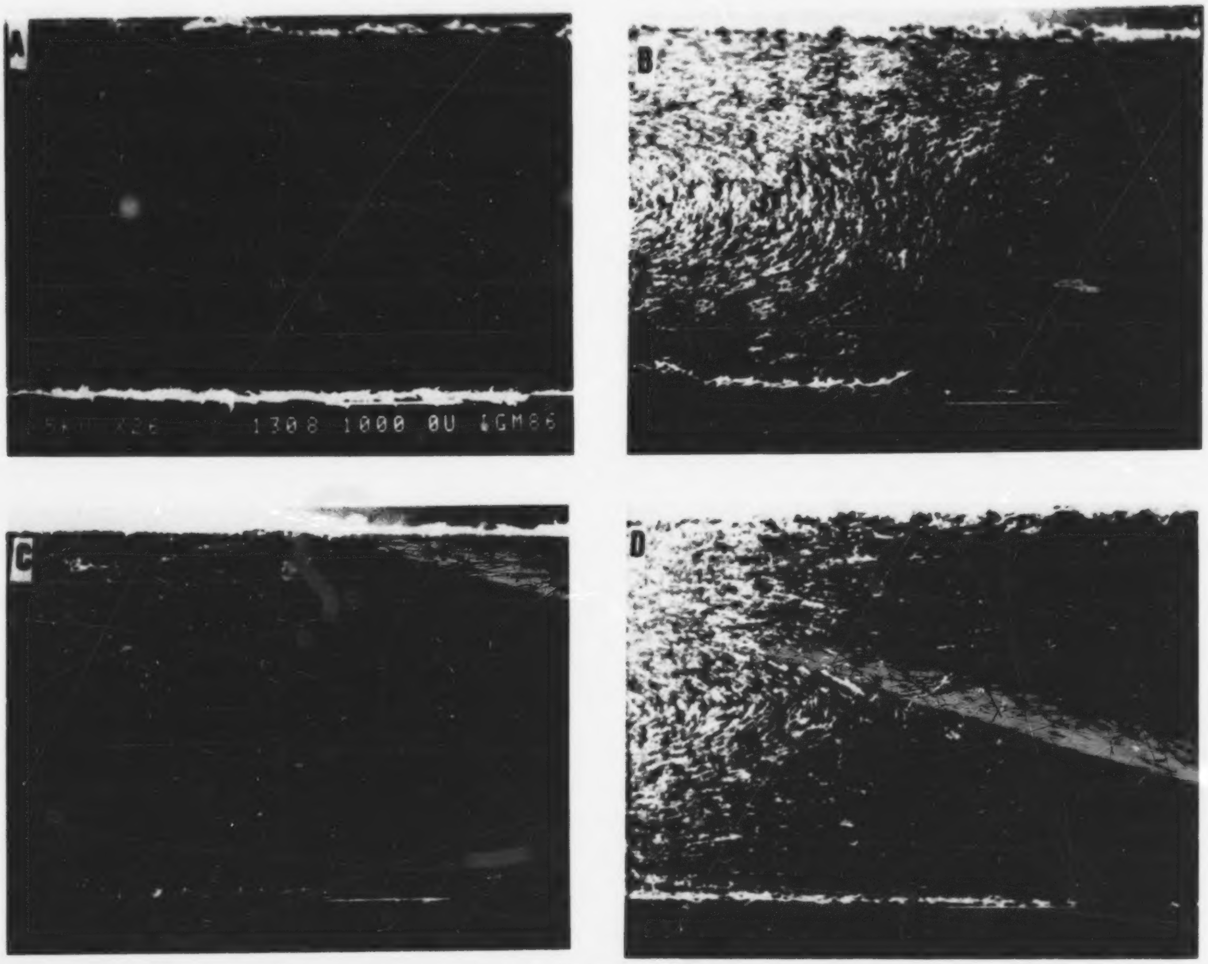

Fig. 11. Development of flake orientation following the merging of melt streams behind the insert. A: All molds with inserts 3 mm behind the insert, B: rectangular mold (2C), 50 mm from insert, C: mold with narrow section (2D), 50 mm from insert, D: laterally expanding mold (2E), 50 mm from insert. Scanning electron micrographs of saw cut sections. Picture plane is perpendicular to the flow direction.

properties of these composites was not a principal goal of this investigation it is interesting to mention their tensile behavior (*Table 3*). Samples were cut from moldings as shown in *Fig. 12*. The effect of mold type on the weldline strength is substantial. As expected, the two-gated mold gives weakest weldlines: the peak stress is only 33 percent compared to weldline free sample. The weldlines formed in the mold 2D are somewhat stronger. With this mold the relatively slow change in flake orientation with distance from the insert is also reflected in these results: the peak stress increases from 13.1 MPa 20 mm from the insert only to 16.1 MPa 70 mm from the insert. On the other hand the mold where the flow around the pin was followed by lateral expansion (2E) gave weldlines with peak stress reaching 80 percent of that of weldline free samples.

Table 3. Results of Tensile Tests Carried on Samples Shown in *Fig. 12*. Polypropylene with 35 wt. Percent of Glass Flakes. Crosshead Speed 10 mm/min.

Mold	Distance from Insert (mm)	Peak Effective Stress* (MPa)	Displacement at Peak Stress* (mm)
2A	—	29.9 ± 0.6	0.99 ± 0.19
2B	—	9.8 ± 0.1	0.26 ± 0.03
2C	20	13.1 ± 0.1	0.25 ± 0.04
2C	70	16.1 ± 0.4	0.23 ± 0.04
2D	70	18.4 ± 0.8	0.41 ± 0.10
2E	70	23.9 ± 0.5	0.59 ± 0.07

* Averages of 6 readings.

SUMMARY AND CONCLUSIONS

Fiber and flake orientation in weldlines of injection molded parts depends on the flow conditions. In weldlines formed by head-on meeting of two melt fronts with no subsequent flow fibers and flakes are oriented perpendicular to the flow. This produces very weak weldlines. Weldlines formed by recombination of melt streams behind an insert remain detectable long after the streams merged. Designing molds

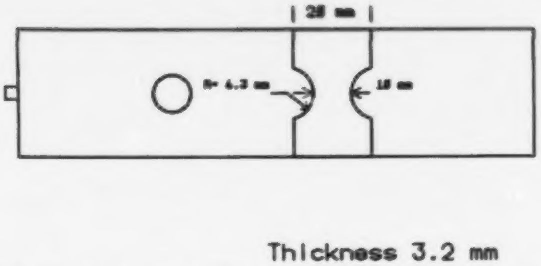

Fig. 12. Shape and dimensions of specimens used in tensile tests (Table 3).

where the melt front expands laterally after the weldline was formed offers an interesting possibility of reducing the negative effect of the weldline both in terms of particle orientation and strength.

ACKNOWLEDGMENTS

The help of Mr. Michel Thibodeau with the scanning electron microscope is gratefully acknowledged.

REFERENCES

1. H. G. Mosle, R. M. Criens, and H. Dick, *SPEANTEC Tech. Papers*, **30**, 772 (1984).
2. S. C. Malguarnera, *Polym.-Plast. Technol. Eng.*, **18**, 1 (1982).
3. E. Nolley, J. W. Barlow, and D. R. Paul, *Polym. Eng. Sci.*, **20**, 364 (1980).
4. A. Salvatori, A . Pelliconi, and D. Romanini, *Plast. Rub. Process. Appl.*, **3**, 215 (1983).
5. P. J. Cloud, F., McDowell, and S. Gerakaris, *Plast. Technol.*, **22**, 46 (1976).
6. N. Burditt, A. King, B. Leonard, and A. Scheibelhoffer, *Plast. Compounding*, **8**, 62 (1985).
7. F. Bataille, T. Vu-Khanh, and B. Fisa, *SPEANTEC Tech. Papers*, **31**, 1174 (1985).
8. M. Svazic, *SPEANTEC Tech. Papers*, **32**, 1136 (1986).
9. M. Christie, *Plast. Eng.*, **42**, 41 (1986).
10. B. Remillard, T. Vu-Khanh, B. Fisa, and S. Naik, *Polym. Compos.*, **6**, 395-(1986).
11. K. Okuno, *Kobunshi Ronbunshu*, **38**, 209 (1981).
12. J. W. Gillespie, Jr., J. A. Vanderschuren, and B. Pipes, *SPEANTEC Tech. Papers*, **30**, 648 (1984).
13. M. J. Bozarth and J. L. Hammill, *SPEANTEC Tech. Papers*, **30**, 1091 (1984).
14. L. A. Utracki, *Rub. Chem. Technol.*, **57**, 507 (1984).
15. B. Sanschagrin, Ecole Polytechnique de Montréal, unpublished data.
16. L. A. Goettler, *Polym. Compos.*, **5**, 60 (1984).
17. P. F. Bright and M. W. Darlington, *Plast. Rub. Mater. Appl.*, **1**, 139 (1981).
18. M. J. Owen and K. Whybrew, *Plast. Rub.*, **1**, 231 (1976).
19. M. Vincent, Dr. Ing. Thesis, Ecole Nationale Supérieure des Mines de Paris (1984).
20. Z. Tadmor, *J. Appl. Polym. Sci.*, **18**, 1753 (1974).
21. L. A. Utracki, B. D. Favis, and B. Fisa, *Polym. Compos.*, **4**, 277 (1984).

B. FISA, J. DUFOUR AND T. VU-KHANH: DISCUSSION

R. T. Woodhams: Your inserts were circular in cross-section. Would it make a difference if they are airfoil shape?

B. Fisa: We did not test the other than circular inserts but it is my feeling that this would not make much difference. The flakes or fibers orient as they flow around the insert, then there is this expanding flow as they come to meet each other, so the filler particle orientation is essentially determined by the fact that there is an expanding flow as a result of an insert.

R. M. Piggott: It seems that you provided me with solution to one of my problems. What I have to do is to put a lot of inserts at the beginning, and I can run my material with fibers and get all aligned all the way down the specimen.

B. Fisa: Probably, but there may be simpler means to orient long fiber composites by a flow through die.

M. Takemori: Would you comment if the converging or the diverging flow is more effective in reducing the weldline effect, in erasing the weldline?

B. Fisa: The results of our tests indicate that laterally expanding flow is preferred over the converging or diverging flow. This has been only an exploratory work. Some aspects are being followed up in more detail in the present time. Clearly the best way to study the effect of filler orientation would be to measure the mechanical properties, but initially we have designed our experiments with untreated filler particles. Clearly the samples were not optimized for studies of mechanical properties.

A. Moet: It looks like weldline provides a material discontinuity. The measurement of this localized discontinuity via total material properties is unfair assessment to the severity of this effect. I suggest that the weldlines be used as a notch to initiate crack propagation and the weldline strength be studied via rate of crack propagation, fracture toughness, K_{1C} or G_{1C} is appropriate. This will accentuate the difference between the bulk properties and the weld line and allow you to study the phenomenon in more detail.

B. Fisa: It is clear that when you have a sample with a weldline it always breaks at the weldline.

S. Newman: In the weldline area, where the fiber is oriented in such a way that it does not contribute to the strength of the material you are basically measuring strength of the matrix, except that now the matrix is diluted by the fibers. In a sense in the weldline you have a reduced cross-section of polymer. Is the measured strength of the specimen essentially that of the matrix material reduced by the volume function of invert material, if you will, not contributing to the strength?

B. FISA: I cannot answer this question. We tried to calculate these effects two years ago for mica, but we could not get quantitative answer.

L. A. Utracki: In Seymour Newman's question for the first time in this discussion the possibility of the filler/matrix interaction was approached. In the weldline the particles are oriented parallel to the weldline. If the adhesion between filler and the matrix is poor, one measures the weakest cross-section of the matrix material, a sort of percolation cross-section. This may lead to a catastrophic failure process.

Electrical Properties of Exfoliated-Graphite Filled Polyester Based Composites

JOHN V. FOY *and* J. THOMAS LINDT*

Department of Materials Science and Engineering
University of Pittsburgh
Pittsburgh, Pennsylvania 15261

Work has been done to develop and optimize a procedure for the preparation of electrically conductive exfoliated-graphite filled unsaturated polyester composites. The exfoliated graphite flakes impart excellent electrical properties to the polyester composite. EMI (electromagnetic interference) shielding effectiveness, comparable to that of exfoliated graphite alone, has been observed over a frequency range of 0 to 1000 MHz with composite samples containing as little as 4 weight percent of exfoliated graphite. The resistivities approached the value for exfoliated graphite in the c-direction (0.03 Ω-cm) at a graphite loading of 11 weight percent. It has been observed that the mechanical integrity of the composite remained good up to graphite loadings of some 17 weight percent. The polyester readily wets the graphite and penetrates most of the graphite open pore volume during processing. Flow visualization measurements have been made in a transparent compression molding apparatus. No effect of the flow conditions on the apparent electrical properties has been found.

INTRODUCTION

It is well known that electrically insulating polymers can be made electrically conductive by incorporating conductive fillers into the polymer (1). The conductivity is due to the formation of a continuous network of filler particles throughout the polymer matrix. Common conductive fillers include electrically conductive carbon blacks, carbon and graphite fibers, metal particulates and metal fibers (2). The electrical properties of such composites depend upon factors such as filler content, aspect ratio and conductivity of the filler, and the processing conditions. The most significant current applications of electrically conductive polymer composites are in the areas of electrostatic discharge dissipation (ESD) and electromagnetic interference (EMI) shielding.

When certain graphite structures are intercalated with bromine or a mixture of nitric and sulfuric acids and subsequently heated past a critical temperature, a large expansion along the c-direction occurs (3). This process is known as exfoliation. Exfoliated graphite flakes have an accordion-shaped appearance and the expansion along the c-direction can be as much as two orders of magnitude. Exfoliated graphite has previously been incorporated successfully into a polyethylene matrix as a conductive filler (4). It was shown that for a given formulation of the initial polyethylene/graphite mixture the electrical properties of the composite were a function of the *in-situ* volume fraction of the graphite particles.

EXPERIMENTAL

Materials

The polymeric system used in this study is STYPOL 40-3941 (Freeman Chemical Corporation) developed primarily for SMC applications. The principal components are an unsaturated polyester (weight average molecular weight 10,000, number average molecular weight 2000) and 38 weight percent styrene monomer.

The bulk density of the exfoliated GTB GRAPHITE flakes (Union Carbide) was 3 kg/m^3 and the specific surface was determined to be approximately 20 m^2/g. The ash content was about 5 percent by weight. A typical graphite flake was about 7 mm long and 1 mm in diameter.

Sample Preparation

The initial mixture of polyester resin and graphite flakes was mixed in a Haake 6000E batch mixer equipped with a set of sigma blades. Subsequently, the charge was placed in the center of a press in which the actual compression molding, including cure took place. The molding was carried out at 200°C for 20 min. The cross-section of the press platens was 381 mm by 381 mm. The mold closed to a gap separation of 6.35 mm (0.25 in). The press was a 75 ton Lawton press and was hydraulically driven and oil heated.

---

* To whom correspondence should be addressed.

Compression Flow Visualization Experiments

A compression flow apparatus shown in *Fig. 1* was used to study the filling of the mold upon compression. A constant linear rate of compression was used and could be varied between 0.005 and 50 cm/min. The bottom plate of the mold was made of a 12.7 mm thick Pyrex glass through which the flowing material could be observed and the location of the advancing front determined as a function of time. The apparatus was placed on top of a load cell (0 to 50 kg) allowing the compression force to be continuously measured. The initial charge was cylindrical in shape and placed in the center of the press. The typical compression time was about 6 s. After the compression was completed, the compression cell was placed in an oven at 200°C for several hours to ensure complete cure.

Measurement of the Electrical Properties

The Four-Probe method was used to measure the electrical resistivity. A schematic diagram of the apparatus is shown in *Fig. 2*. The dimensions of the test specimens were 152.4 mm by 6.35 mm by 6.35 mm and the resistivity was measured lengthwise. The probes penetrated 2 mm into the specimen.

The resistivity was measured as a function of graphite loading and processing history. The test specimens were cut at various locations and orientations from the molded samples. Several specimens were reduced to half their original thickness and the resistivity remeasured to determine whether the electrical resistivity varied with sample depth.

The EMI shielding effectiveness was measured on molded samples containing 4, 5, 7, and 11 percent by weight of graphite over a frequency range of 0 and 1000 MHz. *Figure 3* shows a schematic diagram of the apparatus used to measure the attenuation changes as a result of EMI shielding due to the sample.

Surface Interactions Between the Resin and Graphite

The Sessile-drop test was used to give a measure of wetting between the liquid polyester phase and the graphite surface. A small drop of the unreacted resin was placed on a smooth surface of compressed graphite flakes, of about 10 by 10 mm surface area and the contact angle determined from a photograph of the drop on the graphite surface. The measurement was made at room temperature.

Scanning electron micrographs of the graphite surface were taken to reveal the morphology and the approximate size range of the graphite open pores.

The mercury intrusion apparatus was used to determine the residual open pore volume in a graphite-polyester mixture where part of the pore volume had already been filled by the resin due to capillary flow during mixing. Mercury filled the entire capillary and the bottom of the reservoir of the mercury intrusion penetrometer (*Fig. 4*). Approximately 1 gram polyester-soaked graphite flakes taken from a graphite polyester mixture was placed in the top half of the reservoir. Additional resin was added to completely fill the reservoir. The system was pressurized by the hydraulic fluid. The volume

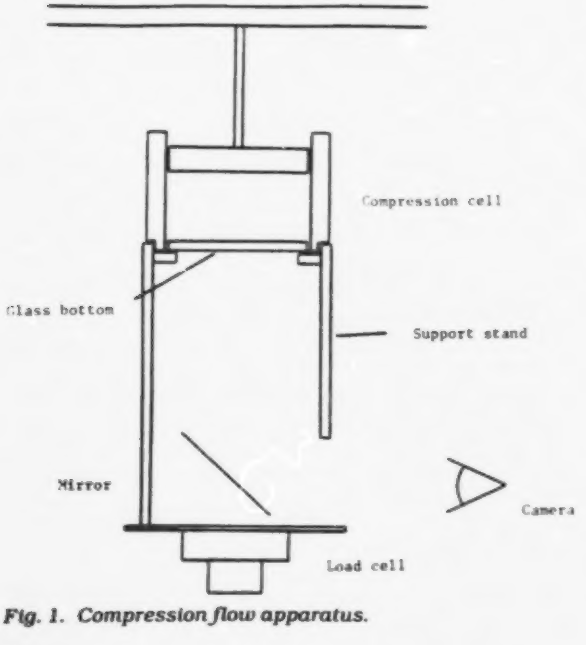

Fig. 1. Compression flow apparatus.

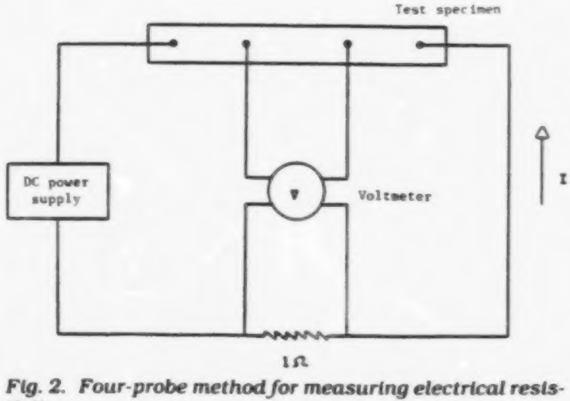

Fig. 2. Four-probe method for measuring electrical resistivity.

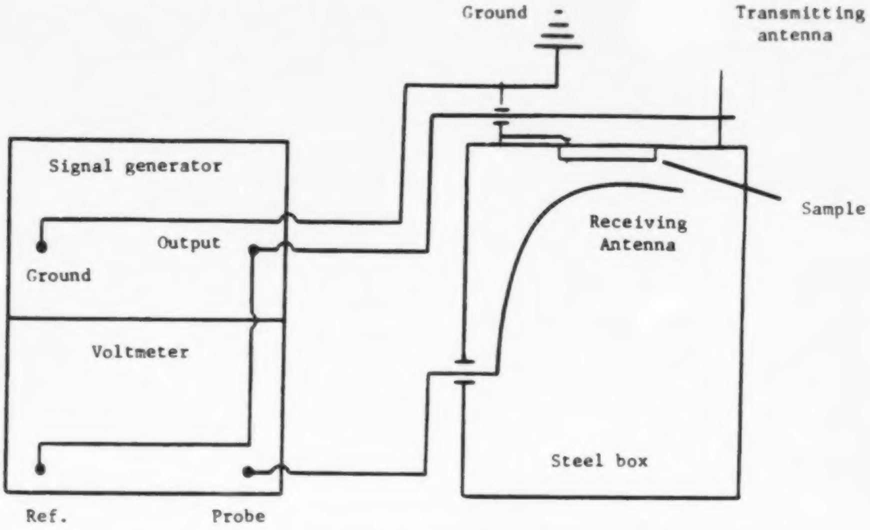
Ground
Transmitting antenna
Signal generator
Sample
Output
Receiving Antenna
Ground
Voltmeter
Steel box
Ref.
Probe

Fig. 3. Apparatus to measure EMI shielding (7).

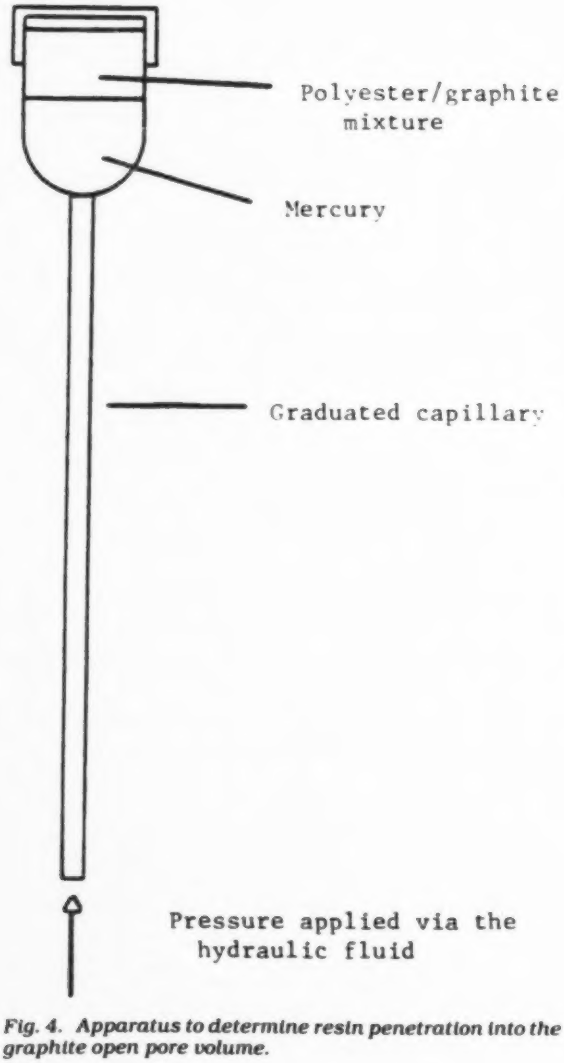
Polyester/graphite mixture
Mercury
Graduated capillary
Pressure applied via the hydraulic fluid

Fig. 4. Apparatus to determine resin penetration into the graphite open pore volume.

of the air remaining in the open pores after mixing was determined from the change in position of the mercury meniscus in the capillary.

RESULTS AND DISCUSSION

The polyester/graphite flake mixture was readily molded into plaques (381 mm by 381 mm) at a curing temperature of 200°C. A negligible amount of resin was squeezed out from the flakes around the perimeter of the mold. Graphite loadings as high as 11 weight percent were used. All samples showed good mechanical integrity.

The density of the composite as a function of applied pressure for graphite loadings of 4 and 7 weight percent is given in *Table 1*. The data were obtained using the transparent compression cell. The results show that the molding pressure can affect the density of these materials due to the presence of air in the pores and between the flakes. The initial and final graphite volume fractions were obtained from the known graphite volume and the initial and final volumes of the charge. The density of the graphite used in these calculations was 2160 kg/m^3, and compressibility of the solid phases was assumed to be negligible.

The morphology of the molded samples was examined using a Scanning Electron Microscope (SEM). *Figure 5* shows a SEM micrograph of a fractured surface of a sample containing 5 weight percent graphite. The micrograph of the fractured surface shows polyester coated graphite flakes indicating good resin penetration and adhesion. No voids are apparent and, within the scale shown here, the graphite flakes appear to be evenly distributed. Further discussion concerning the graphite/resin interface is given below.

The surfaces of the molded samples contain-

Table 1. Pressure Effects During Compression Molding

Graphite w. Fract.	Pressure [N/m²]	Graphite Initial	Vol. Fraction Final	Density [kg/m³]
4	2410	0.01950	0.0139	750
	5480		0.0163	880
	9870		0.0174	940
7	4280	0.03240	0.0142	440
	7680		0.0155	480
	10960		0.0172	530

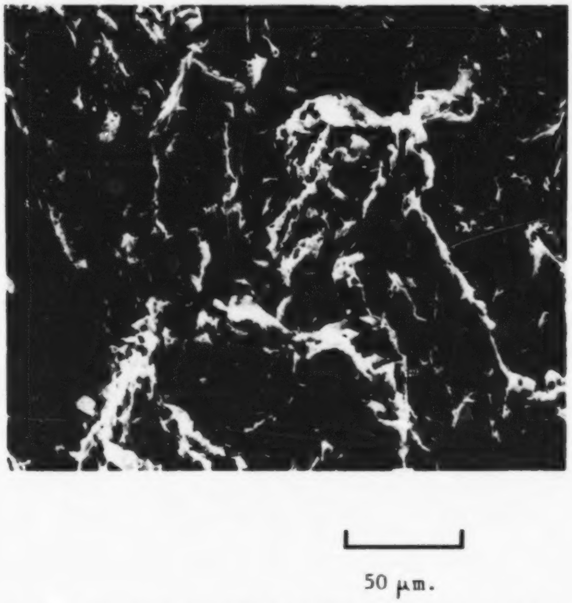

Fig. 5. A SEM micrograph of a fractured surface of a 5 weight percent graphite composite.

ing graphite loadings of 7 weight percent or less were smooth and contained periodically distributed narrow pools or streaks of polyester. They were similar in appearance, and were typically about 0.25 mm deep and 1 mm wide. The origin of these periodic disruptions in the graphite network is discussed below. *Figure 6* illustrates the narrow pools of polyester on the surface of a composite containing 5 weight percent of graphite. At the higher graphite loadings the surface showed a more pronounced silvery appearance caused by shearing and disruption of the surface of the flakes.

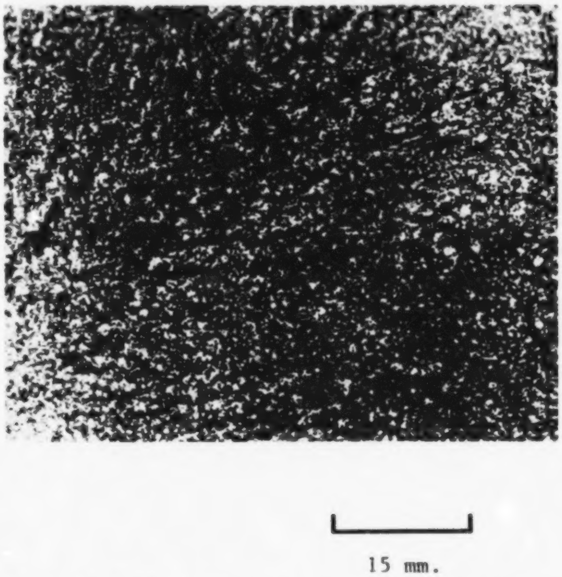

Fig. 6. Surface of a composite containing 5 weight percent graphite.

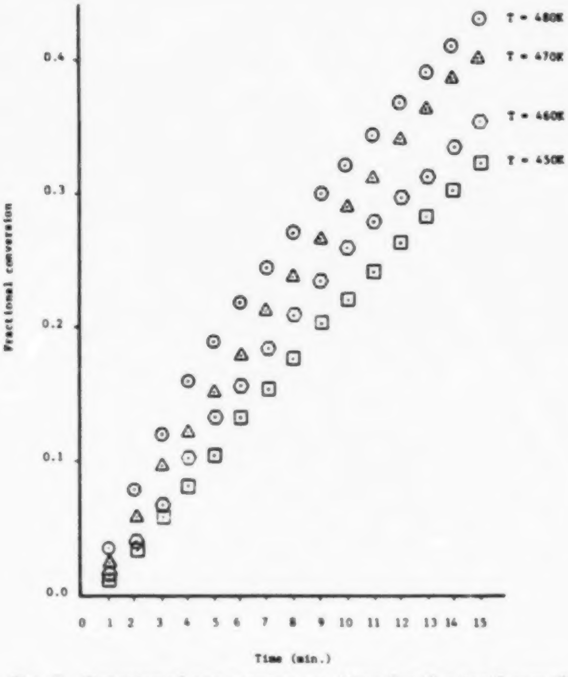

Fig. 7. Fractional conversion vs. time for the isothermal cure of the polyester.

The mechanism of formation of the resin rich areas referred to above was studied using a transparent compression mold. The squeezing flow was studied at room temperature, in the virtual absence of chemical reaction effects. As can be seen from *Fig. 7*, even at a temperature of some 450 K the change in conversion during flow is not large enough to affect the resin viscosity to an appreciable degree. The ram velocity was 50 cm/min giving a total compression time of about 6 s. *Figure 8a* shows successive photographs taken at 0.5 s intervals of the compression process. *Figure 8b* gives the apparent pressure required to maintain the filling process as a function of time, and the rate of energy input as a function of time is shown in *Fig. 8c*. For this experiment the graphite content was 7 weight percent. It should be noted that the molding pressures during the visualization experiments were about an order of magnitude lower than those involved in the compression molding run referred to earlier due

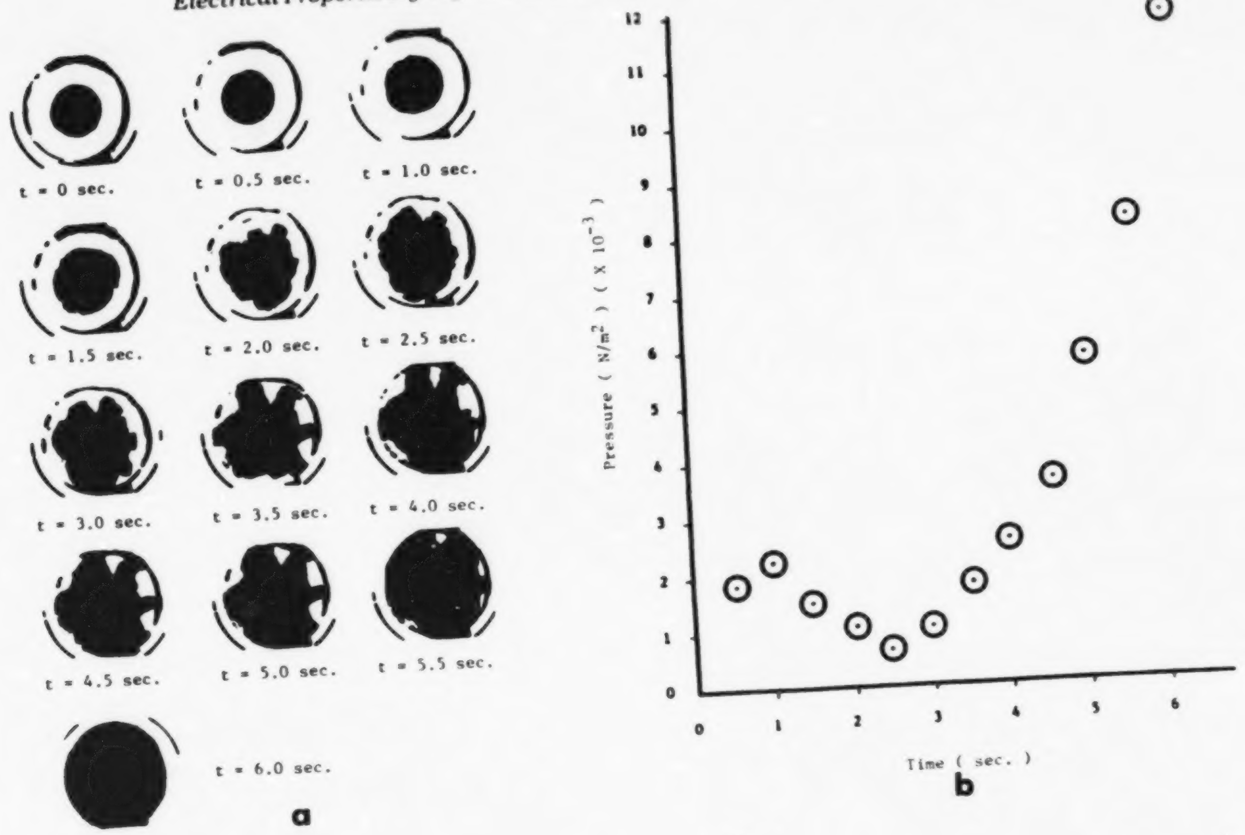

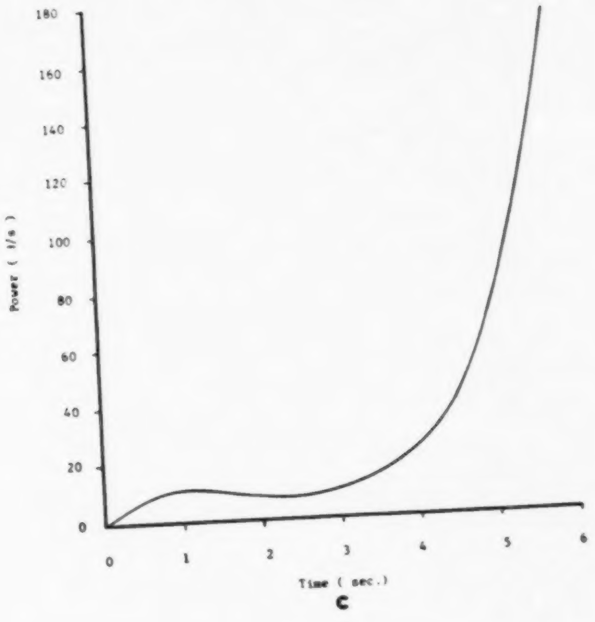

Fig. 8. a. Successive photographs of a compression flow experiment. b. Pressure vs. time for the compression flow experiment. c. Power consumption vs. time for the compression flow experiment.

to the limited strength of the observation glass window. Thus, the results reported in *Fig. 8* should be considered in a broader context of the flow mechanics of the molding process rather than as a direct simulation of compression molding done on the heated press.

In the initial stages of the compression the charge does not show measurable deformation. In the experiment illustrated in *Fig. 8*, the apparent yield stress of the material is exceeded after approximately 1 s. At that point the onset of observable deformation is observed (see *Fig. 8a*) while the compressive stress has reached a temporary maximum (*Fig. 8b*). During approximately the next 1.5 s the compressive stress steadily decreases to the point where the charge touches the wall. Beyond that point a dramatic pressure build-up is observed accompanying the last stage of mold filling and compacting of the material.

It has been observed that once the apparent yield stress is exceeded the charge undergoes a sudden collapse that manifests itself in the formation of "islands" of material. With further compression, the islands flowed radially outward flowing into, and around each other, eventually filling the mold. Through this mechanism resin rich areas were formed, visible as the aforementioned resin pools or streaks.

The good adhesion between the phases can be traced to both the relatively low interfacial energy between the resin and graphite, and to the large driving force for flow discussed above. The contact angle determined by the Sessile drop test was about 30°. Generally, solid and liquid phases are considered non-wetting for contact angles greater than 90° (5). The typical surface of a single flake available for the resin/graphite contact during the molding is shown in *Fig. 9*. The pores appear to be wedge shaped slits. The width of the pores is of the order of 1 to 10 microns. The graphite flakes contain essentially no closed pores (6). The surface texture is relatively rough providing a relatively large area for resin-graphite contact (20 m^2/g). The (unreacted) polyester appears to fill a significant portion of the available open pore volume upon mixing.

Electrical resistivities were measured on test specimens cut from various locations and orientations from the fully cured samples molded on the Lawton press. The electrical resistivities of the molded samples as a function of graphite loading are shown in *Table 2*. It is apparent that as the graphite content was increased the resistivity decreased. A resistivity of 0.03 Ω-cm, corresponding to the resistivity of exfoliated graphite in the c-direction was obtained. The decrease was due to the reduction of the thickness of polyester layers separating individual graphite flakes imposed by the increased loading and compression of the flakes.

Despite the local differences in the flow history, the apparent resistivities were the same throughout a given sample, both along and across the sample. In addition the electrical resistivity near the core of a molded sample was indistinguishable from that near the surface. Similar trends were observed on molded samples compressed in the transparent compression mold and subsequently cured in an oven. These results indicate no significant differences due to flow induced orientation of the graphite flakes. On a smaller scale, however, local resistivities were occasionally observed to be higher, up to as much as three times, when there was a streak of polyester close to the electrode. The presence of the polyester streaks has no appreciable effect on the bulk electrical properties as long as the total volume of these randomly oriented striations are much smaller than the characteristic dimension of the molded part.

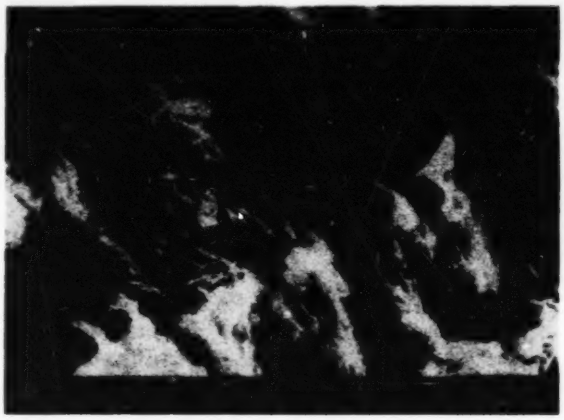

Fig. 9. SEM micrograph of an exfoliated graphite flake.

Table 2. Properties of the Exfoliated Graphite/Polyester Composites

Graphite Weight Fraction [−]	Composite Density [g/cm³]	Resistivity [Ω-cm]
4	0.98	0.22
7	1.03	0.15
9	1.06	0.04
11	1.15	0.03

Figure 10 compares the shielding effectiveness of molded samples containing 4, 5, 7, and 11 weight percent of graphite to that of compressed graphite flakes devoid of resin over a frequency range of short wave electromagnetic radiation between 1 and 1000 MHz. The shielding effectiveness of the compressed graphite flakes varied between 45 to 60 dB over the range of frequencies studied. At the lowest frequencies the molded composite samples shielded as well as the graphite flakes. At higher frequencies the shielding effectiveness of the molded samples compared well with the graphite reference. There was more signal transmission through the test specimens between 100 to 600 MHz than between 600 to 1000 MHz for all the graphite loadings. Furthermore the shielding effectiveness of the composite improved with increased graphite loading.

CONCLUSIONS

1. Exfoliated graphite flakes were successfully incorporated into an unsaturated polyester matrix to form an electrically conductive composite with good mechanical integrity.
2. Kinetic and thermal characterization of the unsaturated polyester curing reaction using DSC showed sufficiently slow chem-

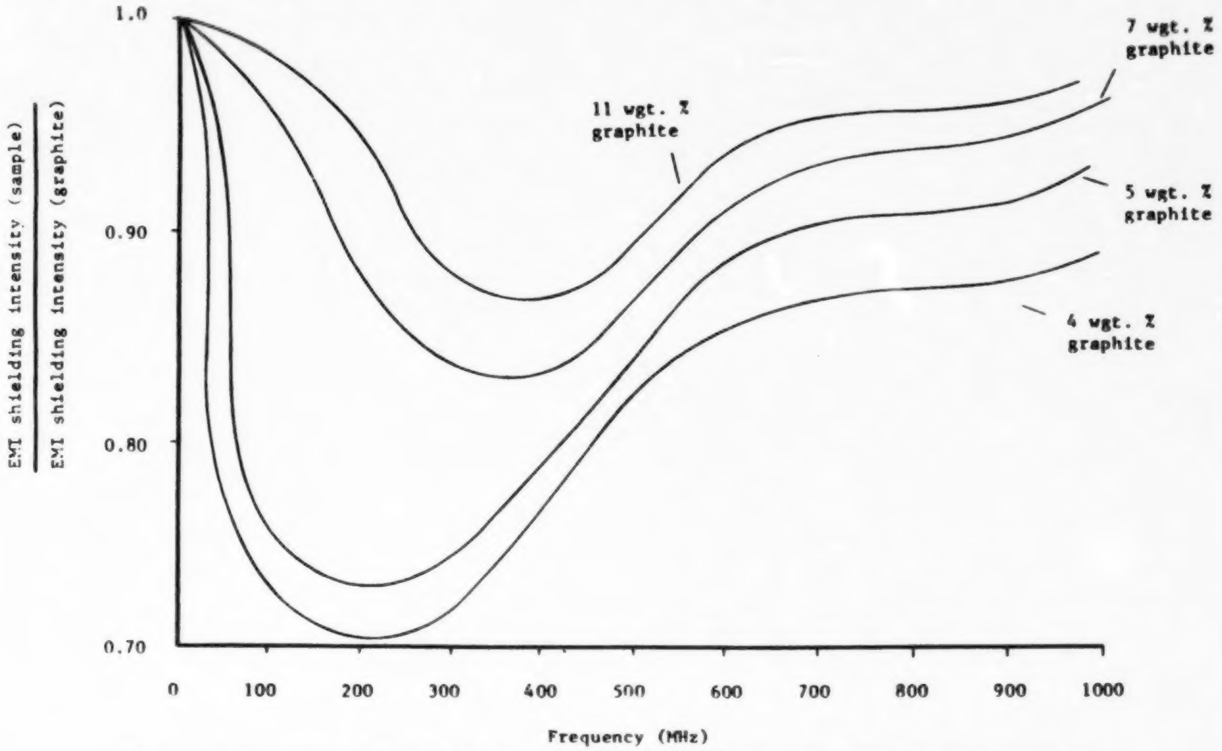

Fig. 10. Comparison of the EMI shielding intensity of molded composite samples to pure graphite.

ical reaction to effectively decouple the flow and cure stages during the formation of the composite.

3. Good wetting between the graphite and polyester has been found. The contact angle was determined to be 30°. The polyester appears to significantly penetrate and fill the open pore volume.
4. The electrical resistivity was essentially constant throughout the molded sample, thus relatively free of flow induced effects.
5. The resistivity of the composite decreased with increasing graphite content, obtaining a value as low as 0.03 Ω-cm at the graphite content of 11 percent by weight.
6. Composites containing between 4 and 11 weight percent of graphite flakes possessed comparable EMI shielding effectiveness to graphite devoid of resin over a frequency range of 0 to 1000 MHz. The EMI shielding effectiveness improved with increasing graphite content.

ACKNOWLEDGMENTS

We gratefully acknowledge the financial and technical support received from the Carbon Division of Union Carbide. The EMI shielding data have been obtained from Union Carbide.

We would also like to thank Dr. Ray Hoffman of the USX Corporation for the use of the heated press for molding the samples, Professor Deborah Chung of the Carnegie Mellon University for the use of her apparatus for measuring electrical resistivity, and Professor Jean Blachere of the University of Pittsburgh for the use of the mercury intrusion apparatus.

REFERENCES

1. B. Jachym and H. Sudolski, *Phys. Stat. Sol.*, (a) **34**, 657 (1976).
2. D. M. Bigg, *Polym. Eng. Sci.*, **19**, 1188 (1979).
3. S. H. Anderson and D. D. L. Chung, "Exfoliation of Intercalated Carbon," submitted to Carbon.
4. Y. S. Wang, M. O'Gurkis, and J. T. Lindt, *Polym. Compos.*, **7**, 349 (1986).
5. A. W. Adamson, Physical Chemistry of Surfaces, John Wiley & Sons, New York, (1982).
6. B. Mercuri, personal commun.
7. D. M. Bigg and P. J. Bradbury, "Conductive Polymeric Composites from Short Conductive Fibers," Polymer Science and Technology, Plenum Press, New York; Vol. 15, p. 27, (1981).

J. V. FOY AND J. T. LINDT, DISCUSSION

S. Newman: Apparently you found a lovely method to obtain good conductivity at 11 wt percent loading, but in view of the low density of the exfoliated graphite particles you have a very high volume fraction. Why has the resistivity reached its limiting value? Is this because at this loading you reached a number of parallel pathways of graphite/graphite continuity, or did you get to the graphite conductivity level?

J. V. Foy: At 11 wt percent graphite the resistivity of the composite has reached its limiting value equal to the resistivity of randomly packed exfoliated graphite flakes. Either the thickness of the polyester layers separating individual graphite particles has become sufficiently small that it does not affect the ability of the charge carriers to jump from particle to particle, or a sufficient number of graphite/graphite contacts have formed throughout the composite.

M. Takemori: What is the origin of these islands of material you observed in compression? Is it due to non-Newtonian flow? Is it commonly seen?

J. V. Foy: Yes, this is a common event with graphite loadings we have investigated. On compression we observed a sudden splattering of material in the mold resulting in island formation. An explanation for this phenomenon was proposed by Dr. Utracki while visiting the University of Pittsburgh. As the charge is compressed, air within the graphite pores and between graphite particles is being compressed. Eventually the internal pressure exceeds the yield stress of the charge and material splatters. In compression molding this phenomenon is much more pronounced.

S. Newman: I do not think that the low molecular weight polyester dissolved in styrene is non-Newtonian. In SMC at high loadings of glass fiber and calcium carbonate there are many situations when resin moves ahead of the filler through the mat, which leads to resin-rich domains within the molding.

G. Benson: I was very interested in your impressive conductivity figures. Can you tell me what was the absolute range of the EMI shielding efficiency of your composite.

J. V. Foy: The shielding effectiveness of compressed graphite flakes is about 45 to 60 dB depending on the transmitted signal frequency. For our composite the shielding effectiveness ranged from 36 to 60 dB depending on graphite loading and signal frequency.

G. Benson: It is very high. How expensive is it?

J. V. Foy: The cost is about $4.75/kg. The graphite filler for this composite was relatively inexpensive.

The Characterization of Thermoset Cure Behavior by Differential Scanning Calorimetry.

Part I: Isothermal and Dynamic Study

PATRICK W. K. LAM

Polysar Limited
Corporate Research & Development Division
Sarnia, Ontario Canada N7T 7M2

A study of the isothermal cure kinetics of an unsaturated polyester resin by differential scanning calorimetry is described. An autocatalyzed second order kinetic model is adopted to elucidate the cure reaction and also assess the kinetic parameters. The rate constant, the maximum cure rate, the extent of cure, and the degree of conversion at the maximum cure rate, all increase with increasing cure temperature, while the half-life and the time required to reach the maximum cure rate both decrease. Discrepancies between the experimental results and the predicted values of some of the kinetic parameters, especially at high degrees of conversion, are attributed to the highly different-controlled cure reaction following the gel point. The activation energy (E) and the pre-exponential factor (ln A) of the polyester cure reaction were estimated, using differential graphical techniques, to be 131 ± 4 kJ/mol and 39 ± 1 respectively. An ASTM method (E698) produces erroneously low values of the Arrhenius parameters, suggesting that the assumptions of the method may be overly simplified.

INTRODUCTION

It is usually difficult to determine the reaction kinetics of a thermosetting material, especially beyond the gel point, because the polymers formed are three-dimensional and insoluble. Although various techniques, including electrical resistivity (1), viscoelasticity (2), and pulsed nuclear magnetic resonance (NMR) (3), have been suggested to study the crosslinking reaction of thermosetting materials, differential scanning calorimetry (DSC) has been shown to be the most effective method of obtaining complete qualitative and quantitative information on the curing process of thermosets.

DSC studies of the cure kinetics of thermoset resins, such as epoxy (4–7) and unsaturated polyester (5, 8–11), have been discussed by a number of workers. Both autocatalyzed (5–7 and 9–11) and n-th order (4, 12) kinetic models have been used to describe the cure reaction of thermoset resins. However, n-th order kinetics failed to depict the auto-acceleration of the reaction (8) and the maximum cure rate, or the maximum heat evolution, at about 30 percent conversion (7, 11). As a result, misleading or invalid kinetic results can be obtained using n-th order reactions.

In this work, an autocatalyzed kinetic model is adopted to re-examine the cure behavior of unsaturated polyester. Mathematical techniques are described to assess all the kinetic parameters, and subsequently, the predicted values are compared with the experimental data in order to verify the consistency of the model. In addition, various graphical methods which are derived from the kinetic model, are demonstrated to determine the Arrhenius parameters. These results are further compared with those obtained from the ASTM E698 method. A modified ASTM method is also suggested in order to obtain reliable values of Arrhenius parameters. It is anticipated that all the techniques presented here will be extended to study the cure kinetics of bulk molding compound/sheet molding compound (BMC/SMC) in future. The symbols used in this work are defined in *Appendix I*.

DATA ANALYSIS

Autocatalyzed Kinetic Model

The exothermic heat evolved during isothermal cure of unsaturated polyester is proportional to the number of double bonds reacted in the system, or the extent of reaction (5, 13). Thus, the relative degree of cure (α) at time t and the total ultimate degree of cure (α_u) after isothermal cure are given by

$$\alpha = Q_t/(Q_T + Q_R) \qquad (1)$$

and

$$\alpha_u = Q_T/(Q_T + Q_R) \qquad (2)$$

where Q_T = heat of cure reaction at constant temperature, Q_t = heat evolved at any time, and Q_R = heat of residual reaction. Based on the DSC thermogram the cure rate ($d\alpha/dt$) is defined as

$$d\alpha/dt = (dQ_t/dt)/(Q_T + Q_R) \qquad (3)$$

where dQ_t/dt = heat flow into or out of the sample.

The curing of unsaturated polyester is, in general, described by an autocatalyzed kinetic equation (5–7, 9–11)

$$d\alpha/dt = k \times \alpha^m \times (1 - \alpha)^n \qquad (4)$$

where m and n are the reaction orders, which are independent of the temperature; and k is the rate constant which follows the Arrhenius equation

$$k = A \times EXP(-E/RT) \qquad (5)$$

where A = pre-exponential factor, E = activation energy, R = gas constant, and T = absolute curing temperature. To a good approximation, the isothermal curing of an unsaturated polyester can be assumed to be a second order reaction (5, 9–11). Mathematically, this is expressed as

$$m + n = 2 \qquad (6)$$

Substituting *Eq 6* into *Eq 4* and rearranging the equation, one obtains

$$\ln[(d\alpha/dt)/\alpha^2] = \ln k + n \ln[(1 - \alpha)/\alpha] \qquad (7)$$

Integrating the equation, the following relation is obtained:

$$t = [k(n - 1)]^{-1} \times [\alpha/(1 - \alpha)]^{n-1} \qquad (8)$$

The half-life of polyester ($t_{1/2}$) at any curing temperature can be computed by substituting *Eq 5* and $\alpha = 0.5$ into *Eq 8*:

$$t_{1/2} = [A(n - 1)]^{-1} EXP(E/RT) \qquad (9)$$

Differentiating *Eq. 4* with respect to α and setting the derivative to zero, one obtains

$$\alpha_{max} = m/2 \qquad (10)$$

where α_{max} = degree of cure at the maximum cure rate. Thus, when *Eqs 5* and *10* are substituted into *Eq 4*, the maximum cure rate $(d\alpha/dt)_{max}$ can be estimated by the equation

$$(d\alpha/dt)_{max} = A \times EXP(-E/RT) \times (m/2)^m \times (n/2)^n \qquad (11)$$

Similarly, when *Eq 10* is substituted into *Eq 8*, the time required to attain the maximum cure rate (t_{max}) is given by

$$t_{max} = [A(n - 1)]^{-1} \times (m/n)^{n-1} \times EXP(E/RT) \qquad (12)$$

Arrhenius Parameters

Arrhenius parameters, such as the activation energy of reaction (E) and the pre-exponential factor ($\ln A$), are usually determined using graphical techniques. For example, by plotting the logarithmic scale of the quantity on the left-hand side of *Eq 5, 9, 11*, or *12 vs. 1/T*, the Arrhenius parameters can be estimated by linear regression methods.

Another approach to determine these parameters is the ASTM E698 method (14) in which the variations of exothermic peak temperatures (T_p) are measured as functions of the linear programmed DSC heating rates. Usually, the peak maximum temperature increases with increasing heating rate for the cure reaction of unsaturated polyester.

In the ASTM E698 method, three basic assumptions are made for the calculations:

1) The peak maximum represents a point of constant conversion which is independent of the heating rate.
2) The cure reaction follows n-th order kinetics.
3) The reaction rate constant obeys the Arrhenius equation.

Based on these hypotheses, the activation energy and the pre-exponential factor are approximated by the equations

$$\ln \beta \simeq Z - (1.05\, E)/(R \cdot T_p) \qquad (13)$$

where Z = a constant and

$$\ln \beta \simeq \ln[R \cdot T_p^2/E - E/(R \cdot T_p)] + \ln A \qquad (14)$$

EXPERIMENTAL PROCEDURES

Koppers polyester resin 3702–5, which contained 39 percent of styrene monomer, was selected as the thermoset material for this work. The polyester is the condensation product of orthophthalic anhydride (OPAH), maleic anhydride (MAH), and propylene glycol (PG) with the ratio OPAH:MAH:PG 1.0:1.3:3.5. The weight average molecular weight of the resin was estimated to be 2800 based on the intrinsic viscosity measurement (15). Lucidol t-butyl peroctoate (50 percent W/W solution in dioctyl phthalate) was the initiator for the curing of the polyester resin.

Cure kinetics were monitored using a DuPont Model 9900 thermal analyzer which was equipped with a DSC cell and a computer. The onset cure temperature and peak maximum temperature were determined by heating a polyester sample in the DSC cell at a rate of 5°C/min, producing a thermal curve. The temperatures for isothermal kinetic studies were selected from an interval defined about 20°C below the onset temperature and a point midway to peak maximum temperature. In this work, the isothermal kinetics experiments were performed at 75, 80, 90, and 95°C under a dry nitrogen atmosphere.

A catalyzed polyester resin sample was prepared by mixing thoroughly, in a vial, the polyester resin with 1 percent by weight of a t-butyl peroctoate solution. About 10 mg of the resin sample was sealed in a hermetic sample pan and weighed before and after the experiment to check whether there was any loss of styrene monomer during the cure reaction.

The DSC was calibrated using high-purity indium and an isothermal baseline was established at the present cure temperature by means of two empty sample pans. Then the sample was placed in the DSC cell immediately and the data acquisition system was triggered. Usually, equilibrium in temperature between the sample and reference holders was achieved in less than one minute, as indicated by a steady temperature readout on the computer. During the isothermal measurements, the change of temperature never exceeded 1.5°C. The experiment was stopped when the DSC thermogram leveled off to a baseline. At the end of each run, the sample was cooled rapidly to room temperature. A temperature scan from ambient to 250°C at a 10°C/min heating rate was initiated to determine the residual activity of the sample.

The integral heat generated from the reaction at any time was obtained by integrating the partial area of the thermogram using a DuPont Instrument 9900 Computer/Thermal Analyzer and General Thermal Analysis software.

In the ASTM E698 DSC kinetics experiments, the samples were scanned at various heating rates (2.5, 5.0, 7.5, 10.0, 12.5, and 15.0 °C/min) from ambient to 250°C. The exothermic peak maximum temperatures were analyzed using a computer and General Thermal Analysis software, and corrected according to the ASTM procedures.

RESULTS AND DISCUSSION

Autocatalyzed Kinetic Model

The residual exotherm, which is due to the presence of remaining monomers, begins to appear just beyond the temperature of isothermal cure. The residual reactivity of the polyester is caused by the highly diffusion-controlled reaction at advanced stages of cure. Thus, a very long time is required to reach completion under isothermal conditions. This is supported by results showing that viscosity increases tremendously in the vicinity of the gel point (11, 15). The effect of curing temperature on the residual reactivity of polyester is expressed as the total ultimate degree of cure (α_u) as indicated by *Eq 2* and shown in *Fig. 1*.

The results in *Fig. 1* reveal that the completion of cure increases as the curing temperature is increased. The cessation of the reaction at a certain conversion is probably dependent upon the crosslink density of the system. Hence, it is essential to postcure the polyester composites at higher temperatures in order to achieve complete cure of the matrices. This conjecture is confirmed by the fact that after the residual reactivity of the sample is determined (second scan), rescanning of the sample (third scan) no longer shows any residual exotherm. The minimum postcuring temperature is probably indicated by the peak maximum temperature in the residual exotherm, and is about 120 to 130°C in this case.

The glass transition temperature of the cured resin, which was determined in the dynamic mechanical testing (15), is about 171°C. Thus, the optimum curing temperature of thermoset materials should be at least 40 to 50°C above the minimum postcuring temperature or above the glass transition temperature. The loss of styrene monomer during the experiments is not critical because the weight of the sample does not decrease significantly during the experiments.

The reaction orders m and n, and the rate constant k, are estimated according to *Eqs 6* and *7*. These results are shown in *Fig. 2* and summarized in *Table 1*. All the plots in *Fig. 2* are linear and almost parallel to each other because the reaction order n (or m) is independent of the temperature. The average values of m and n for the polyester are 0.68 ± 0.03 and 1.32 ± 0.03, respectively. The rate constants,

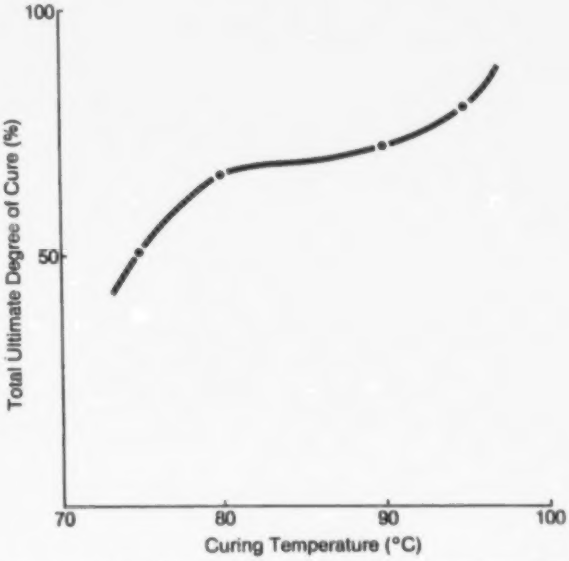

Fig. 1. Total ultimate degree of cure of unsaturated polyester resin vs. curing temperature.

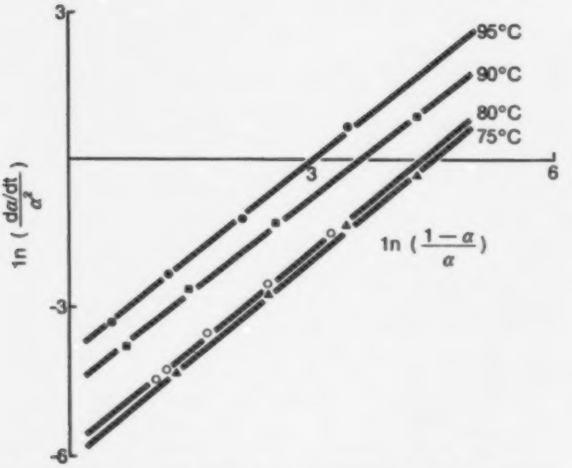

Fig. 2. Determination of rate constants and reaction orders of isothermal cure kinetics of unsaturated polyester resin.

Table 1. Rate Constants and Reaction Orders of Unsaturated Polyester Resin at Different Curing Temperatures

Curing Temperature (°C)	k (min^{-1})	m	n	r*
75	0.11	0.64	1.36	0.9982
80	0.20	0.70	1.30	0.9986
90	0.63	0.71	1.29	0.9998
95	1.10	0.66	1.34	0.9985
	average	0.68 ± 0.03	1.32 ± 0.03	

* r = Correlation coefficient.

as predicted by the Arrhenius equation, increase with increasing cure temperature. The results of m and n obtained in this work are compared with literature values in *Table 2*. The values of the reaction orders appear to be dependent upon the type of polyester, the concentration of styrene monomer in the resin, and the initiator. The value of m is, in general, less than that of n. The curing of an unsaturated polyester is a second order reaction in all cases.

The degrees of cure (α) at different temperatures are calculated using *Eq 3* and the results are shown in *Fig. 3*. The symbols represent the experimental data and the solid sigmoidal curves are the predicted values based on *Eq 8*. The degree of conversion increases with increases in either the curing time or the curing temperature. The experimental results, especially at high curing temperature, are in good agreement with the computed values up to 40 to 60 percent conversion. The discrepancies at high conversion are attributed to the residual reactivity of the polyester, which is a consequence of the diffusional resistance of polymeric segments.

The experimental cure rates (the symbols) are compared with the predicted values (the solid curves) in *Fig. 4*. They agree well with each other, particularly below the maximum cure rates. The cure rate goes through a maximum

Table 2. Comparison of Reaction Orders of Autocatalyzed Kinetics of Unsaturated Polyester Resin

Resin	Initiator	m	n	Reference
Ashland Polyester (72%)	MEK*	0.45	1.55	10
Reichhold Polyester (70%)	MEK	0.25	1.75	9
Reichhold Polyester (70%)	MEK	0.33	1.67	5
Ashland Polyester (64%)	BP**	0.34	1.66	11
Koppers Polyester (61%)	TBPO***	0.32	1.68	present study

* MEK = Methyl ethyl ketone peroxide.
** BP = Benzoyl peroxide.
*** TBPO = T-butyl peroctoate.

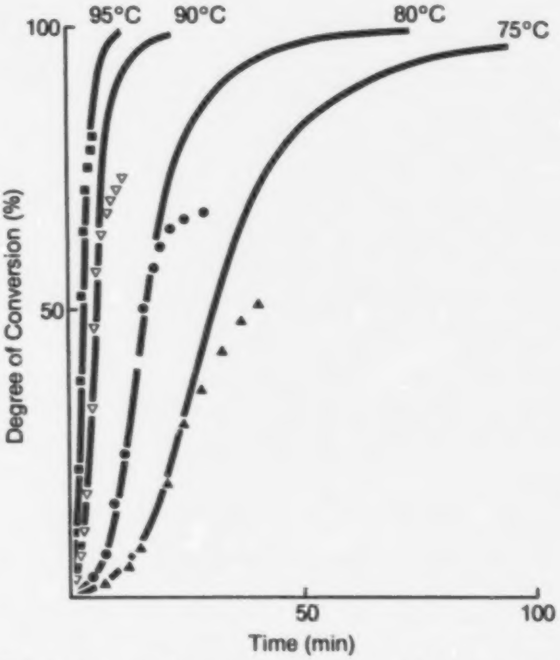

Fig. 3. Degree of conversion of unsaturated polyester resin vs. time at different curing temperatures.

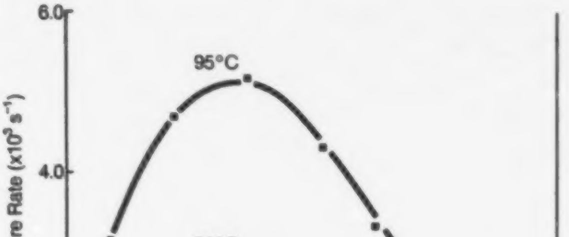

Fig. 4. Cure rate of unsaturated polyester resin vs. degree of conversion at different curing temperatures.

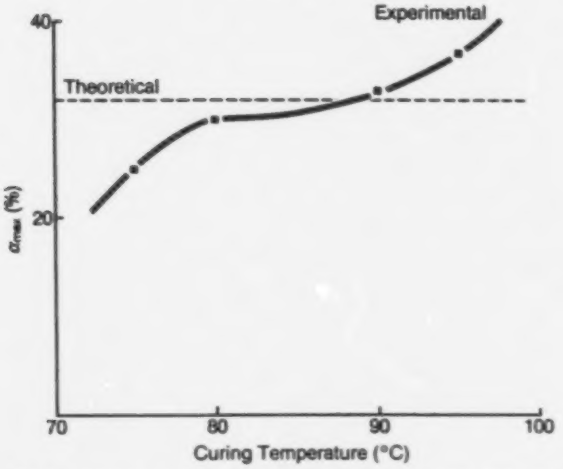

Fig. 5. Degree of conversion at maximum cure rate vs. curing temperature compared with theoretical values (Eq 10).

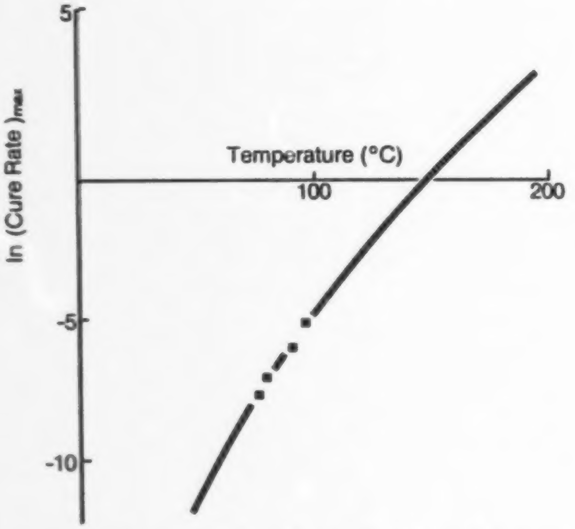

Fig. 6. Maximum cure rate of isothermal curing of unsaturated polyester resin vs. curing temperature.

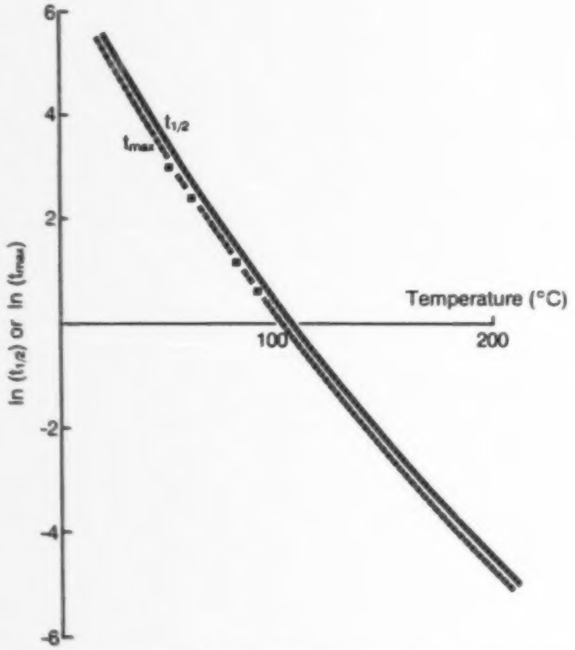

Fig. 7. Half-life and time required to attain maximum cure rate vs. curing temperature.

and then decreases as the degree of cure is increased. This peculiar cure behavior, as described by an autocatalyzed rate equation (*Eq 4*), is usually observed for thermoset materials. Again, the deviation of the experimental results from the theoretical curves at high conversion is caused by the low molecular mobility of the gel structure.

Theoretically, the degree of conversion at the maximum cure rate (α_{max}) should be 0.32 (*Eq 10*) and independent of the curing temperature. However, our experimental results indicate that α_{max} increases with increasing cure temperature and is in the range of 25 to 40 percent (*Fig. 5*). The variations of α_{max} and α_u with curing temperatures are very similar in nature (*Figs. 1* and *5*). This suggests that the dependence of α_{max} on the temperature is due to different residual reactivity in the polyester at different curing temperatures.

The maximum cure rate increases with increasing cure temperature (*Fig. 6*). This is consistent with the results shown in *Fig. 4*. The experimental data agree with the theoretical values within ±5 percent. Although the autocatalyzed kinetic model (*Eq 11*) can predict the maximum cure rate at any temperature, in practice the kinetic experiments are confined within certain temperature limits. This is because the cure kinetics may be too fast to be followed by DSC at high temperature or too slow at low curing temperature.

The time required to attain the maximum cure rate (t_{max}), is also temperature dependent and determined by the reaction orders m and n as described by *Eq 12*. The experimental values of t_{max} (the symbols) are in good agreement with the predicted values (solid curves) (*Fig. 7*). They appear to decrease as the curing temperatures are increased. Furthermore, t_{max} also decreases with increasing values of n or decreasing values of m. In a special case, when $n = 2$ and $m = 0$ (second order kinetics) t_{max} becomes zero. This indicates that the maximum cure rate or maximum heat evolution occurs at time = 0 which is a typical characteristic of the n-th order kinetics.

The half-lives of polyester ($t_{1/2}$) as predicted by *Eq 9*, at 75, 80, 90, and 95°C are 28.6, 16.2, 5.0, and 2.9 min respectively. The half-life also decreases with increases in either the curing temperature or the reaction order n. In this case the values of $t_{1/2}$ differ from those of t_{max} by a factor of $(m/n)^{n-1}$ or 0.81. Thus, parallelism between t_{max} and $t_{1/2}$ is observed in *Fig. 7*.

The rate constants (k), as expected, closely follow the Arrhenius equation and increase rapidly with increasing cure temperature, as shown in *Fig. 8*. Again, the variations of rate constant and maximum cure rate with temperature are very similar in nature (*Figs. 6* and *8*). These two kinetic parameters differ by a factor of $(m/2)^m \times (n/2)^n$ or 0.28 (see *Eqs 5* and *11*).

Arrhenius Parameters

Figure 9 shows that ln k is linearly correlated with $1/T$. This yields values of $E = 130$ kJ/mol and ln $A = 39$. Similarly, the plot of $\ln(d\alpha/dt)_{max}$ *vs.* $1/T$ (*Fig. 10*), and the plot of $-\ln(t_{max})$ *vs.* $1/T$ (*Fig. 11*), give the results E = 135 and 126 kJ/mol, and ln A = 39 and 38 respectively. No doubt, the Arrhenius parameters can be assessed using one of these three methods, as they all produce consistent results.

Figures 12 and *13* show the results of E and ln A obtained from the ASTM E698 method. The logarithm of the heating rate (ln β) is a linear function of the reciprocal of the peak maximum temperature ($1/T_p$) (*Fig. 12*). Based on *Eq 13*, the values of E and Z are estimated to be 115 kJ/mol and 40 respectively, using the linear regression technique. The pre-exponential factor is obtained from the intercept of the plot in *Fig. 13* (see also *Eq 14*). In principle, the slope of the straight line in *Fig. 13* should be unity, but the experimental data yield the results of slope = 0.97 and ln A = 35.

The results of activation energy and pre-exponential factor obtained using different graphical methods are compared in *Table 3*. Most of the techniques used in this work, except the ASTM E698 method, produce the same results. The lower values of E and ln A obtained from the ASTM method are probably due to the oversimplification of the assumptions in this technique.

It is of interest to note that the ratio E/ln A obtained by different methods is almost constant and independent of their actual values or the method used, (*Table 3*). The constancy of the ratio is about ±4 percent. Reed, *et al.* (16)

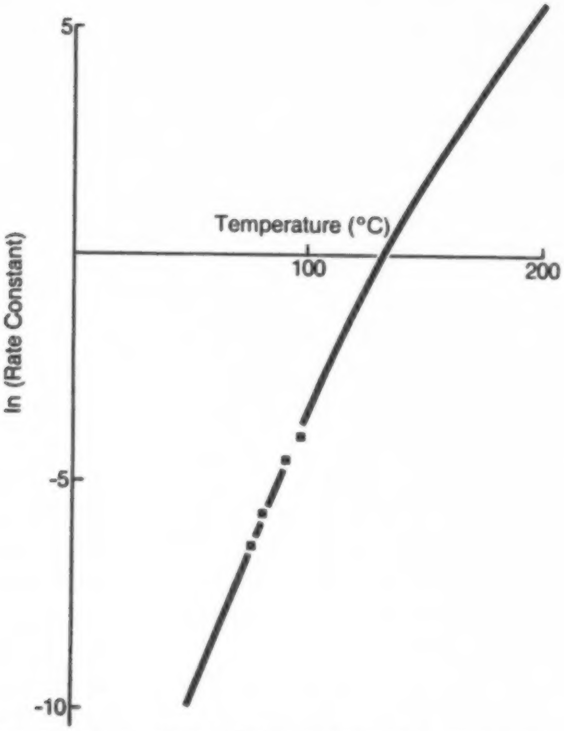

Fig. 8. Rate constant of isothermal curing of unsaturated polyester resin vs. curing temperature.

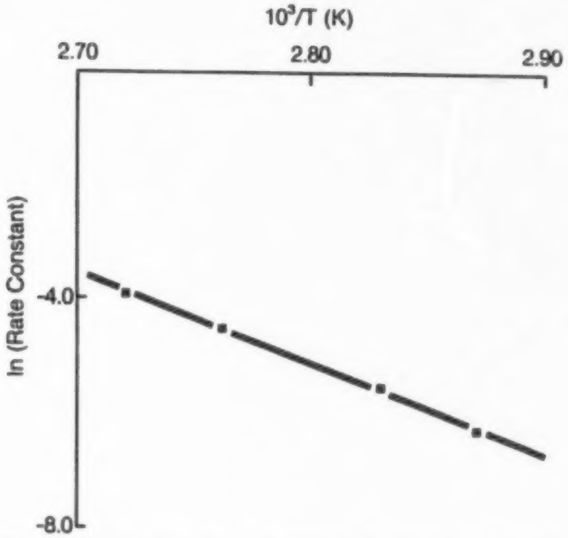

Fig. 9. Logarithmic scale of rate constant vs. reciprocal of absolute curing temperature.

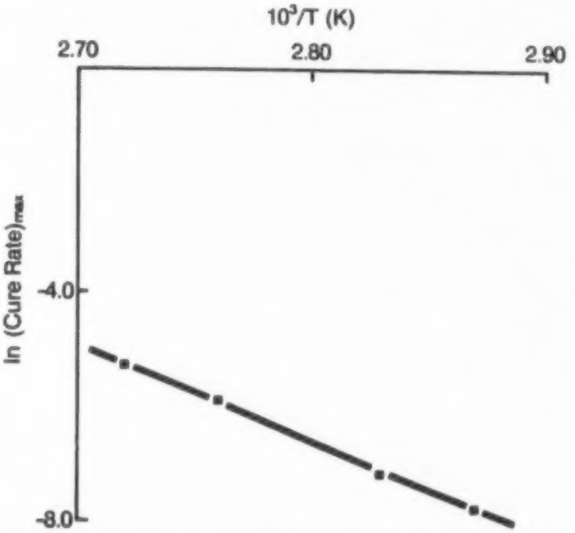

Fig. 10. Logarithmic scale of maximum cure rate vs. reciprocal of absolute curing temperature.

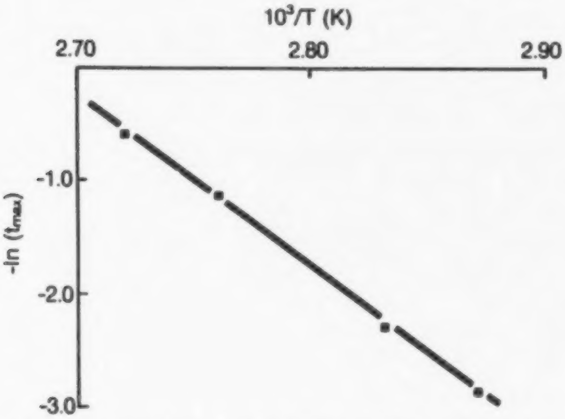

Fig. 11. Logarithmic scale of time required to attain maximum cure rate vs. reciprocal of absolute curing temperature.

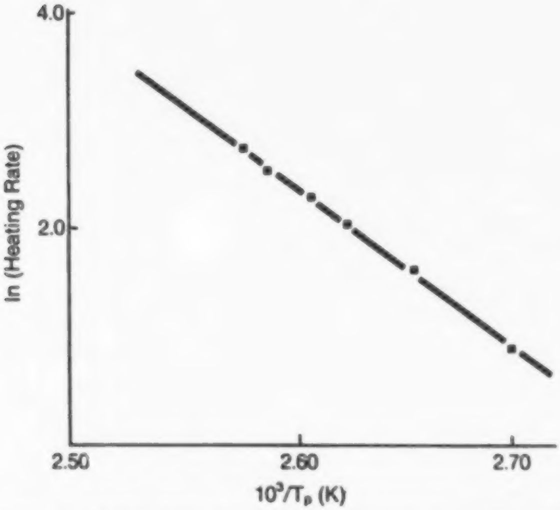

Fig. 12. Logarithmic scale of heating rate vs. reciprocal of absolute peak maximum temperature.

have also observed the striking constancy of $E/\ln A$ for the decomposition of benzenediazonium chloride, while Prime, *et al.* (4) have shown that this constancy did not exist for epoxy systems.

In the calculation of activation energy, the ASTM method assumes that the degree of cure at the peak exotherm (α_{max}) is constant and independent of heating rate. However, our experimental results reveal that both α_{max} and T_p increase slightly with increasing heating rate (*Fig. 14*). This may account for the lower value of activation energy obtained by the ASTM method. Also, *Eq 14*, which is adopted by the ASTM method, is only an approximation for $\ln A$ of n-th order reaction (4, 17). The accurate expression for the pre-exponential factor is given by the equation

$$A = \frac{E \times EXP(E/RT_P)}{RT_P^2[n(1-\alpha_{max})^{n-1}]} \qquad (15)$$

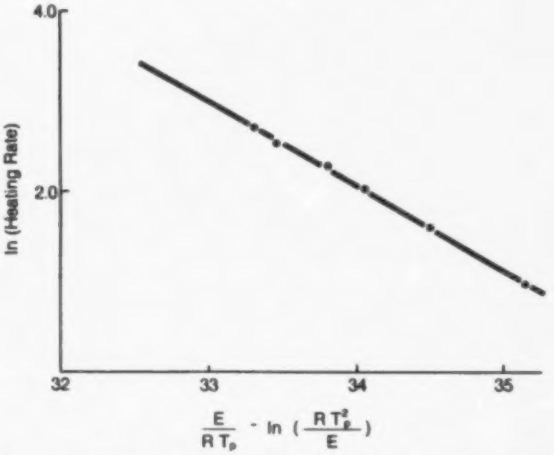

Fig. 13. Determination of pre-exponential factor using ASTM E698 method.

Table 3. Comparison of the Activation Energy and the Pre-Exponential Factor of Unsaturated Polyester Resin Obtained by Different Methods

Method	E (kJ/mol)	$\ln A$	$E/\ln A$ (kJ/mol)	r**
$\ln k$ vs. $1/T$	130	39	3.33	0.9996
$\ln(d\alpha/dt)_{max}$ vs. $1/T$	135	39	3.46	0.9993
$-\ln(t_{max})$ vs. $1/T$	126	38	3.32	0.9991
$-\ln$ (Gel Time) vs. $1/T$*	127	40	3.18	0.9901
ASTM E698	115	35	3.29	0.9972
$\ln(\beta) + \ln f(\alpha_{max})$ vs. $1/T_p$	125	40	3.13	0.9980

* Data from *Ref.* 15.
** Correlation coefficient.

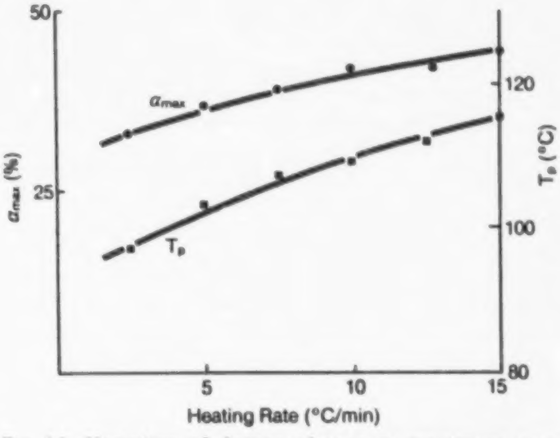

Fig. 14. Variation of degree of cure at maximum cure rate and peak maximum temperature with heating rate during the ASTM E698 experiments.

Although Kissinger (17) agreed that the quantity $n(1 - \alpha_{max})^{n-1} \sim 1$ and is independent of heating rate, apparently *Eq 14* is obtained by setting $n = 1$ in *Eq 15* or assuming a first order cure reaction. Also, α_{max} is dependent upon the heating rate or the temperature (*Fig. 14*). Therefore, the assumptions in the ASTM method seem to be oversimplified to describe the autocatalyzed cure reaction of thermosets.

If *Eqs 13* and *14* are modified in such a way as to account for the variations of α_{max} and T_p with heating rates, then the following equation is obtained (see *Appendix II* for derivation).

$$\ln \beta + \ln f(\alpha_{max}) \simeq \ln\left(\frac{AE}{R} - 5.33\right) - \frac{1.05\,E}{RT_p} \quad (16)$$

$$\text{where} \quad f(\alpha_{max}) = \frac{1}{n-1}\left(\frac{\alpha_{max}}{1-\alpha_{max}}\right)^{n-1}$$

Both E and $\ln A$ can be determined simultaneously from a single plot of $(\ln \beta + \ln f(\alpha_{max}))$ *vs.* $1/T_p$ according to *Eq 16*. *Figure 15* illustrates the determination of Arrhenius parameters using *Eq 16*. The straight line in *Fig 15* yields values of $E = 125$ kJ/mol and $\ln A = 40$, which are about the same as the other results shown in *Table 3*. Since $1/T_p$ varies only slightly with heating rate (order of magnitude $10^{-4} - 10^{-5}$), the slope of *Eq 16* is, therefore, very sensitive to a small change of $\ln f(\alpha_{max})$. This probably explains why a better approximation for Arrhenius parameters can be obtained by using *Eq 16*.

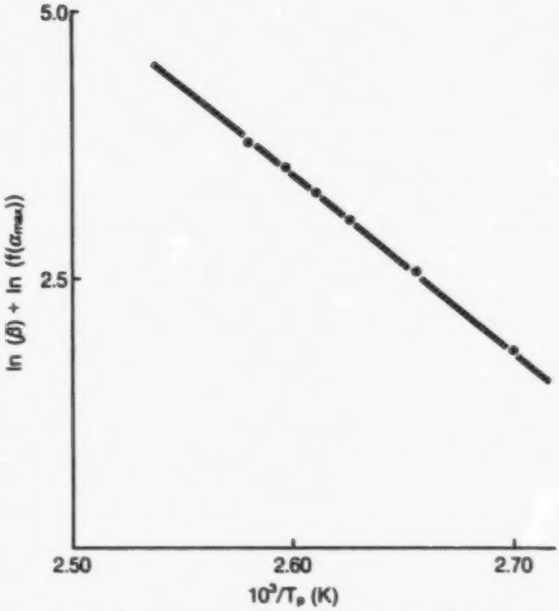

Fig. 15. Determination of activation energy and pre-exponential factor using modified ASTM method.

CONCLUSIONS

Isothermal curing of a representative unsaturated polyester resin is an autocatalyzed second order reaction with $m = 0.68$ and $n = 1.32$. An autocatalyzed kinetic model is capable of predicting all the kinetic parameters, such as the degree of cure, cure rate, conversion at maximum cure rate, maximum cure rate, time required to attain the maximum cure rate, half-life, and rate constant of the reactions. The theoretical values of these variables are, in general, in good agreement with the experimental results at 40 to 60 percent conversion. Discrepancies at high degrees of conversion are probably due to the highly diffusion-controlled cure reaction of the polymer gel.

The total ultimate degree of cure, conversion at maximum cure rate, rate constant, and maximum cure rate all increase with increasing temperature, while the half-life and the time required to obtain the maximum cure rate decrease. The cure rate goes through a maximum and then decreases as the curing time or degree of conversion is increased.

Arrhenius parameters can be determined from the rate constants, maximum cure rates, and times required to attain maximum cure rates. The average values of the activation energy of reaction (E) and the pre-exponential factor ($\ln A$) are 131 ± 4 kJ/mol and 39 ± 1 respectively. The oversimplification of the assumptions in the ASTM E698 method results in erroneously low values of E and $\ln A$. However, the ratio of $E/\ln A$ obtained from different techniques is almost constant. The degree of conversion at peak exotherm and peak maximum temperature increases with heating rate. Thus, reliable results of Arrhenius parameters can be obtained using *Eq 16* instead of *Eqs 13* and *14*.

ACKNOWLEDGMENTS

The author wishes to thank his colleagues at Polysar for their assistance, and Polysar Limited for permission to publish.

POLYSAR

POLYSAR, KRYLENE, KRYMIX, KRYNAC, KRYNOL, SS 250, TAKTENE, TORNAC and TRANS-PIP are registered trade marks of Polysar Limited, Sarnia, Ontario, Canada.

Information given herein is furnished in good faith, without warranty, representation, inducement or a license of any kind. Polysar does not assume any legal responsibility for use of or reliance upon same. No warranty or representation is given that Polysar products described will be suitable in purchasers' formulations or processes for any particular end use. No representation is given as to freedom from patent infringement.

Materials not manufactured or supplied by Polysar may present hazards in handling and use. Reference should be made to the manufacturer or supplier for all information relating to such materials.

REFERENCES

1. T. Imai, *J. Appl. Polym. Sci.*, **11**, 1055 (1967).
2. G. S. Learmonth, G. Pritchard, and J. Reinhardt, *J. Appl. Polym. Sci.*, **12**, 619 (1968).
3. M. Paci, E. D. Vecchio, and F. Campana, *Polym. Bull.*, **15**, 21 (1986).
4. R. B. Prime, *Polym. Eng. Sci.*, **13**, 365 (1973).
5. M. R. Kamal, S. Sourour, and M. Ryan, *SPE ANTEC Tech. Paper*, **19**, 187 (1973).
6. M. E. Ryan and A. Dutta, *Polymer*, **20**, 203 (1979).
7. J. Mijovic, *J. Appl. Polym. Sci.*, **31**, 1177 (1986).
8. K. Horie, I. Mita, and H. Kambe, *J. Polym. Sci., Part A-1*, **8**, 2839 (1970).

9. M. R. Kamal and S. Sourour, *Polym. Eng. Sci.*, **13**, 59 (1973).
10. S. Y. Pusatcioglu, A. L. Fricke, and J. C. Hassler, *J. Appl. Polym. Sci.*, **24**, 937 (1979).
11. C. D. Han and K. W. Lem, *J. Appl. Polym. Sci.*, **28**, 3155 (1983).
12. L. W. Crane, P. J. Dynes, and D. H. Kaelble, *J. Polym. Sci., Polym. Lett.*, **11**, 533 (1973).
13. H. J. Borchandt and F. Daniels, *J. Am. Chem. Soc.*, **79**, 41 (1956).
14. Annual Book of ASTM Standards, E698–79 Method, Vol. 14.02, 601 (1979).
15. Patrick W. K. Lam, Unpublished data.
16. R. L. Reed, L. Weber, and B. S. Gottfried, *Ind. Eng. Chem., Fundam.*, **4**, 38 (1965).
17. H. E. Kissinger, *Anal. Chem.*, **29**, 1702 (1957).
18. C. D. Doyle., *Anal. Chem.*, **33**, 77 (1961).
19. R. B. Prime, "Thermal Characterization of Polymeric Materials", Ed. by E. Turi, Chap. 5, P. 541, Academic Press, New York, (1981).

APPENDIX I

Definition of Symbols

Q_T = Total heat of cure reaction which is measured at the end of an isothermal run at temperature T (J/g).

Q_t = Heat which is evolved isothermally corresponding to a partial cure condition at time t (J/g).

Q_R = Heat evolved due to the residual isothermal reactivity of the sample at temperature T (J/g).

α = Degree of conversion.

α_{max} = Degree of conversion at maximum cure rate.

α_u = Total ultimate degree of cure.

dQ_t/dt = Heat flow into or out of the sample (W/g).

$d\alpha/dt$ = Cure rate (min^{-1}).

$(d\alpha/dt)_{max}$ = Maximum cure rate (min^{-1}).

k = Rate constant (min^{-1}).

m, n = Reaction Orders which are independent of temperature.

T = Curing temperature (K).

T_p = Exothermic peak maximum temperature (K).

$t_{1/2}$ = Half-life of cure reaction (min).

t_{max} = Time required to attain a maximum cure rate (min).

E = Activation energy of cure reaction (kJ/mol).

A = Pre-exponential factor (min^{-1}).

β = Linear programmed DSC heating rate (°C/min).

Z = A constant (see *Eq 13*).

$f(\alpha_{max})$ = Function of α_{max} (see *Eq 16*).

APPENDIX II

Derivation of *Eq 16*

Combining *Eqs 4*, *5*, and *6* and integrating the resulting equation, it becomes

$$\int_o^{\alpha_{max}} \frac{d\alpha}{\alpha^{2-n}(1-\alpha)^n} = A \int_o^{t_{max}} EXP(-E/RT)dt \qquad \text{(a)}$$

If $dT = \beta\, dt$ is defined and substituted into *Eq a*, then one obtains

$$f(\alpha_{max}) = \frac{1}{n-1}\left(\frac{\alpha_{max}}{1-\alpha_{max}}\right)^{n-1} = \frac{A}{\beta}\int_o^{T_p} EXP(-E/RT)dT \qquad \text{(b)}$$

For $20 < E/RT < 60$, the right-hand side integral of *Eq b* can be determined using Doyle's approximation (18, 19). This yields,

$$f(\alpha_{max}) \simeq \frac{AE}{\beta R} \times EXP\left(-5.33 - \frac{1.05\,E}{RT_p}\right) \qquad \text{(c)}$$

Rearranging *Eq c*, the following equation is obtained,

$$\ln \beta + \ln f(\alpha_{max}) \simeq \ln \frac{AE}{R} - 5.33 - \frac{1.05\,E}{RT_p} \qquad (16)$$

P. W. K. LAM: DISCUSSION

L. A. Utracki: The way you wrote your kinetic equation as a product of concentration of growing polymeric radicals (proportional to conversion) and concentration of remaining monomer with the assumption that exponents $m + n = 2$, suggests to me a second order polymerization kinetics. However, you called it systematically "autocatalytic"; where the autocatalytic part comes from? Furthermore, why did you have to assume the second order reaction, while there are methods of representation of the kinetic data from which the reaction order can be determined? Finally, this is a symposium on composites. Your paper treats kinetic of the polyester resin without taking into account presence of a filler. Are you implying that filler will not affect the kinetics, that the same dependencies you proposed for neat polyester will be valid for such composites as SMC or BMC? Did you check if and to what extent filler affects the reaction?

P. W. K. Lam: The second order kinetic is one of n-order kinetic schemes. In n-order kinetics you do not see maximum in the reaction rate. Here we have maximum at about 34 percent conversion and this is why it is called autocatalytic. In fact, the "autocatalytic effect" or "gel effect" was also observed by Horie, *et al.* (8) for a similar system. Now, the assumption of the 2-nd order makes the mathematic analysis much simpler; you can integrate the rate equation, you can get exact solution. Without this assumption one has to go through a numerical solution. The relations I proposed are very simple so anyone can use to calculate.

L. A. Utracki: Did you check if indeed it is a second order reaction?

P. W. K. Lam: Yes. I have done a bit of literature survey summarized in *Table 2*. Everybody assumes the second order. Presently we are studying the effect of fillers and additives on the kinetics, and the results will be published in the subsequent paper in the same journal.

L. A. Utracki: Can you tell us if the filler affects the kinetics and in what sense?

P. W. K. Lam: I have tried a lot of additives. Plotting half-life or t_{max} *vs.* T there is a crossover. The reaction starts at slower rate but at certain temperature it accelerates.

W. T. Stevenson: Your isothermal curves are up and down and you said that this is autocatalytic. Could it be that this is the old Tromsdorff effect?

P. W. K. Lam: The typical isothermal curves shown in the paper are probably the consequences of the interplay at the autocatalytic effect and the diffusion-controlled reaction.

W. T. Stevenson: I have seen a lot of autocatalysis in amine-cured epoxies. There the effect is genuine. But here, as the reaction progresses the viscosity increases, the termination rate goes down, and the concentration of radicals goes up.

P. W. K. Lam: I see your point. Yes, to get the maximum the reaction simply can be diffusion controlled.

L. A. Utracki: The maximum is a natural consequence of the assumed kinetic scheme, summarized in the initial *Eq 4*. Differentiating it one gets an expression for conversion at the maximum rate $\alpha_{max} = m/(m + n)$. Assuming $m + n = 2$ your *Eq 10* is obtained. Two conclusions: (i) the presence of maximum is a natural consequence of the initially assumed two-body reaction kinetics where the concentration of radicals is proportional to α^m and concentration of monomer to $(1 - \alpha)^n$, and (ii) that if α_{max} is independent of temperature the reaction to quite high conversion is not affected by the diffusion processes associated with approach of the glass transition.

PANEL DISCUSSION ON: THERMOPLASTICS VS THERMOSETS IN ADVANCED COMPOSITES

R. C. Tennyson: Our next topic is a panel discussion on the subject of "Thermoplastics *vs.* Thermosets in Advanced Composites". I have three other colleagues who will also contribute to this discussion: S. Newman, M. Takemori, and T. A. Waterhouse.

Earlier today I had the opportunity to review what I believed are the major advantages of utilizing thermoplastic based composites, compared to current generation thermoset composites. In summary, the points I made in favor of thermoplastics were:

- increased toughness
- better impact resistance
- some have higher service temperatures
- less hygroscopic
- more easily repaired
- lower cost processing—the materials are already "cured", thus unlimited shelf-life, with no requirement for refrigerated storage
- some metal forming operations will be transferable to thermoplastic forming
- quality of material may be better in terms of less variation from batch to batch.

On the negative side, several points should be noted. In processing thermoplastics one can encounter:

- higher pressure and temperature
- the higher molecular weight can lead to difficulties with fiber wet-out, thus yielding higher void contents
- possible environmental stress cracking
- higher CTE values at equivalent fiber volume fractions
- some thermoplastics are susceptible to organic solvent exposure.

Having said this, I strongly believe that the aerospace industry will be moving towards substantial increased utilization of thermoplastic composites.

One panelist from whom we have not heard is Alain Waterhouse. He is from Bell Helicopter Textron in Ste-Thérèse, Québec, and will present an industrial point of view.

T. A. Waterhouse: I was very pleased to see Prof. Tennyson's presentation with all the slides and viewgraphs illustrating application of composites in the aerospace industry. I want only to reinforce some of his points. Bell Helicopter Textron has had a long involvement with high performance composites. I graduated in 1972 with a masters degree in aircraft engineering and since then have been involved in the application of composites to high performance structures. Bell Helicopter, as other helicopter manufacturers in North America, has been involved for a long time in primarily glass fiber composites because of their increased fatigue performance over metals. That automatically led into the use of high performance composites such as those based on graphite, bismaleamides, polyamides, and various other materials currently used in the aerospace industry.

Helicopters were probably the first major application of primary composite structures in the aerospace industry. Helicopter blades are mainly made of composites. We followed on from there. Recently the US Army funded two all-composite airframe helicopter programs, one of which was at Sikorsky and the other with us at Bell. In terms of the amount of composite used in airframe, Kevlar and graphite fiber were nearly identical, only the performance details are somewhat different.

In the new model we are building at Mirabel, the majority of the airframe structure is aluminum but the blades, yoke, fuel tanks, etc. are of glass fiber composites. We are taking advantage of the damage tolerance characteristics of the material in certifying these parts.

Our next project is going to be Model 440 with a very large percentage of the airframe made out of high performance composites. When we planned it two years ago, the assumption was that it would be graphite-epoxy. However, presently we are thinking seriously about using thermoplastics. This is one reason for my being here. I would like to get some input on that subject. One of the problems we are facing in the aerospace industry when we come to new materials is that there is a lot of investment in capital equipment involved, personnel training, etc. Every time a new material comes along, there has to be a very good reason for scrapping that investment. In the case of a new material with new properties, such as is the case for replacing epoxies with thermoplastics, there is also a large time delay in selecting the material, characterizing it, and arriving with statistically viable properties which can be used throughout the industry for design purposes.

Looking at the thermosets/thermoplastics issue, we think that thermoplastics are more attractive because of performance, hot/wet behavior, impact resistance, etc. One of the attractions for us is that currently with thermosets, every manufacturer is essentially his own "materials" producer. The quality and performance of a composite depends on how the manufacturer handles it. With thermoplastics this is not the case. The quality and performance is in the hands of the material supplier and this is where we would like to have it for the sake of reproducibility of batch-to-batch performance. The other benefits are: the low storage cost, long shelf-life time, lower production cost (in some instances), and applicability of well known metal forming practices (rolling, hydropress).

In conclusion, I would like to say that when we are looking at a new material like graphite/epoxy, it took about 10 years from the date the industry became aware of the potential to actually seeing it in production. From where I stand, it seems to me that as far as thermoplastics are concerned, we are in the middle of that period. At least five years will pass before anybody flies in an aircraft which has a significant proportion of thermoplastic composites in it.

S. Newman: In the automotive industry we have been continuously faced with new material choices. There is a constant competition between new materials and those we are familiar with. I suspect that, as in other cases, each new material will find its own niche. It is very difficult for us to discuss the topic on thermosets *vs.* thermoplastics in advanced composites unless we begin to get down to "brass tacks" of particular applications: where is it going to be used, what are the environmental conditions, and what function must it perform. There are obvious advantages to thermoplastics but there are also some disadvantages which may or may not be relevant depending on the application and environmental conditions. For instance, thermoplastics by and large, are more prone to environmental stress cracking than thermosets. Secondly, I suspect that thermoplastics also tend to have higher coefficients of thermal expansion since they do not have the same degree of restraint due to crosslinking. Furthermore, it is more difficult to control anisotropy in thermoplastics than in thermosets. In general, due to higher viscosity, you may also have more difficulties with fiber wet-out. In short, I can think of pluses and minuses and only when dealing with specific classes of applications and conditions may we be able to realistically balance the equation.

T. A. Waterhouse: I appreciate your point. I think that we may be further along than you are suggesting. There has been a lot of work done in the UK starting more than 10 years ago, which has been followed by additional R & D in the USA. There is a lot of published data on some types of thermoplastic composites and laminated reinforced thermoplastic composites of a similar type to those thermosets used by industry. For instance, the control of anisotropy is quite equivalent. Judging from published data, the properties (e.g. stress corrosion, moisture pickup, mechanical properties, whole-part performance, etc.) are the same or better in comparison to thermosets. What is missing is the solid data base that is currently available to thermoset materials.

S. Newman: Could you comment on creep and stress relaxation characteristics of these systems?

T. A. Waterhouse: At the temperatures we are proposing to use them in civil aviation (excluding supersonics), the materials are operating so far below T_g that we do not think that there are any problems.

M. Takemori: I would like to present another view point. General Electric is both a raw material producer and user. As a material user, we see some of the problems Alain Waterhouse has mentioned: large capital investment, data base is not there, and high risk situation. GE supplies engineering thermoplastics through its Plastics Business Division, PBD. Since the growth projection of the use of engineering resins in commercial aircraft, military and space usage for 1985 to 1992 is steady but not outstanding, PBG is more interested in what can be called "industrial composites", rather than advanced composites. These industrial composites are short or long fiber composites, but not produced by typical injection molding or SMC/BMC type of operations. One offshoot of GE's interests is a recently formed joint venture between GE and PPG, called Azdel, Inc., whose initial products are glass filled PP and PET. Soon to follow are poly(butyleneterephthalate) (PBT), polycarbonate (PC), PBT/PC blends, and polyetherimide. For GE as the resin supplier, the lower temperature, high volume application market, particularly the automotive, offers the greatest growth potential. The aircraft market is still a few years down the line.

S. Newman: Obviously, the automotive market offers tremendous incentive but not for the top performance and cost of advanced composites that I thought we were supposed to discuss. Azdel is currently being used in the automobile industry; it is a polypropylene sheet with continuous strand glass mat. Presumably, it can be made with a higher temperature resin and can be compression molded at 1000 to 1500 psi. Very costly systems are not likely to be used in large amounts.

Additionally, the thermoset people are not standing still. There are new, interesting technologies coming along which allow one to use continuous fibers. I am citing in particular the resin transfer technique where you preplace fiber in a mold. It can be a continuous strand mat, a wound structure or some type of preform. The matrix phase is then pumped in as in RIM technology. It is a low pressure technique, therefore, large parts can be made at relatively low capital costs. In the automotive industry when you want to make a large part, you have to invest in enormous injection molding machines, or compressing presses. There is considerable resistance to that sort of investment. Thermosets are not standing still; they offer a great deal of attractiveness for making large parts with relatively low cost equipment. In summary, one has to make a case-by-case decision in the choice of thermoplastics over thermosets.

M. Takemori: I agree with you. Nonetheless, the advantage in being a material supplier is that there are so many opportunities to choose from. The growth potential is everywhere you look.

A. N. Wright: I like what Seymour Newman said about knowing what your particular application is. That really has to be the driving factor. We have an excellent example of a tradeoff to use a filled thermoplastic. GE just formed a joint venture for the exploitation of Ultem polyetherimide. They join with a company which know how to make circuit boards. Because of Ultems high heat distortion temperature capability, filled or not, they will make the circuit boards by injection molding. The product will have high temperature stability in terms of dimensional tolerances that can get you into all sorts of new microcircuitry. There will be thousands and thousands of pounds involved. The venture is application driven where the thermoplastic resin fits like a glove.

R. C. Tennyson: I am going to ask Alain if he agrees. Aren't we looking at the aircraft industry in terms of the replacement of thermoset systems like epoxy-graphite by a thermoplastic materials which you can design in a very similar way for specific conditions and properties? At the same time, gaining more ductility and less susceptibility to delamination and cracking as a bonus.

T. A. Waterhouse: These are the drivers in our industry, but first is the improvement of impact resistance. Certainly if we go this route, one would replace all the graphite/epoxy we are using with graphite/thermoplastic.

L. A. Utracki: In five or six years, new military aircraft will contain large structural parts made of reinforced thermoplastics. The material does not exist at the moment, at least noboby knows what material will be used, but in the plans they are supposed to fly with thermoplastic composites. This will require serious, accelerated R & D to scan various candidate materials, build a data-base and to develop new processors and test procedures.

At the present moment, we are experiencing an explosion of engineering thermoplastics on the market. There are several companies manufacturing poly(phenylene ether), poly(phenylene sulfide), poly(etheretherketone), or liquid crystal polymers. There is also a new, so called "long fiber" technology, where the continuous fibers pass through a pultrusion process for perfect wetting, then are cut into about 2 to 10 mm long strands. The strands can be processed using standard processing equipment: injection molding or extrusion. Since the fibers are wetted and in bundles they do not undergo the same mechanical degradation as short fibers do, and the properties of parts formed by this method compare fairly well with those made using continuous filaments. Kevlar in various thermoplastics is already available on the open market. The material is not cheap since it has to go through a pultrusion process, chopping, then a forming stage. However, it will be attractive for replacement of numerous parts in the aerospace industry. In the future, one would like to develop a single step process in which all the individual steps: fiber/matrix feeding, wetting, cutting, and forming steps can be combined, generating long fiber reinforced materials. The chopped Kevlar fibers now on the market, may also provide a new interesting method of going into advanced technology without outrageously new and costly processes. We have to learn how to wet these fibers, how to control their orientation by rheological forces and how to design the pieces. All this will require an increased R & D effort, not its erosion as we have seen in recent years.

During the 10th International Plastics and Rubber Exhibition, K-86, in Düsseldorf, the number of new engineering resins was quite astonishing. Besides Dartco and Celanese, there are four other companies manufacturing LCP. Bayer came with a new single step polymerized poly(phenylene sulfide) with a long term use temperature of 250°C, available in various colors and at very attractive pricing. There were several new sources of PPO, a new source of PEEK (not yet on the market), etc. Most of these are available with reinforcements at loadings exceeding 50 wt percent. I do not have to remind you that thermoplastic anisotropic sheets can be piled and welded to generate appropriate structural properties. It seems that we are at the doorstep of a new era in polymer technology, where new materials and new processing techniques provide us with great potential and also a challenge. I would like to close with a warning to our industry. Seeing European research efforts and the demonstration of new technological developments, the name "Old Continent" seems to be more appropriate to ours. The challenge to North America does not come exclusively from the Asian countries.

S. Newman: The moderately long fiber systems made by several people, for instance ICI or Polymer Composites in the USA, have a significant potential outside the aerospace industry. They do seem to have good properties, better impact behavior than short fibers, and better creep characteristics. However, the aircraft people often need to be able to achieve orientation of the fiber in a controlled fashion. Basically the long fiber system is an injection molding compound and therefore you are at the mercy of the machine and part configuration in regards to fiber orientation.

L. A. Utracki: Yes, as far as injection molding is concerned, to a degree you are right—weld or seam-lines are difficult to control. I have been mainly addressing extrusion, where with a properly designed die, you know how to control fiber alignment down to about 10 to 15° of uniformity.

S. Newman: Some automotive parts, such as steering wheels, have already been made using these materials and indeed they seem to have a large potential. I do not understand the claims that there is very little fiber degradation during injection molding of these long fibers. I presume that you must make some alteration to the machine to prevent this degradation. The mechanism for fiber degradation is often considered to be fiber-fiber friction and I cannot see that this is eliminated. I am curious as to why there should be little degradation!

L. A. Utracki: In our Institute, Bo Fisa studied the mechanism of anisometric particle degradation during processing. He and his co-workers demonstrated quite convincingly that indeed inter-particle contact is responsible for attrition of flakes. However, in agreement with Czarnecki and White observations, he found that fiber (at least glass fibers) break by rheological forces, independent of concentration. Single fibers will be broken by virtue of the stresses created in the polymeric matrix. Now, regarding your question I can only summarize how I explain this to myself. To the feeder of the injection molding machine you introduce thermoplastic/fiber strands or bundles. The bundle is much stronger than a single fiber. The polymer acts rather like a binder than a matrix, the aspect ratio of the fiber is in excess of 1000, so there is nearly uniform plug flow both in the extruder as well as in the runners, sprue, and mold. One has to remember that channel depth and runner diameter are smaller than the fiber length. The only way the material can flow is to have a good extensional field orientation at the entrance to the runner system. Neither irrotational nor plug flow generates mechanical attrition. The 20 to 30 percent reduction of statistical fiber length seems to be reasonable.

S. Newman: Obviously, this is a very promising system combining processability of short fiber composites with properties or characteristics of long or continuous fiber composites. Regarding your comment on liquid crystal polymers, it seems to me that again here, it is very difficult to control the orientation especially in injection molding. People are using LCP primarily for high temperature characteristics, rather than for their so-called molecular composites properties. Maybe we should learn to produce oriented tapes of LCP.

L. A. Utracki: LCP are interesting matrix materials for long fiber technology. In the isotropic state, melt viscosity is low and they provide attractive fiber wetting materials. Due to high crystallinity, the thermal expansion coefficient is low and dimensional stability very good. There are at least six companies manufacturing LCP, so the price should come down as well.

D. J. Carlsson: CIL provides PEEK in Canada. I want to come back to the problem of using thermoplastic composites. Prof. Tennyson was stressing their advantages, that one can lay them up, fuse, heat treat, etc. A lot of people are worrying that these materials are fabricated at very high temperatures. Then they crystallize, creating a lot of stresses in the system. I wonder if someone could comment on how much of a problem this is. There is a large literature on annealing of PEEK to overcome the stresses, but how much is this going to limit the applications of these materials?

M. Takemori: I cannot comment on PEEK. I do know though that residual curing stresses, even in epoxies, are enough to cause creep relaxation, microcracking and changes in mechanical performance over time. This is a problem that will have to be addressed.

L. A. Utracki: If you have a problem you will find a solution. If you want to lay several plies and heat up a thick construction by thermal welding, indeed you will have a serious problem. On the other hand, if you selectively soften only the adjacent layers to be welded together (for instance by inductive heating) then your problem will be significantly smaller. Stresses do have a tendency to relax below T_g so a method of conditioning can be devised. I do not think that this is a technical problem. Financially, it may be, but then one has to develop better, less expensive methods.

R. C. Tennyson: What you are saying is that we can anneal thermoplastics whereas the cross-linked thermosets will not relax by this process.

D. J. Carlsson: As Utracki was saying the approach is annealing but this will add to the cost. Another aspect is that the apparent simplicity of thermoplastics is probably overstated. If you are processing at temperatures exceeding 400°C there are very few organic materials that are stable at that temperature. Already, there are comments that PEEK (annealed at these temperatures to control crystallinity to eliminate skin-core effects) undergoes serious chemical changes resulting in about 60 percent cross-links. It is no longer a simple thermoplastic.

L. A. Utracki

U.S. POSTAL SERVICE

STATEMENT OF OWNERSHIP, MANAGEMENT AND CIRCULATION

(Required by 39 U.S.C. 3685)

1. TITLE OF PUBLICATION Polymer Composites	**A. PUBLICATION NO.**	**2. DATE OF FILING** 10/87
3. FREQUENCY OF ISSUE (Feb, Apr, June Bi-Monthly Aug, Oct, Nov.)	**A. NO. OF ISSUES PUBLISHED ANNUALLY** 6	**B. ANNUAL SUBSCRIPTION PRICE** $40.00 member $100.00 nonmember

4. COMPLETE MAILING ADDRESS OF KNOWN OFFICE OF PUBLICATION *(Street, City, County, State and ZIP Code) (Not printers)*

14 Fairfield Drive, Brookfield Center, CT 06805

5. COMPLETE MAILING ADDRESS OF THE HEADQUARTERS OR GENERAL BUSINESS OFFICES OF THE PUBLISHERS *(Not printers)*

14 Fairfield Drive, Brookfield Center, CT 06805

6. FULL NAMES AND COMPLETE MAILING ADDRESS OF PUBLISHER, EDITOR, AND MANAGING EDITOR *(This item MUST NOT be blank)*

PUBLISHER *(Name and Complete Mailing Address)*

Robert D. Forger, 14 Fairfield Drive, Brookfield Center, CT 06805

EDITOR *(Name and Complete Mailing Address)*

Dr. Roger S. Porter, 14 Fairfield Drive, Brookfield Center, CT 06805

MANAGING EDITOR *(Name and Complete Mailing Address)*

Daniel J. Domoff, 14 Fairfield Drive, Brookfield Center, CT 06805

7. **OWNER** *(If owned by a corporation, its name and address must be stated and also immediately thereunder the names and addresses of stockholders owning or holding 1 percent or more of total amount of stock. If not owned by a corporation, the names and addresses of the individual owners must be given. If owned by a partnership or other unincorporated firm, its name and address, as well as that of each individual must be given. If the publication is published by a nonprofit organization, its name and address must be stated.) (Item must be completed)*

FULL NAME	COMPLETE MAILING ADDRESS
Society of Plastics Engineers, Inc.	14 Fairfield Drive Brookfield Center, CT 06805

8. KNOWN BONDHOLDERS, MORTGAGEES, AND OTHER SECURITY HOLDERS OWNING OR HOLDING 1 PERCENT OR MORE OF TOTAL AMOUNT OF BONDS, MORTGAGES OR OTHER SECURITIES *(If there are none, so state)*

FULL NAME	COMPLETE MAILING ADDRESS
None	

9. FOR COMPLETION BY NONPROFIT ORGANIZATIONS AUTHORIZED TO MAIL AT SPECIAL RATES *(Section 411.3, DMM only)*
The purpose, function, and nonprofit status of this organization and the exempt status for Federal income tax purposes (**Check one**)

☒ *(1)* **HAS NOT CHANGED DURING PRECEDING 12 MONTHS**

☐ *(2)* **HAS CHANGED DURING PRECEDING 12 MONTHS**

(If changed, publisher must submit explanation of change with this statement.)

10. EXTENT AND NATURE OF CIRCULATION	AVERAGE NO. COPIES EACH ISSUE DURING PRECEDING 12 MONTHS	ACTUAL NO. COPIES OF SINGLE ISSUE PUBLISHED NEAREST TO FILING DATE
A. TOTAL NO. COPIES *(Net Press Run)*	817	900
B. PAID CIRCULATION 1. SALES THROUGH DEALERS AND CARRIERS, STREET VENDORS AND COUNTER SALES		
2. MAIL SUBSCRIPTION	500	630
C. TOTAL PAID CIRCULATION *(Sum of 10B1 and 10B2)*	500	630
D. FREE DISTRIBUTION BY MAIL, CARRIER OR OTHER MEANS SAMPLES, COMPLIMENTARY, AND OTHER FREE COPIES		
E. TOTAL DISTRIBUTION *(Sum of C and D)*	500	630
F. COPIES NOT DISTRIBUTED 1. OFFICE USE, LEFT OVER, UNACCOUNTED, SPOILED AFTER PRINTING	317	270
2. RETURN FROM NEWS AGENTS		
G. TOTAL *(Sum of E, F1 and 2 - should equal net press run shown in A)*	817	900

11. I certify that the statements made by me above are correct and complete

SIGNATURE AND TITLE OF EDITOR, PUBLISHER, BUSINESS MANAGER, OR OWNER

Circulation mgr
10-16-87

Subject Index

A

Acoustic emission, during fracture of short glass fiber reinforced poly(vinyl chloride), 109
Adhesion, fiber-matrix, fatigue fracture of glass-fiber-reinforced poly(vinyl chloride), 298

B

Bis-maleimide/bis-cyanate/epoxy thermosetting resin, thermal characteristics, 39

C

Calorimetry, differential scanning, thermoset cure behavior by, 427
Center sprue-gated cavities, short fiber reinforced thermoplastics in, 8
Chemical exposure, EMI shielding of conductive plastics and, 1
Composite materials: *see also* specific type of composite
  advanced, thermosets vs. thermoplastics, panel discussion, 437
  bis-maleimide/bis-cyanate/epoxy thermosetting resin, thermal characterization of, 39
  epoxy and carbon fiber, Shuttle filament-wound case, 149
  exfoliated-graphite filled, electrical properties, 419
  fabricated, ambient aging of 5245C/graphite prepeg, 245
  fiber, interface/interphase effects, 291
  fibrous, controlled energy dissipation in, 94
  graphite/epoxy
    damage tolerance, 352
    interlaminar fracture and fatigue properties, 342
  high temperature liquid crystalline copolyester, self-reinforced matrix phase, 379
  lamination, thermoanalytical investigation, 222
  mode II delamination, crack-arrest study, 331
  polyester, isothermal cure kinetics, 427
  polymer, optothermal analysis, 396
  poly(phenylene sulfide) and poly(etherketone), thermal and rheological properties, 256
  reinforced plastic, current status and future trends, 363
  resin flow during processing, model, 29, 123
  self-reinforced melt processible, 158
  thermoplastic, unidirectionally reinforced, viscoelastic response of, 237
Compression molding
  flow dynamics in, sheet molding compound, 176
  self-reinforced melt processible polymer composites, 158
Conductive plastics, EMI shielding of, chemical exposure effects, 1
Copolyester composites, high temperature liquid crystalline, self-reinforced matrix phase, 379
Crack-arrest study, mode II delamination, composites, 331
Cryogenic temperatures, fiber-epoxy composites, energy applications, 188
Curing behavior, unsaturated polyester resins, pressure effects, 133

D

Detergents, exposure, EMI shielding of conductive plastics and, 1
Di-methylolmelamine, modification, cellulose fibers, 199, 203

E

Electromagnetic interference shielding, conductive plastics, chemical exposure effects, 1
Electronic speckle pattern interferometer, material property determination, orthotropic plates, 103
EMI: *see* Electromagnetic interference shielding
Energy
  controlled dissipation, fibrous composites, 94
  fiber-epoxy composites for, cryogenic failure mechanisms of, 188
Epoxies: *see also* Resins
  engineering analysis of reaction injection molding process, 208
  neat, measurement of thermal conductivity, 53
Extrusion, self-reinforced melt processible polymer composites, 158

F

Fiber: *see also* specific type of fiber
  orientation, thermoplastic properties of PEEK and, 74
Fiber-epoxy composites, cryogenic failure mechanisms of, energy applications, 188
Fiber-matrix adhesion, fatigue fracture and, glass-fiber-reinforced poly(vinyl chloride), 298
Fiber-polyester connposites, cellulose, reduced water sensitivity, 199, 203
Fillers
  inorganic, mechanical properties of, 115
  shape effects, weldline integrity of reinforced plastics, 408
Formaldehyde, modification, cellulose fibers, 199, 203
Fracture and fatigue properties, interlaminar, micromechanisms of, 342
Fracture tests, scanning electron microscope, 324

G

Glass fibers
  length, effect on creep and impact resistance of thermoplastics, 8
  poly(vinyl chloride) reinforced with, fatigue fracture of, fiber-matrix adhesion, 298
  reinforced poly(vinyl chloride), fracture, acoustic emission during, 109
  short, orientation in sheet molding compound, 82
Graphite composites, ductile polymeric coating application, 46
Graphite-epoxy composites
  damage tolerance, 352
  interlaminar fracture and fatigue properties, 342

I

Injection molding
  reaction, epoxy resin, 208
  self-reinforced melt processible polymer composites, 158
  short fiber reinforced thermoplastics, center sprue-gated cavities, 8
Interphase, dynamic mechanical analysis studies of, 308
Isopropyl alcohol, exposure, EMI shielding of conductive plastics and, 1

L

Laminates, graphite/epoxy, unidirectional, numerical analysis for, 123
Lamination, composite, thermoanalytical investigation, 222

M

Microdielectric monitoring, prepeg cure, 232
Microscopy, scanning electron, fracture tests in, 324
Models, resin flow, composite processing, 29, 123

N

Nylon fiber, reinforcement, polyurethane composites, 253

O

Optothermal analysis, polymer composites, 396
Orthotropic plates, material properties in, nondestructive method of determination, 103

P

Particles, heavily-filled, reinforced epoxide resin, 265
Particulate, epoxy resin filled with, strength and toughness, 314
PEEK
  advanced composites and, 57
  short carbon fiber reinforced, thermoplastic properties of, fiber orientation effects, 74
Poly(aryl-ether-ether-ketone): *see* PEEK
Polyester composites
  exfoliated-graphite filled, electrical properties, 419
  isothermal cure kinetics, differential scanning calorimetry, 427
  unsaturated, curing behavior of, pressure effects, 133
Poly(etherketone), thermal and rheological properties, 256
Polymeric coatings, ductile, application onto graphite fibers, 46
Polymers
  filled, ultrasonic evaluation, 22
  nondestructive evaluation, optically generated thermal waves, 283
  optothermal analysis, 396
  particulate filled, mechanical properties of, 115
  self-reinforced melt processible, 158
  semicrystalline, high speed spun, composite characterization, 271
  short carbon fiber reinforced, thermoplastic properties of, fiber orientation effects, 74
Poly(phenylene sulfide), thermal and rheological properties, 256
Polypropylene
  injection molded reinforced, weldline integrity, 408
  ordered, thermoforming of, 371
Polyurethane composites, nylon fiber reinforcement for, 253
Poly(vinyl chloride)
  glass-fiber-reinforced, fatigue fracture of, fiber-matrix adhesion, 298
  short glass fiber reinforced, fracture, acoustic emission during, 109
Prepreg
  5245/C graphite, effects of ambient aging, 245
  cure, microdielectric monitoring, 232

R

Resin: *see also* Epoxies
  flow, during composite processing, model, 29, 123
  heavily-filled particle reinforced, slow crack propagation, 265
  particulate-filled, strength and toughness, 314
  poly(phenylene sulfide) and poly(etherketone), thermal and rheological properties, 256
  thermosetting, thermal characterization of, 39
  toughening of, ternary blends in, 141
  unsaturated polyester, curing behavior, pressure effects, 133

S

Semicrystalline fibers, high speed spun, composite characterization, 271
Sheet molding compound
  flow dynamics, in compression molding, 176
  short glass fibers in, 82
Slow crack propagation, reinforced epoxide resin, 265
Space shuttle, filament-wound case, cure-rate model for, 149

T

Ternary blends, toughening of epoxy resins, 141
Thermal conductivity, neat epoxies and their composites, 53
Thermal waves, optically generated, polymer evaluation, 283
Thermoforming, ordered polypropylenes, 371
Thermoplastics
  reinforced
    glass fiber length effects, 8
    short fiber, center sprue-gated cavities, 16
  unidirectionally reinforced, viscoelastic response of, 237
  vs. thermosets, advanced composites, panel discussion, 437
Thermosets
  cure behavior, differential scanning calorimetry, 427
  vs. thermoplastics, advanced composites, panel discussion, 437

U

Ultrasonic evaluation, filled polymers, 22

W

Weldline, integrity, reinforced plastics, filler shape effects, 408

Author Index

Appelt, B., 222
Appelt, B. K., 39

Baer, E, 109
Bell, J. P., 46
Bigg, D. M., 1, 115
Bozarth, M. J., 74
Busse, G., 283

Cagliostro, D. E., 149
Cantwell, W. J., 314
Chang, J., 46
Chang, Y. S., 188
Chua, P. S., 308
Chung, W. C., 94
Cielo, P., 396
Cordova, C. W., 253
Cudré-Mauroux, N., 324

Darlington, M. W., 16
Dave, R., 29, 123
Draughn, R. A., 265
Duduković, M. P., 29, 123
Dufour, J., 408

Ellis, T., 222
Eyerer, P., 283

Fällström, K-E., 103
Felsen, M., 244
Fisa, B., 408
Fitzgerald, J. J., 221
Flodin, P., 199, 203
Foy, J. V., 419
Frayer, P. D., 379
Frosini, V., 141

Gillespie, J. W., Jr., 74
Gotro, J., 222
Gotro, J. T., 39

Hagerman, E. M., 176
Hamel, A., 22
Han, C. D., 133
Hiltner, A., 109
Hsia, H-C., 256
Hsu, M-T., 149
Hu, J-T., 256
Hua, L., 199, 203
Hwang, L. R., 94, 188

Iaboni, S., 371
Isayev, A. I., 158
Ishida, H., 57
Islas, A., 149

Jang, B. Z., 94, 188
Joseph, R., 46

Kardos, J. L., 29, 123
Kau, H. T., 82, 176
Kausch, H. H., 314, 324
Kim, D. H., 208
Kim, S. C., 208
Koenczoel, L., 109
Krapez, J. C., 396

Lam, P. W. K., 427
Lazzeri, A., 141
Lee, D-S., 133
Levita, G., 141
Lieu, Y. K., 94, 188
Lindt, J. T., 419
Liu, W-L., 256

Ma, C-C. M., 256
Maldague, X., 396
Marchetti, A., 141
McCullough, R. L., 74
Mei, H. L., 53
Mijović, J., 53
Modic, M., 158
Moet, A., 298
Molin, N-E., 103
Montes-G., G. M., 265

Nguyen, H. X., 57
Nguyen, P. X., 298

Papathomas, K. I., 39
Piché, L., 22
Piggott, M. R., 291
Pournoor, K., 271

Rhee, H. W., 46
Rief, B., 283
Rönnhult, T., 203
Roulin-Moloney, A. C., 314, 324
Rowan, H. H., 253
Roy, C., 352
Russell, A. J., 342

Scola, D. A., 244
Seferis, J. C., 271
Silverman, E. M., 8
Simpson, T. H., Jr., 265
Smith, A. C., 16

Tasnon, M., 352
Tomkinson, G. D., 237

Utracki, L. A., 289, 361, 396, 437

Vallance, M. A., 237
Vassilatos, G., 271
Vontell, J., 244
Vu-Khanh, T., 289, 331, 361, 363, 408

Weiss, R. A., 221
Wentworth, S. E., 232
Woodhams, R. T., 371

Yandrasits, M., 222
Young, J. A., 253

Zadorecki, P., 199
Zukas, W. X., 232

INFORMATION FOR AUTHORS

Submission of original and review articles is encouraged. There is no limit on length. Three copies of the manuscript should be submitted, which should be typed, one side only, double space, with at least a 2.5-cm (1-inch) margin. Submission will be taken to imply that the paper has not been previously published, that it is not being considered elsewhere for publication, and that if accepted it will not be published elsewhere in the same form, in any language, without the consent of the editor or publisher. Authors must agree to transfer copyright to the publisher when an article is accepted for publication. Unless notified to the contrary by the authors, the publisher assumes that the act of submitting the article signifies the author's agreement to such copyright transfer to the publisher. The journal carries a voluntary page charge. Each manuscript should include:

A separate title page, headed by a concise, meaningful title (no abbreviations). This page should provide:

- The name and affiliations of each contributing author at the time the paper was prepared.
- Indicate by asterisk any changes of address for each author since article preparation.
- Acknowledgment of any prior oral presentation and original source of the material.

A separate abstract page, consisting of a single paragraph, text only, of 100–200 words to include the title and the names and addresses of the authors. Define any abbreviations for substances or methods (such as ABS, SAXS, etc.).

A list of references, on a separate page at the end of the text, numbered in order of text citation. The references are to be abbreviated in the form used in Chemical Abstracts using the names of all authors preceded by initials; see Bibliographic Guide for Editors and Authors, American Chemical Society, Washington, D.C.

- Within the text, the reference citations are typed in parentheses in line with the main copy (no superscripts or subscripts), thus:

According to Cohen, et al. (1) . . .

- In the list of references the general style is as follows:

For periodicals:

1. D. Cohen, A. Siegmann, and M. Narkis, *Polym. Eng. Sci.*, 27, 286 (1987).

The journal name and volume are to be underlined and the year is placed in parentheses. The issue number is given only when needed for identification. The article name is eliminated unless the reference is unclear without it.

For books: The title to be spelled out in full.

9. J. E. G. Lipson and J. E. Guillet, in "Macromolecular Solutions," R. D. Seymour and G. Allen Stahl, Eds., Pergamon Press, New York (1982). (Include the state when the city is not identifiable.)

A list of nomenclature, identifying symbols and abbreviations, commonly desirable at the end of the text. Footnotes are to be avoided.

Equations, numbered and typed in the appropriate place in the text. Where symbols cannot be typed, write them neatly in ink.

Tables, each typed on a separate page, with a heading, and numbered with arabic numerals that correspond to the order in which they are cited in the text. The tables should be inserted in the manuscript after the references and before the figures.

Figures, assembled at the end of the manuscript and preceded by a separate typed list of captions that explain them. Please also supply a set of original figures or sharp glossy photos thereof, on 8½ × 11 paper or attached to sheets of this size, one sheet for each figure. Each should be identified on the front edge or on the back (photographs) with the name of the first author and the figure number (e.g., Smith, Fig. 1). Originals are to be prepared with high contrast India ink and to bear uniformly stencilled notations. Line drawings and photos should be of a quality suitable for good photographic reproduction and retained legibility upon size reduction to one quarter. Manuscript transmittal letter should indicate if the figures need be returned.

Send manuscripts to:
Roger S. Porter, Editor
POLYMER COMPOSITES
℅ Polymer Science & Engineering
University of Massachusetts
Amherst, Massachusetts 01003

For information concerning publication dates, page charges and reprint orders contact:
Editorial Department
Society of Plastics Engineers
14 Fairfield Drive
Brookfield Center, Connecticut 06805